The Influence of Wind Flow Over a Long-Walled Asymmetric Coastal Parabolic Dune – Morphodynamic Feedback, Evolution and Migration.

Frances A. Mowling
Graduate Diploma of Environmental Studies (Honours), B.A.

Submitted to the School of Geography and Environmental Studies
in fulfilment of the requirements for the degree of
Doctor of Philosophy

University of Tasmania
Hobart

2006

STATEMENT OF AUTHOR

This thesis contains no material that has been accepted for a degree or diploma by any University or any other institution, except by way of background information that is duly acknowledged in the thesis. To the best of my knowledge, information and belief, the thesis contains no material previously published or written by another person, except where due reference is made in the text of the thesis.

Frances Mowling
13.9.2006.

This thesis may be made available for loan. Copying of any part of this thesis is prohibited for 1 year from the date this statement was signed; after that time limited copying is permitted in accordance with the *Copyright Act 1968.*

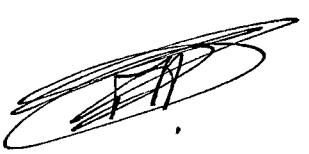

Frances Mowling
13.9.2006.

Abstract

Mobile transgressive dune systems are often overlooked in the study of coastal morphodynamics and sediment budgets. Inundation by sand of abutting agricultural land and infrastructure has recurred throughout the 20th century, frequently accompanied by requests by farming communities to the government to stabilise the dunes. In addition, the association of sea-beach-coastal dunes provides an attractive setting for residential / holiday developments on dune systems. Yet little is known about the pattern of dune mobility in response to changing atmospheric conditions (rainfall, air temperature and wind speed) and their effect on dune mobility and the rate of actual and predicted dune migration. The work presented in this thesis addresses the evolution of a parabolic dune, dune mobility and migration.

Quantitative data were collected to determine process-response in an actively mobile long-walled asymmetric parabolic dune located on the western coastline of northeast Tasmania, Australia. The data were acquired over a period of four years from a composite of geomorphic survey techniques that incorporated repeated surveys of the ground surface topography using kinematic GPS and arrays of erosion pins, which were linked to analysis of wind flow patterns acquired from an on-site 2 m high meteorology station, and analysis of sediment that forms the dune. Wind shear velocity ($u*$) and roughness length (z_0) were measured close to the ground on windward slopes, and speed-up ratios were determined. Analysis of temporally-spaced ortho-rectified and georeferenced aerial photography extended the duration of the survey by fifty years to establish the longer term evolution of the parabolic dune, including the downwind and lateral migration rates of the dune system.

The level of accuracy (planimetric accuracies typically in the range of 2-5 cm and vertical accuracies of 3-10 cm) achieved in the six epochs of kinematic GPS surveys provided reliable GPS data that were used to construct three-dimensional topographic models of the dune system on 5 m x 5 m grids using kriging. The topographic models displayed the general patterns of displacement and accretion of sediment that maintain dune form. Using cross-sectional profiles, at representative locations across the dune, the pattern of process–response between wind speed / wind direction on the direction of sand movement and on morphodynamics was clearly evident. A series of morphological parameters were extracted from the kinematic GPS data to quantify dune migration rates, dune volumes, and dune reconstitution time.

The measured migration rate of the parabolic dune head was 21.5 m/yr (mean value) measured over 4 years, and 27.3 m/yr measured from a fifty-year sequence of ortho-rectified, georeferenced, digitised aerial photography. The head of the dune reconstitutes at the rate of 8.9 years, with a volume of 100,800 m^3. Volumetric change for the study site over an interval of thirty months was in the range of 656,400 m^3. The majority of sand transport is generated by moderate velocity wind flows which have a higher frequency of occurrence. Forty one percent of wind events occur in the moderate velocity category (4 to < 12 m/s), twenty seven percent occur in the high velocity category of > 12 to > 20 m/s. Measurement of flow close to the ground on windward slopes indicated that shear stress does not progressively increase from toe to crest of slope due to interaction between flow and bed form.

Some seventy percent of wind events are topographically aligned; across dune flow from the SW sector results in lateral migration of the trailing arms, with the smaller south trailing arm migrating ENE at more than twice the rate of the north trailing arm. This rate of lateral displacement maintains the 3:1 length to width ratio of the asymmetric parabolic dune by maintaining the dimensions of the deflation plain which in turn maintains the dynamic equilibrium of the aerodynamic envelope of the dune form.

This integrated approach has provided quantitative evidence that demonstrates the dynamic feedback between the prevailing wind regime and seasonal and discrete wind flow events on the dune bed, and the influence of atmospheric conditions on dune mobility.

ACKNOWLEDGEMENTS

The completion of this thesis would not have eventuated without the assistance, support, and encouragement of many people. In particular I thank the following people who provided special assistance.

My supervisors Richard Coleman and Jamie Kirkpatrick who provided sound advice, expert criticism, and encouraged me throughout the study. Thanks especially to Richard for the recommendation to trial GPS technology, followed by the foot slog over the dunes measuring ground surface level with GPS followed by the GPS data analysis. Mick Russell, who has been an absolute diamond throughout the study, from teaching me the intricacies of the Excel program and the obscure delights of equations, to the joy of wiring up the thermo anemometers to data loggers; for the good hearted humour with the calibrations; for assistance with the downloading of data, and for being an absolute brick when we measured wind flow in the field. Thanks to all three of you for proofreading the thesis and for your comments, which increased the rigour. Without your invaluable guidance, this thesis would not have been completed.

Kate Brown supervised in the early phase of the study and introduced me to my research supervisor Patrick Hesp. Patrick generously visited Croppies Bay with me twice, demonstrating how to collect wind flow data with cup anemometers, and provided sound advice and guidance on field research techniques during the early stages of the study. Manuel Nunez both encouraged and challenged me, and in this process he constructively guided me in selecting thermo anemometers to measure close to the ground wind flow and in close to the ground wind flow analysis.

I am grateful to third year Geomatics students Sam Bucknell, Keith van der Schoor and Michael Walsh for surveying the Croppies Bay dune as a component of their course work. Cati Greve who earned some money by ortho rectifiing and georeferencing the aerial photographs in *Arcview*.

To Mike Power, Department of Primary Industry Water & the Environment (DPIWE), thanks for the discussions about surface wind flows and providing easy access to the Department's computer program 'WinRose' to analyse the surface wind data.

Many thanks to Mike Pemberton from DPIWE and to the Bridport Landcare group who supported the Coastcare funding application. The financial support of the Coastcare grant was invaluable in facilitating the purchase of equipment and providing travel expenses for a team of volunteers from the Tasmanian Environment Centre. Like the loaves and fishes parable, the small grant increased eighteen-fold through in-kind donations. To the volunteers, Susan Gunter, Julie von Platen, Moira Lavis, Margaret Steadman, John Hunter, Sahn Cramer, thanks so very much – your labours with the fences yielded good results and a practical methodology that has been printed in several community coastal management reports.

Denis Charlesworth cheerfully assisted with the provision of field and lab equipment and proof read the soils analysis. Darren Turner wrote the computer program for sorting the wind data, and was always there with an answer when 'something' went

wrong with a program or the computer – "Have you tried turning it off?" will resonate for years to come. Kate Charlesworth has always been resourceful and generous in her assistance.

John Davies built the thermo anemometers from a simple design and made them function. Joanna Elliston, Geography Department, Launceston, provided access to the Rapid Sediment Analyser and demonstrated how to use it.

The University of Tasmania, particularly the School of Geography and Environmental Studies, provided funds, a diversity of Department facilities, and the means to network into the Tasmanian community, for which I am most grateful.

Field assistance from Mick Russell, Susan Gunter, Karyl Michaels, Julie von Platen, Darren Phillips, Nicholas Fitzgerald, Vicky Hewitt, and Paul Smart.

Vernon Graham, from the Tasmanian Aboriginal Land Council, visited Croppies Bay to assess for site impact prior to the study commencing.

To the friends who have asked encouragingly 'How's it going?' and I responded 'Gawd, don't ask' or 'Well, I think I'm getting there'. In particular Celia Karpfen, Darren and Jos Phillips, and Andrea Breen. Darren Phillips, in the last year of the thesis provided support, laughter and a productive sounding board.

Table of Contents

CHAPTER 1 Introduction 1

1.0 Overview 1

1.1 Climate of coastal northeast Tasmania 2

1.2 Objectives 3

1.3 Thesis outline 3

CHAPTER 2 Theoretical context 5

2.0 Introduction 5

2.1 Near-surface wind flow in blowouts and parabolic dunes 5

2.1.1 Calculation of shear velocity 9

2.2 Measurement of wind flow and wind velocity to derive sand transport rates 11

2.2.1 In-situ measurement of wind flow 11

2.2.2 Fryberger wind resultant sand roses 11

2.2.3 Measuring close to the ground wind flow 13

2.2.4 Calculation of the sand transport rate 13

2.3 Regulators of dune mobility - wind speed, rainfall and air temperature 14

2.4 Conclusion 19

CHAPTER 3 Grain-size analysis and composition of parabolic dune sediments 20

3.0 Introduction 20

3.1 Aims 22

3.2 Methods 23

3.2.1 Collection and analysis of sediment samples 23

3.2.2 Loss on ignition 23

3.2.3 Moisture content 23

3.2.5 Wet bulk density measurements 24

3.2.6 Sediment grain size distributions 24

3.3 Results and discussion. Existing knowledge of sediment source parameters 26

3.3.1 Sea floor and beach 26

3.3.2 Reworked sediment 26

3.4 Sediment analysis 29

3.5 Variability within and between morphological units 37
3.5.1 Lee slipface 37
3.5.2 North trailing arm 38
3.5.3 Stoss 39
3.6 Sediment moisture content 42
3.7 Summary 43
3.8 Conclusion 45

CHAPTER 4 Wind Regime, Atmospheric Parameters and Wind Flow Pattern over a Long-Walled Parabolic Dune 46

4.0 Introduction 46
4.1 Methods 47
4.1.1 Wind data acquisition and analysis 47
4.1.2 Wind data processing 48
4.1.2.1 Short wind phases 49
4.1.2.2 Flow visualisation 49
4.1.2.3 Flow and form: airflow on stoss and the windward flank of the north trailing arm 50
4.1.3 Design, construction, and calibration of thermo anemometers 51
4.2 Results and discussion 56
4.2.1 Croppies Bay climate 56
4.2.1.1 Air temperature 56
4.2.1.2 Rainfall and evaporation 56
4.2.1.3 Solar radiation 57
4.3 Wind Pattern 59
4.3.1 Seasonal and diurnal wind pattern 59
4.4 Remote and on-site wind data 66
4.5 Wind resultant sand roses 67
4.6 Sand Transport Rate 73
4.7 Airflow up the windward slopes of a long-walled parabolic dune 76
4.7.1 Introduction 76
4.7.2 Shear Stress 77
4.7.3 Flow acceleration on windward slopes 80
4.7.4 Wind velocity profiles and flow visualisation 82
4.7.5 Parabolic windflow pattern 90
4.8 Sand dune mobility 93
4.9 Future trends 98
4.10 Summary 102

CHAPTER 5 Flow and morphodynamics 105

5.0 Introduction 105

5.1 Methods 106

5.1.1 Reconnaissance and ground truthing 106

5.1.2 Rectification of aerial photographs 106

5.1.3 Ground survey 107

5.1.3.1 Erosion pins 107

5.1.3.2 Copper erosion pins measuring changes in surface elevation during measurement of close to the ground wind flow 108

5.1.3.3 GPS Surveys 110

5.2 Results and Discussion 113

5.2.1 Reconnaissance and ground truthing 113

5.2.2 Aerial photography 116

5.2.2.1 1949 aerial photograph 116

5.2.2.2 1964 aerial photograph 120

5.2.2.3 1984 aerial photograph 120

5.2.2.4 1999 aerial photograph 120

5.2.3 Downwind and lateral migration 121

5.2.4 Relationship between flow dynamics, direction of sand transport and morphodynamics 126

5.2.4.1 Repeated Kinematic GPS surveys 126

5.2.4.2 Topographic models 126

5.2.5 Surface elevation change 129

5.2.5.1 Erosion pins 129

5.2.5.2 Copper erosion pins measuring changes in surface elevation during measurement of close to the ground wind flow 130

5.2.6 Wind resultant sand roses, combined with erosion pin and GPS 132

5.2.6.1 South Trailing Arm 132

5.2.6.2 Lateral displacement 140

5.2.6.3 Head of parabolic dune 145

5.2.6.4 North Trailing Arm 152

5.3 Summary 155

5.4 Conclusion 157

CHAPTER 6 Conclusions 158

6.0 Introduction 158

6.1 Sediment sources 158

6.2 Site wind flow 159

6.3 Atmospheric parameters 160

6.3.1 Dune mobility 160

6.3.2 Measurement of potential sand movement rate 160

6.3.3 Measurement of dune migration rate 160

6.4 Wind flow over a parabolic dune – interaction between wind flow and dune form 162

6.5 Future trends 164

6.6 Proposed characteristic features of parabolic dunes 165

References and Bibliography 168

Appendix 1. Wind data – Figures 4.9 to 4.13. 187

Appendix 2. Prècis of average annual atmospheric parameters, 1940 – 2003. 202

Appendix 3. Erosion pin data for the periphery of the deflation plain, Croppies Bay, NE Tasmania, Australia. 203

Appendix 4. Summary of close-to-the-bed wind flow and Aerial photography. 205

Appendix 5. Measurement of enclosure sensor and probe. 206

List of Figures

Figure 1.1. Location of study area. 2

Figure 1.1a. An aerial view of Croppies Bay transgressive dunefield, and the study site parabolic dune. 3

Figure 1.1b. The contextual location of bedforms that form the Croppies Bay transgressive dunefield, and the locations of the study site dune bedforms. 3

Figure 2.1. Robertson-Rintoul's (1990:73) interpretation of near-surface flow structures on a parabolic dune. Taken from Robertson-Rintoul (1990:73). 6

Figure 2.2. The Jackson and Hunt (1975) model of boundary flow over low hills. 8

Figure 3.1. Lee slipface and lee north trailing arm. Grain size frequency histograms of lee bedforms, Croppies Bay, north east Tasmania. 31

Figure 3.2. North trailing arm. Grain size frequency histograms, Croppies Bay, north east Tasmania....32

Figure 3.3. Stoss. Grain size frequency histograms of stoss, Croppies Bay, north east Tasmania. 33

Figure 3.4. Grain samples slides. 36

Figure 3.5. A plot of mean grain size against sorting. 41

Figure 4.1. 2 m mast with cup anemometer and wind vane located on crest of south trailing arm... 49

Figure 4.2. Thermo anemometer with protective cover removed to show circuitry....52

Figure 4.3. Thermo anemometer calibration technique. 52

Figure 4.4a. An example of the initial method of calibration of cup and thermo anemometers....54

Figure 4.4b. An example of the optimal method of calibration of cup and thermo anemometers....54

Figure 4.5. Light weight aluminium 2 m mast with thermo anemometers and wind vanes. 55

Figure 4.6. Mean monthly rainfall and evaporation, 1960 – 2003....57

Figure 4.7. Full year wind rose, Croppies Bay. 61

Figure 4.8. Winter wind rose, Croppies Bay....62

Figure 4.9. Spring wind roses, Croppies Bay. 63

Figure 4.10. Summer wind rose, Croppies Bay. 64

Figure 4.11. Autumn wind rose, Croppies Bay....65

Figure 4.12. Comparison of mean remote (Low Head, 10 m mast) and on-site (Croppies Bay, 2 m mast) wind speeds. 66

Figure 4.13a. Wind resultant sand roses, 1 to 6. 69
Figure 4.13b. Wind resultant sand roses, 1 to 6. 70
Figure 4.14. Stoss wind flow illustrating temporal fluctuations in wind speed due to gustiness close to ground surface, recorded at heights of 15 cm, 45 cm and 190 cm, over a thirty–minute period using thermo anemometers 75
Figure 4.15. Wind shear velocity (u_*) profiles on windward slopes, Croppies Bay parabolic dune. 77
Figure 4.16. Relationship between friction velocity (u_*) and roughness length (z_0). 79
Figure 4.17. Measured wind velocity profiles from a transect aligned north to south, across the parabolic dune profile, with the location of masts.. 84
Figure 4.18. Measured wind velocity profiles on stoss and the location of masts.. 85
Figure 4.19. Location of azimuths and wind speeds for eight wind profiles. 86
Figure 4.20a. Flow visualisation on stoss. GPS surveyed profile 89
Figure 4.20b. Examples of toe and crest flow visualisation on stoss. Arrows indicate the direction of flow towards crest 89
Figure 4.21. Wind flow pattern over Croppies Bay parabolic dune. 92
Figure 4.22 . Running mean of annual wind speed, air temperature and rainfall for the period 1940 to 2003, Croppies Bay. 98
Figure 5.1. Location of the erosion pins on stoss, periphery of deflation plain, and central alignment; central erosion pins. Location of GPS profiles 1 to 17 109
Figure 5.2a. Control network for the dune survey - comprised of 6 stations sited on the periphery of the parabolic dune system and toe of NTA. 112
Figure 5.2b. Epoch 5 survey profiles, displayed on a scanned image of the 1999 aerial photograph. 112
Figure 5.3a. Croppies Bay parabolic dunefield. 113
Figure 5.3b. Scanned image of the 1:42,000 1997 aerial photograph, showing the Croppies Bay transgressive dunefield and the study site parabolic dune 114
Figure 5.4a. Croppies Bay parabolic dune viewed west (2004). 114
Figure 5.4b. Croppies Bay parabolic dune viewed east (2004). 115
Figure 5.5. 1949 Arcview aerial photo (black and white image), showing the western portion of the Croppies Bay parabolic dune 117
Figure 5.6. 1964 Arcview aerial photo (black and white image), showing Croppies Bay parabolic dune 117

Figure 5.7. Temporal and spatial changes in the morphology of Croppies Bay parabolic dune. 118
Figure 5.8. Location of transects 1 to 4 119
Figure 5.9. 1984 Arcview aerial photo (black and white), showing Croppies Bay parabolic dune. 123
Figure 5.10. 1999 Arcview aerial photo, showing Croppies Bay parabolic dune. 123
Figure 5.11. Temporal and spatial morphological changes between Epochs 1 and 4. 128
Figure 5.12. Ripple bedform mid slope, NTA with copper erosion pins in a 1 m^2 grid. 131
Figure 5.13. North trailing arm. Profiles 1, 2, 3 134
Figure 5.14. North trailing arm and stoss. Profiles 4 and 5. 135
Figure 5.15. Stoss and head of dune. Profiles 6, 7, 8. 136
Figure 5.16. STA and head of parabolic dune. Profiles 9, 13, 17. 137
Figure 5.17. STA. Profiles 10, 11, 12. 138
Figure 5.18. South to North traverses. Profiles 14, 15, 16. 139
Figure 5.19. Seasonal surface elevation changes at the periphery of the deflation basin. 146
Figure 5.20. Head of parabolic dune, oblique low altitude air photo, 2003. 148
Figure 5.21. Stoss: change in mm ground surface elevation per day by wind resultant sand rose. 149
Figure 5.22. The crest of the NTA showing the distribution of relict vegetation on eroding knolls (background) and shadow dunes formed in the lee of *Spinifex sericeus* (foreground). Located between GPS profiles 14 to 16. 154

List of Tables

Table 2.1. Comparison of weighting factors for wind speed measurements in m/s and knots. 12

Table 3.1. Sediment texture of three soil types within study area after Hubble (1946:58, 60). 27

Table 3.2. Sediment analysis of bulk density, porosity, grain density and grain size distributions; loss on ignition. 30

Table 3.3. Grain shape characteristics and mineral origin, representative samples. 34

Table 3.4. Sand moisture content of sediment samples. 42

Table 4.1. Seasonal air temperature (°C), Waterhouse Station 1994 to 2003. 56

Table 4.2. Seasonal solar radiation (MJ/m^2) for Croppies Bay, 1990 – 2003. 58

Table 4.3. Croppies Bay wind pattern. 59

Table 4.4. Croppies Bay drift potentials (DP) and annual drift potential. 71

Table 4.5. Vector average wind speed by season 72

Table 4.6. Units used to calculate the sand transport rate. 73

Table 4.7. Wind shear velocity (u_*) and roughness length (z_0) on windward slopes, Croppies Bay parabolic dune. 78

Table 4.8. Speed-up ratios on stoss and north trailing arm, south flank 80

Table 4.9. Wind velocity (m/s) north to south over the dune profile, and up the axis (west to east) of the parabolic dune. 82

Table 4.10. Croppies Bay units for calculating M by six monthly intervals and M by seasons. 93

Table 4.11. Croppies Bay units for calculating q by dry and wet six month periods. 95

Table 4.12. Predicted trends on dune mobility: applying Lancaster's (1997) indices to calculate M and P:E. 99

Table 4.13. Predicted trends on dune mobility: applying Tsoar and Arens (2004) index to calculate DP (q) 99

Table 5.1. Kinematic GPS survey dates, sampling rates at Croppies Bay parabolic dune 110

Table 5.2. Temporal and spatial changes in the morphology of Croppies Bay parabolic dune, derived from the fifty-year sequence of digitised, ortho rectified, and georeferenced aerial photographs 119

Table 5.3. Lateral migration (m), 1949 – 1999 125

Table 5.4. Stoss erosion pin data. 130

Table 5.5. Surface elevation changes (mm) measured over a thirty-minute period. 131
Table 5.6. Annual and intra-year wind resultant drift directions..... 142
Table 5.7. Intra-year and seasonal deflation rates on the stoss by sand rose over a period of 721 days. 145
Table 5.8. Surface elevation changes (mm) on the stoss – 721 days..... 147
Table 5.9. Progressive mean migration rate of the lee slipface. 147
Table 5.10. Temporal-spatial changes in the width and height by selected Epochs. 151
Table 5.11. NTA morphology data. 153

List of Equations

Equ 2.1 8
Equ 2.2 9
Equ 2.3 9
Equ 2.4 10
Equ 2.5 10
Equ 2.6 13
Equ 2.7 14
Equ 2.8 14
Equ 2.9 15
Equ 2.10 16
Equ 2.11 16
Equ 2.12 17
Equ 3.1 23
Equ 4.1 80
Equ 5.1 108
Equ 5.2 108
Equ 5.3 111

Table of frequently uscd symbols.

Symbol	Function
M_z	distribution of mean grain size
ϕ	phi – size scale for grain size
%	percent
mm	millimetre
km/hr	kilometres per hour
m/s	metres per second
km	kilometre
m	metre
cm	centimetre
gm	gram
g cm^{-3}	grams per cubic centimetre
gm/cc	grams per cubic centimetre
DP	Drift Potentials measure the energy of surface winds and their effectiveness in transporting sand
EP	Erosion pins
NTA	North trailing arm
RDP	Resultant drift potential expresses, in vector units, the net sand transport potential when winds from various directions interact
RDP/DP	Ratio of the resultant drift potential to the drift potential index of the directional variability of the wind
RDD	Resultant drift direction expresses the direction and magnitude of the vector resultants
STA	South trailing arm
VU	Vector units
q	in all equations represents the sand transport rate
z_0	At ground surface velocity is zero, so the gradient starts at the height of the roughness length, z_0
u_x	the friction velocity is an expression of the velocity gradient.
$u*$	shear velocity
u_z	wind speed at height z
z	height
MI	moisture index
P	precipitation
PE	potential evapotranspiration
M	dune migration
W	the percentage of days during a year when the sand moving capacity of the wind is > 5 m/s
P/E	the ratio of the mean annual precipitation to mean annual potential evaporation
u_t	threshold wind velocity
BoM	Bureau of Meteorology
TAs	Thermo anemometers

CHAPTER 1

Introduction

1.0 Overview

Coastal parabolic dunes occur within both actively mobile and fixed transgressive dune fields. They remain one of the least studied geomorphic bedforms. The influence of wind flow and wind direction on their process and form, sediment sources and sediment textural and compositional parameters have received relatively little attention. This thesis is concerned with the processes that drive the morphodynamic evolution of a long-walled, asymmetric, actively mobile, coastal parabolic dune. In particular, the study examines the sediment that is available for entrainment from the distinct morphological units that form a parabolic dune; the control that an effective wind regime has on dune evolution; the feedback between specific wind flow events and morphodynamics, and the predicted influence of selected atmospheric parameters on coastal dune mobility.

The initial reason for undertaking the present study was the encroachment on agricultural land, roads and dams by sediment from the Waterhouse transgressive dune system, northeast Tasmania. The Tasmanian State Government expended about six million dollars on a dune stabilisation program using marram grass (*Ammophila arenaria*) during the 1970s and 1980s. By the late 1990s, sediment from this dune field continued to encroach upon abutting farmland and dams, and farmers requested that the State Government recommence the marram grass stabilisation program. Measurement of the dune migration rate, or predicted potential alienation rate of agricultural land, is a simple measure that may assist in the formulation and implementation of policy by government and land management practices by farmers. The measurement of dune mobility, both actual and potential, proved complex, opening up the questions addressed in the present study.

The Waterhouse transgressive dune field, although extensive in area, was unsuitable for an extended survey where equipment needed to be deployed. The dune field is readily accessible to the public and is used recreationally by drivers and riders of off-road vehicles and by game shooters; in addition, the dune morphology has been modified by bulldozer activities to form beds for marram grass (*Ammophila arenaria*). A suitable study site needed the following criteria: a coastal area exposed to prevailing westerly winds; a transgressive mobile dune field devoid of marram grass (*Ammophila arenaria*); sufficiently remote to discourage pedestrian or off-road vehicle access, thus deterring vandalism on the 2 m meteorology station and erosion pins; a landscape unmodified by domestic stock grazing, mining, or bulldozer activities. Essential to the study was access to a series of sequential aerial photography and a large-scale topographic map. For logistical reasons, the site also needed to be close enough (within a day return visit of

Hobart) to enable repeated downloading of wind data and recording of changes in ground surface elevation.

An area situated immediately north of Waterhouse, Croppies Bay, was located which fulfilled the research criteria. The Croppies Bay transgressive dune field is five square kilometres in area, and occupies a shallow basin between dolerite headlands and marl ridges. The dune field has transgressed across earlier Quaternary sediment, the Ainslie sand (Bowden, 1981), which overlays an indurated coffee rock that impedes drainage.

The study area, shown in Figure 1.1, is in coastal northeast Tasmania, Australia, at approximately latitude 41° S, longitude 151°E; a region with a humid temperate climate (Thornthwaite (1931) and extensive transgressive dune fields.

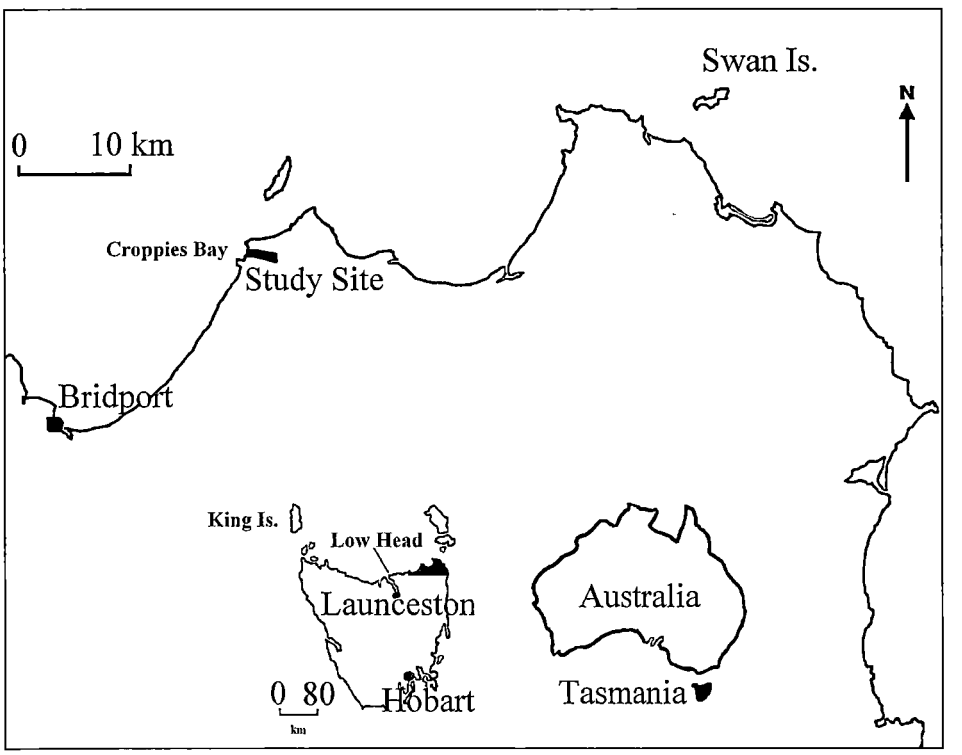

Figure 1.1. Location of study area.

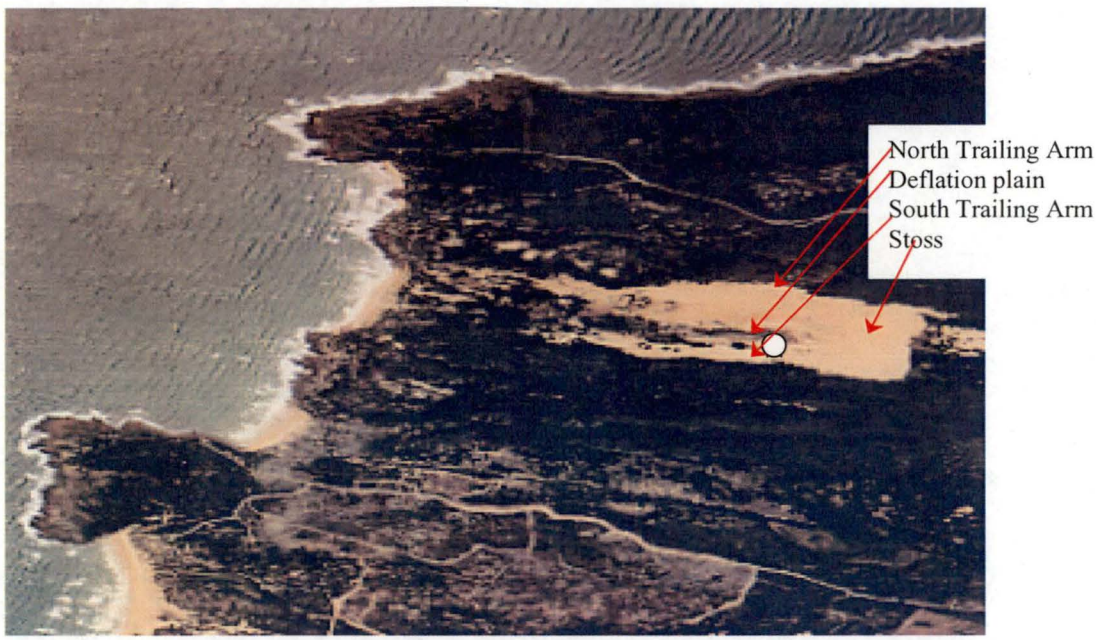

Figure 1.2a. An aerial view of Croppies Bay transgressive dunefield, and the study site parabolic dune (1:42,000 1997 aerial photograph). The location of the on-site meteorology station on the south trailing arm is indicated by ○.

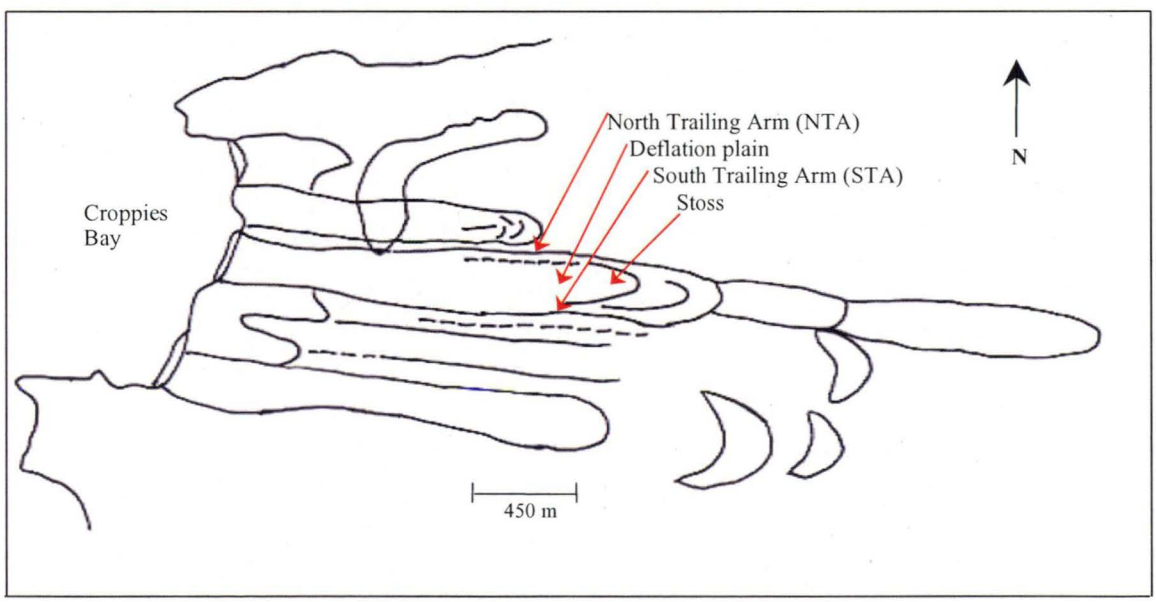

Figure 1.2b. The contextual location of bedforms that form the Croppies Bay transgressive dunefield, and the locations of the study site dune bedforms. The components of this diagram are described in section 5.2.1.

1.1 Climate of coastal northeast Tasmania

Northeast Tasmania is influenced by a broad zonal westerly flow, popularly known as the Roaring Forties, and the seasonal position of the anticyclonic belt. The zonal westerly flow occurs in all seasons of the year, varying in intensity. During winter the anticyclonic belt is located over mainland Australia and is associated with cyclonic depressions and frontal systems that generate strong westerly winds. During summer, the zonal westerlies move southward and the subtropical high-pressure belt is associated with lighter winds (MacKinnon, 1980). Summer is also associated with a higher proportion of northerly winds that vary in intensity between light to strong winds. Northerly winds are generally associated with warm to hot (25 to 33°C) air temperatures.

The western coastline of northeast Tasmania is exposed to a high-energy onshore wind regime (Bowden 1981) and an ocean swell that originates from storm activity in the Southern Ocean. King Island refracts the southwest swell around northern Tasmania onto the exposed shoreline (Bird, 1993). This swell typically consists of predominant 3 m high sea waves, which are widely spaced with periods of 10 – 16 seconds. Locally generated waves produced by onshore winds in coastal waters (Hamilton, 1997) have periods of less than 6 seconds.

1.2 Objectives

The study has two principal objectives. One is to determine the processes that drive the morphodynamic evolution of a long-walled, asymmetric, actively mobile, coastal parabolic dune. The second objective is to determine the nature and correlates of the aerodynamic envelope of the parabolic dune.

To accomplish these objectives it was necessary to determine a range of parameters:

- the composition of the sediment available for transport, particularly its size range, and the shear velocity ($u*$) of the wind flow close to the ground surface;
- the prevailing wind regime and seasonal wind flow; and
- other climatic parameters, such as the long-term and seasonal patterns of rainfall, air temperature, and the evapotranspiration rate.

1.3 Thesis outline

Chapter 2 provides a literature review relevant to coastal dunes, and of particular relevance to coastal parabolic dunes. The review summarises the principal methods of measuring and calculating surface wind flow and close to the ground wind flow. The equations available for calculating sediment transport by wind, the regulators of dune mobility, and indices for calculating dune mobility are reviewed and discussed in the context of coastal parabolic dunes.

Chapter 3 commences with a succinct review of the textural and compositional parameters of sediment that form coastal parabolic dunes. The chapter then presents the results from an analysis of sediment samples collected from the windward and lee slopes of a parabolic dune in the study area.

Chapter 4 describes the local wind regime, and analyses close to the ground wind flow and other atmospheric parameters that have affected the surface conditions of the Croppies Bay parabolic dune and its mobility over a period of fifty-five years, focusing in particular on the period 2000 to 2004, when extensive field surveys were conducted.

Chapter 5 presents quantitative data on the temporal and spatial influence of wind flow on the morphodynamics of the dune. This chapter incorporates a published paper, namely: (Mowling and Coleman 2003) *Temporal spatial analysis of dune morphology.* In Coastal GIS 2003: an integrated approach to Australian coastal issues, edited by C.D. Woodroffe and R.A. Furness. Wollongong Papers on Maritime Policy, 14.

The final chapter, Chapter 6, integrates the results from the previous chapters in light of the objectives of the present study.

CHAPTER 2

Theoretical context

2.0 Introduction

This chapter presents the literature review that informs the research framework for Chapters 4 and 5; the review on the textural and compositional parameters of sediment is presented contextually in Chapter 3. The review in this chapter works sequentially, commencing with a contextual appraisal of near-surface wind flow on coastal parabolic dunes, and an evaluation of the methods and the equations available for calculating shear velocity. This is followed by the rationale for the collection of wind data on-site. The methods of analysing wind data and an evaluation of equations for calculating the sand transport rate follow. This is followed by an evaluation of the methods available for calculating dune mobility and relevant atmospheric parameters.

2.1 Near-surface wind flow in blowouts and parabolic dunes

Simple parabolic dunes are U or V shaped in planform due to two trailing arms that point upwind. Most dunes have a steep terminal lee slipface located at the downwind end. The trailing arms may be partially mobile on the windward side, or partially or wholly fixed by vegetation. Continued movement of parabolic dunes is governed by the source and the amount of sand available, the strength and directional variability of the wind, and the terrain over which the dunes move (Pye, 1990). The long axes of coastal parabolic dunes lie almost parallel with the onshore wind (Jennings, 1957). However, wind conditions can be changed due to topographic steering within the dune system that may generate left or right-handed asymmetry in the arms (Hesp, 1996).

A number of coastal studies describe wind flow in blowouts. These blowouts have generally been located in foredunes. They range in size from several square metres in area (Olsen 1958; Jungerius et al 1981; Jungerius and van der Meulen 1988; Mikkelsen 1990; Pluis 1992; Gares and Nordstrom 1995), to a twenty hectare trough blowout (Hesp and Hyde, 1996), and a twenty five hectare elliptical blowout in a transverse dune (Fraser and Bennett et al., 1998). Anderson and Walker (2006:2) measured airflow, sand transport, vegetation density and surface elevation changes in an area measuring 325 x 30 m in a backshore foredune-parabolic dune plain complex. Consistent themes in these coastal studies have been the relevance of winds that flow up the dune axis and the erosion patterns that result within blowouts.

Pye and Tsoar (1990:204) report that airflow along U-shaped parabolic dunes "is especially enhanced because the flow is compressed both laterally and vertically towards

the crest". During this process of compression, flow accelerates and sediment is entrained. As airflow passes over the crest, air pressure is reduced and flow separates, depositing sand on lee slopes (Oke, 2000).

The work of Robertson-Rintoul (1990:58, 61, 70) remains the only detailed descriptive field study of near-surface wind flow over a three-dimensional parabolic dune using arrays of cup anemometers and flow visualisation. Her work was undertaken on a parabolic dune in Scotland with a form ratio[1] of 1.2, compared with the form ratio of 3.1 at Croppies Bay. Thus the form of her dune (width of 200 m, length of 215 m and crest height of 15 m, tapering to 8 m on the north trailing arm ridge), other than the crest elevation, was substantially smaller than the dune in this study, and thus her work may not be of direct relevance to the Croppies Bay site.

Robertson-Rintoul (1990:73) described four flow structures, shown in Figure 2.1, associated with near-surface airflow. These were, closed windward eddies on the stoss

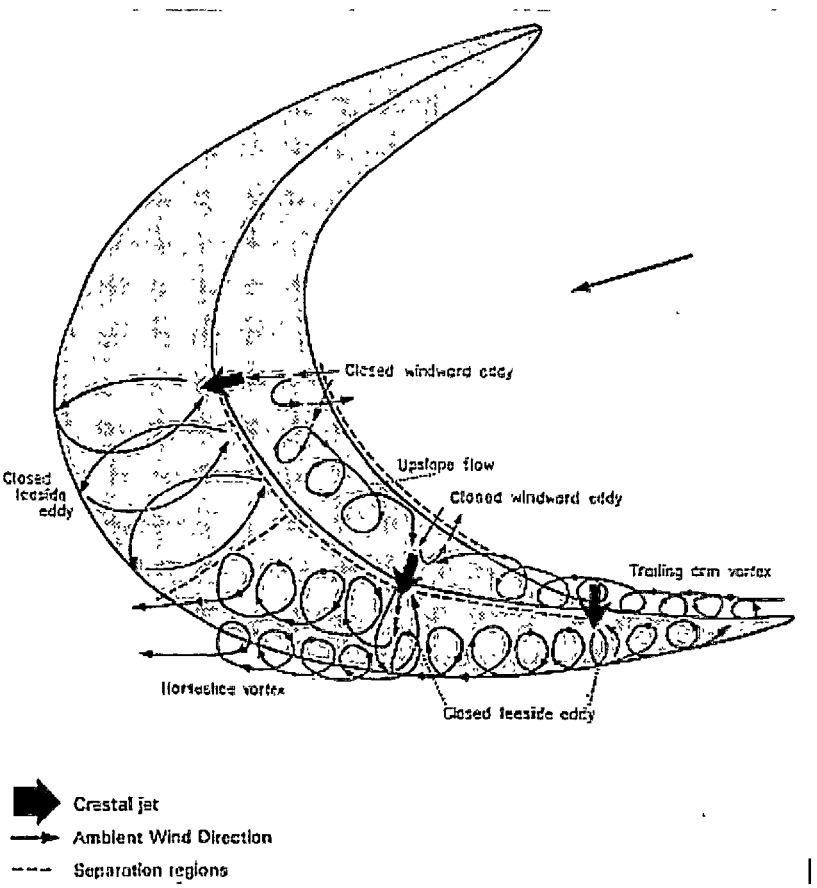

Figure 2.1. Robertson-Rintoul's (1990:73) interpretation of near-surface flow structures on a parabolic dune. Taken from Robertson-Rintoul (1990:73).

[1] The planform of parabolic dunes are frequently described using a ratio of length to width of the dune.

and north trailing arm, leeside eddies, spiral vortex flows along the windward north trailing arm and toe of lee north trailing arm, and jet flows associated with the crest of the stoss and north trailing arm. On windward slopes, flow was characterised by stalling and closed eddies at the toe resulting in reduced sediment transport. Wind flows at the dune crest had the characteristics of high turbulence and increased velocity.

Finigan and Neil et al. (1990:93) investigated the wind flow pattern around a 1000:1 scale model of a symmetrical parabolic dune in a wind tunnel. They found that it was the orientation and extent of the separation zones[2] that indicated the direction of the dune growth. For their dune form, winds flowing at horizontal angles of less than 15° off the axis (that is, winds flowing up the axis of the dune), the surface winds are topographically steered. A zone of separation formed a depositional lobe at the crest of the head of the dune, contributing to growth along the dune axis. As the wind vector approached 30° off axis, the dune was more aligned with the wind vector, not the dune axis, and the dune was no longer steering the wind. Their model indicated that the separation zone behind the crest on the north trailing arm, which was aligned east-west, became more complex, and, although of similar area to the up axis flow, was replaced by areas of high shear stress. The authors proposed that this probably resulted in vortex rolls forming in the lee, "a feature known to occur when the angle between a ridge and the approaching wind approaches 45° ".

Oke (2000:184) provided a succinct and fundamental explanation of typical patterns of airflow over steep topography (> 17° slope), including conditions that create lee eddies and vortex flows. To date, empirical field-based studies of flow on windward and lee slopes have been located largely in desert dunes. They include studies of: wind flow on the stoss slope of sand dunes (Lancaster and Nickling, et al., 1996; Frank and Kocurek, 1996); variation in wind velocity on windward flanks of dunes (Lancaster, 1985); velocity profiles on a windward slope of a transverse dune (Mulligan, 1988); flow in the lee of a transverse dune (Walker and Nickling, 2002); and airflow over sand dunes (Weng, et al., 1991). Non-logarithmic wind profiles result when sediment is being transported (Bagnold, 1941; Pye and Tsoar, 1990; Wang and Dong et al., 2002), when flow perturbations occur, or multidirectional or oscillating surface winds occur (Walker and Nickling, 2002:50), and when wind speed is recorded below a height of 1.6 m (Mulligan, 1988). Frank and Kocurek (1996) measured velocity profiles on the stoss of 13 desert dunes to determine the principal trends in these profiles. They determined that stoss wind profiles are not log-linear; that acceleration of flow occurs very close to the ground surface (generally in the order of ten centimetres to about one metre above the dune surface) in an internal boundary layer that increases in depth downwind. Their results indicate that it is difficult to determine which segment of the wind profile drives saltation, thus rendering an accurate calculation of sand transport from velocity profiles (derived from $u*$ which drives saltation) questionable.

The internal boundary layer, comprised of a compression of airflow in a thin layer over a dune, described by Frank and Kocurek (1996:51), corresponds with earlier work by

[2] Called separation regions by Robertson-Rintoul (1990:73). The author of the present study adopts the Finigan and Neil et al. (1990:93) descriptor of separation zones.

Jackson and Hunt (1975) who modelled boundary layer flow over gently sloping symmetrical hills. The Jackson and Hunt (1975) model divided boundary layer flow into inner and outer regions, shown in Figure 2.2, with the inner region comprised of two sub-layers: (1) a thin inner surface layer empirically measured (Burkinshaw, et al., 1993; Frank and Kocurek, 1996, 1994; McKenna Neuman and Lancaster et al., 1997) within a few centimetres above ground surface on small to moderate sized dunes, and (2) a shear stress layer "where shear effects decrease with height until considered negligible at the outer region" (Walker and Nickling, 2002:51). Jackson and Hunt (1975) proposed the following equation to approximate the thickness of the inner boundary layer:

$$\frac{l}{z_0} = \frac{1}{8}\left[\frac{L}{z_0}\right]^{0.9} \qquad \text{Equ 2.1}$$

where l = the thickness of the inner layer,

L = the half length of the hill at its half height, taken generally as the length of the stoss slope (Frank and Kocurek, 1996:51).

z_0 = the roughness length of the ground surface, found to be approximately d/30, where d is the diameter of the sand grains forming the surface and their ground area density (Pye and Tsoar, 1990:31).

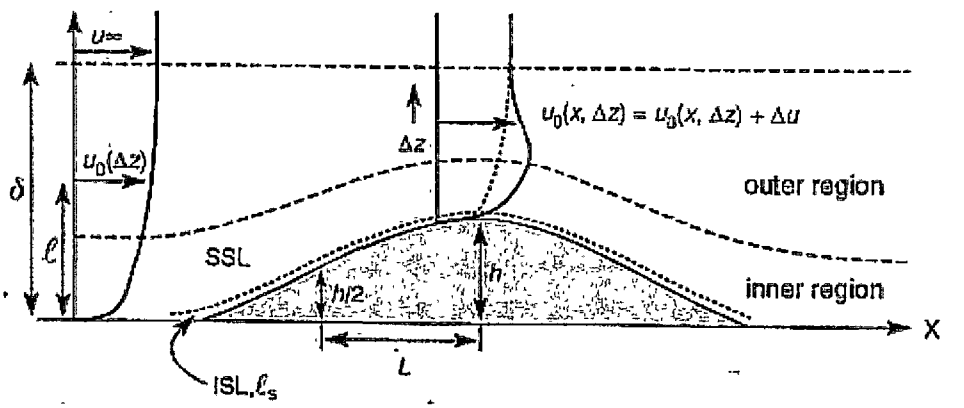

Figure 2.2. The Jackson and Hunt (1975) model of boundary flow over low hills. The Jackson and Hunt model divides flow into inner (ISL – inner surface layer) and outer regions. SSL – shear surface layer (taken from Walker and Nickling, 2002:50).

Walker and Nickling, (2002:51) reported that estimates of l using Equation 2.1 are slightly more sensitive to changes in z_0 than to values of L. This is due in part to measurements of L being more certain than measurements of z_0, which is dependent upon wind speed profile measurements. Consequently, an inaccurate estimation of z_0 would result in unreliable estimates of the depth of l (Walker and Nickling, 2002:51).

To date, there is empirical evidence that acceleration of flow up a windward slope on a moderate sized dune occurs between 0.1 to 1.0 m above the ground surface. However, the thickness derived from Equation 2.1 remains estimation, being only an indicative rather than a specific height at which something occurs. The results of Equation 2.1 are presented in Chapter 4, 4.7.3.

Several authors (Bagnold, 1941; Gerety, 1984; 1985 in Pye and Tsoar, 1990; Butterfield, 1993; Frank and Kocurek, 1996) report kinks (at heights of the deflection zones) in wind velocity profiles. Bagnold (1941:62) described wind velocity profiles during saltation that had distinct kinks up to a height of 3 cm above the ground surface, indicating a change in the velocity gradient and a deviation from the logarithmic profile law. Bagnold (1941:62) observed that the width and height of the kink (i.e. departure from the log profile) increased with friction velocity ($u*$) and that the height of the kink corresponded to the average trajectory path of uniform grains in saltation. Both Bagnold (1941) and Gerety (1984, in Pye and Tsoar, 1990) found that the kink in velocity curves may not be as clearly defined when sediment is comprised of mixed grain sizes and trajectory heights. Bagnold (1941:58, 62) observed negative and positive kinks in velocity profiles and proposed that the negative deviations correspond approximately to the saltation trajectory height, whereas the positive deviations reflect a speeding up of the wind due to grains accelerating just prior to hitting the ground surface. In effect, the saltation layer extracts momentum from the flow by imparting an aerodynamic roughness to the flow. Butterfield (1993:319), based on wind tunnel experiments, reported that with increasing velocity and transport rate, the height of the deflection zones, or kink, increased, and the slope above the kink decreased until the profile segments followed the logarithmic profile law.

2.1.1 Calculation of shear velocity

Surface shear stress cannot be measured directly, rather it is inferred from wind velocity profiles (Bagnold, 1941; Frank and Kocurek, 1994; 1996; Arya, 1988). The present study applied the method described by Frank and Kocurek (1994:737; 1996:49) and Arya (1988:148), which is regularly applied in the literature to derive $u*$ (Bagnold, 1941; Hsu, 1971a; Hsu, 1971b; Hsu, 1973; Frank and Kocurek, 1994; 1996; Arya, 1988). In the Frank and Kocurek (1994:737) method the value of shear velocity ($u*$) is substituted for shear stress to describe the transport capacity of a wind:

$$u_* = (\tau o / \rho)^{1/2} \qquad \text{Equ 2.2}$$

where τo = surface shear stress,
ρ = air density.

Shear velocity is calculated by applying time-averaged velocity profiles to the logarithmic velocity profile (the 'law-of-the-wall'):

$$u_* = \frac{k}{\ln z/z_0} u_z \qquad \text{Equ 2.3}$$

where k = von Karman's empirical constant with a value of approximately 0.40[3],
z = height above the ground surface,
z_0 = a dimensional constant of integration commonly referred to as the surface roughness parameter or roughness length,
u_z = wind speed at height z.

There are a number of constraints embedded in the above equation, namely that flow is measured over a flat surface and the roughness length is fixed. Hence, the equation is based on the assumptions that the flow field is steady and uniform, and the wind is carrying as much sediment as it can at all times (Bauer, et al., 1990). Previous empirical field studies (for example, Bauer, et al., 1990; Frank and Kocurek, 1994; 1996; Mikkelsen, 1990) have established that flow is unsteady and non-uniform close to the ground. Arya (1988:146) reports that the equation does acquire a logarithmic velocity profile, which describes a log-linear velocity profile for the boundary layer down to z_0, and that wind profiles have confirmed the validity of this equation up to heights of 20 – 200 m.

Thus u_* and z_0 can be determined graphically by plotting points from the wind velocity profile data on a semi-log scale and fitting a straight line through the data. The slope is inversely proportional to u_*, and z_0 is the y-intercept.

Frank and Kocurek (1994) rearranged the logarithmic velocity profile to give

$$\log z = \frac{1}{5.75u_*} u_z + \log z_0 \qquad \text{Equ 2.4}$$

This equation can be written in terms of a linear regression model, where (using the equation $y = mx + b$) we have $y = \log z$, $x = u_z$, $m = 1/(5.75u_*)$, and $\log z_0$ = b the y axis intercept. For flat, homogeneous surfaces, with no saltation, Bagnold (1941) found the roughness length approximated $d/30$ (d being the sand grain size); Zingg (1953, in Pye and Tsoar, 1990:32) found that d/z_0 decreases rapidly with increasing grain size above 2 ø, where ø is related to the grain size by $\text{ø} = -\log_2 d$ (Krumbein, 1936) such that $2^{-\text{ø}} = d$, where d is in mm. Since ø units are dimensionless, it is strictly more correct to state that $\text{ø} = -\log_2(d/d_0)$, where d_0 is the standard grain size of 1 mm (Pye and Tsoar, 1990:45).

Owen (1964, in Frank and Kocurek, 1996:49) found that during saltation, the saltation layer responds as an increased aerodynamic roughness to the flow outside it, and z_0 increases with u_*:

[3] Arya (1988:144) states that it has not been possible to determine von Karman's constant with an accuracy better than 5%.

$$z_0 = \alpha\left(u^{2}{}_{*} / 2g\right) \qquad \text{Equ 2.5}$$

where α = 0.02 for wind tunnel work, g is the gravitational constant .

The present study has adopted the more recent approaches of Frank and Kocurek (1996), Burkinshaw et al. (1993) and Burkinshaw and Rust (1993) who argue from empirically derived field data that "flow in the amplification layer does not drive saltation, but rather sediment flux is governed by an underlying surface shear stress layer, only a few centimetres thick and roughly equivalent to the inner surface layer in the model of Hunt et al. (1988)" (Frank and Kocurek, 1996:52). Thus, this diverges from Owen's (1964) hypotheses that the saltating cloud is self-regulating, and that the shear stress above the saltating cloud drives sediment transport.

To conclude, one of the intents of the Croppies Bay study is to describe general airflow and near surface patterns of flow that gives form to a parabolic dune. There is no intention to contribute to an analysis of wind shear velocity profiles per se, or towards calculation of an absolute shear stress.

2.2 Measurement of wind flow and wind velocity to derive sand transport rates

2.2.1 In-situ measurement of wind flow

The empirical field work of Hesp and Hyde (1996:522) established that wind speeds within blowouts may be significantly higher than remotely sensed wind speeds acquired from meteorological data collected on 10 m masts. This is due in part to topographic acceleration and topographic steering of wind flow within the dune. Hesp and Hyde (1996) argue that the use of remotely sensed wind speeds to derive potential sand transport is questionable due to the effect of topographic acceleration on wind flow. Pluis (1992:671) suggested that on-site wind data collected to derive regression equations to calculate surface level changes might not fully express the relationship between wind velocity at the blowout and at the remote meteorological station.

Similarly, Walker and Nickling (2002:51), in their review of wind flow over transverse dunes, found that topographically induced flow perturbations pose difficulties for modelling flow and sediment transport over dunes.

2.2.2 Fryberger wind resultant sand roses

The Fryberger (1980) method links the measuring of wind velocity with relative rates of sand transport over a fixed time period, with the results expressed visually as sand roses.

This method uses only effective wind velocities, and makes the assumption that stronger winds are more effective than lighter winds in transporting sediment.

Drift potentials (DP) measure the energy of surface winds and their effectiveness in transporting sand; the higher the DP value, the higher is the potential for sand transport. Resultant drift potential (RDP) expresses, in vector units, the net sand transport potential when winds from various directions interact, and the ratio of the resultant drift potential to the drift potential – the RDP/DP – is an index of the directional variability of the wind (Fryberger, 1980:148). Lower values in the RDP/DP ratio are indicative of a higher directional variability in effective winds. Fryberger (1980:149) arbitrarily grouped the RDP/DP values into 3 classes – 0.0 to less than 0.3 is equivalent to high directional variability in the wind, 0.3 to less than 0.8, intermediate variability, and 0.8 or greater is equivalent to low variability. The resultant drift direction (RDD) expresses the direction and magnitude of the vector resultants.

To generate the sand roses, wind velocities are treated as vectors by Fryberger (1980) and drift potentials are designated as vector units (VU[4]). Fryberger (1980:146) modified the sand transport equation (see section 2.3.4) by substituting values for wind velocity, and providing weighting factors for velocity classes where strong winds have higher weightings than lighter winds. Table 2.1 gives in tabular form the wind ranges of Fryberger. To simplify the plotting of sand roses, the value of $V^2(V - Vt)$ is divided by 100 to reduce the magnitude of the weighting factors so that the length of the vectors are comparable and can fit onto an A4 page.

Bullard (1997:500) converted Fryberger's (1980) classification of wind-energy environments, which were calculated in knots, to m/s, as follows in Table 2.1

Table 2.1. Comparison of weighting factors for wind speed measurements in m/s and knots. V, average wind velocity at 10 m height; Vt, impact threshold wind velocity at 10 m (minimum velocity at 10 m to keep sand in saltation (Fryberger 1980:146).

Velocity category nearest equivalent m/s	Mean velocity of winds in category V	V^2	$(V - V_t)$	Weighting factor $V^2 (V - V_t)/100$ for measurements in m/s	Equivalent weighting factor for wind speeds in knots
6.5–7	6.75	45.56	0.775	0.353	2.7
9–10	9.5	90.25	3.525	3.182	25.3
12–13	12.5	156.25	6.525	10.196	75
15–16	15.5	240.25	9.525	22.885	172.1
18–19	18.5	342.25[5]	12.5	42.781	342.3

[4] The 'units' that Fryberger uses in vector units (VU) are dimensionless.
[5] Bullard (1997:500) had a conversion error which has been corrected in this text.

2.2.3 Measuring close to the ground wind flow

Thermo anemometers (TAs) have been used effectively by many researchers undertaking aeolian transport studies in the field, for example Jensen and Rasmussen et al. (1984), Rasmussen et al. (1985), Lee (1987), Kocurek et al. (1994), Wiggs and Livingstone et al. (1996), and Rasmussen and Sørensen (1999). Butterfield (1999:33), in his review of TAs and high-frequency measurement of mass flux to aeolian sediment transport, stated that their primary advantages over cup-anemometers are: the small dimensions, the robustness of the sensors and their fast response, and not stalling during sediment saltation, but continuing to record in grain saturated air flows.

2.2.4 Calculation of the sand transport rate

There have been a number of equations proposed for calculating sediment transport by wind, for example von Karman (1934), Bagnold (1941), Kawamura (1951), Skidmore (1965), Hsu (1973). Mostly these equations apply over ideal surfaces within a narrow range of sediment sizes, or without reliable variables that are predictive of the influence of moisture content on aeolian transport (Namikas and Sherman, 1995). Hence results have met with mixed success when used in field conditions (Sherman and Hotta, 1990). Pye and Tsoar (1990:119), in summarising their review of equations developed to predict the mass transport of wind blown sand, stated that 'In most cases the sand transport equations provide estimates of the maximum rate of sand movement which is likely under specific meteorological and topographical conditions'. A number of field-based studies reported that equations either underestimated or overestimated the actual transport rate (Inman and Ewing et al. 1966; Watson, 1987; Sarre, 1989; Sherman et al., 1998).

Bagnold (1941, in Pye and Tsoar, 1990:113) derived a method of determining a sand transport rate (q) in g cm^{-1} s^{-1}. His equation is based on the relationship between the wind velocity and the rate of sand movement such that

$$q = C_1 (d/D)^{1/2} (\rho/g) u_*^3 \qquad \text{Equ. 2.6}$$

where C_1 is an empirical coefficient based on grain size, D is the diameter of a standard grain of sand (taken as 0.025 cm), d is the mean grain diameter of sand from the windward slopes, cm, g is the gravitational constant, ρ is the density of air, $u*$ is the shear velocity at designated height above ground surface, cm s^{-1}. C_1 has the values of 1.5 for a nearly uniform sand, 1.8 for naturally graded sand, and 2.8 for a wide range in grain sizes (Bagnold, 1941:67). Pye and Tsoar (1990:113) reported that Equation 2.6 has its limitations, in that it predicts unrealistic transport rates when $u*$ is below threshold.

Kawamura (1964, in Pye and Tsoar, 1990:113) formulated a transport equation, which includes a threshold velocity term:

$$q = K(\rho / g)(u_* - u_{*_t})(u_* + u_{*_t})^2 \qquad \text{Equ 2.7}$$

where K = a constant; u_{*t} = the minimum shear velocity (in cms^{-1}) required to keep sand in saltation. In field measurements K ranges from 2.3 to 3.1 for beach sand with a size range of 0.1 to 0.8 mm and a median diameter of 0.3 mm (Pye and Tsoar, 1990:114).

In turn, Lettau and Lettau (1978) refined Kawamura's (1964) equation by incorporating a different threshold term:

$$q = C_2(d / D)^{1/2}(\rho / g)u_*^2(u_* - u_{*_t}) \qquad \text{Eqn 2.8}$$

where the constant $C_2 = 4.2$ (Pye and Tsoar, 1990:114).

The sand transport rate (q) has units of mass per unit width per unit time measured in c.g.s units.

2.3 Regulators of dune mobility - wind speed, rainfall and air temperature

One of the primary goals of the present research is to identify the influence of specific atmospheric parameters on aeolian processes. Namely, under what circumstances does dune mobility increase, remain stable or decrease? To evaluate this, an analysis of the relationship between wind speed, air temperature and rainfall has been undertaken over a sixty-three year interval using Bureau of Meteorology (BoM)[6] data collected at Low Head (wind speed, air temperature), Waterhouse Station (rainfall 1960 – 2003) and Bridport[7] (rainfall 1940 – 1959). Analysis of these data is given in Chapter 4.

Sherman and Hotta (1990) and Namikas and Sherman (1995) reported that rainfall increases the threshold shear velocity by increasing the moisture content in sand and promoting the growth of plants. Gaylord and Stetler (1994:113), following an evaluation of climatic conditions that promote or diminish aeolian activity in inland dune fields, reported that prolonged phases of a decline in rainfall associated with values above the average wind speed and air temperature directly influenced the volume of unvegetated dune sand. Hesp and Hyde (1996) and Wolfe and David (1997) established that prolonged drought accompanied, or followed by, strong winds, can lead to a reduction in vegetation cover, the remobilisation of fixed or partially fixed dunes,

[6] http://www.bom.gov.au/weather/tas/

[7] Bridport receives slightly higher rainfall in specific months than Waterhouse Station, the mean difference was calculated over a common time period and subtracted from the relevant rainfall records to form a combined record.

accompanied by an increase in the number of blowouts, leading to the merging of parabolic dunes into an actively mobile sand sheet or transgressive dunefield.

Several indices have been developed to calculate sand dune mobility (Chepil et al., 1962; Ash and Wasson, 1983; Lancaster, 1997; Tsoar and Illenberger, 1998; Tsoar and Blumberg, 2002; Tsoar and Arens, 2003). These indices share two common components:

- the combining of the influence of wind speed, expressed as the percentage of days the wind is above the threshold velocity to transport sand (Chepil et al., 1962); and
- a modification of Thornthwaite's (1957) 'precipitation – effectiveness index' which links vegetation cover and soil moisture content, and is taken as a function of the ratio between average annual rainfall (P) and evaporation (E). The original component of Thornthwaite's climate classification is his moisture index which describes whether a region has a positive or negative water balance, expressed as,

$$MI = \frac{100(P - PE)}{PE} \qquad \text{Equ. 2.9}$$

Where MI = moisture index,
P = precipitation,
PE = potential evapotranspiration.

UNESCO (1979) used the P/PE ratio as a means to classify the degree of aridity of lands:

P/PE ≥ 0.75	Humid
0.50 ≤ P/PE < 0.75	Sub–humid
0.20 ≤ P/PE < 0.50	Semi–arid
0.03 ≤ P/PE < 0.20	Arid
P/PE < 0.75	Hyper–arid

Lancaster (1997:336) reviewed the common components of the P/PE index and proposed the following mobility index for inland dunes[8] based upon the assumption that there is a relationship between plant cover and soil moisture content and sand dune activity, where

$$M = \frac{W}{P/PE} \qquad \text{Equ 2.10}$$

with M = dune migration,

[8] The P/PE dune mobility index has also been applied to describe dune activity in sub-humid to semi-arid environments (Ash and Wasson, 1983; Wolfe, 1997; Jorgensen, 1992; Muhs and Maat, 1993; Muhs and Holliday, 1995).

W = the percentage of days during a year when the sand moving capacity of the wind is > 5 m/s;
P/PE = the ratio of the mean annual precipitation to mean annual potential evaporation (Lancaster, 1997; Tsoar and Blumberg, 2002).

Potential evaporation, for the purposes of this study, is calculated as mean pan evaporation (Bowden, 1981; MacKinnon, 1980).

Lancaster (1997:336) developed a mobility index (M), which he calculated using 5 m/s as the wind threshold velocity. Using this index, dunes are:

fully active when *M* exceeds 200;
partially fixed by vegetation on slopes and interdune corridors when *M* is between 100 and 200.
Only the crests are active when *M* is between 50 and 100, and when *M* is less than 50, dunes are fixed.

The dominant component of this mobility index is the average rainfall and average potential evaporation, which are constrained only by the percent duration of effective wind speeds. What is lacking are components expressing wind direction (for example, narrow unimodal compared with a bimodal) and the magnitude of single or clustered wind events when wind speeds are in excess of 12 m/s (strong wind events), and the proportion on a yearly basis of these events. Bagnold (1941:70) found that the rate of sediment transport is related to the cube of the wind velocity:

$$q = 5.2 \times 10^{-4} \ (u - u_t)^3 \qquad \text{Equ 2.11}$$

where u = wind velocity measured at 1 m height above dune surface,
u_t = threshold wind velocity.

Based on Equation 2.11, Bagnold (1941:70) gives the example of a strong wind blowing at 16 m/s, which moves the same volume of sand in 24 hours, as a wind blowing steadily at 8 m/s moves in 3 weeks.

Tsoar and Blumberg (2002:1151; Tsoar and Illenberger, 1998; Tsoar and Arens, 2004) argue that rainfall is neither a decisive factor nor a limiting factor for plant growth in coastal dunes. These authors propose that dune sand has large pore spaces and high infiltration rates resulting in deep percolation of frequent inputs of rainfall. Moisture is retained within the dune and evaporation is reduced in dry periods by a layer of dry sand to a depth of 30 cm. They argue that wind erosion is the main limiting factor for vegetation growth on dunes due to the following:

1. *wind magnitude above the threshold speed: the rate of sand erosion is in proportion to the cube of the wind velocity.*
2. *wind direction variability: winds above the threshold, with a low rate of directional variability, will form dunes whose windward surfaces are undergoing constant erosion. However, the intensity of wind erosion from a multidirectional*

wind regime is distributed over more than one slope of the dune, and the total erosion of each slope is lower (Tsoar and Blumberg, 2002:1152).

Tsoar and Arens (2003:9) propose that the drift potential (DP) values developed by Fryberger (1980) are a better predictor of dune mobility than indices based on P/PE ratios. They offer a modification of the Fryberger (1980) equation, adapting it into an index:

$$DP = \sum q = \sum_{t'} \frac{u^2(u - u_t)}{100} t \qquad \text{Equ 2.12}$$

where q = the rate of dune migration,
u = wind velocity in m/s, at a height of 10 m above ground surface,
u_t = the threshold wind velocity,
t' = time over which the transport occurs,
t = is equal to W in Equation 2.10, i.e. the percent time the wind blows above the threshold velocity.

The DP value is a measure of the potential wind energy – it is an indicator of the rate of sand transport and the time over which the transport occurs; it is also an expression of the maximum quantity of sand that could be transported downwind (Tsoar and Arens, 2004). The issue of variability in wind direction is resolved with Fryberger's (1980:149) index of directional variability – the resultant drift potential (RDP), and the ratio of the RDP to the drift potential – the RDP/DP.

Following an analysis of 40 wind stations distributed globally, Tsoar and Arens (2003:9) established that the two parameters of DP and W are related, with W increasing in most instances with DP. The strongest correlation occurred in the low range of vector units, W<25; DP<400. They also established that when the RDP/DP ratio is low (indicating an increase in the directional variability of effective winds), wind energy is distributed on more than one slope of the dune and the energy exerted on each slope is lower than the same DP with high RDP/DP (Tsoar and Arens, 2004:9).

Tsoar and Arens (2003) identified a relationship between wind energy and vegetation cover on dunes, observing that a decrease in wind energy is associated with an increase in vegetation cover. Conversely, they found that an increase in wind energy over vegetated dunes did not cause the loss of vegetation cover. In both instances, the authors cite a decrease or increase below or above DP 500 (measured in m/s), which in Fryberger's (1980) classification of wind-energy environments is high-energy.

Within the context of the present study site, which is located in a humid temperate climate, an objective is to determine whether Lancaster's (1988) mobility index adequately explains vegetation cover, or whether wind erosion is the main limiting factor for vegetation growth on dunes as proposed by Tsoar et al. (1998; 2002; 2004). Another question to consider is, 'is there merit in the Tsoar and Arens (2003) proposal that Fryberger's (1980) DP values are a better predictor of dune mobility?'

2.4 Conclusion

This chapter has presented a brief literature review of topics relevant to this study. It commenced by reporting the findings of previous studies on near-surface wind flow in dune blowouts, and the empirical measurement of wind flow over desert linear dunes, in particular on the compression of airflow close to the ground and the resultant acceleration of flow. The salient methods and findings were evaluated.

Practical methods of measuring wind flow and wind velocity, with the intention of deriving a sand transport rate, were presented and their respective limitations in the field reviewed, resulting in the decision to install an on-site meteorology station, and construct a number of thermo anemometers with which to sample close to the ground wind flow. Methods of analysing wind data were presented, in particular the Fryberger (1980) method, which links the measuring of wind velocity with relative rates of sand transport over a fixed time period.

A series of indices that have been developed to calculate sand dune mobility were reviewed to assess the feasibility of determining the influence of specific atmospheric parameters on aeolian processes at Croppies Bay.

Based on a wide-ranging literature search it is evident that the observation by Fraser and Bennett et al. (1998:451) remains current: "studies that integrate data on wind flow patterns with geomorphic mapping and sedimentological characteristics of blowout dunes are scarce ... especially the feedback between wind flow and shape, as well as the role of wind erosion in subsequent deposition." In addition to these general observations by Fraser and Bennett et al. (1998:451), there are a number of gaps in our understanding of the downwind evolution of coastal parabolic dunes in temperate sub-humid climates, in particular:

- data on the textural and compositional parameters of sediment;
- the sediment composition of actively mobile long-walled parabolic dunes,
- the influence that reworking of earlier phases of late Quaternary deposits, remote from beach, has on the textural parameters of the morphological units forming the dune;
- how dune morphology is controlled by an effective wind regime,
- the measurement of acceleration of wind on the windward slopes,
- the influence of atmospheric parameters on coastal dune mobility.

CHAPTER 3

Grain-size analysis and composition of parabolic dune sediments

3.0 Introduction

Landward transport of aeolian sediment is a significant geomorphic process in coastal zones, and during the present still stand in sea-level, large volumes of aeolian sediment have accumulated. Within the context of the present study of bedform evolution and migration rate of a long-walled parabolic dune, an understanding of the sediment available for entrainment by effective winds is necessary. Entrainment of sand grains is influenced by the characteristics of individual grains-size, shape and density, and bulk sediment properties grain size distribution (sorting), porosity, moisture content, packing and cohesion (Pye and Tsoar, 1990; Allen, 1970).

There is a limited amount of data on the textural and compositional parameters of sediment that forms long walled, actively mobile, coastal parabolic dunes (Pye, 1982; Anthonsen and Clemmensen 1996; Arens, 2004; Stapor, 1983). Several authors have undertaken research on temperate climate coastal parabolic dunes that have been partially (Anthonsen and Clemmensen, 1996) or fully remobilised by removing vegetation (Arens and Slings, 2004). Pye (1982) described variations in textural parameters in a humid tropical transgressive dunefield that contains parabolic and elongated parabolic dunes that are fixed by heath or forest vegetation, except for occasional slipfaces. Stapor and May (1983) investigated aeolian shape sorting and aerodynamic traction equivalence by sampling only stoss surfaces in an actively mobile parabolic dune system. Anton and Vincent (1986) reported the reworking of a poorly sorted sand sheet in a desert environment, which resulted in dune sands being poorly sorted, and coarse grained.

To date, research on coastal dune grain size analysis (Ahlbrandt, 1980; Mason and Folk, 1958; Mattox, 1954; Visher, 1969; Inman, 1952; Stapor and May, 1983; Pye and Tsoar, 1990; Abuodha, 2003) has focused on winnowing processes from beach to frontal dune to dune. Mason and Folk (1958:216) reported progressive sorting from beach (0.309 ø) to dune (0.273 ø) to aeolian flat (0.286 ø), with dune sands exhibiting a bimodal distribution of mean grain size (M_z), with most grains about 2.80 ø and a smaller cluster at about 2.96 ø, and mesokurtic distribution of grain size. Ahlbrandt (1980:25) analysed 291 predominantly Brazilian coastal dune samples that were comprised almost entirely of very well sorted (0.15 to 0.24 ø) fine to very fine grained sand (2 to 3 ø) that were platykurtic to mesokurtic in grain size distribution. Abuodha (2003) reported winnowing of fine mean grain sand from beach (2.06 ø) to berm zone (2.17 ø) to foredune (2.23 ø) to dunefield (2.05 ø), and associated slight increase in sorting from beach (0.39 ø) to berm zone (0.39 ø) to foredune (0.37 ø) to dunefield (0.41 ø). Predominantly, his samples were leptokurtic in distribution from beach, foredune and dune areas, and mesokurtic in distribution in the berm zone.

In the Anthonsen and Clemmensen (1996) description of an asymmetric, mobile parabolic dune, standing 20 m high, and located at Rabjerg Mile, Denmark, the authors reported well-sorted sand with a mean grain size of 0.2 – 0.85 ø. Pye (1982:255) in his study of partially mobile parabolic and elongate parabolic dunes in North East Queensland established that crest dune sands are comprised of fine (0.5 – 4.0 ø), well sorted predominantly negatively skewed distributions of grain sizes. He also reported considerable variability between samples in their grain size distributions, with some unimodal and mesokurtic ranging to bimodal. Stapor and May (1983) sampled the stoss surfaces of 28 active parabolic and barchan dunes in Hout Bay, South Africa. Stapor and May (1983) differentiated their samples by density, distinguishing the quartz fraction from calcite fraction. Consistently, the calcite fraction was larger than quartz by 0.2 ø. Sediment was comprised of coarse to fine grains (1.63 to 2.42 ø), very well sorted (0 to 0.34 ø) with 28% fine skewed quartz fraction and 62 % fine skewed calcite fraction. The Stapor and May (1983:163) study indicated that wind "preferentially selects grains of lower sphericity" and that both creep and saltation modes of transport occur in the stoss surface deposits.

Thus, Mason and Folk (1958), Ahlbrandt (1980), Allen (1970), Abuodha (2003), Inman (1952) and Stapor and May (1983) determined that coastal dune sands contain finer size grains which are fine skewed, indicative of better sorting. These characteristics can be attributed, generally, to maintenance of the link between compositionally similar sediment source (beach) and dunes. Bigarella and Alessi (1969) noted that coarse and poorly sorted beach sands usually translate into finer and better-sorted sand in adjacent dunes, which is congruent with the findings of other research cited above. However, Pye (1982) and Stapor and May (1983) confined their samples and textural parameter analysis to a narrow range of morphological units on parabolic dunes, but their studies are still considered representative for Croppies Bay.

There are a number of gaps in our understanding of the downwind evolution of coastal parabolic dunes in temperate sub-humid climates, in particular, of the sediment composition of actively mobile long-walled parabolic dunes, and of the influence that reworking of earlier Quaternary deposits, remote from beach, has on the textural parameters of the morphological units forming the dune.

3.1 Aims

The present study contributes towards an understanding of an actively mobile, long walled, coastal parabolic dune as it migrates downwind displacing and re-accumulating an earlier phase of aeolian Quaternary deposition. Specifically the study

- determines the variation in grain size and textural parameters by morphological units;
- identifies the sources of sediment that are available for reworking;
- determines the grain size and textural parameters of the sediment sources;
- determines the contribution of the various sources to each morphological unit.

Previous studies have been undertaken within the vicinity of the present study site, which are relevant to this sediment analysis. The Royal Australian Navy (1989) undertook a bathymetric survey of Bass Strait, and Geoscience Australia surveyed the sediments on the floor of Bass Strait (Butler and Althaus et al, 2002). Davies (1978) surveyed the sediments on beaches in Tasmania, including an area near Croppies Bay. Hubble (1946) surveyed and mapped the distribution of soils of part of the Waterhouse estate in the mid 1940s and analysed a number of soil profiles. Of relevance to the present study are his descriptions, analysis and mapped distribution of aeolian Quaternary sand, subsequently described by Bowden (1981, 1983) as part of the 'Ainslie Sand' formation. The findings of these regional studies contribute cumulatively to the analysis of the source of sediments available for reworking by a parabolic dune at Croppies Bay.

3.2 Methods

3.2.1 Collection and analysis of sediment samples

Twelve sand samples, comprised of three transects (Figures 3.1, 3.2, 3.3), were collected from deflation and deposition sites located on the north trailing arm, stoss and lee slipface to determine bulk density, and differences in grain size and porosity within and between these morphological units. The status of deflation and deposition was determined through comparison and analysis of contour maps and dune profiles generated from the series of six kinematic GPS surveys (Chapter 5, Section 5.2.5) that distinguished relevant deflation and deposition areas on the parabolic dune over a period of three years. Data derived from erosion pins located at the majority of sample sites (Chapter 5, Figure 5.1) corroborated analysis of the six GPS derived maps.

To derive samples, which characterised the sediment of each morphological unit, the top 2 cm layer of sand was removed prior to collection to eliminate recently transported lag and / or fine sediments. Each sample was collected by inserting by hand individual 72 mm diameter x 50 mm high PVC tube into the sediment. Both ends of each sampler were sealed with lids, labelled by transect and morphological unit, then wrapped with airtight plastic film and placed in an airtight clipseal plastic bag, then located in an Esky portable fridge. Airtight sealing of each sample was undertaken to maintain moisture content and the profile of grain size distribution within each sample. The horizontal position of each site was determined using a Garmin GPS, accurate to about 5 m – 20 m.

3.2.2 Loss on ignition

The calcium carbonate ($CaC0_3$) carbon content was determined through the loss on ignition procedure (Dean, 1974). Crucibles were weighed prior to sub-samples of the initial 12 field samples being placed in these crucibles, and reweighed. These samples were then oven dried for 18 hours at 104° C to remove moisture, reweighed, then placed in a SEM Laboratory Muffle Furnace and heated to 1,000° C for one hour. The weight loss between the second and last weighing is the total amount of $C0_2$ evolved from carbonate minerals (Dean, 1974:242). Weight loss was converted to weight of $CaCO_3$ by multiplying by a factor of 2.273 (Molecular wt. $CaCO_3$/M.wt CO_2).

3.2.3 Moisture content

Moisture content was calculated as:

$$M = \frac{wf - wd}{wd} x100 \qquad \text{Equ. 3.1}$$

where M is moisture content (%), wf is the weight of the field sample, and wd is the weight of the dried sample (Davidson-Arnott, et al., 2005:119).

3.2.4 Shape, texture and mineral characteristics of grains

Twelve sub-samples were mounted on slides in resin and ground to thin section for analysis by a petrographic microscope. With the aid of a polaroid filter mounted on the petrographic microscope, texture and origin of the grains were determined. A series of photographs, taken by a camera mounted on the microscope, enabled a visual analysis of grain shape and an assessment of the proportion of different origin grains.

3.2.5 Wet bulk density measurements

Sediment bulk density and porosity were analysed by A. Heap of Geoscience Australia as follows.

After equilibration with ambient laboratory conditions (between 18° and 20°C), wet bulk density (WBD), P-wave Velocity (Vp), and Fractional Porosity (FP) were determined at 1 cm intervals down each core using a GEOTEK™ MS2 multi-sensor core logger (Heap et al., 2001).

Wet bulk density was determined by measuring the gamma attenuation of the sediment from a Cs-137 source. WBD of the sediment is positively correlated with gamma attenuation. The relationship between density and gamma attenuation was initially calibrated using a graduated density standard consisting of water and aluminium density components (Best and Gunn, 1999). The calibration was undertaken using a water density of 1.001 g cm^{-3}, and an aluminium density of 2.71 g cm^{-3}, which is approximately equal to the mineral densities of siliciclastic (2.65 g cm^{-3}) and carbonate (2.67 g cm^{-3}) grains. Using this calibration, repeat density measurements were within 0.05 gm cm^{-3}.

3.2.6 Sediment grain size distributions

Sediment grain size distributions were analysed using a MacArthur Rapid Sediment Analyser, comprised of PVC inner (240 mm) and outer (290 mm) water-filled tubes. Sediment falls through the inner 2 m tube onto a Mettler electronic balance, accurate to 0.01 gm, and is computer read at time intervals of at least 1 second. Settling speeds were corrected for air temperature variation by regularly measuring the temperature of the column of water by immersion of the thermometer, and recalibrating the temperature-corrected settling speed within the computer program. Graphical statistical parameters were used to obtain measures of mean grain size, sorting, skewness and kurtosis (Folk and Ward, 1957; Mason and Folk, 1958) to describe the grain size spectrum in log–normal space and to distinguish different grain-size populations. The selected grain-size parameter is phi ϕ, which is a logarithmic measurement of the statistical relations of the diameter of sediments, where $\phi = -\log_2 (d/d_o)$ of the diameter in millimetres, where d_o is the standard grain size of 1 mm, and d is the specimen grain size (Inman, 1952:126; Pye and Tsoar, 1990:45).

Throughout the present study Wentworth's (1922) terminology for sediment size classes are used (McDonald and Isbell, 1984).

3.3 Results and discussion

Existing knowledge of sediment source parameters

3.3.1 Sea floor and beach

Sediment overlaying the floor of Croppies embayment has a mean grain size of 0 ø (coarse sand) that is poorly to very poorly sorted ($1 - 3\phi$) and comprised inshore of 30% carbonate, grading to 50% carbonate at distances greater than1 km offshore. This sediment is not fixed by sea grass and extends offshore ~ 2.5 km in shallow water with a gradual incline to the 20 m bathymetry contour (Butler and Altheus et al, 2002; Royal Australian Navy, 1989). Cyclic inundation and denudation of dolerite bedrock by sediment, accompanied by formation and subsequent incision of foredunes, indicates active seasonal sediment replenishment and erosion of beach and foredunes. Davies (1978:160) collected beach sediment in the vicinity of Croppies Bay and indicated that the mean grain size is about 1.83 ø (coarse sand) and poorly sorted (2.0 ø), comprised of 20% carbonate and 26% coarse angular quartz due to sand being derived from granite catchments. Relatively high wave energy, derived from refracted swell from the west and northwesterly gales, weather the beach and inshore sediments.

Sediment from the embayment and beach continues to be transported into frontal dunes that are fixed (~ 65% ground cover) by natural vegetation, and subsequent downwind sediment transport is an on-going process. Sediment accumulates on the abutting deflation basin (Figure 5.4b, Chapter 5), which extends 585 m to the neck, as knolls, sand sheet and shadow dunes.

3.3.2 Reworked sediment

As parabolic dunes migrate downwind, they incorporate, or rework, sediment from underlying sources. They are constrained from increasing their width by coastal vegetation surrounding the mobile dune and on the outer flanks of the trailing arms (Pye and Tsoar, 1990). The following section outlines the sand formations predating Holocene parabolic dune emplacement at Croppies Bay.

The low relief coastal plain that the Holocene dunes inundated in the area of the present study is a continuation of the inundated Bassian Plain with dolerite bedrock overlain by an aeolian Quaternary mantle of quartz sediment ('Ainslie Sand' formation) that reworked an earlier phase of late Quaternary marine sediment ('Stumpys Bay Sand' formation) (Bowden, 1981, 1983). Hubble (1946) surveyed and mapped the distribution of soils of part of the Waterhouse estate in the mid 1940s and analysed a number of soil profiles. Of relevance to the present study are his descriptions, analysis and mapped distribution of 'Tomahawk sand' and 'Tomahawk sand, deep phase'. The map accompanying his report also locates the 'Unstable coastal drifts of calcareous sand' that occurred within the boundaries of the present study site. Table 3.1 indicates the range of grain sizes associated with the Hubble soil types. Hubble (1946) did not undertake quantitative comparisons

between grain size distributions to distinguish statistical parameters of phi sorting, phi skewness or kurtosis.

Table 3.1 Sediment texture of three soil types within study area after Hubble (1946:58, 60).

Sediment Texture	Tomahawk sand (depth 1.5 m)		Tomahawk sand, deep Phase (depth 2.1. m)	
	%[1]	phi (ø)	%	phi (ø)
Coarse to very coarse	67	-1 to 0	86	-1 to 0
Fine	26.5	3.8	10.3	3.8
Silt	2.4	6	1.0	6
Clay	2.16	8	1.6	8

[1]averaged particle sizes derived from Hubble's (1946) soil profile horizons.

The following components of Hubble's (1946) survey are of relevance to the present study.

Firstly, Hubble (1946) located hard pans (B_2 horizon of indurated coffee rock that impedes drainage) in both phases of 'Tomahawk sands'. Both phases have a mantle of sand overlying the hard pan. The 1.5 m soil profile of 'Tomahawk sand' typically has a hard pan located 53 cm from ground surface, with a thickness of 25 cm. The 2.1 m soil profile of 'Tomahawk sand, deep phase' has a hard pan typically located 75 cm from ground surface, with a thickness of 26 cm Hubble (1946:31). An indurated B_2 horizon (coffee rock) extends west to within 150 m of present day high water mark, indicative of the extent of the 'Tomahawk sand' phases prior to inundation by Holocene dunes. The present study area has a large deflation plain comprised of a B_2 horizon of indurated coffee rock 26 cm thick. The parabolic dune has migrated downwind displacing and reforming 'Tomahawk sand' phases occupied previously by low (~ 1.2 m) heath communities (Thomas, 1991; Hubble, 1946; Kirkpatrick and Harris, 1999). Remnant root bowls of *Banksia* are embedded in the coffee rock.

Secondly, both 'Tomahawk sands' are predominantly coarse textured quartz sands, 67% and 86 % respectively, of -1 – 0 ø. Fine sand grains are present; higher (26%) in the Tomahawk sand and lower (10%) in the deep phase. Silt and clay particles are present in very low proportions in both. The silt and clay fractions are higher below the hard pan, (9.5 % and 6% respectively) (Hubble, 1946:60). Bioturbation by rabbits and wombats has broken <20% of the surface of the hard pan up-wind, resulting in wind erosion of the sub-surface, liberating the silt and clay fractions.

Hubble's (1946) description of 'unstable coastal drifts of calcareous sand' was management rather than analysis based. The boundary indicated on his map confirms that the parabolic dune of the present study site was mobile in the early 1940s.

Bowden's sediment analysis (1981) of the aeolian 'Ainslie Sand' formation was designed to characterise the longitudinal dunes. It was derived from samples collected over an extensive area and may be indicative rather than actual for the

present study site. In this portion of North East Tasmania, Bowden's 'Ainslie Sand' formation occurs as sand sheet and undulating dunes and has almost identical boundaries to Hubble's (1946) 'Tomahawk sand' phases. The 'Ainslie Sand' longitudinal dunes are comprised of unconsolidated quartz sands that are moderately well sorted (0.68 ± 0.38 ϕ) and fine-grained (mean grain size 2.08 ± 0.38 ϕ) (Bowden, 1983:160).

In summary, source sediment that forms the dune at Croppies Bay is derived from:

- coarse (0 ø) and poorly to very poorly sorted (1 – 3 ø) sediment that continues to be available from the floor of the embayment, comprised inshore of 30 % carbonate, grading to 50% carbonate >1 km offshore (Butler and Althaus et al, 2002);
- indicative beach sand which is coarse grained (1.83 ø) and poorly sorted (2.0 ø), comprised of 20% carbonate and 26% coarse angular quartz, due to the sand being derived from granite catchments (Davies,1978:160);
- a 53 - 75 cm deep mantle of late quaternary aeolian quartz sand ('Ainslie Sand' formation) overlaying an indurated B_2 horizon prior to inundation by Holocene sand, is comprised predominantly of coarse to very coarse sediment (67 – 86 %), some fine (26 – 10 %) and a low proportion of silt and clay (4.5 – 1.7 %) (Hubble, 1946) and moderately well sorted (0.68 ± 0.38 ϕ) (Bowden, 1983).

3.4 Sediment analysis

Given the research findings discussed above, which indicate a tendency towards an increase in sorting and a decrease in grain size as the distance from the beach to dunes increases, the following questions are posed: what do the sediment analysis results at Croppies Bay reflect, and are there variations between morphological units? The source sediment available for replenishment from the embayment is poorly to very poorly sorted (1 – 3 ø) coarse carbonate grains (0 ø), and beach sediment is poorly sorted (2.0 ø) coarse grain (1.83 ø), 20% carbonate and 26% coarse angular quartz grains. This is congruent with Bigarella's (1969) observation. However, sediment available for reworking is derived from a 53 – 75 cm deep mantle of late Quaternary aeolian quartz sand ('Ainslie Sand' formation) overlaying an indurated B_2 horizon, and comprised predominantly of coarse to very coarse sediment (67 – 86 %), some fine (26 – 10 %) and a low proportion of silt and clay (4.5 – 1.7 %) (Hubble, 1946), that may be moderately well sorted (0.68 ± 0.38 ϕ) (Bowden, 1983).

Within the context of temporal / spatial reworking of sediment downwind, the trailing arms and present lee slipface extend 1.9 km from the rear of the frontal dune. The sampled morphological units, shown in Figures 3.1, 3.2, 3.3 and Table 3.2, are located 1.5 to 1.9 km downwind with a large B_2 horizon of indurated coffee rock forming a hard, pitted deflation plain upwind.

Analysis of sediment that forms the windward and lee slopes of the parabolic dune at Croppies Bay indicates about 95% of the grains are sub-angular (mean 68%) to well rounded (mean 6.5%) quartz (mean 68%), with metamorphic[1] (mean 12%) and feldspar[2] (mean 18%) grains in 11 of the 12 samples. Five percent of the grain size distribution is sub-angular to well rounded biogenic calcite[3] ($CaC0_3$). With twelve percent of grains occurring as granules to very coarse sand (< 1 ø), 49% occur as medium to fine sand (1 to 3.75 ø) and 39% occur as very fine sand to silt (> 3.8 ø). Mean grain size is 2.45 ø, indicating a fine moderately well sorted sand (mean sorting 0.62 ø) (Table 3.2). This range of grains suggests that the late Quaternary aeolian quartz sand, designated 'Ainslie Sand' formation by Bowden (1983), has been substantially reworked. In the process of downwind reworking, the grains have reduced in size and textural parameters. The proportions of coarse to very coarse grains that Hubble (1946) analysed are significantly transformed (coarse to very coarse sediment, 67 – 86 %) to the finer sediment size classes of medium to fine sand. Biogenic calcite occurs in all samples, with elevated proportions in Samples 1 (25%) and 6 (6%).

Section 3.6 presents the analysis of the sediment samples by morphological units.

[1] Metamorphic grains originate from hinterland undifferentiated granitic rocks.
[2] Microcline and authoclase.
[3] Derived from loss on ignition (Dean, 1974).

Table 3.2 Sediment analysis of bulk density, porosity, grain density and grain size distributions; loss on ignition.

Sample	Bedform	Status	DBD[1] gm/cc	DBD[2] kg/m^3	Volume m^3	Total Mass kg	Percent[3] Porosity	Grain Density gm/cc	M_z ϕ		ϕ Sorting σ		ϕ Skewness		ϕ Kurtosis	Loss on ignition $CaC0_3$ gm	Loss on ignition $CaC0_3$ %
1	Nth trailing arm	Deposition	0.8934	893.4	656400	586427760	68.16	1.575	3.74	VF[4]	0.43	W[5]	-0.28	F[6]	1.33	8.118	25.3
2	Nth trailing arm	Deposition	0.9684	968.4	656400	635657760	65.4	1.6224	1.46	M	0.39	W	+0.03	S	0.77	1.696	3.94
3	Nth trailing arm	Deflation	1.0851	1085	656400	712259640	61.12	1.6963	1.55	M	0.07	VW	+1.0	SF	0.87	1.59	3.9
4	Nth trailing arm	Deflation	0.8162	816.2	656400	535753680	70.99	1.5261	2.84	F	0.44	W	-0.77	SC	0.85	0.938	3.07
5	Nth trailing arm	Deflation	0.9118	911.8	656400	598505520	67.48	1.5866	0.47	C	1.23	P	-0.87	SC	0.42	0.934	2.34
6	Lee Nth trail arm	Deposition	0.7561	756.1	656400	496304040	73.2	1.4881	3.84	VF	0.08	VW	-0.34	SF	0.6	0.994	2.14
7	Stoss	Deflation	0.6662	666.2	656400	437293680	76.5	1.4312	3.59	VF	0.37	W	-0.26	C	1.27	0.812	2.51
8	Stoss	Deflation	0.7691	769.1	656400	504837240	72.72	1.4963	1.69	M	2.08	VP	-0.4	SC	0.43	0.91	2.76
9	Stoss	Deflation	0.8058	805.8	656400	528927120	71.37	1.5195	1.43	M	2.15	VP	-0.3	C	2.53	1.796	3.71
10	Lee slipface	Deposition	0.7293	729.3	656400	478712520	74.18	1.4711	4.06	S	0.08	VW	-1.0	SF	0.77	1.312	3.3
11	Lee slipface	Deposition	0.5675	567.5	656400	372507000	80.12	1.3687	3.88	VF	0.08	VW	-0.0	S	0.74	1.126	2.36
12	Lee slipface	Deposition	0.7517	751.7	656400	493415880	73.36	1.4853	0.87	C	0.14	VW	+0.71	SF	0.62	2.986	6.09
		Mean	0.81005	810.1	656400	531716820	71.2	1.5222	2.45		0.62						

[1]DBD, dry bulk density.

[2]The density of a particle is defined as its mass per unit volume expressed in kg m^{-3} (Pye and Tsoar,1990:47).

[3]Porosity is defined as the percentage of the total volume of bulk sediment which is occupied by voids (Pye and Tsoar,1990:64) and reflects the packing arrangement of the grains, which in turn influences the ease with which grains are entrained by the wind. Grain shape influences the packing arrangement; voids are filled with air or another fluid.

[4]Sediment size class, Wentworth categories (McDonald, 1984) VF, very fine; M, medium; F, fine; S, silt; C, coarse

[5]Textural description (Folk & Ward, 1957). Sorted: W, well; VW, very well; P, poorly; VP, very poorly.

[6]Inclusive phi skewness (Folk & Ward, 1957). F, Fine skewed; SF, strongly fine skewed; S, symmetrical; SC, strongly coarse skewed; C, coarse skewed.

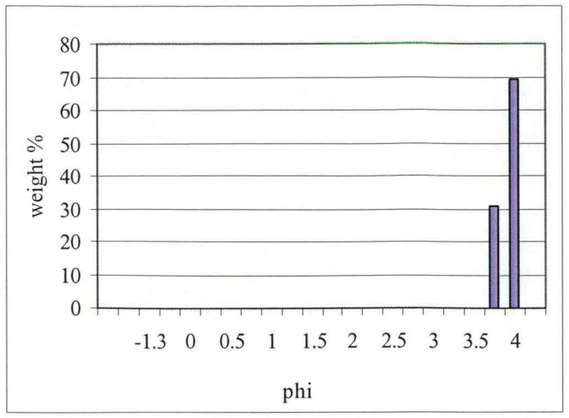

Sample 6. Deposition, lee north trailing arm.

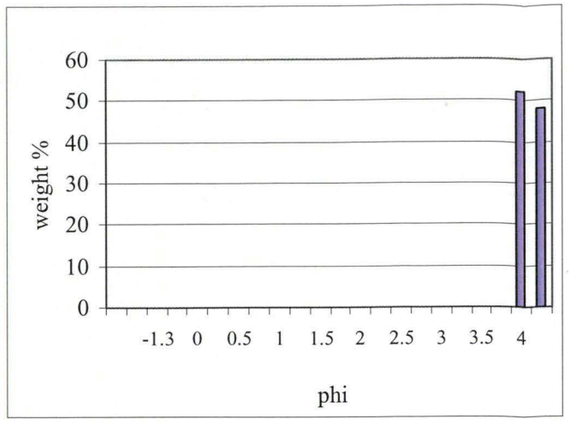

Sample 10. Deposition, 1 m below crest

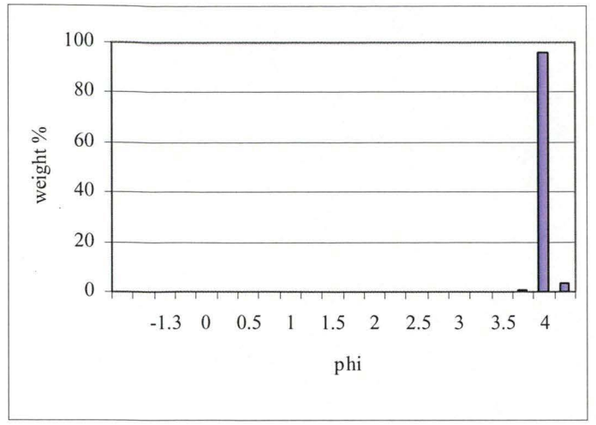

Sample 11. Deposition, mid slope, lee slipface

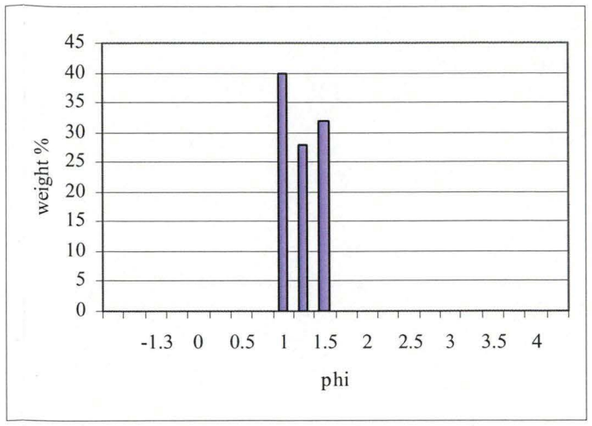

Sample 12. Deposition, base of lee slipface.

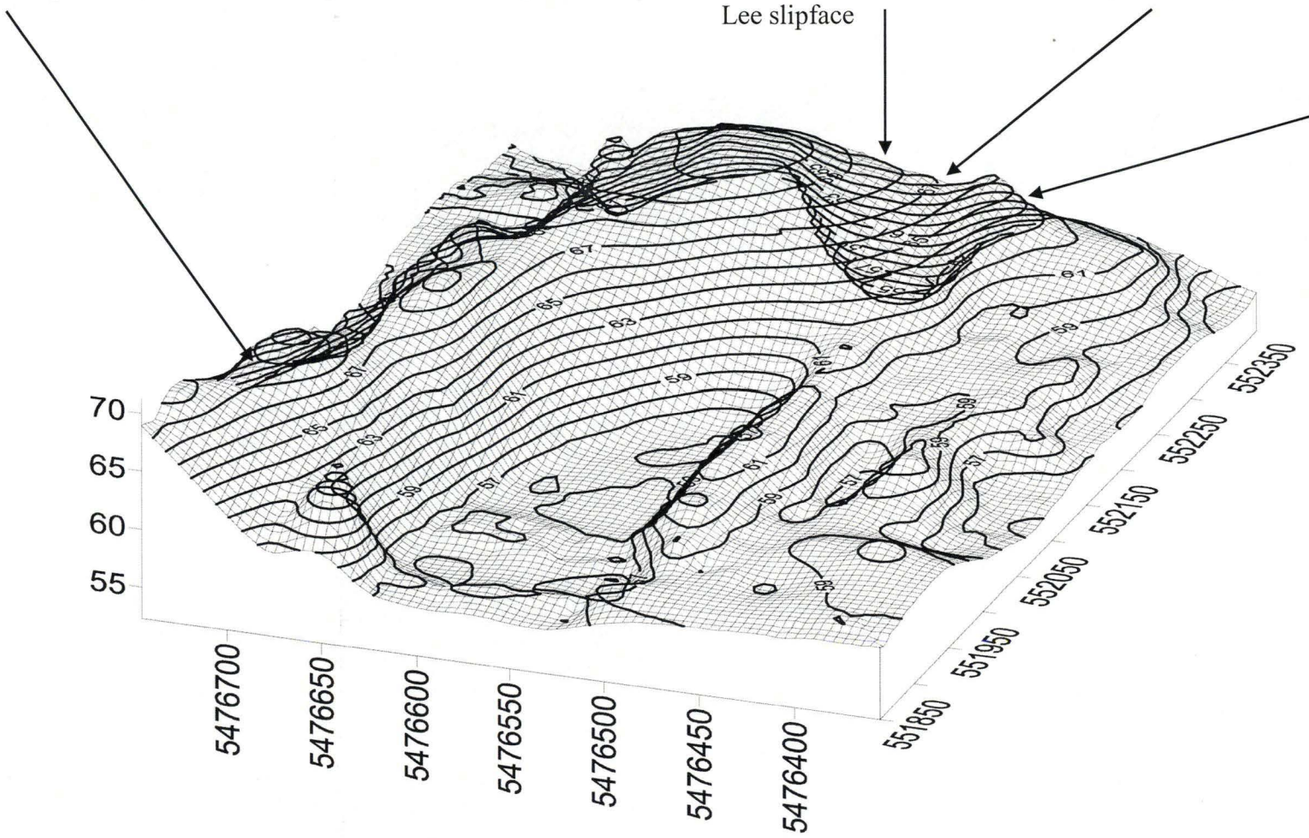

Figure 3.1. Lee slipface and lee north trailing arm. Grain size frequency histograms of lee bedforms, Croppies Bay, north east Tasmania.

From Table 3.2. Sediment analysis of bulk density, porosity, grain density and grain size distributions; loss on ignition.

Sample	6	10	11	12
DBD[1] gm/cc	0.7561	0.7293	0.5675	0.7517
DBD[2] kg/m^3	756.1	729.3	567.5	751.7
Volume m^3	656400	656400	656400	656400
Total mass kg	496304040	478712520	372507000	493415880
Percent Porosity[3]	73.2	74.18	80.12	73.36
Grain Density gm/cc	1.4881	1.4711	1.3687	1.4853
$M_z \phi$	3.84	4.06	3.88	0.87
	VF[4]	S	VF	C
ø sorting	0.08	0.08	0.08	0.14
	VW[5]	VW	VW	VW
ø skewness	-0.34	-1	-0	+0.71
ø kurtosis	0.6	0.77	0.74	0.62
Loss on ignition gm	0.994	1.312	1.126	2.986
CaCo[3] %	2.14	3.3	2.36	6.09

[1]DBD, dry bulk density.
[2]The density of a particle is defined as its mass per unit volume expressed in kg m^{-3} (Pye and Tsoar,1990:47).
[3]Porosity is defined as the percentage of the total volume of bulk sediment which is occupied by voids (Pye and Tsoar,1990:64).
[4]Sediment size class, Wentworth categories (McDonald, 1984) VF, very fine; M, medium; F, fine; S, silt; C, coarse.
[5]Textural description (Folk & Ward, 1957). Sorted: W, well; VW, very well; P, poorly; VP, very poorly.

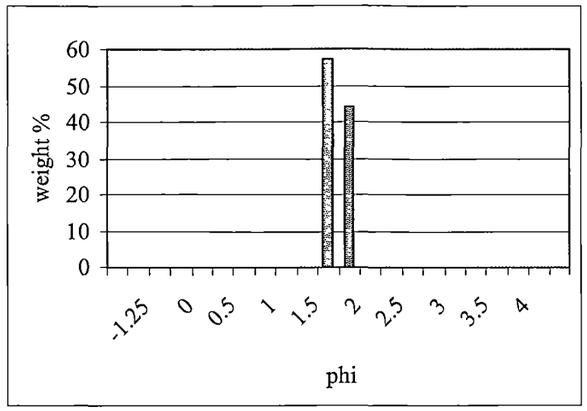

Sample 3. Deflation.

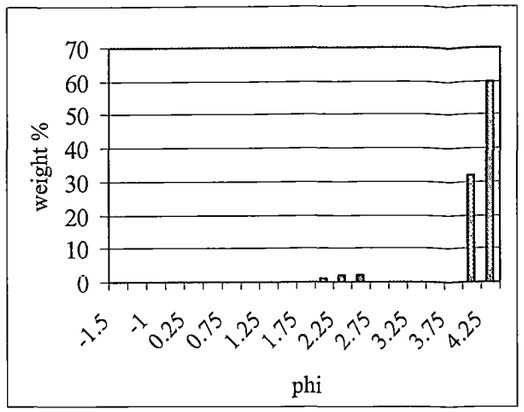

Sample 1. Deposition.

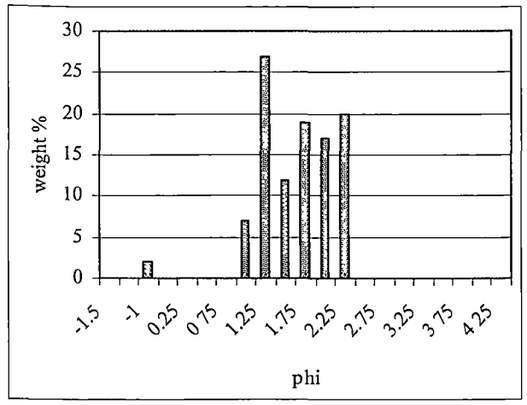

Sample 2. Deposition, crest.

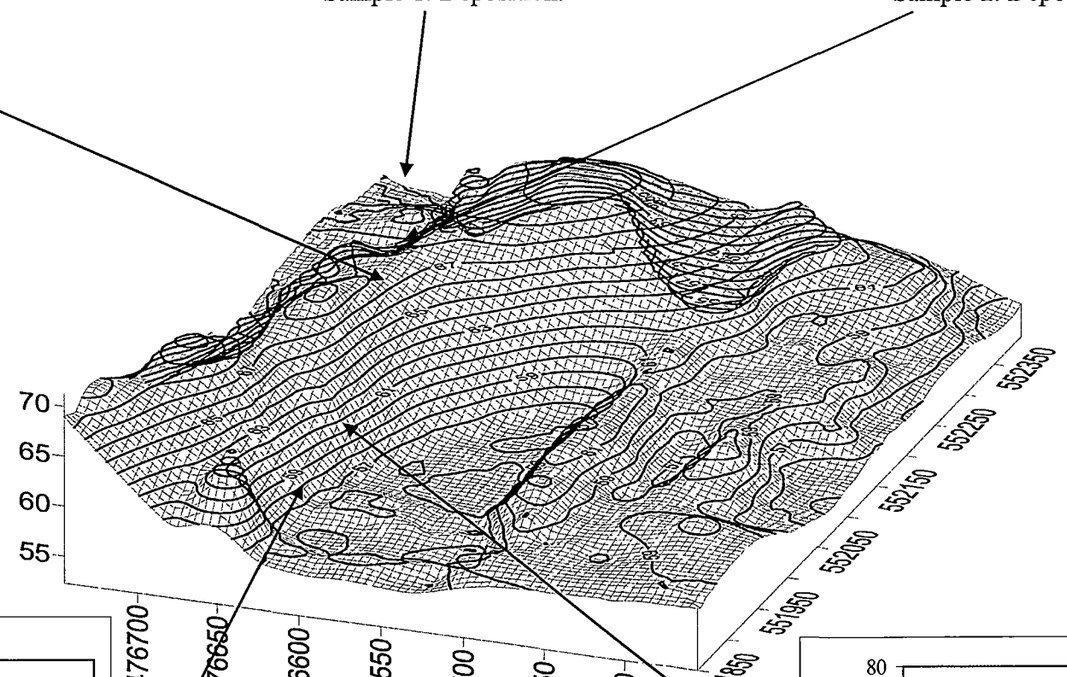

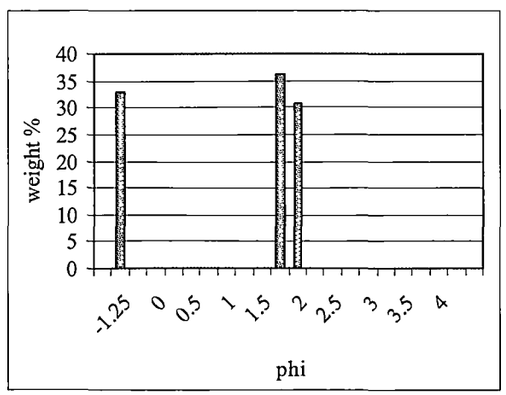

Sample 5. Deflation, South aspect.

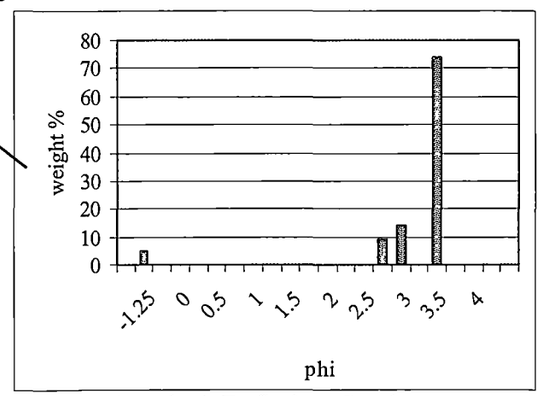

Sample 4. Deflation, South aspect.

From Table 3.2. Sediment analysis of bulk density, porosity, grain density and grain size distributions; loss on ignition.

Sample	1	2	3	4	5
DBD[1] gm/cc	0.8934	0.9684	1.0851	0.8162	0.9118
DBD[2] kg/m^3	893.4	968.4	1085	816.2	911.8
Volume m^3	656400	656400	656400	656400	656400
Total mass kg	586427760	635657760	712259640	535753680	598505520
Percent Porosity[3]	68.16	65.4	61.12	70.99	67.48
Grain Density gm/cc	1.575	1.6224	1.6963	1.5261	1.5866
M_z ϕ	3.74	1.46	1.55	2.84	0.47
	VF[4]	M	M	F	C
ø Sorting σ	0.43	0.39	0.07	0.44	1.23
	W[5]	W	VW	W	P
ø Skewness	-0.28	+0.03	+1	-0.77	-0.87
ø Kurtosis	1.33	0.77	0.87	0.85	0.42
Loss on ignition gm	8.118	1.696	1.59	0.938	0.934
$CaCo_3$ %	25.3	3.94	3.9	3.07	2.34

[1]DBD, dry bulk density.
[2]The density of a particle is defined as its mass per unit volume expressed in kg m^{-3} (Pye and Tsoar, 1990:47).
[3]Porosity is defined as the percentage of the total volume of bulk sediment which is occupied by voids (Pye and Tsoar,1990:64).
[4]Sediment size class, Wentworth categories (McDonald, 1984) VF, very fine; M, medium; F, fine; S, silt; C, coarse.
[5]Textural description (Folk & Ward, 1957). Sorted: W, well; VW, very well; P, poorly; VP, very poorly.

Figure 3.2. North trailing arm. Grain size frequency histograms, Croppies Bay, north east Tasmania.

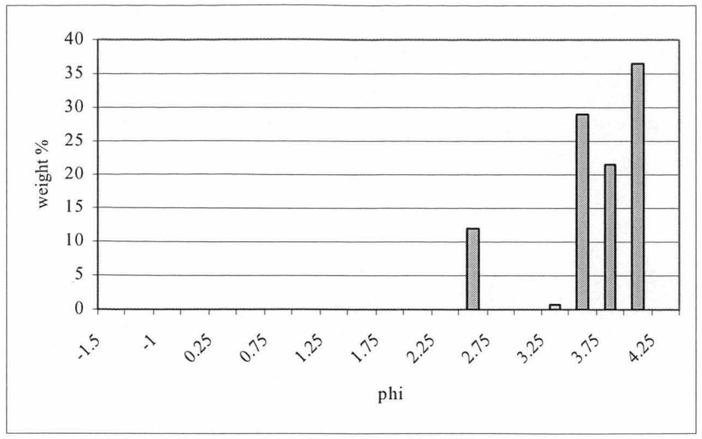

Sample 7. Deflation, Contour 59 m

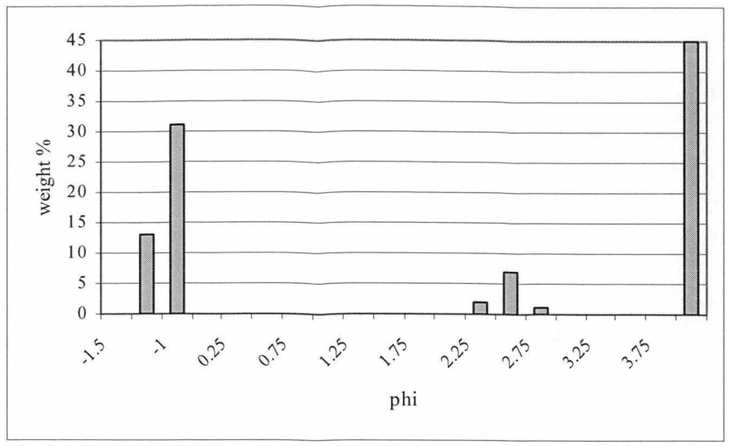

Sample 8. Deflation, Contour 61 m

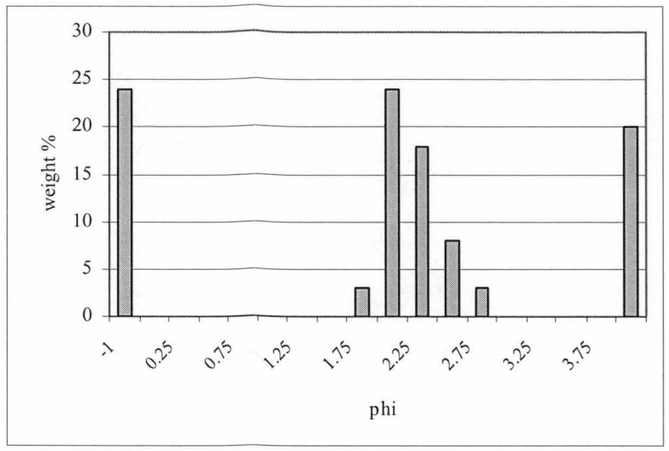

Sample 9. Deflation, crest of parabolic head.

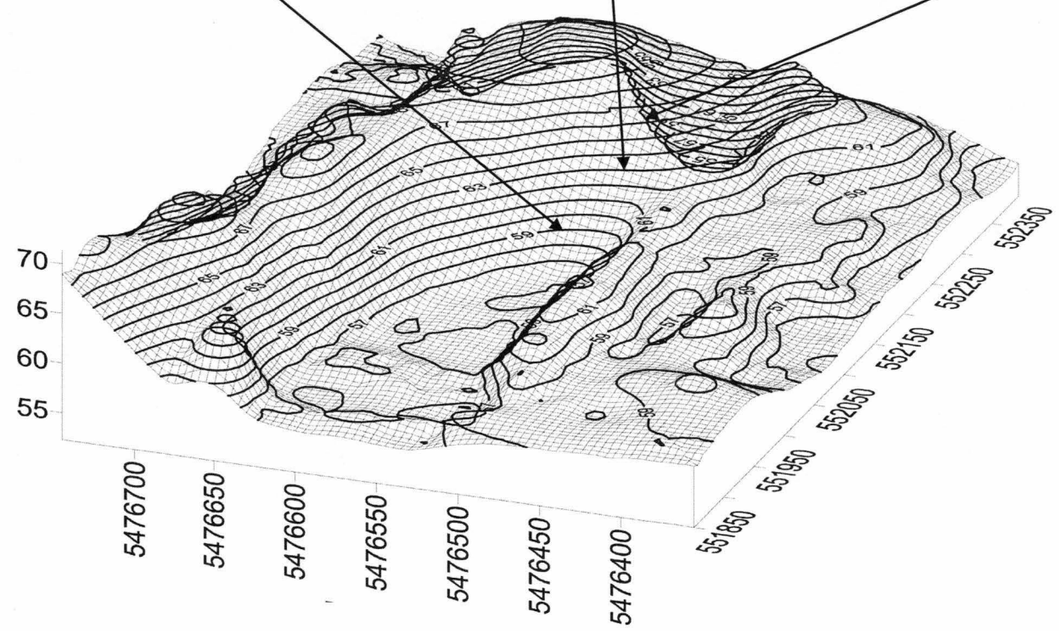

Figure 3.3. Stoss. Grain size frequency histograms of stoss, Croppies Bay, north east Tasmania.

From Table 3.2. Sediment analysis of bulk density, porosity, grain density and grain size distributions; loss on ignition.

Sample	7	8	9
DBD[1] gm/cc	0.6662	0.7691	0.8058
DBD[2] kg/m^3	666.2	769.1	805.8
Volume m^3	656400	656400	656400
Total mass kg	437293680	504837240	528927120
Percent Porosity[3]	76.5	72.72	71.37
Grain Density gm/cc	1.4312	1.4963	1.5195
$M_z\ \phi$	3.59	1.69	1.43
	VF[4]	M	M
ϕ sorting	0.37	2.08	2.15
	W[5]	VP	VP
ϕ skewness	-0.26	-0.4	-0.3
ϕ kurtosis	1.27	0.43	2.53
Loss on ignition gm	0.812	0.91	1.796
CaCo3 %	2.51	2.76	3.71

[1]DBD, dry bulk density.
[2]The density of a particle is defined as its mass per unit volume expressed in kg m^{-3} (Pye and Tsoar,1990:47).
[3]Porosity is defined as the percentage of the total volume of bulk sediment which is occupied by voids (Pye and Tsoar, 1990:64).
[4]Sediment size class, Wentworth categories (McDonald, 1984) VF, very fine; M, medium; F, fine; S, silt; C, coarse.
[5]Textural description (Folk & Ward, 1957). Sorted: W, well; VW, very well; P, poorly; VP, very poorly.

Table 3.3 Grain shape characteristics and mineral origin, representative samples.

Sample		Grain Shape[1] %				Sphericity%			Mineral origin %		
		well rounded	rounded	sub-rounded	sub-angular	high	low	Quartz	Meta morphic	Feldspar	Biogenic calcite
1	NTA	5	6.8	8.2	79.9	20	80	67	9.5	19.5	4
2	NTA	0.7	9.8	9	80.4	19.5	80	63	7.6	17	12.5
5	NTA	7.4	6	16.3	70.2	29.7	70	61.1	10.3	17.8	10.8
7	Stoss	10.6	11.8	21.3	56.2	43.7	56.2	61.7	15.3	14.2	8.8
8	Stoss	7.3	16.4	18.2	57.9	42	57.9	69	6	22	3
10	Slipface	8.1	14.9	12.9	63.9	36	64	50	23	19.6	7.4
		6.5	10.9	14.3	59.5	31.8	68	61.9	11.9	18.3	7.7

[1] Grain roundness and sphericity classes based on Powers (1953) visual comparator in Pye and Tsoar, (1991:60).

Table 3.3 and Figure 3.4 show the range in grain sizes and grain shapes. The grains are dominated by mature sand, and are comprised predominantly of quartz with feldspar and a proportion of metamorphic grains derived from hinterland undifferentiated granitic rock. There are also large and small fragments of biogenic carbonate calcite indicative of downwind transport of modern beach material derived from calcareous algae, foraminifera and bivalve molluscs[4].

The density of particles is similar: quartz, undifferentiated granitic rock and feldspar (microcline and authoclase) 2650 kg/m^3, calcite 2710 kg/m^3. The calcite particles are perforated (Figure 3.4 'C'), probably resulting in a lighter, more buoyant particle relative to the densities of the quartz and feldspar particles.

The high proportion of very fine sand to silt (Figures 3.1, 3.2, 3.3) is probably a derivative of three processes. Firstly, reworking of sand grains by wind entails abrasive churning of grain sediment, in combination with the process of selective entrainment[5]. Very coarse to coarse sized grains, transported by creep (surface traction), are probably less subject to aeolian abrasion than grains transported in saltation or suspension (Pye and Tsoar, 1990). Mineral composition of on-site grains, quartz, metamorphic rock, feldspar (microcline and authoclase) and biogenic calcite ($CaCO_3$), also influences the rate of rounding by aeolian abrasion. Marsland and Woodruff (1937, in Pye and Tsoar, 1990:75) found that the rate of rounding by aeolian abrasion depends on the hardness of different minerals. "The relative susceptibility to rounding by abrasion was found to be gypsum > calcite > apatite > magnetite > orthoclase > garnet > quartz" (Marsland and Woodruff (1937), in Pye and Tsoar (1990:75). Given Hubble's (1946) sediment analysis of coarse to very coarse sediment, with a low proportion of silt and clay, it is evident that the reworked sediment has reduced in grain size by three sediment size classes to a medium to fine sand and remains moderately well sorted.

[4] Pers com Dr. Pat Quilty, 3.3.04.

[5] Selective entrainment, or the process of winnowing, contributes to a decrease in grain size and increased sorting in the direction of transport. Where a decrease in the direction of transport of effective wind speed, momentum exchange between grains and bed, and dependence of threshold speed on grain size, combine together to reduce the probability that grains of a given size will continue to be transported (Allen, 1970).

Secondly, silt grains exhumed upwind from the B_2 horizon of indurated coffee rock and C horizon (beneath coffee rock) is available for downwind transport. Hubble (1946) indicated a composition of 26% fine sand and 2.4% silt. Aeolian abrasion and chemical weathering of feldspar grains may also have contributed to the silt component.

Thirdly, aeolian silt deposited in advance of the lee slipface to a depth of 30 – 60 mm is arguably available for recycling to the deflation basin and stoss, as the head of the parabolic dune migrates downwind.

Selective entrainment also occurs as a derivative of the lateral migration of trailing arms of the dune. Two examples are illustrative of the process. Firstly, coarse to medium grains are exhumed from the base of the northern flank, Sample 5 (see Figure 3.2), in which quartz granules (-2 to -1.5 ø) and very coarse sand (-1 to 0.5 ø) are concentrated at the base of the flank. These lag deposits form mega ripples in a zone of wind acceleration. Secondly, medium to fine sediment, derived from the advancing south trailing arm, is liberated for downwind transport, accumulating on the deflation plain in the lee of shadow dunes and low lying areas subject to inundation. Subsequent strong wind events transport a proportion of this sediment onto the stoss.

Currently, the sediment that forms the parabolic dune at Croppies Bay is comprised predominantly of well to very well sorted sand grains (0.44 to 0.07 ø), mean 0.23 ø. Twenty five percent of samples contain poorly to very poorly sorted grains (1.23 to 2.15 ø) increasing mean sorting to 0.62 ø. Mean grain size for the site is 2.45 ø. This mean grain size is comprised of 50% coarse to medium grains, 0.47 to 1.69 ø (mean 1.24 ø), and fifty percent of fine to very fine to silt grains 2.06 to 4.06 ø, (mean 3.52 ø). Within this mode, there is some variability between morphological units, initiated by windward and lee factors. Consequently, samples vary between strongly fine to strongly coarse skewed grains, which are very platykurtic to platykurtic in grain size distribution. Twenty five percent of samples are fine to coarse skewed and leptokurtic in grain size distribution. Thus, contemporary analysis of sand indicates that the Quaternary aeolian coarse grained quartz, designated 'Ainslie Sand' formation by Bowden (1983), has been substantially reworked by downwind transport, reducing quartz, feldspar and calcite grains from angular to sub-angular and rounded, accompanied by a reduction in grain size. These results are consistent with the findings of Goudie and Watson (1981) that quartz sand grains are well rounded where they have been recycled from older sedimentary phases. The distribution and variability of grain sizes are discussed below.

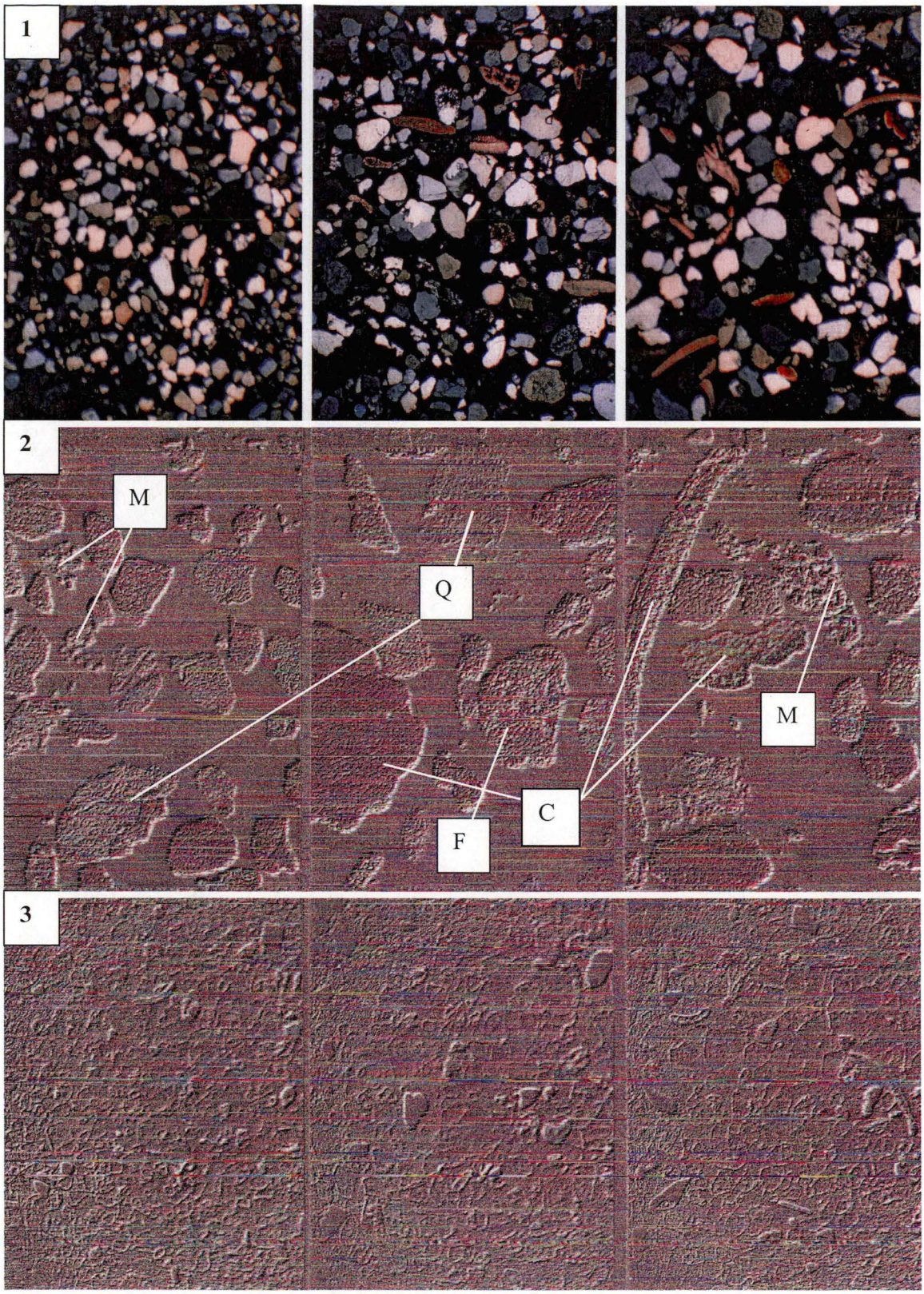

Figure 3.4. Grain samples slides.

Grain size (**1**); grain texture and origin (**2**); grain shape (**3**). (Q, quartz; F, feldspar; C, biogenic calcite; M, metamorphic). The 2.5 mm scale applies to sample slides 1 and 2.

3.5 Variability within and between morphological units

Analysis of 12 samples, shown in Table 3.2, Figures 3.1, 3.2, 3.3, indicates variability between and within morphological units, which are discussed in the following descriptions.

The three modes of aeolian sediment transport are creep (surface traction), saltation and suspension. The true value of the different size classes depends upon the intensity of effective wind speed, and there may be some intermingling of the coarse (creep) and upper size margin of the saltation classes. At Croppies Bay, 12% of grains (creep) occur as granules to very coarse sand (< 1 ø); 49% (saltation) occur as medium to fine sand (1 to 3.75 ø) and 39% (suspension) occur as very fine sand to silt (>3.8 ø). All modes are represented within Samples 1 to 12.

3.5.1 Lee slipface

Lee slipface grains are finer and consistently very well sorted compared with grains on windward slopes (Figure 3.1). Three of the four lee samples, S 6, S10 and S11, contain very well sorted (0.08 ϕ) sediment. Sample 6, located on the lee of the north trailing arm, is comprised of very fine sand (3.75 – 4 ϕ), compared with the silt (4 – 4.25 ϕ) of S10 and S11, which are located on the lee slipface. Twenty percent of grains are sub-rounded to well rounded (Table 3.3, Figure 3.4). These three samples are negatively skewed in distribution. S12, located at the base of the 33° lee slipface, contains very well sorted (0.14 ϕ) medium sand (1 – 1.5 ø) positively skewed. The presence of larger grains at the base of the slipface is due to cascading of larger grains down the slipface, six percent of these grains are biogenic calcite. Tongue-shaped avalanching, commencing just below the crest, is generally shallow, surface dry sediment moving over a moist subsurface. Field observation indicates that grains on the margins of the tongue are generally coarse, with fine grains located mid-tongue. Coarse silt (4.5 ϕ) is transported downwind, up to 30 m in advance of the lee slipface, inundating ground cover plants and tussock grasses to a depth of 30 – 60 mm, in the process 'smoothing' roughness features in front of the migrating dune. The low proportion of fine particulate in source material and resistance of material to weathering, suggests that this particulate fraction is recycled to the stoss / deflation plain as the dune migrates downwind.

Sediment on this lee slipface is uniformly low in bulk density and high in porosity; for example, S11 has a bulk density of 567.5 kg/m^3, where the average is 810.1 kg/m^3, and a porosity of 80%, indicative of very loosely packed sediment with a large proportion of voids (Figures 3.1; 3.2). Pye (1983:200) indicated that the typical porosity range of recently deposited dune sand is 25% to 65%, but is dependent upon sediment sorting, the packing arrangement of grains and particle shape. Pryor (1973:175) collected a total of 116 samples from coastal dunes at St Andrews State Park, near Panama City, Florida. Pryor reported a porosity range of 49% to 55%. Loss on ignition indicates up to 95% of the grains are quartz, metamorphic rock and feldspar, with the exception of 6% biogenic calcite. Sixty four percent of grains have a low sphericity.

3.5.2 North trailing arm

Samples S5, S4, S3, S2 and S1 are aligned in the direction of transport from the base of the north trailing arm, south aspect, (S5) up the deflating north trailing arm (S4 and S3) to the crest (S2) and into a zone of deposition (S1). Figure 3.2 illustrates a gradation from poorly sorted, strongly coarse skewed sediment to well sorted, strongly fine skewed sediment from the base of the trailing arm across the crest to a deposition zone. This sequence illustrates sediment has undergone a process of selective winnowing in response to wind flow converging and accelerating up the flank of the north arm (S5, S4, S3). Progressively, a process of selective entrainment has resulted in coarse, heavier-density quartz particles (-1.5 ø) remaining on the lower flank of the dune; whilst medium and fine grained sand (1.5 – 2.25 ø) has been transported up the dune flank. Converging wind flow at S 3 (Chapter 4, 4.7.2) deflates medium sand grains (1.5 – 1.75 ø), followed by separation of wind flow at the crest (S2) where a range of particle sizes have fallen out of saltation, and silt, probably in suspension, has continued downwind to S 1. Kurtosis for S5, S4 and S3 is very platykurtic, with S2 near symmetrical platykurtic, and S1 very leptokurtic. Bulk density and grain density (Figures 3.1, 3.2) are higher on this morphological unit, porosity lower, possibly indicative of an earlier phase of emplacement, i.e., the duration of time has reduced voids and increased grain packing. There is a gradation from S 5 to S 1 of an increasing proportion of biogenic calcite, 2.3% to 25% respectively.

The gradation along the sample sites is as follows:
S5 located near the base (~ 1.5 m above deflation plain, 58 m contour) of the north trailing arm, is comprised of the coarsest sediment 33% at -1.5 ϕ, 30% at 1.5 ϕ, and 36% at 1.75 ϕ (medium sand), 97.6% of grains are quartz, feldspar and metamorphic rock. Seventy percent of grains have a low sphericity, with 30% of grains sub-rounded (16%) to well rounded (Table 3.2, Figure 3.4, S 5 and S 2). A bimodal distribution results in a poorly sorted sediment of 1.23 ϕ, with a bulk density of 911.8 kg/m^3 and porosity of 67%, one of three samples in this upper range for the study site.

S4 located ~ 4 m above deflation plain, is located in the lee of a truncated arm buttress which forms a shadow dune tail extending to the 60 m contour on the north trailing arm, southerly aspect. Figure 3.2 shows increased sorting of sediment (0.05 ϕ) with the majority of the sample occurring within 2 and 2.5 ϕ (medium to fine sand) and 5% occurring in the -1.5 ϕ (very coarse sand) range. Ninety seven percent of grains are quartz and feldspar. Bulk density is 816.2 kg/m^3 and porosity 71%, the lowest figures on the deflating exhumed surface, possibly indicative of deposition sourced from the tail of the shadow dune.

S3 located ~ 9 m above deflation plain, 67 m contour, exhibits a unimodel distribution of sediment of 1.5 – 1.75 ϕ (medium sand) with very well sorted sediment (0.07 ϕ); 96% of grains are quartz and feldspar. Bulk density at 1085 kg/m^3 and porosity of 61% indicates less voids and possibly better packing.

S2 located ~ 10 m above the deflation plain at crest of the north trailing arm (70 m contour), exhibits an increased range of sediment size, with 2% very coarse sand and

the majority distributed between 1 ϕ to 2.5 ϕ (medium to fine sand). Ninety six percent of grains are quartz, metamorphic and feldspar. 80% of grains have a low sphericity. Bulk density and porosity are lower than S3.

S1 located in a depositional corridor (Figure 3.2) is comprised of 5% fine and very fine sand and 92 % silt. The fine skew (-0.28 ϕ) is probably indicative of the increased elevation selectively winnowing coarse particles from sediment transport downslope. Why this depositional corridor contains 25% biogenic calcite remains open to speculation. However, Stapor (1983;162) established that quartz and biogenic calcite have different settling speeds, with biogenic calcite being the slower, and that grains of lower sphericity are preferentially selected in transport. Although it is beyond the scope of the present study to critically analyse the settling-speed distributions of individual grains, analysis of grain characteristics in the present study indicates that biogenic calcite grains are perforated (Figure 3.4) probably resulting in a lighter, more buoyant particle relative to the densities of the quartz, feldspar and metamorphic particles, thus likely contributing to a slower settling rate. The images illustrated in Figure 3.4 are representative of the remaining nine samples, and indicate that, generally, biogenic calcite has a lower sphericity.

3.5.3 Stoss

Ripples are a key morphological feature on the stoss, varying in wavelength from 9 to 30 cm dependent on wind speed, building in length and steepness towards the crest, and reducing in wavelength again on the plateau located between stoss and lee slipface crests. In strong sustained wind events, ripples flatten out (filling up with grains) and the stoss and plateau are devoid of ripples. Bagnold (1941:151), in wind tunnel experiments, found that with a nearly uniform grain size of 0.25 mm (2 ϕ), ripples disappeared when wind shear velocity ($u*$) was three times its threshold value; this factor would probably increase with a mixture of grain texture and sizes. Given the mean grain size on the stoss of 2.23 ϕ, this equates to ~ 14 m/s. The variability in the range of grain sizes contained in Samples S7, S8, S9, may be partially explained by the amplitude of the ripples and the concentration of coarse grains on the crest of ripples. Bagnold (1941:34) found that grains transported as surface creep are moved forward by saltating grains, rather than wind velocity, and "a high-speed grain in saltation can by impact move a surface grain six times its diameter, or more than 200 times its own weight".

Unlike the north trailing arm, no pedestals form, due in part to high porosity (average of 73% to a depth of 1 m), and the sustained churning of sediment. Sediment is derived from the deflation plain, base of the north trailing arm, and south trailing arm from the deflation basins inset within this arm, and lateral migration. Loose packing enables sand entrainment to commence at lower wind speeds, compared with sediment on the flank of the north trailing arm.

Samples S7, S8, S9 (Figure 3.3) were aligned up the midline of the 23° slope.

S7 Sediment in S7 (~ 2 m above the deflation plain, 56 m contour) is very well sorted, fine skewed with very fine sand and coarse silt (2.5 – 4 ϕ). This fine sediment is primarily derived from the deflation plain and transported onto the lower

flank of the stoss. Field observation found that silt and very fine sand particles are available for entrainment and transport in low wind speeds of 3 to 3.8 m/s, a selective winnowing process. The gradient of the measured wind shear velocity (Chapter 4, 4.7.2) on this concave portion of the stoss is lower and momentum of sediment entrainment by bombardment during saltation reduced. As the head of the parabolic dune migrates downwind, fine particulate, transported in advance of the lee slipface, is exhumed, in addition to the up-wind sediment exhumed from horizon C. Density is low at 666.2 kg/m^3 and porosity high at 76%. Ninety seven percent of sand grains are quartz, (metamorphic rock and feldspar, 2.5% calcite (Table 3.3). Grains are predominantly sub–angular (56%), with low sphericity.

S8 (~ 6 m above deflation plain, 61 m contour) is tri modal in distribution, with 42 % very coarse sand, 10% fine, and 45% silt, resulting in a very poorly sorted, negative skewed, leptokurtic grain distribution. Shear stress close to the bed is sufficient to transport grains in the coarse lag range up a 23° slope. Bagnold (1941) stated that a saltating cloud of grains bombarding lag-sized sediment is required to dislodge and transport lag. High porosity (72.7%) is probably indicative of loose packing of grains (grain density 1.4963 gm/cc), which would assist the dislodging of grains during bombardment. Ninety seven percent of sand grains are quartz, metamorphic and feldspar, 2.7% biogenic calcite.

S9 (~ 12 m above deflation plain, 67 m contour) is located on the crest of the stoss. Grain distribution is tri modal, with 24% of very coarse sand grains (-1 ø) in creep mode possibly advancing on the crest of ripples. Fifty six percent of grains are 1.75 to 2.75 ø, indicative of moderating shear stress resulting in grains falling out of saltation at the crest, similar to S 2. Twenty percent of grains are silt. The tri modal distribution results in a very poorly sorted negatively skewed leptokurtic grain size distribution. A bulk density of 805.8 kg/m^3, although below the average of 810.1 kg/m^3, is the highest on the stoss, which is reflected in percent porosity of 71% and grain density of 1.5 gm/cc. Ninety six percent of sand grains are quartz, metamorphic and feldspar, 3.7% biogenic calcite.

In summary, there is variation between the morphological units that form the Croppies Bay parabolic dune. Namely, the deflating north trailing arm, south aspect, has a higher proportion of coarse grains, yielding a moderately well sorted sand (0.53 ø) with a mean grain size of 1.58 ø. The windward stoss has a high proportion of poorly sorted (1.53 ø) medium sized grains 2.4 ø. Depositional surfaces, which are characteristically lee, are comprised of very well sorted sand, 0.16 ø, ranging between coarse sand (base of lee slipface) to silt grains (0.87 to 4.06 ø). The plotting of mean grain size against sorting indicates no relationship between the two variables (Figure 3.5). Similarly, no relationship is evident between mean grain size against skewing. This is probably due to the reworking and mixing of sediment.

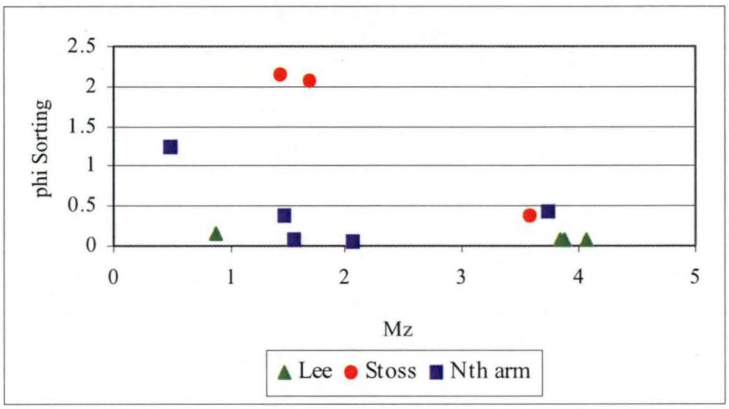

Figure 3.5 A plot of mean grain size against sorting.

3.6 Sediment moisture content

A thermal blanket of dry sand overlays the persistently moist morphological units that comprise the parabolic dune to variable depths, consistent with seasonal precipitation, effective wind speed and solar radiation (Chapter 4, section 4.2.1).

Table 3.4 shows the results of applying Equation 3.1 to the sediment samples. The Croppies Bay average sand moisture content is 4.6%. There is no evident pattern to the distribution of higher or lower moisture contents either between morphological units, or from toe to crest, or between deflation and deposition bedforms. In addition, there is no apparent pattern associated with the porosity of the sand. S12, located at the toe of the lee slipface with a moisture content of 6.4%, may be explained by the weight of the advancing dune depresses the deflation basin, which, in turn, releases moisture to the ground surface.

Gardner and McLaren (1999:942) reported moisture content on unvegetated frontal dunes rarely exceeded 14% within the top 1.3 m and commonly ranged between 2% to 10%.

Field observation indicates that sustained wind speeds above 9 m/s deflate moist sediment, evident by beds of perched pedestals 0.5 to 2 cm high with deflation wind tails. Belly (1964), in laboratory experiments, established that 1% moisture content impedes sediment transport by elevating wind shear (fluid threshold velocity).

Table 3.4. Sand moisture content of sediment samples.

Sample	Bedform	Status	Moisture content (%)	Percent Porosity
1	Nth trailing arm	Deposition	0.14	68.2
2	Nth trailing arm	Deposition	0.2	65.4
3	Nth trailing arm	Deflation	22.4	61.1
4	Nth trailing arm	Deflation	9.8	71
5	Nth trailing arm	Deflation	0.4	67.5
6	Lee Nth trail arm	Deposition	9.2	73.2
7	Stoss	Deflation	0.2	76.5
8	Stoss	Deflation	0.1	72.7
9	Stoss	Deflation	5.8	71.4
10	Lee slipface	Deposition	0.5	74.2
11	Lee slipface	Deposition	0.2	80.1
12	Lee slipface, toe	Deposition	6.4	73.4
		Average	4.6 %	71.2

3.7 Summary

Previous scientific literature on coastal parabolic dunes reported on textural parameters derived from remobilised dunes (Anthonsen, 1996; Arens, 2004), on specific morphological units, for example stoss (Stapor and May, 1983) or crests (Pye, 1982). Although reworking of sediment is commonly understood as a process, there is limited reporting (Anton and Vincent, 1986) on the process and outcome. This research presents an analysis of a reworked Quaternary quartz mantle and, based on a search of the scientific literature, the first analysis of textural parameters on morphological units that form a long-walled coastal parabolic dune.

The sediment that forms the parabolic dune at Croppies Bay is comprised predominantly of well to very well sorted sand grains (mean 0.23 ø), 25% of samples are poorly to very poorly sorted (mean 1.8 ø). There is a bimodal distribution delineated extensively by deflation and deposition surfaces. Deflation surfaces are comprised of medium to coarse grains (mean 1.24 ø), deposition surfaces predominantly of very fine grains (mean 3.65 ø). Consequently, there is variation between strongly fine to strongly coarse skewed grains, resulting in a very platykurtic to platykurtic grain size distribution. Twenty five percent of samples are coarse or fine skewed and leptokurtic in grain size distribution. Twelve percent of grains occur as granules to very coarse sand (< 1 ø); 49% occur as medium to fine sand (1 to 3.75 ø) and 39% occur as very fine sand to silt (> 3.8 ø).

Grains are dominated by mature sand comprised predominantly of sub angular low sphericity quartz (mean 62%), feldspar (mean 18%) and metamorphic grains derived from hinterland undifferentiated granitic rock (mean 12%). Biogenic carbonate calcite occurs generally as fragments (mean 7.7%) indicative of downwind transport of modern beach material derived from calcareous algae, foraminifera and bivalve molluscs. The density of particles is similar (2650 ± 60 kg m $^{-3}$), however calcite particles are perforated probably resulting in lighter, more buoyant particles relative to the densities of the quartz, feldspar and metamorphic particles. Five percent of grains are sub-angular to well rounded biogenic calcite ($CaC0_3$).

This present day sediment is derived extensively from a 53 – 75 cm deep mantle of late Quaternary aeolian quartz sand, designated 'Ainslie Sand' formation by Bowden (1981) and 5% biogenic calcite overlaying an indurated pitted B_2 horizon. The mantle was comprised predominantly of coarse to very coarse sediment (67 – 86 %), some fine (26 – 10 %) and a low proportion of silt and clay (4.5 – 1.7 %) (Hubble, 1946). The proportions of coarse to very coarse grains that Hubble (1946) analysed are significantly transformed (coarse to very coarse sediment, 67 – 86 %) to the finer sediment size-classes of medium to fine sand. Evidently, the reworked sediment has reduced in grain size by three sediment size classes to a medium to fine sand. Thus, contemporary analysis of sand indicates that the mantle has been substantially reworked by downwind transport, reducing the quartz, feldspar and metamorphic grains from angular to sub-angular and rounded, accompanied by a reduction in grain size.

The sediment available for entrainment by effective winds at Croppies Bay are creep (surface traction) with 12% of grains occurring as granules to very coarse sand (< 1

ø); 49% (saltation) occur as medium to fine sand (1 to 3.75 ø) and 39% (suspension) occur as very fine sand to silt (> 3.8 ø).

Variability is exhibited in the textural parameters between morphological units, initiated by windward and lee factors, these include:

a) deflating north trailing arm, south aspect, has a higher proportion of coarse grains, yielding a moderately well sorted sand (mean 0.5 ø) with a mean grain size of 1.58 ø;
b) the windward stoss has a high proportion of poorly sorted (mean 1.5 ø) medium sized grains 2.2 ø;
c) depositional surfaces, which are characteristically lee, are comprised of very well sorted sand, mean 0.09 ø, ranging between coarse sand (base of lee slipface) to silt grains (0.87 to 4.06 ø), yielding a mean grain size of 3.16 ø.

The present study identifies a range of characteristic textural parameters derived from several morphological units that form an actively mobile parabolic dune, including:

a) the dune base contains grains which are coarser, poorly sorted and positively skewed;
b) the dune crests contain very well sorted grains that are fine grained, resulting in a platykurtic grain size distribution that is strongly fined skewed;
c) lee slipface grains are finer and consistently very well sorted compared with grains on windward slopes;
d) high proportion (66%) of samples contain very fine sand to silt, for example the stoss, lee and depositional surfaces;
e) large and small fragments of biogenic carbonate calcite, indicative of downwind transport (up to 1.9 km) of modern beach material derived from calcareous algae, foraminifera and bivalve molluscs;

Field and laboratory analysis identified examples of selective entrainment occurring,

a) as a derivative of lateral migration of trailing arms coarse to medium grains are exhumed from the base of the northern flank;
b) as medium to fine sediment, derived from the advancing south trailing arm, is liberated for downwind transport, accumulating on the deflation plain in the lee of shadow dunes;
c) as aeolian silt deposited in advance of the lee slipface to a depth of 30 – 60 mm is arguably available for recycling to the deflation basin and stoss, as the head of the parabolic dune migrates downwind.

Subsequent strong wind events transport a proportion of these sediments onto stoss and lee bedforms.

3.8 Conclusion

Grain size and sorting at Croppies Bay parabolic dune contrasts with the results of Mason and Folk (1958), Ahlbrandt (1980), Allen (1970) and Abuodha (2003) who determined that coastal dune sands contain finer size grains which are fine skewed, indicative of better sorting. They attributed these characteristics, generally to maintenance of the link between compositionally similar sediment source (beach) and dunes. Bigarella and Alessi (1969) noted that coarse and poorly sorted beach sands usually translate into finer and better-sorted sand in adjacent dunes. In contrast, parabolic dunes often initiate as blowouts, remote from a beach source and derive their sediment by cannibalising earlier Quaternary phases of deposition that may be comprised of coarse-grained sediment.

Thus, unlike most coastal dunes that are formed from material sourced from beach deposit, the Croppies Bay sediment is sourced predominantly from an aeolian Quaternary mantle and is relatively diverse in size range and sorting. Therefore, in this example of downwind migration of a Holocene dune that is the product of the reworking predominantly *in situ* of aeolian quartz material, the degree of subsequent sorting is likely to be the result of wind action rather than the more usual derivative of a limited size-range of beach material.

CHAPTER 4

Wind Regime, Atmospheric Parameters and Wind Flow Pattern over a Long-Walled Parabolic Dune

4.0 Introduction

This chapter describes the wind regime and atmospheric parameters that have affected the surface conditions of a parabolic dune system and its mobility over the last fifty-five years, focusing especially over the last four years. Yearly and seasonal wind patterns and the wind resultant sand roses are analysed, followed by analysis and description of the near-surface wind flow on an asymmetric parabolic dune. An evaluation of primary regulators of dune mobility, namely wind speed, rainfall and air temperature, are assessed for feedback mechanisms in parabolic dune dynamics.

This chapter addresses a series of gaps in the understanding of how dune morphology is controlled by an effective wind regime. In particular, the gaps addressed are: (i) the measurement of acceleration of wind on windward slopes of an actively mobile, coastal parabolic dune, and (ii) the influence of atmospheric parameters on coastal dune mobility.

The sediment characteristics of the windward and lee slopes that were described in Chapter 3 are incorporated into the wind shear calculations in this chapter, and the feedback between wind flow and dune form described. The analysis of wind flow patterns described in this chapter are integrated in Chapter 5 along with the temporal and spatial geomorphic mapping.

4.1 Methods

Field observation, backed by empirical evidence, informs us that a certain range of atmospheric parameters influence sediment transport within the study region. These include wind speed and wind direction and the linked parameters of air temperature and solar radiation, precipitation and surface moisture (Sherman and Hotta, 1990). Within the context of the Croppies Bay study, questions linked to dune morphodynamics are: how often do effective wind events occur? Is there a distinct seasonal pattern? Are the summer months, with higher incoming solar radiation and higher air temperatures, associated with higher migration rates? What are the long-term atmospheric trends, and what is their influence on migration rates? Determining answers to these questions requires elaboration upon: i) the control that an effective wind regime has on the downwind evolution of an actively mobile long-walled parabolic dune; ii) understanding feedback mechanisms between wind flow and dune shape; iii) the predicted influence of selected atmospheric parameters on coastal dune mobility, and iv) developing short and long-term land management strategies for coastal dunes that abut agricultural land and/or infrastructure (for example, access and arterial roads, water, powerlines).

To answer these questions an in-situ meteorological station was installed to collect wind data over a 2-year period, 2001 to 2003, followed by a detailed analysis of wind speed and wind direction. A large scale (i.e., site remote) analysis of air temperature and solar radiation, precipitation and surface moisture was also undertaken. Rainfall and air temperatures were derived from a Bureau of Meteorology (BoM) site located within 5 km of our study site, and solar radiation data were obtained from a national BoM database. A remote coastal BoM site, Low Head, provides comparative and contemporaneous wind speed data recorded at three-hour intervals, collected on a 10 m mast.

4.1.1 Wind data acquisition and analysis

The wind pattern for the Croppies site was recorded for 511 days by installing a climate station on the eastern portion of the south trailing arm. A Campbell 03101-5 plastic cup anemometer and Met-1 024A wind vane were installed on a 2 m mast (Figure 4.1) and connected to a Campbell 10X data logger powered by a 12 volt closed cell battery. Wind speed was recorded at half hourly intervals and wind direction was recorded by resistance and then vector-averaged, also at half hourly intervals.

The 3-cup anemometer has an operating range of 0 to 50 m/s, gust survival of 60 m/s, and a relatively fast start up threshold of 0.5 m/s. The output frequency is 1 cycle per cup wheel revolution at 0.75 m/s per Hz. This low maintenance instrument is constructed from non-corrosive materials and is specifically designed for long-term use in remote locations with good precision of measurement.

Surface wind data were analysed using the 'WinRose' v0.95, MS-Windows based program (Freeman,.2002). Wind direction and speed were calculated for 8 sectors (sector bins of 45 degrees).

The Bureau of Meteorology provided wind speed and wind direction data for Low Head, Bridport and Swan Island in Excel spreadsheet format. For the period 2000 to 2003, the data are provided in the format of year-month-day, at three hourly intervals (0, 3, 6, 9, 12, 15 18 and 21 hours). The data for the three remote sites were then transposed using a macro function in Excel to acquire day/month/year compatibility with the Croppies Bay wind data. The compatibility of the three remote sites with the Croppies Bay site was determined by applying a standard linear regression analysis, resulting in the selection of Low Head. For the period 1940 to 2003, BoM generated the mean monthly wind speed and wind direction for Low Head in spreadsheet format.

4.1.2 Wind data processing

Data collection from remote field sites is often fraught by equipment failure. For our field program, data collection extended over 700 days resulting in 511 days of wind data that generated 28,134 wind speed/wind direction records (recording rate an average for each 30 minutes). Irregular corruption of data occurred due to equipment failure, including bearing failure in an initial cup anemometer. A "hungry" wombat severed cables to both cup anemometer and wind vane! Corrosion of wiring occurred in a wind vane. A new battery failed to generate adequate power, resulting in the loss of about 12 weeks of data.

The irregular corruption of data due to the above failures resulted in the deletion of nominal sequences of data that, on comparison with Bureau of Meteorology remote site data, were evidently erroneous. This included sequences of calm winds running for several days (235 values, 0.83%), wind speeds above the maximum wind gust (16 values, 0.05%), and wind direction 'fixed' over several days (310 values, 1%). Cumulatively, equipment failure (177 days, or 25%) and cleaning of data (12 days, or 1.7%) resulted in 189 days of lost recording days or edited data.

A field experiment was designed and implemented to measure wind flow that typified the predominant flow pattern close-to-the-bed on windward slopes. The experiment involved the following repetitive actions prior to leaving for Croppies Bay: close monitoring of the national and local meteorological weather pattern on the Bureau of Meteorology web site http://www.bom.gov.au/weather/tas/; coordination of a team of willing field workers who were happy to camp and work in exposed conditions; vehicle bookings; programming the Geography Departments laptop computer; booking access to four data loggers; wiring the thirteen thermo anemometers to the data loggers; followed by a calibration of the thermo anemometers. There were successive attempts at getting into the field, and several separate field trips, to achieve a good representative sample of downwind flow on windward slopes.

A key objective for this experiment entailed establishing a benchmark that linked the close-to-the-bed wind measurements with the on-site climate station (Figure 4.1) to correlate both sets of collected wind speeds with each other. A second option to acquire correlation of data was the remote Bureau of Meteorology site at Low Head, which was statistically evaluated.

4.1.2.1 Short wind phases

The full Croppies Bay wind data set was analysed in a number of ways, one option was to investigate short wind phases that coincided with the intermittent measuring of erosion pin elevation changes and downwind migration of the parabolic dune head. The relationship between wind speed, wind direction and changes in ground surface level are discussed in Chapter 5.

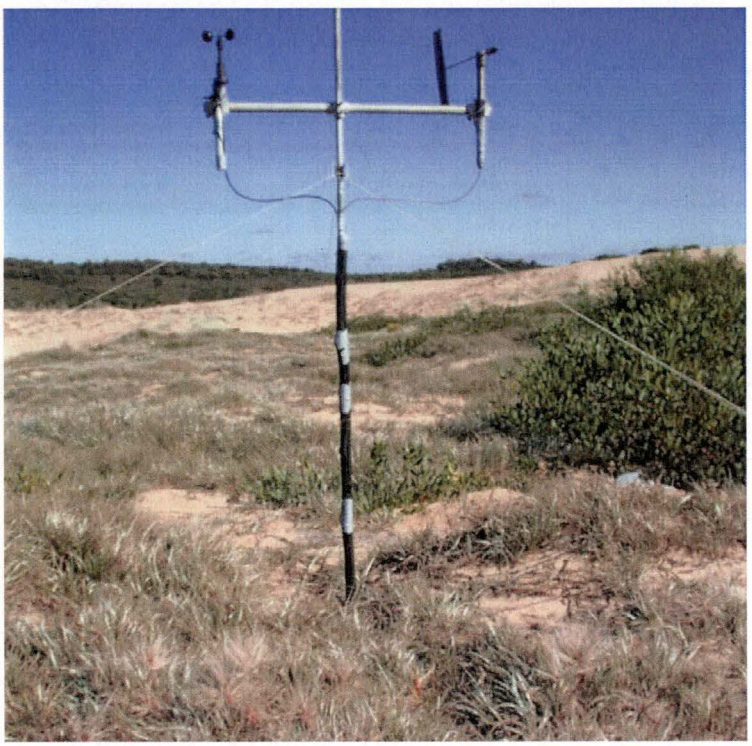

Figure 4.1 2 m mast with cup anemometer and wind vane located on crest of south trailing arm. The cladding is pvc pipe to protect the wiring and deter wombats. View is towards the east with a section of the parabolic dune head mid-field.

4.1.2.2 Flow visualisation

A series of smoke flares were deployed along the stoss, stoss plateau and crest of the lee slip face to enable visualisation of the flow pattern up the stoss and flow separation on the crest and lee slipface. Each smoke flare discharged for an interval of three minutes downwind in wind speeds averaging 7.5 m/s at 45 cm, and 14 m/s at 190 cm above ground surface. The smoke flares were out-of-date standard issue sea distress signals. The flow visualisation was contemporaneous with the measurement of near-surface flow, with the arrays of thermo anemometers mounted on 2 m masts and wind direction finders, between 13.00 and 15.00 hours on September 5, 2003. The results are presented in this Chapter 4.8.4.

4.1.2.3 Flow and form: airflow on stoss and the windward flank of the north trailing arm

The patterns of erosion and deposition in this parabolic dune determine dune morphology and demonstrate the relationship between flow and form. A component of the present study is to elaborate upon the relationship between flow and form by the collection and analysis of airflow on windward slopes, and by the description of wind velocity and wind shear profiles.

To accomplish this task, arrays of thermo anemometers (TAs) and wind vanes were deployed on the stoss and across the dune profile, accompanied by flow visualization. The flow visualisation was recorded photographically, generating a qualitative image of airflow and bedform ripples. The assessment of wind velocity is indicative and reasonably representative of flow at spatial scales of approximately 200 to 500 m along flow, being constrained by the number of TAs and non-sequential measurements between the stoss and across the parabolic dune profile.

Wind velocity was measured along the axis perpendicular to the stoss crest in one simultaneous sample. The across-dune profile was measured from north to south across the lee crest of the north trailing arm (NTA), the windward crest, mid slope and toe of the north trailing arm, the deflation basin and ridge of the south trailing arm (STA). This across-dune transect was undertaken in two separate samples. The locations of the masts on the dune profiles are shown in Figures 4.17 and 4.18. All samples were measured with a downwind flow along the axis of the parabolic dune.

Wind velocity profiles were measured with vertical arrays of three TAs at heights of 15 cm, 45 cm and 190 cm. This placed the lower two TAs (15 cm and 45 cm height above ground surface) within the active saltation layer, and the upper TA within the inner-layer, as defined by Jackson and Hunt (1975). The thirty-minute recording period of each array was synchronised, and one-second measurements from each TA were recorded onto a data logger. Data were downloaded after each sequence on to a laptop computer, and data from each array plotted to ensure data quality. All arrays were sampled during phases of active saltation, with the exception of the deflation basin and south trailing arm crest arrays that had vegetation to a height of 45 cm.

The rate of deflation and deposition was measured simultaneously on windward and lee slopes using a grid of very fine (1 mm) copper erosion pins (welding rods) located 1 m upwind from selected arrays. The results are discussed in Chapter 5, 5.2.5.2.

4.1.3 Design, construction, and calibration of thermo anemometers

An initial field experiment measuring wind flow close-to-the-bed on the stoss with lightweight low inertia cup anemometers was found to be ineffective. The cups stalled due to sediment bombardment or inundation. Subsequently, 13 light, durable TAs were designed, based on circuitry principles illustrated in Unwin (1980:58), and constructed by staff at the Central Science Laboratory (CSL), University of Tasmania, for a total of $1,200.00 ($92 each).

The design used a pair of small platinum resistance sensors (thermistors) with thin film elements (PT100 721-8850) that have a fast response to temperature change (0.3 s) and a temperature range of -50°C to +500°C. One of the sensors is mounted within the circuitry box to measure ambient air temperature; the second sensor (probe) is mounted at the end of a 13 cm length of fibreglass tube (recycled 0.6 mm diameter flexible tent pole) as illustrated in Figure 4.2. Sensors were calibrated in the laboratory to zero air speed by covering the probe in an enclosure to eliminate exposure to small air currents. The circuit design is arranged to pre-heat the probe to 160°C (powered by a 12 volt sealed cell battery) and is compared with the ambient temperature of the covered sensor. The differential between the heated sensor and ambient sensor is conditional on the amount of convective cooling, and hence on wind speed. Within the circuit diagram (Unwin, 1980:58), a resistor (potentiometer) is pre-set to a zero point by shielding the resistor behind a draft excluder, and another component of the circuit sets the range of speeds (0.02 – 20 m/s). Following initial field trials, a thin film of clear nail varnish was painted on the probe sensor to protect against corrosion. Subsequent laboratory calibrations indicated that the varnish did not impede temperature heating or cooling on the probe sensor.

A laboratory experiment was undertaken to determine whether differential heating of the enclosure occurred over the duration of a recording period, with the potential to influence the ambient temperature. The findings (see Appendix 5) indicate that over a thirty-three minute period, there is a drift in the range of 1 m/s between the ambient temperature and the probe (Figure 4.2).

The TAs were calibrated using a standard factory calibrated[1] cup anemometer (Met-One 014A wind speed sensor) mounted on the cabin cross bar of a Toyota utility[2] illustrated in Figure 4.3. The cup and 13 TAs were wired and programmed to a Campbell 10X data logger. A manual on/off switch, operated from within the cabin of the vehicle, controlled the data logger externally. The vehicle was driven continuously at a range of different speeds (6, 10, 15, 20, 25, 40, 50 and 60 km/hr[3]) on a calm day with an average four-minute recording period for each speed category, alternating with short duration intervals with the TAs switched 'off' between each recording sequence. The 'off' intervals enabled the calibration of the duration of effective heating for each sensor.

---

[1] Calibration speeds for the TAs were derived solely from the factory calibrated cup anemometer.

[2] The vehicular method of calibrating the TAs was adopted due to the prohibitive expense of calibrating in the wind tunnel.

[3] Equivalent m/s: 1.66; 2.77; 4.16; 5.55; 6.94; 11.1; 13.88 and 16.6.

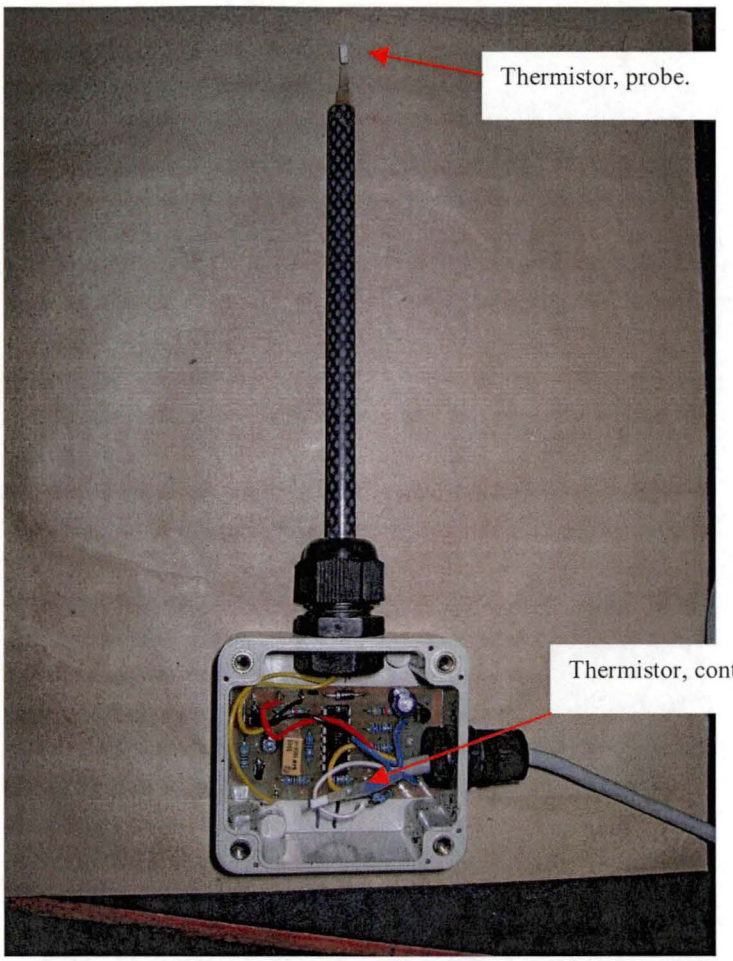

Figure 4.2. Thermo anemometer with protective cover removed to show circuitry.

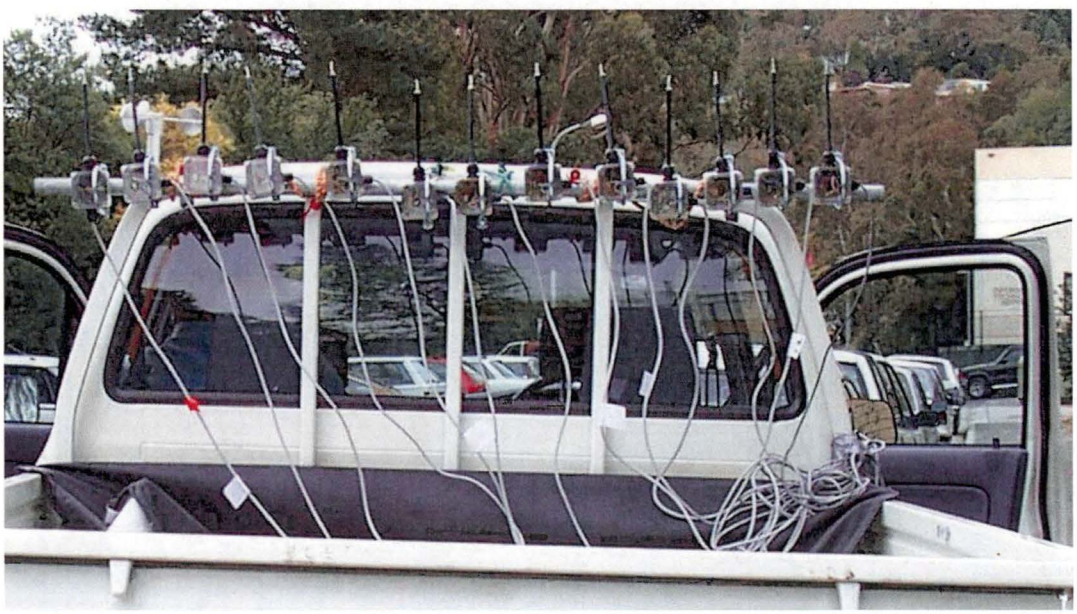

Figure 4.3 Thermo anemometer calibration technique.

To acquire a comparison with the vehicular calibration method, the 13 TAs and cup anemometer were calibrated at night in windy conditions with the instrument array placed on the sports ground oval. The output from this stationary calibration, with a range of outputs in the lower range of wind speeds – 1 to 10 m/s, gave equivalent results (within instrumental uncertainty) to the outputs from the vehicular calibration in the same range of wind speeds. Butterfield (1999:32) established that '*the primary response of saltation to change in wind velocity occurs in about 1 s*'. His finding informed the recording interval for this study.

The data from the cup and 13 TAs were then calibrated against each other to derive a regression equation that could be applied to the subsequent conversion of field wind speeds. Figures 4.4a,b are representative examples of this method, with all thirteen sensors having correlation coefficients > 0.92, with regression equations typically in the form of polynomial equations or exponential equations.

Figure 4.4a illustrates the initial method of calibration, which was derived using polynomial equations, to fourth order. However, it was not deemed to be the best fit for lower wind speed values, despite the high correlation coefficient (r^2) values. Figure 4.4b illustrates the optimal method, which entailed sorting values into bins of 1 m/s increments through to 20 m/s. This was followed by a two stage curve fitting, comprised of mean wind speed values in individual categories of < 4 m/s [(0 to 4 m/s) with a range in the r^2 values between 0.90 and 0.96], and increments of 1 m/s through to the highest wind speed category (5 to 20 m/s) [with a range in the r^2 values between 0.97 and 0.99], and fitting equations to the data. The mean wind speed value for each bin was used in subsequent calibrations.

The form of the wind speed calibration curves indicates that higher wind speeds could be accurately determined using the calibration curves.

For data acquisition in the field, four all-weather instrument boxes, each containing a sealed 12 volt battery and data logger wired to 3 TAs and an external on/off switch, were deployed on four light weight 2 m aluminium masts (Figure 4.5). Thermo anemometers were set at heights of 190 cm, 45 cm and 15 cm and run for 30-minute intervals, preceded by a programmed 'warm-up' phase of 3 minutes. Each sequence of data collection was downloaded on-site to a laptop computer. The data collected from each mast were assessed for data quality and data intercompared between masts. Twelve manual wind direction sensors were deployed on the 2 m masts at the same heights (15 cm, 45 cm, 190 cm) as the TAs, and wind directions were recorded at three-minute intervals with a magnetic compass.

An in-situ climate station was used as the benchmark for correlation with wind speeds collected with the TAs, complemented with data collected by the BoM at the remote site of Low Head, located 50 km south west of Croppies Bay.

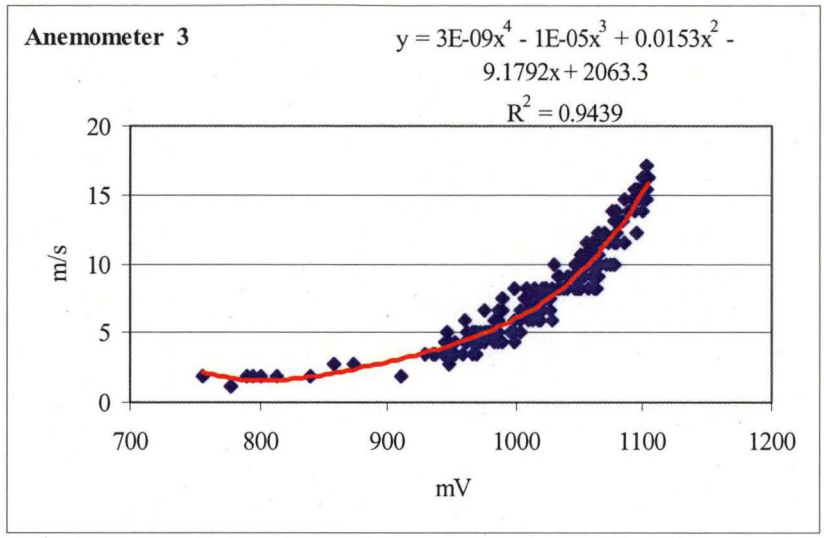

Figure 4.4a. An example of the initial method of calibration of cup and thermo anemometers.

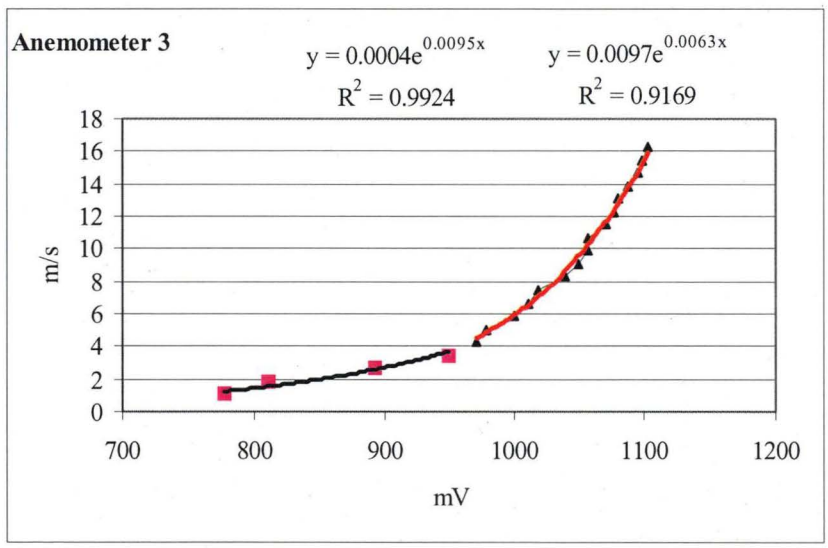

Figure 4.4b. An example of the optimal method of calibration of cup and thermo anemometers.

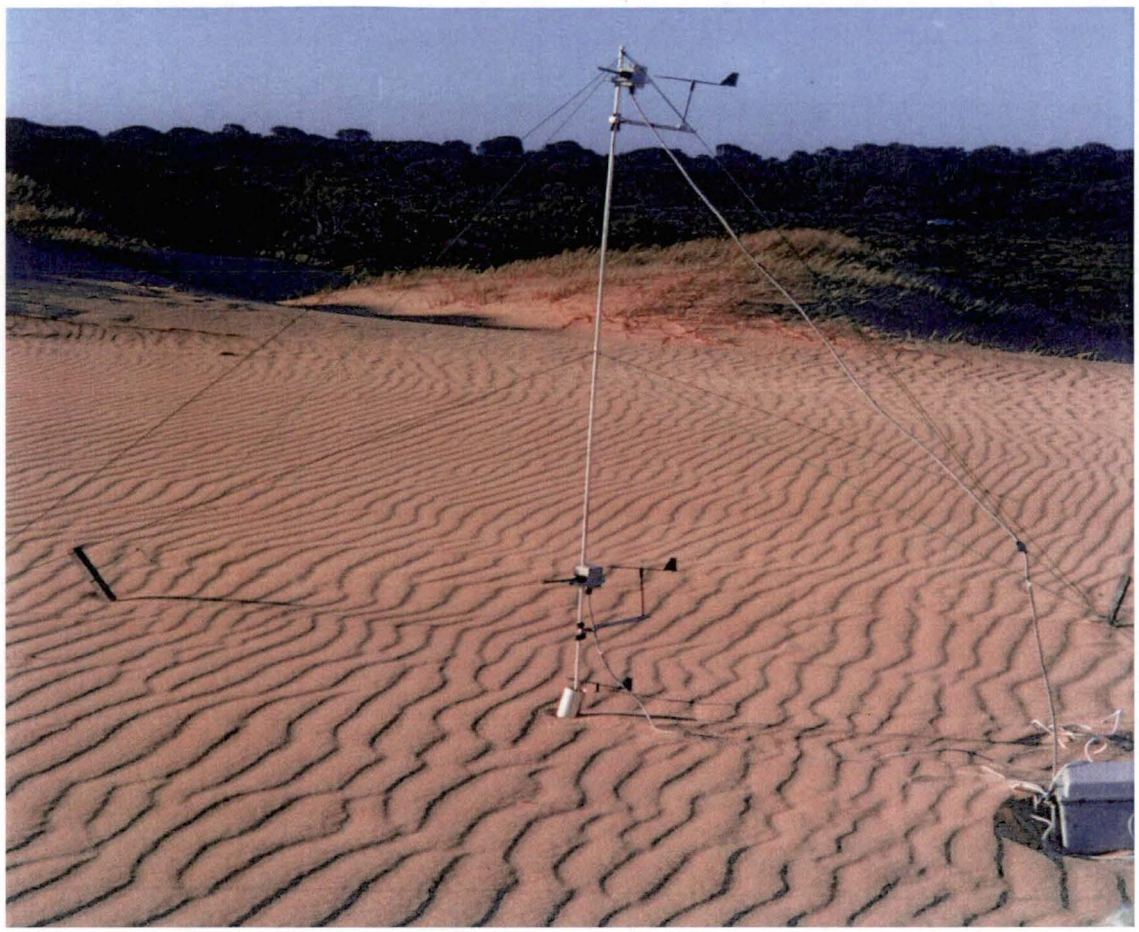

Figure 4.5. Light weight aluminium 2 m mast with thermo anemometers and wind vanes connected to a data logger powered by a 12 volt closed cell battery housed in an instrument box. Thermo anemometers and wind vanes at heights 15 cm, 45 cm and 190 cm above the ground surface. The 15 cm thermo anemometer remains to be installed in this photograph. Figure 4.19 shows the location of the transect sample sites.

4.2 Results and discussion

This section of the thesis presents the results generated from measuring the wind regime. Components of the previous chapter on sediment and grain characteristics are included in the analysis. This section progresses sequentially from the large scale regional climate pattern that influences the Croppies Bay study site, such as wind flow, air temperature, evaporation, rainfall and solar radiation, to the site specific wind patterns and wind resultant sand roses that result in sand transport. This, in turn, is followed by the more specific measurements of wind flow close to the bed on windward slopes, incorporating wind shear velocity, speed-up ratios and flow visualisation. The results of the site-specific wind patterns and the close-to-the-bed measurements are then integrated to generate an understanding of the feedback between flow and form in a parabolic dune. This is followed by an analysis of sand dune mobility indices, based on selected atmospheric parameters, to gauge their capacity in assessing coastal dune mobility. To finish, there is an analysis of the atmospheric parameters of air temperature, rainfall and wind speed, to investigate future trends in dune activity.

4.2.1 Croppies Bay climate

4.2.1.1 Air temperature

BoM data collected at Bridport and Low Head for the period 1940 to 2003 indicate that the pattern of maximum air temperatures range between mid 20s in summer to mid teens in winter. July and August are the coolest months (diurnal range 16°C to -0.2°C). Frost was experienced on site. Characteristically, summer minimum temperatures are higher, winter lower. Table 4.1 indicates the range of seasonal and monthly air temperatures recorded at Waterhouse Station, 5 km south of the Croppies Bay study site.

Table 4.1. Seasonal air temperature (°C), Waterhouse Station 1994 to 2003.

	Summer			Autumn			Winter			Spring			
Month	Dec	Jan	Feb	March	April	May	June	July	Aug	Sept	Oct	Nov	Year
Maximum	25.6	27	26.7	25	21.6	19.4	16.8	15.6	16.3	18	21.3	23.3	21.4
Minimum	6	7.6	7.25	5.5	2.74	2.17	1.25	0.02	0.02	1.5	2.15	3.1	3.2

4.2.1.2 Rainfall and evaporation

The average yearly rainfall for the site is 670 mm. The general rainfall pattern is a dry summer period that extends into early autumn, with an average monthly rainfall of 41 mm. Winter is moist with an average monthly rainfall of 69 mm, followed by a decline in spring to a monthly average of 59 mm. Dews contribute moisture to the ground surface during autumn and early spring. Fifty-nine percent of the total annual rainfall falls between late autumn and spring, 17% of rainfall falls mid summer to early autumn.

Figure 4.6 compares rainfall and pan evaporation for Tomahawk, located 14 km east of Croppies Bay. Figure 4.6 shows that over the duration of six months, incorporating late spring, summer and autumn, pan evaporation exceeds rainfall, generating a deficit of 253 mm (average annual pan evaporation is 923 mm; mean pan evaporation is 77 mm). The average evaporation values in Figure 4.6 are indicative because the values were obtained from pan evaporation rates obtained from a site 35 km inland. Bowden (1981) established that the pan evaporation rate at Tomahawk is 1.3 times greater than at Scottsdale (35 km inland) probably due to the higher insolation of the sand plains. Bowden found that "pan evaporation at Scottsdale is approximately 77 percent of that at Tomahawk, and as evapotranspiration in Tasmanian conditions is estimated to be between 70 percent and 80 percent of pan evaporation, the figures for Scottsdale can be used as an approximation to Tomahawk" (Bowden, 1981:235). Based on Bowden's (1981) finding, and contemporaneous analysis of pan evaporation data for the northeast region of Tasmania (MacKinnon 1980; BoM, 2004), the present study finds the Scottsdale evapotranspiration data contextually relevant for the study site.

Effective precipitation occurs between early April to mid September, declining during the summer months when evapotranspiration rises to its maximum.

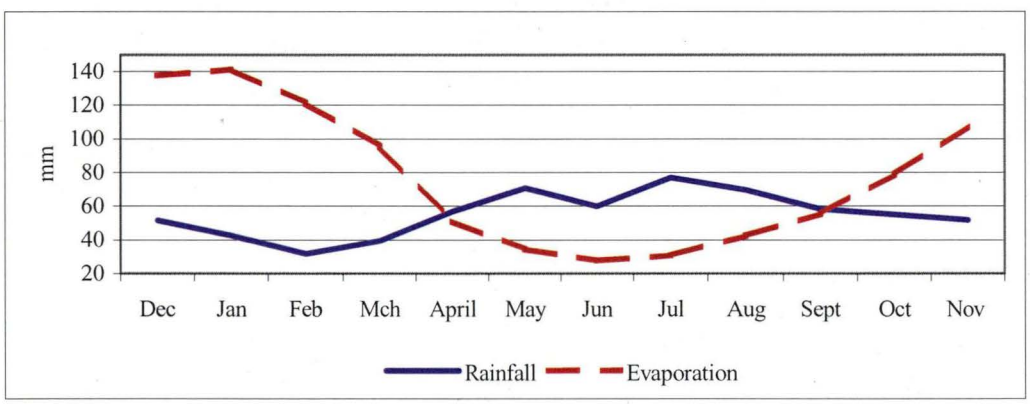

Figure 4.6 Mean monthly rainfall and evaporation, 1960 – 2003.
Rainfall data collected at Waterhouse Station; evaporation data from Scottsdale, BoM, Hobart.

4.2.1.3 Solar radiation

Incoming short-wave radiation on sand surfaces influences sand moisture content by controlling evaporation rates.

The latitude of Croppies Bay is S 40° 9', and results in a mid-summer sun reaching an elevation of 72°, and mid-winter elevation of 25°. The longest day is 15.1 hours and shortest day 9.2 hours. Summer receives the highest average sunshine hours of 8.6 hrs, followed by spring (7.0 hrs), and winter 4.2 hours (Table 4.2).

Incoming solar radiation follows a similar pattern to sunlight hours, with late spring and summer averaging 25.8 MJ/m^2, (BoM, 2003) and declining sharply to mid winter averaging 5.5 MJ/m^2. The BoM 1990-2003 solar radiation measurements are actual and recorded at 40.5°S, 147.3°E.

Table 4.2. Seasonal solar radiation (MJ/m^2) for Croppies Bay, 1990 – 2003.

Month	Dec	Jan	Feb	Mar	April	May	June	July	Aug	Sept	Oct	Nov
Mean	27.28	25.31	24.86	18.95	13.2	9.43	5.51	8.04	9.59	16.31	20.63	26.18
Std Dev	8.16	8.57	5.15	4.94	3.72	2.2	1.71	1.91	3.51	3.84	5.34	7.18

4.3 Wind Pattern

The predominant wind pattern at Croppies Bay[4] (Figure 4.7), based on approximately two years of measurements, is typified by a prevailing westerly and southwesterly flow with a mean site wind speed of 8.1 m/s, and site maximum wind speed of 48 m/s. Thirty-two percent of wind flow occurs below 4.5 m/s, which represents the threshold below which effective sediment transport does not occur; about seventeen percent of this class is comprised of wind speeds below 1 m/s. Sediment transport winds occur from the east and southeast for twenty percent of the year, effectively 'stalling' downwind migration.

High velocity wind events, characterised by the average number of days with records of wind speeds greater than 12 m/s occur 29% of the year[5], summer and autumn have the highest frequency of high velocity winds (Table 4.3). Spring and winter have the highest frequency of wind speeds below 4.5 m/s.

Table 4.3. Croppies Bay wind pattern.

	Frequency (%)				
Classes (m/s)	Year	Summer Dec – Feb	Autumn March – May	Winter June – Aug	Spring Sept – Nov
< 4.4	29	23	25	36	34
4.5 to 11.9	42	41	48	37	41
>12 to >20	29	36	27	26	25
Wind direction (W) and Maximum wind speed (m/s)	(SW) 48	(W) 39	(W) 29	(SW) 48	(W) 28
Ave maximum wind speed (m/s)	35	24	23	34	16
Wind direction (W) and Minimum wind speed (m/s)	(S) 8	(S) 7	(S) 7	(N) 7	(SE) 7
Ave minimum wind speed (m/s)	10	11	10	10	10

4.3.1 Seasonal and diurnal wind pattern

There is a distinct seasonal and diurnal pattern to the wind flow, as indicated in Figures 4.8 to 4.11, although the prevailing wind flow from the west is strongest in all seasons in the daytime period 12:00 – 18:00.

During winter (June – August), effective wind flow is predominantly from the west exceeding threshold velocity on average 16% of the day, and progressing in duration sequentially from 0:00 – 06:00 hrs (14%), to an average of 22% between 12:00 – 18:00 hours, and declining to 16% between 18:00 – 24:00 hours. Figure 4.8 indicates a consistent easterly flow which exceeds on average 20% diurnally, but characterized, with the exception of the 12:00 – 18:00 period, by a higher proportion of wind speeds in the > 4 to < 8 m/s category, compared with westerly winds.

[4] Determined from an on-site climate station at a height of 2 m above ground surface.
[5] For the entire recording period of 511 days, 3,682 hours recorded wind speeds > 12 m/s (30%), and within this class, 647 hours recorded wind speeds > 20 m/s (5%).

Notably, the winter season experiences the lowest influence of northerly sector winds, due in part to seasonal zonal flow.

The spring (September – November) wind pattern, Figure 4.9, is characterized by westerly and south westerly flows, with a higher proportion of westerly winds exceeding > 20 m/s. The influence of easterly winds persists, but with a lower proportion of effective sediment transport flows, compared with the westerly sector flows. Northerly sector winds increase their influence on the site, increasing in proportion from morning to afternoon, and declining between evening and midnight.

The summer (December – February) wind pattern (Figure 4.10) is again dominated by an effective westerly flow particularly 12:00 – 18:00 hours, when 38% of wind flow exceeds threshold velocity. Evening to early morning (18:00 – 06:00) has a higher proportion of southwesterly flow, which is replaced by predominantly northeasterly wind as the day warms. The influence of easterly flow remains present but is of least influence during this season.

Autumn (March – May), Figure 4.11, has the lowest proportion of 'calm'[6] periods for all seasons (25%, yearly mean 36%) consistent with a seasonal transition in the westerly wind belt. West and southwest sector winds predominate, with the exception of the 12:00 – 18:00 period, when the southwesterly winds are replaced by northeasterly winds.

The thermally driven land-sea breeze system has been observed at this study site and is associated with the warmer months, commencing generally in late spring and occurring intermittently throughout summer until late autumn. The duration of this wind is longest during summer, extending over 4 to 5 hours. Wind direction generally changes late morning, re-changing direction in mid afternoon. Commencement of this wind orientation occurs later in the day, and is of shorter duration in spring and autumn. Progressively, this window truncates as solar radiation declines. Field observation and on-site wind data indicate this land-sea breeze is effective in transporting sediment and its influence is incorporated in the sand roses, which are discussed below.

[6] Calculated wind flow occurring below 4.5 m/s is the threshold below which effective sediment transport, with a mean grain size for the site of 2.45 ø, does not occur.

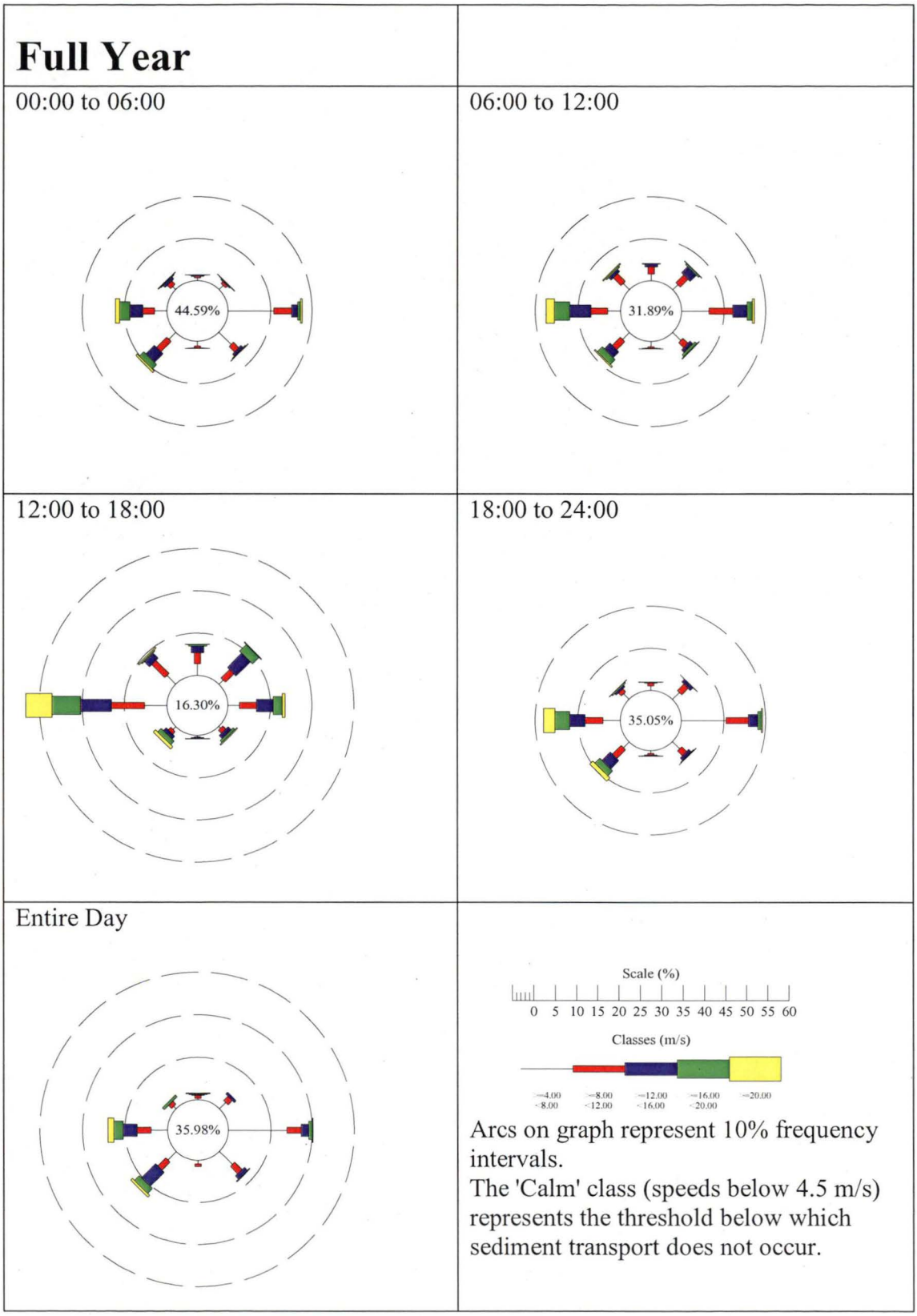

Figure 4.7. Full year wind rose, Croppies Bay.

Winter

00:00 to 06:00

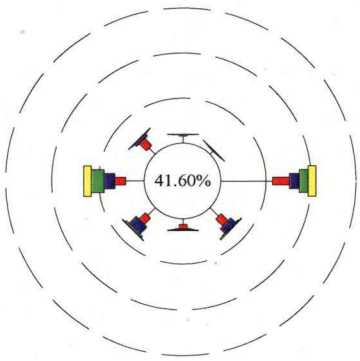

06:00 to 12:00

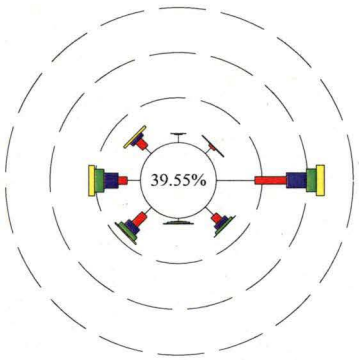

12:00 to 18:00

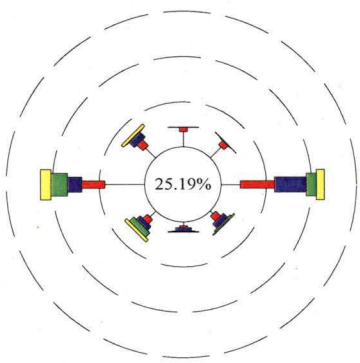

18:00 to 24:00

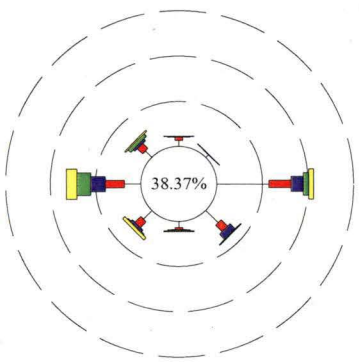

Entire Day

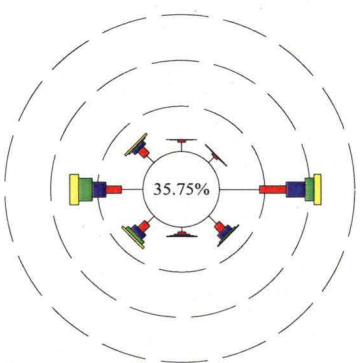

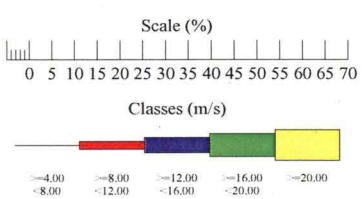

Arcs on graph represent 10% frequency intervals.
The 'Calm' class (speeds below 4.5 m/s) represents the threshold below which sediment transport does not occur.

Figure 4.8. Winter wind rose, Croppies Bay.

Spring

00:00 to 06:00

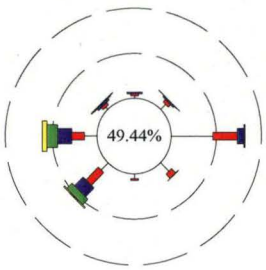

06:00 to 12:00

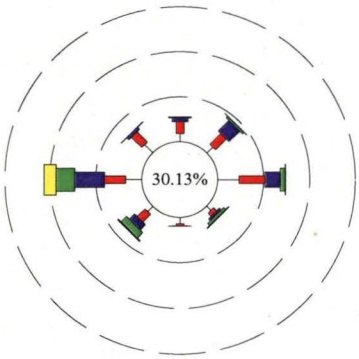

12:00 to 18:00

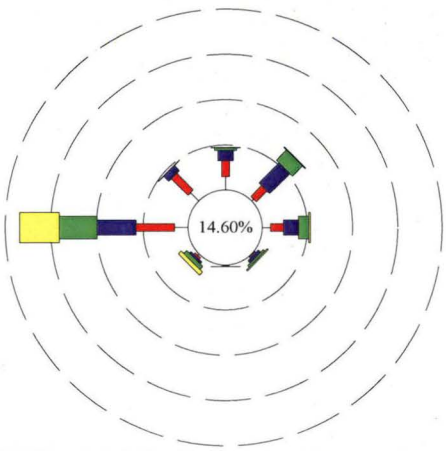

18:00 to 24:00

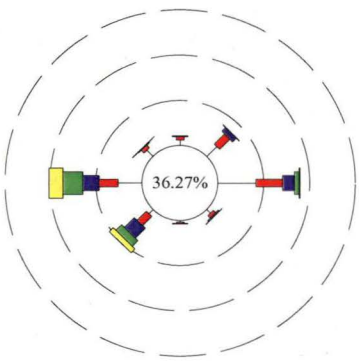

Entire Day

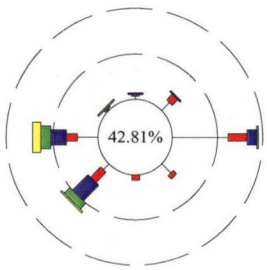

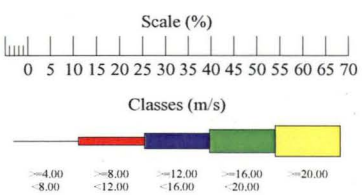

Arcs on graph represent 10% frequency intervals.
The 'Calm' class (speeds below 4.5 m/s) represents the threshold below which sediment transport does not occur.

Figure 4.9. Spring wind roses, Croppies Bay.

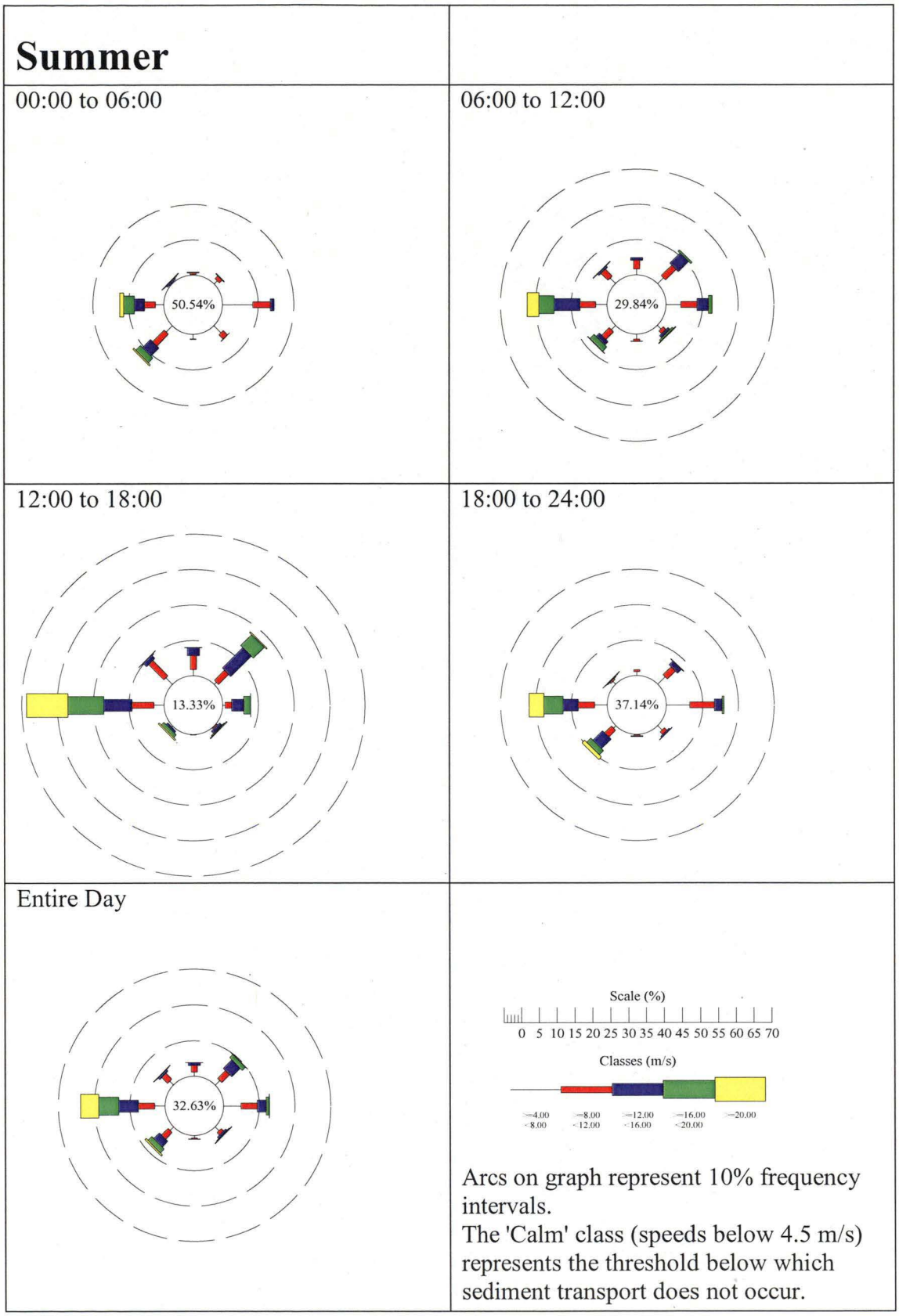

Figure 4.10. Summer wind rose, Croppies Bay.

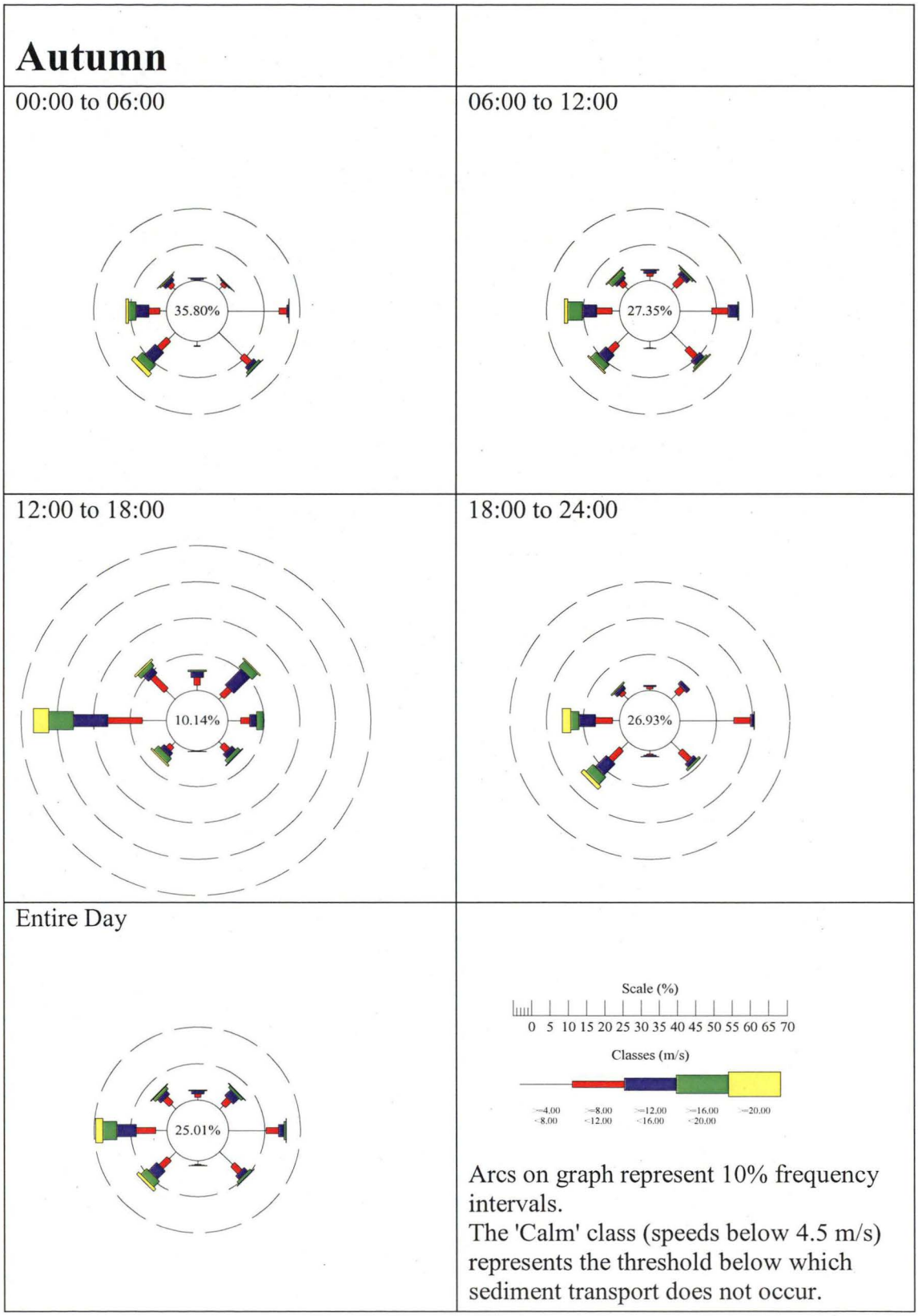

Figure 4.11. Autumn wind rose, Croppies Bay.

4.4 Remote and on-site wind data

To determine the influence of long (fifty years) and short period (seventeen months) wind patterns on dune morphodynamics at Croppies Bay, a comparative analysis of the compatibility of remote BoM sites – Bridport (20 km South West), Swan Island (45 km North East) and Low Head (65 km West) – was undertaken, with the aim of acquiring a remote benchmark which had wind speeds and wind direction that may be correlated with Croppies Bay. Subsequent analysis of the wind data from the three BoM sites resulted in the selection of Low Head. Low Head and Croppies Bay have correlation coefficient values of 0.47 using three hourly data for wind speed and wind direction, with increasing correlation for data comparisons at daily (0.66) and monthly (0.64) intervals.

Figure 4.12 confirms the findings of other authors (Hesp and Hyde, 1996; Pluis, 1992; Wiggs and Livingstone et al, 1996; Walker and Nickling, 2002; Jackson and Hunt, 1975) that dune morphology is not effectively explained by regional or remote wind patterns. The wind speeds collected from an in-situ 2 m mast indicate that wind speed values extend over a wider range representing a higher proportion of ineffective sediment transport (< 4.5 m/s), and a broader spectrum of potential sediment transport including a higher proportion of high velocity winds. In comparison, the remote site, in this instance, indicates that the pattern of wind speeds derived from a 10 m mast have a higher proportion of low wind speeds and lower proportions of calms and high velocity winds, and a higher proportion of wind speeds occurring in the 6 to 12 m/s categories. Therefore, no wind speed proxy could be used for Croppies Bay.

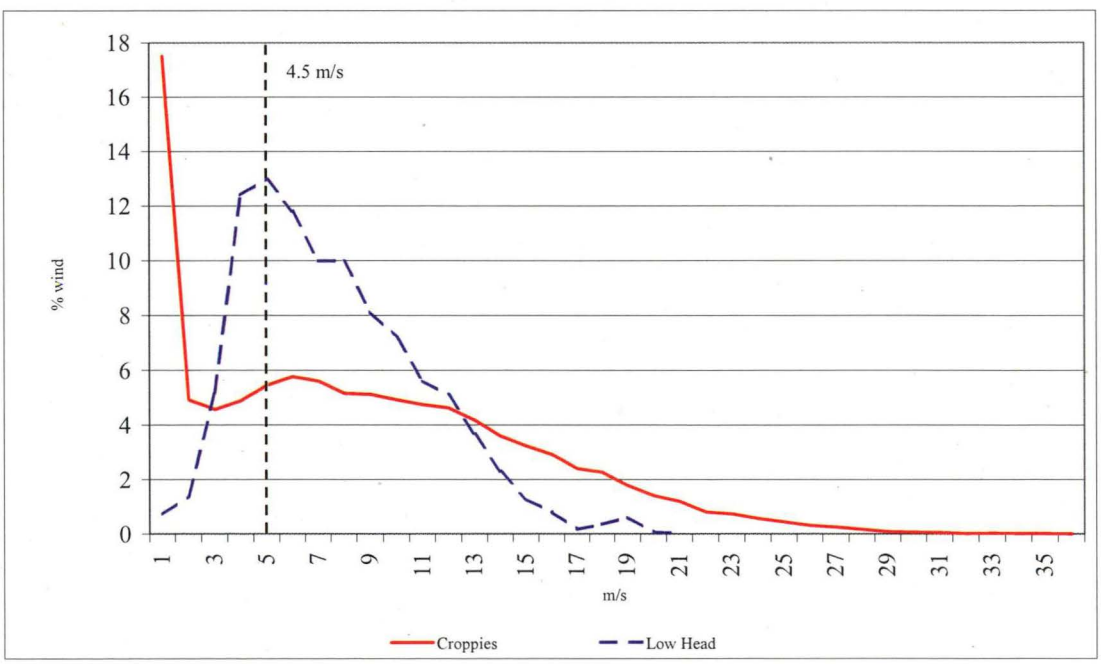

Figure 4.12. Comparison of mean remote (Low Head, 10 m mast) and on-site (Croppies Bay, 2 m mast) wind speeds.

4.5 Wind resultant sand roses

The present study applied Fryberger's (1980) method to generate a series of wind resultant sand roses (bins of 22.5 degrees) to evaluate the potential sediment transport by wind with speeds of 6 m/s and above. To achieve consistency in comparison between the present study and similar studies, (for example Anthonsen (1997), Bailey and Bristow (2004), Tsoar and Arens (2004), Fryberger (1980)) a threshold wind speed of 6 m/s was applied, rather than the Croppies Bay 4.5 m/s. Wind resultant data were analysed using the WRPlot program located at www.lakes-environmental.com website to generate the roses. Conversion of the wind data to sand roses (Fryberger, 1980: Bullard, 1997:500) generates the drift potential (DP[7]), resultant drift direction (RDD), resultant drift potential (RDP) and the measure of variability in wind direction (RDP/DP). These parameters express the net trend of sand transport and net trend of dune migration occurring under the influence of effective sand moving winds. This index provides a measure of potential rather than actual sand flow due to reliance on estimated variables in Bagnold's Equation 4.1 (Pye and Tsoar, 1990)

Figure 4.13b shows that the annual resultant drift potential (RDP) for the present study site is 7652 Vector Units (VU), with an annual resultant drift direction (RDD) of 69° azimuth. This figure, and Table 4.4, also shows the range in RDP (150 to 2659 VU) that corresponds with the intervals of measuring elevation changes on erosion pins. Sixty percent of recorded wind events generated DPs greater than 1000, with an autumn recording period generating a DP of 2671 VU (Table 4.4). This high DP demonstrates that the site experiences narrow unimodal wind events that translate into relatively short and effective high rates of sediment transport. It also demonstrates the merit in recording and analysing on-site short-term wind events rather than relying on averaged annual rates to assess the process-response feedback, entailed in the morphodynamic evolution on dune form.

When compared with other coastal parabolic dune studies, the RDP of 7652 VU for the Croppies Bay site is moderate. This can be partially explained by the distinction between on-site recording of wind pattern at Croppies Bay and the remote recording of wind pattern from 10 m masts by other authors. Bailey and Bristow (2004) reported an RDP of 1657 VU and a DP of 2084 VU for parabolic dunes at Aberffraw, Anglesey, north Wales over a period of 29 years. Arens (Tsoar and Arens, 2004) reported a DP of 1224 VU for coastal parabolic dunes at IJmuiden, Netherlands.

Anthonsen (1997) reported a low RDP of 379, a DP of 3598 VU, RDP/DP of 0.11 for a parabolic dune at Skagen Odde, Denmark for 1986. Anthonsen (1997) demonstrated that DP fluctuated over the 109 years (1877 to 1986) of her study, commencing at RDP 650, DP 2131 VU in 1877, declining to RDP 475, DP 2185 VU in 1924, and RDP 382, DP 2291 VU in 1966, followed by an increase to RDP 582, DP 3371 VU in 1977, and another decrease in 1986.

---

[7] The unit of measurement used for winds throughout this study is m/s (SI units). The vector units that comprise the DPs have been derived in m/s.

Table 4.4 shows the results of an analysis of the seasonal variability in DP and RDP/DP (a measure of variability in wind direction). Seasonal vector averaged wind speeds indicate that summer, autumn and spring have potentially higher resultant distances of sand transport than winter. The data are constrained by the 511 days duration of field measurements.

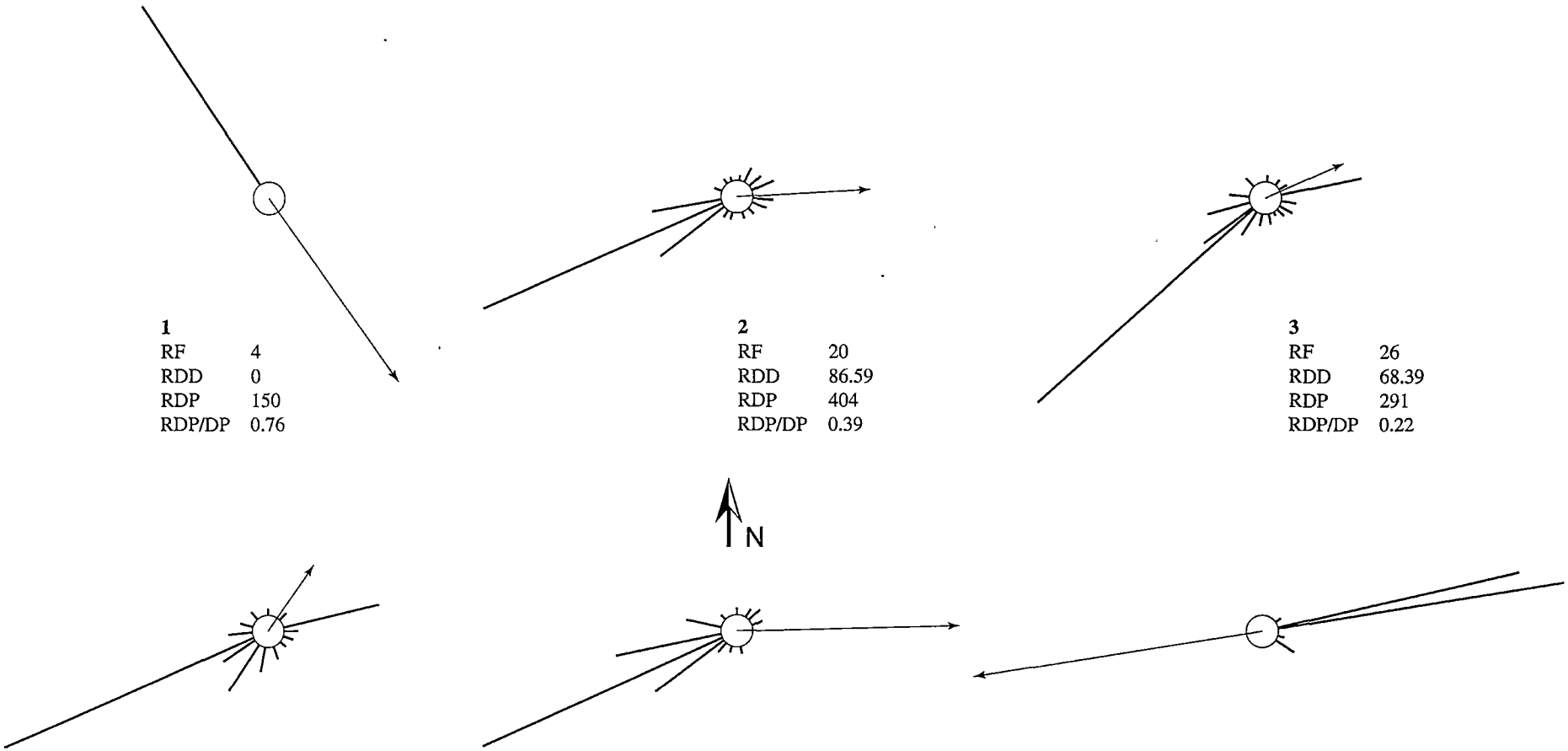

Figure 4.13a. Wind resultant sand roses, 1 to 6 (bins of 22.5°). RF: reduction factor; RDD: resultant drift direction; RDP: resultant drift potential.

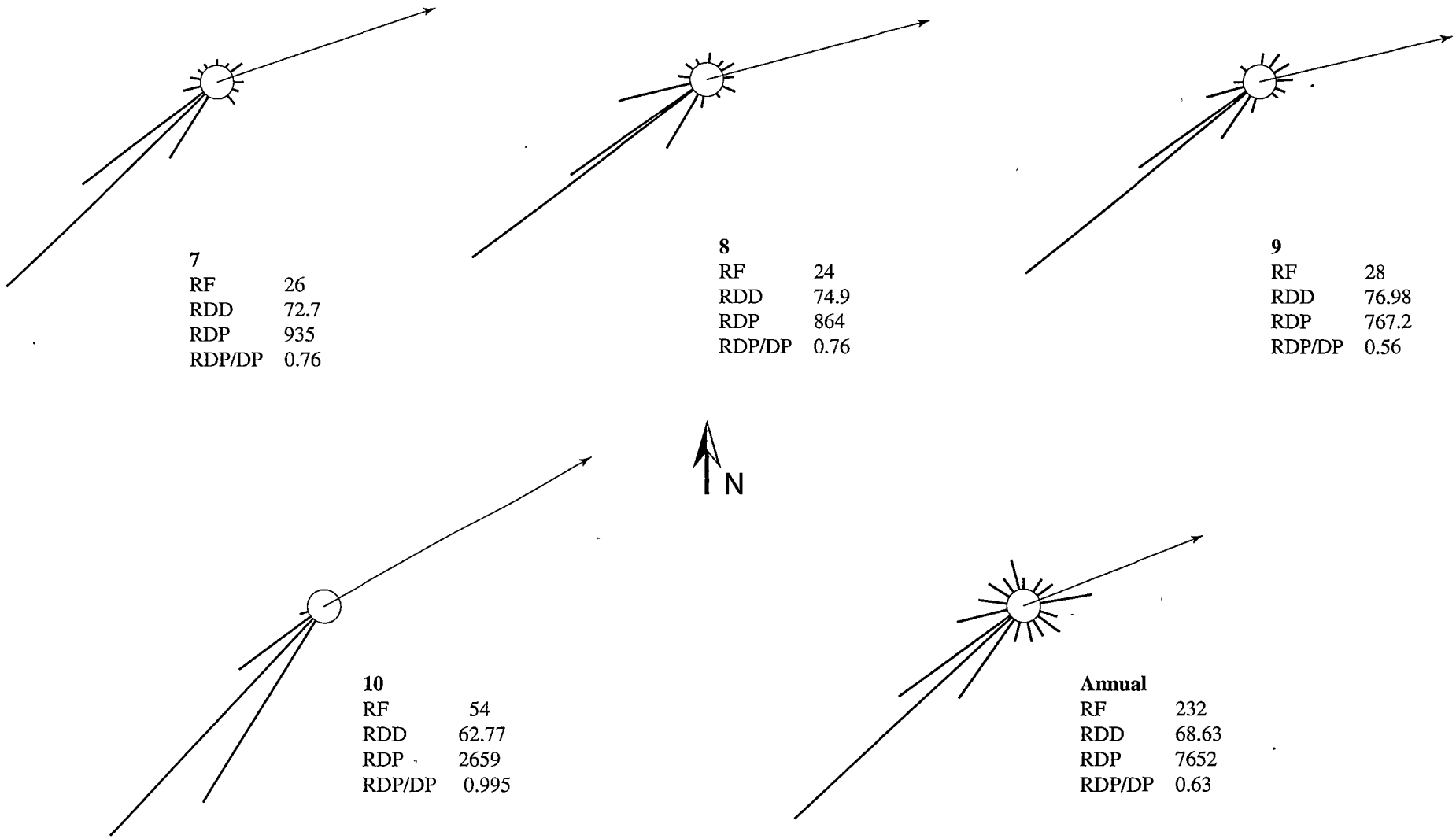

Figure 4.13b. Wind resultant sand roses, 7 to 10, Annual (bins of 22.5°). DP: Drift potential.-

Table 4.4. Croppies Bay drift potentials (DP) and annual drift potential (data is linked to the measurement of ground surface elevation changes at erosion pins, 5.2.5 Surface Elevation Changes, pp 129-131. Appendix 3).

Sand Rose Number		1	2	3	4	5	6	7	8	9	10	**Annual Drift Potential**
Wind Direction		Total Drift Potential (DP)										
N	10 °	0	23.73	10.22	8.71	2.17	0	21.54	18.62	27.7	0	**112.7**
NNE	32.5	0	51.89	6.45	5.9	15.08	0	19.41	18.6	62.7	0	**180.0**
NE	55	0	56.828	17.58	17.18	33.93	12.87	42.2	40.77	81.2	0	**302.5**
ENE	77.5	0	60.426	355.03	431.93	14.76	797.17	21.74	20.77	59.5	0	**1761.3**
E	100	0	65.493	60.16	54.27	0.25	15.99	0.64	0.59	43.3	0	**240.7**
ESE	122.5	0	50.917	28.35	36.39	0	67.55	28.97	23.79	11.8	0	**247.8**
SE	145	0	1.022	5.02	11.19	0	17.43	1.22	1.02	2.28	0	**39.2**
SSE	167.5	0	9.045	29.36	23.07	3.4	0	1.13	1.63	3.02	0	**70.7**
S	190	0	13.075	31.18	27.08	6.56	0	17.58	15.7	34.4	0	**145.6**
SSW	212.5	0	15.3	109.19	92.69	36.47	0	282.6	234.5	211.0	1910.2	**2892.0**
SW	235	0	275.466	263.08	216.92	229.47	0	654.8	572.4	592.3	747.2	**3551.6**
WSW	257.5	0	237.778	210.38	176.58	297.8	0	78.9	125.2	176.7	13.9	**1317.3**
WSW	280	0	53.47	113.9	92.69	81.71	0	29	38.66	25.5	0	**435.0**
WNW	302.5	0	40.03	50.5	40.91	7.33	0	10.29	9.67	13.02	0	**171.8**
NW	325	0	10.88	8.73	7.43	1.29	0	9.85	8.18	7.84	0	**54.2**
NNW	347.5	150.46	9.64	3.16	3.1	0.43	0	6.64	5.61	15.74	0	**194.8**
Total DP for all directions		150.46	974.99	1302.29	1246	730.65	911.01	1226.5	1135.6	1368.0	2671.4	**11716.9**
Reduction factor [1]		4	20	26	26	16	18	26	24	28	54	232
RDD °		0	86.59	68.39	34.29	88.83	265.04	72.7	74.9	76.98	62.77	480.41
RDP		150	403.54	290.9	127.38	579.7	874.4	935.38	864.3	767.15	2658.5	7651.65
RDP/DP		0.76	0.39	0.22	0.1	0.79	0.959	0.76	0.76	0.56	0.995	0.629

[1]Reduction factor – all vector unit totals are divided by 2 until the longest arm of a sand rose can be plotted at < 50 mm (Fryberger, 1980:147).

A comparative analysis of Fryberger's (1980:149) RDP/DP categories of low (0.0 to < 0.3), intermediate (0.3 to < 0.8) and high (> 0.8) indicates the categories are transferable to the wind regimes of coastal environments.

Figure 4.13b, 'Annual' shows that the annual RDP/DP for the study site has an intermediate variability in wind direction at 0.63, with a wide unimodal wind regime. Outliers from this intermediate category are the autumn (RDP/DP 0.96) and spring (RDP/DP 1.0) high categories (Figure 4.13a, b, wind resultants 6 and 10), with narrow unimodal wind regimes, indicative of low directional variability in wind flow resulting in high RDP and RDD values. The winter outlier occurs in a low category (RDP/DP < 0.2), indicative of greater variability in wind direction resulting in lower resultant drift directions (RDD) and resultant drift potentials (RDP) (Figure 4.13a, wind resultants 3 and 4; Table 4.4).

Table 4.5. Vector average wind speed by season

Season	Year	Speed m/s	Direction
Summer	2000	7	267
Autumn	2000	1.1	248
Winter	2000	1.1	284
Spring	2000	2	357
Summer	2001	2.4	283
Autumn	2001	1.4	249
Winter	2001	1	162
Spring	2001	1.4	258
Summer	2002	0.5	262
Autumn	2002	3.2	249
Total		**1.7**	**258**

Each of the prime 16 compass directions contain effective winds, as illustrated in Figures 4.13a and b and Table 4.5. The predominant sand transport direction originates from the SW sector (with an aggregate annual drift potential (DP) of 7761, comprising sixty six percent of the annual drift potential) and drives the downwind and lateral migration of the parabolic dune. However, the short-term effective winds originating from the east, shown in Figure 4.13a and b, wind resultants 3, 4, 6 and Annual, truncate the RDP and skew the RDD towards the ENE. This easterly sector influence directly influences the morphodynamics of the dune, and this will be discussed in the next chapter.

In summary, Croppies Bay has an intermediate-energy wind environment, with an annual drift potential of 7652 (VU). Seasonal, vector-averaged, winds speeds indicate that summer and autumn have higher resultant drift potential than spring and winter. The predominant sand transport direction originates from the SW sector and drives lateral migration of the parabolic dune.

4.6 Sand Transport Rate

Potential sand movement rates were calculated using the Lettau and Lettau (1978) Equation 2.8. The values for Croppies Bay are shown below in Table 4.6.

Table 4.6. Units used to calculate the sand transport rate applying Equation 2.8.

c.g.s. units	Stoss	Flank
C_2	4.2	4.2
u_* cms^{-1} (mean)	145	126
u_{*t} cms^{-1}	450	450
d (mean cm)	0.025	0.037
D (cm)	0.025	0.025
q	16.8	15.2

Actual transport rates on the stoss at Croppies Bay are significantly lower than those predicted by Equation 2.8. Equation 2.8 predicted annual values of sediment transport in the range of 1,000 m. To achieve the field measured distances of 21.5 m / year downwind migration, the calculated q value for Equation 2.8 would need to equal 0.077, rather than the q value of 16.8 shown in Table 4.6 for the stoss.

Rasmussen (1989:138) reported similar discrepancies resulting from measurements of near surface flow on a beach with saltation, giving a $z_0 \approx 3$ mm for a friction speed of 0.63 m/s, nearly 7 times greater than that predicted by the equation. Rasmussen could not identify a clear cause for these discrepancies.

Some of the discrepancies between the actual and predicted rates of transport may be attributed to the original laboratory based methods that were applied to formulate the equations. These methods were based on wind tunnel studies using steady and uniform wind speeds flowing over dry, uniform sand grains for periods of 10 minutes.

Field conditions are more complex for determining transport rates. For example at Croppies Bay the following factors were observed: mixed sand grain characteristics (4.06 to 0.47Ø; variable sorting from very fine to coarse, and variable grain density – packing of the bed), and slope angles between 23° to 30°. Solar radiation dries the bed, which increases the availability of sediment for transport, arguably resulting in an increase in fetch. This drying process is offset by intermittent periods of cloud cover, which may reduce drying of sediment. All of these field-based variables are accompanied by fluctuations in wind speed, which probably dampens the feedback between effective wind velocity and sediment transport rate. This is exemplified in Figure 4.14, which shows the temporal fluctuations in wind speed on the stoss due to gustiness over a thirty-minute recording period, suggesting that the actual transport rate fluctuates and is dynamic over periods measured in seconds[8] and is probably intermittent over a period of several minutes. Thus the mean transport rate will be lower.

[8] Butterfield (1999:32) established that the primary response of saltation to a change in wind velocity occurs in about one second.

There is a need for the components of the sediment transport equations to be refined to accommodate field conditions, but this is beyond the scope of this study. The present study will rely on the field-measured rates of migration and deflation / accretion, rather than equations based on laboratory-derived constants.

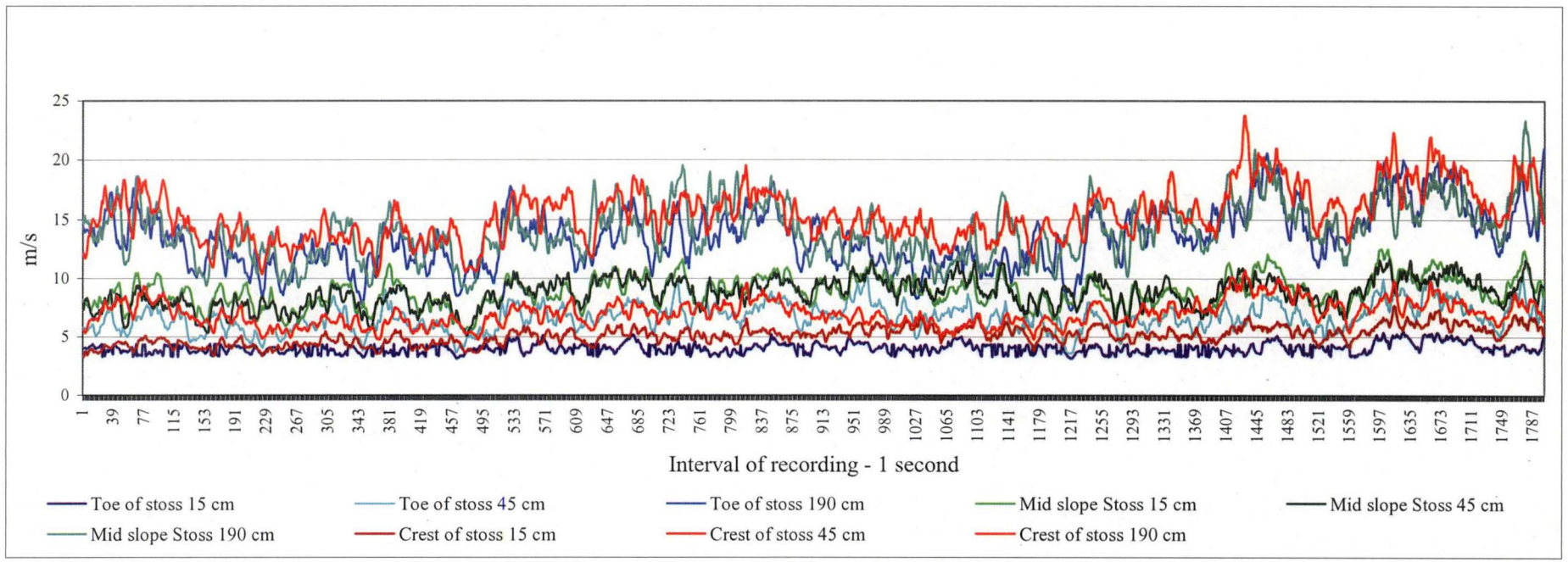

Figure 4.14. Stoss wind flow illustrating temporal fluctuations in wind speed due to gustiness close to ground surface, recorded at heights of 15 cm, 45 cm and 190 cm, over a thirty–minute period, using thermo anemometers.

4.7 Airflow up the windward slopes of a long-walled parabolic dune

4.7.1 Introduction

This section of the thesis addresses the results of the field experiment that measured close-to-the-bed wind flow, with arrays of thermo anemometers mounted on light weight 2 m masts deployed on the deflation basin and windward slopes of a parabolic dune[9]. Unfortunately, attempts to acquire a correlation between the benchmark on-site climate station and the arrays of deployed thermo anemometers failed due to a computer programming interface failure between the climate station logger and the laptop computer.

The Croppies Bay long walled parabolic dune is asymmetric in form – the north trailing arm (NTA) is 8 m higher than the south trailing arm; the stoss has a 23° gradient slope and the lee slope is abrupt and steep (30°). The parabolic form indicates that the predominant pattern of airflow is downwind along the axis of the dune, with asymmetry created by flow over the lower wall of the south trailing arm (RDD 68.6°, Figure 4.13b). Both windward slopes (1,800 m on the south flank of the north trailing arm, and the stoss) are erosional in form, devoid of vegetation and actively migrating downwind or laterally.

The topography of the windward slopes both influence and are influenced by wind flow. For example, the stoss is concave under the influence of westerly sector winds, from approximately the 60 m to the 65 m height contours (see Figure 4.19), and convex under the influence of easterly sector flows. In contrast, the windward flank of the NTA remains convex between the 60 m to 65 m contours in all wind flows, but most pronounced following sustained high velocity SW flows. The convex topography on the NTA is the result of lateral migration, revealing a previously emplaced shoulder of a trailing arm.

[9] The close-to-the-bed wind flow measurements are summarised in Appendix 4.

4.7.2 Shear Stress

Empirical studies in desert dunes (Lancaster, 1985; Lancaster and Nickling et al. 1996: Mulligan, 1988; Frank and Kocurek, 1996; Burkinshaw, et al. 1993; McKenna Neuman and Lancaster et al. 1997; Weng, et al. 1991; Wang, et al. 2002) have found that due to compression of flow up the slope of a dune, shear stress progressively increases. Table 4.7 and Figure 4.15 show the findings of the present study, specifically that on the flank of the NTA, shear stress ($u*$) more than doubles between toe (1.03 $u*$ m/s) and mid-slope (2.27 $u*$ m/s), decreasing nearly five-fold at the crest to 0.48 $u*$ m/s. Mid-slope on the flank

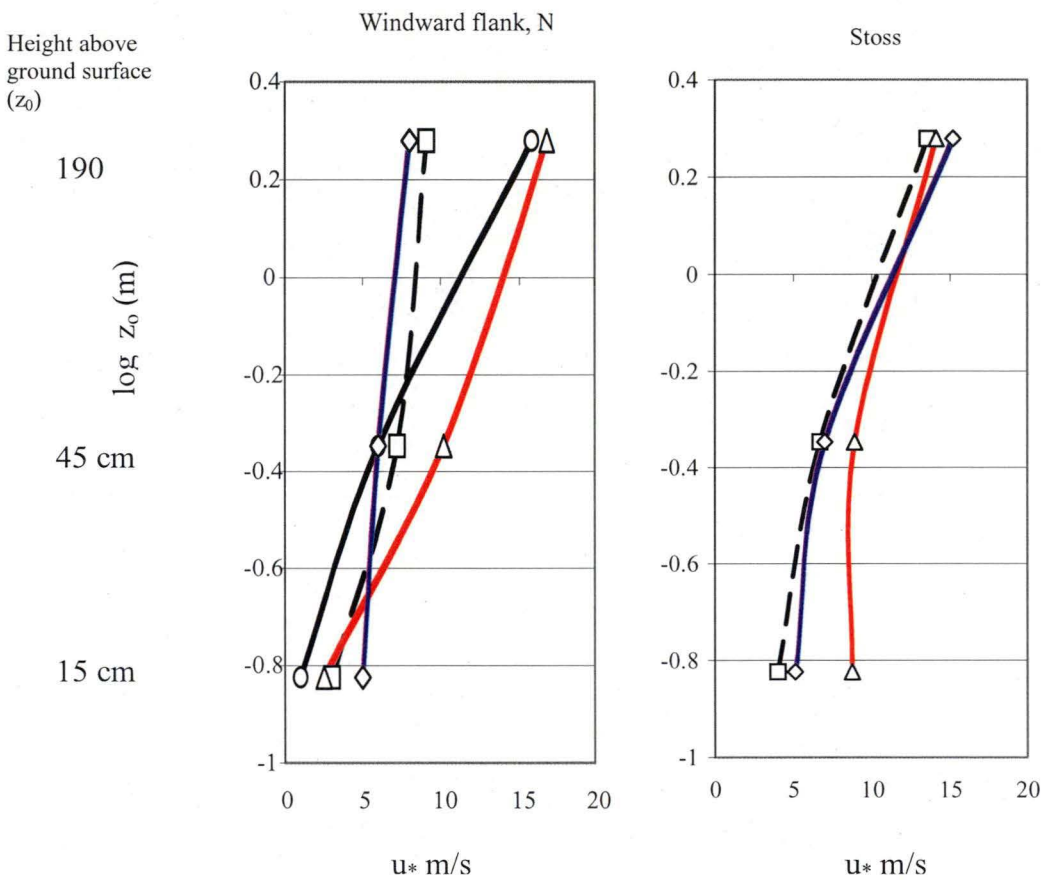

Figure 4.15. Wind shear velocity (u*) profiles on windward slopes, Croppies Bay parabolic dune.

For each profile: (O) black line is deflation basin; (---) black dash line is toe of slope; (△) red line is mid slope; (◊) blue line is crest. The height difference between the toe of dune and crest for the stoss is 13 m over a distance of 350 m, slope 23°; for the flank of the north trailing arm height is 12 m over a distance of 86 m, slope 28°.

Table 4.7. Wind shear velocity (u*) and roughness length (z_0) on windward slopes, Croppies Bay parabolic dune.

	Flank of north trailing arm (28°)				Stoss (23°)		
	Deflation basin	Toe	Mid slope	Crest	Toe	Mid slope	Crest
$u*$ m/s	2.38	1.03	2.27	0.48	1.56	1.05	1.75
z_0 m	0.140	0.041	0.089	0.003	0.063	0.009	0.062
r^2	0.989	0.913	0.986	0.987	0.971	0.835	0.93

$u*$ is convex (protrudes into the air flow), thus apparently contributing to a convergence of streamlines, generating an increase in pressure (Walker and Nickling et al., 2002), which results in an increase in $u*$ with a roughness length (z_0) of 0.041 m. In contrast, $u*$ on the stoss from toe (1.56 $u*$ m/s) to crest (1.75 $u*$ m/s) does increase, but not progressively. Rather, it increases mid-slope, where the stoss is distinctly concave, $u*$ is 1.05 m/s, with the shortest roughness length (z_0) of 0.009 m.

The on-site shear stress, with a correlation coefficient of 0.88, is 0.2 $u*$ m/s compared with Owen's (1964) 0.02 $u*$ m/s. The ten-fold difference between these values may be attributed to the larger and mixed grain sizes, and the compression of flow up the 28° (flank) and 23° (stoss) slopes. Hsu (1971), following measurements of wind speed close to the ground on a beach, also reported a shear stress more than ten times those predicted by Equation 2.8.

Figure 4.15 and Table 4.7 show that the measured velocity profiles, with the exception of the crest of the NTA, are not log-linear. Kinks, or deviations from a straight line, characterise the velocity profiles indicating a causal relationship (r^2 >0.86) between a saturated inner saltation layer and wind velocity, shown in Figure 4.16. The roughness length (z_0) of the deflation basin (0.14 m) is higher in response to sparse tussock grass to a height of 12 cm.

In Figure 4.15 the stoss velocity profiles display negative kinks, or distinct curvature within the lower 40 to 50 cm boundary, indicative of saltation (Bagnold, 1941, in Pye and Tsoar, 1990). The variability between roughness lengths (z_0) in Figure 4.15 is probably indicative of inconsistencies between bed characteristics, namely transitions between toe and crest in ripple wavelength, sand grain size and bed porosity. Field observation of bed characteristics during the process of sampling wind close to the ground with the TAs, indicated the following transitions. The ripple length at the toe of the stoss at the time of sampling wind velocity had an average interval of 15 cm; the bed was comprised of very fine sand grains (3.59 M_z ϕ) with a bed porosity of 76%. Mid slope, ripples rapidly filled with sediment, resulting in a flatter ground surface with the bed comprised of medium sand grains (1.69 M_z ϕ) and a bed porosity of 73%. The ripple bedform on the crest had a symmetric mean wavelength of 10 cm; the bed was comprised of medium sand grains (1.43 M_z ϕ), with a bed porosity of 71%. The height of 'kinks' for mid slope and crest, shown in Figure 4.15, are close to the ground surface on the stoss, lying below the height of the 15 cm thermo anemometer. The trend of a positive 'kink', below 15 cm for the stoss mid slope, probably reflects a consistent 10° divergence from the primary flow direction of up the stoss.

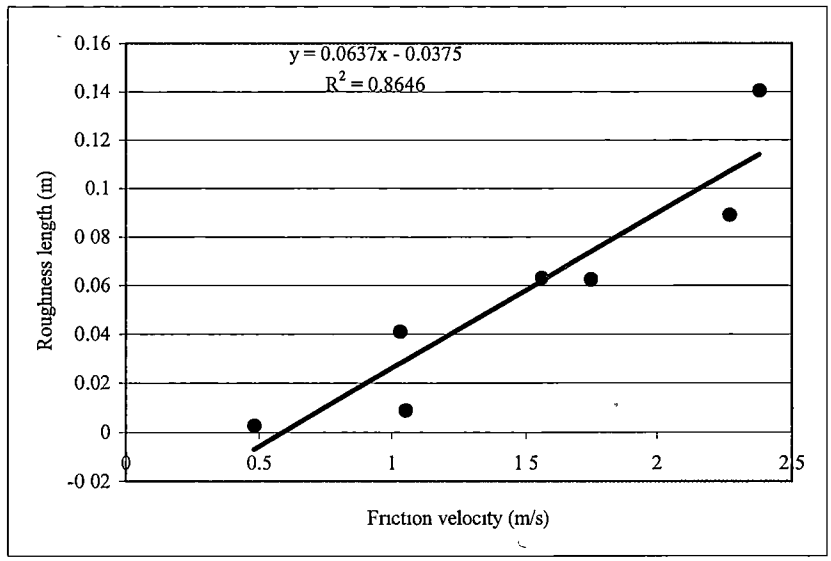

Figure 4.16. Relationship between friction velocity ($u*$) and roughness length (z_0).

The north trailing arm velocity profiles shown in Figure 4.15, illustrate diversity in flow between the toe, mid slope and crest, contrasting with the pattern of flow up the stoss. Both the flank toe and mid slope velocity profiles have positive kinks, which Bagnold (1941) hypothesised to reflect a speeding up of the wind due to grains accelerating just prior to hitting the ground surface. However, given the asymmetric parabolic bedform of the site, positive kinks probably reflect topographic variations between the slope angles of stoss (23°) and flank (28°), accompanied by distinctions between sand grain sizes and porosity of the bed on stoss and flank. Mid slope on the flank is convex due to deflation of the shoulder of a trailing arm emplaced during an earlier phase of mobility, accompanied by medium sand grain size (1.55 M_z ϕ) and higher compaction of the bed (porosity 61%; mean 71%). Thus, airflow is compressed, resulting in pressure increasing over the convex flank, accompanied by an increase in z_0, which is also responding to the increased compaction of the bed, and to medium sand grains.

Other contrasts between stoss and flank flows include: wind velocity on the flank crest is log-linear; the mid slope flank $u*$ is double that on the stoss, and crest $u*$ on the stoss is three and a half times greater. The z_0 at the mid slope on the stoss is ten times higher than on the flank.

Given the variation in height of $u*$ up the windward slopes and the non-linear profiles, it is evident that the flow structure is complex – probably reflecting topographically induced variations in pressure and surface roughness – thus rendering the calculation and quantification of sand transport problematic. Bagnold (1941:60) assumed a fixed z_0 determined from a focal point (the point where a range of profiles with different $u*$ values converge). Frank and Kocurek (1996:52) doubt the robustness of this method, finding that a clear definition of a focal point is generally not available to substitute for a measurement. Butterfield's (1993:311) findings support the doubts of Frank and Kocurek (1996), reporting that "during

saltation the 'effective roughness', z_0, of the surface varies with the height of the grain cloud, and there can be no fixed roughness length constraining velocity rays to a focus, as suggested by Bagnold (1941)". Frank and Kocurek (1996:52) report that adopting a fixed z_0 averages the effects of the inner layer and generates an increased $u*$ value for windward slopes. This may explain in part the large discrepancies between migration rates derived from erosion pins deployed in the field and migration rates derived from remote and on-site wind data reported by other researchers (Inman and Ewing et al. (1966), Jensen and Rasmussen et al. (1984), Pluis (1992).

4.7.3 Flow acceleration on windward slopes

Flow acceleration up windward slopes at Croppies Bay are characterised by applying the Mason and Sykes (1979 in Walker and Nickling et al. (2002:54)) speed-up factor, S:

$$S = Uc / Ut \qquad \text{Equ 4.1}$$

where S is a ratio of crest (Uc) to toe of stoss (Ut) wind speeds at the same height above the surface.

This study, based on the precedent established by Walker and Nickling et al. (2002), Lancaster, (1985) and Wang and Dong et al. (2002) has applied the Mason and Sykes (1979) equation, modified to:

$$\frac{\text{velocity at dune crest}}{\text{velocity at dune toe}} = \frac{5}{3} = 1.66$$

Table 4.8. Speed-up ratios on stoss and north trailing arm, south flank.

Height above ground surface in cm	Stoss (23° slope)			North trailing arm, south flank (28° slope)		
	Crest to Toe	Crest to Mid slope	Crest to Deflation basin	Crest to Toe	Crest to Mid slope	Crest to Deflation basin
15	1.3	0.6	5.1	1.7	2	0.2
45	1	0.8	1.2	0.8	0.6	1
190	1.1	1.2	1.0	0.9	0.5	0.5

The speed-up ratios are determined by the dune height and the windward shape of the dune profile (Lancaster, 1985; Mikkelsen, 1980) and confined to an inner layer close to the surface (Jackson and Hunt (1975) in Walker and Nickling, (2002:50)), exemplified by the 1.3 and 1.7 ratios for the thermo anemometer located closest to ground surface (15 cm). Equation 2.1 applied to the stoss indicates that the thickness of the inner layer $l = 5.95$ m.

Convergence of streamlines results in an acceleration of flow that, in a mean wind speed of 4 m/s (see Table 4.9 below), increases wind speed 1.7 times on the flank. The doubling in wind speed between mid slope and crest on the NTA confirms that

changes in dune morphology (convex) determine acceleration of flow. Lancaster (1985:587) suggested that the main effect of velocity speed-up on windward slopes is to increase the volume of potential sand movement towards the dune crest.

The ratios in Table 4.8 exhibit some variation when compared with field measurements on windward slopes of desert dunes (Lancaster, 1985; Mulligan, 1988; Wang and Dong et al., 2002; McKenna Neuman and Lancaster et al., 1997). The ratios for the thermo anemometers located closest to the ground surface (15 cm) are consistent with the measurements of Lancaster (1985), Mulligan (1988), Wang and Dong et al. (2002) and McKenna Neuman and Lancaster et al. (1997); the stoss ratios are also within a range consistent with the measurements of the authors cited above. However, the ratios of the higher elevation thermo anemometers on the NTA are approximately half the averaged ratios (1.52; range 1.81 to 1.31) measured by the above authors. This could partly be explained by morphological distinctions of dune shape, by the oblique direction of wind flow, and by the lateral and vertical compression of flow in a parabolic dune.

Table 4.8 shows the distinctions between the speed-up values for the stoss and NTA, indicating that flow up the axis (west to east), under the field measurement conditions, is the predominant flow. Apparent convergence of streamlines results in a wind speed 5.1 times that of the deflation basin to crest of stoss in the inner layer, compared with 0.2 times on the flank. Stoss speed-up ratios are higher than NTA ratios in the same category. This supports the Pye and Tsoar (1990) report that flow is compressed both vertically and laterally by the blunt intrusion of the trailing arms and stoss into boundary layer flow.

4.7.4 Wind velocity profiles and flow visualisation

Figures 4.17 and 4.18 illustrate the measured wind velocity profiles and the location of the masts and thermo anemometers across the parabolic dune profile (north to south) and on the stoss (west to east), respectively. The wind velocity profiles on the windward slopes, shown in Figures 4.17 and 4.18, demonstrate that the intrusion of the dune into the stream flow affects the vertical velocity gradients close to the dune surface, and that flow acceleration varies over the dune profile and between windward slopes. The wind velocity profiles located on the crests of the south and north trailing arms indicate the influence of vegetation, which is reflected by the muted magnitude of vertical increase in wind speed.

Table 4.9. Wind velocity (m/s) north to south over the dune profile, and up the axis (west to east) of the parabolic dune.

Height above ground surface in cm	North to south over dune profile					Up-the-axis		
	South trailing arm, crest	Deflation Basin	North trailing arm, flank			Stoss profile		
			Toe	Mid slope	Crest	Toe	Mid slope	Crest
	m/s	m/s	m/s	m/s	m/s	m/s	m/s	m/s
15	0.41[1]	1	3	2.5	5.1	4	8.7	5.1
45	3.1	6	7.2	10.2	6	6.7	8.9	7
190	4.5	15.8	9.1	16.8	8.4	13.5	14.1	15.2

[1]Wind speed values are averages of measurements derived from 1-second intervals during 30 minute recording periods.

The wind velocity profiles shown in Table 4.9 and the azimuths in Figure 4.19 indicate that wind accelerates up the axis from the deflation basin to the crest of the stoss. The magnitude of the vertical wind speed on the stoss is significantly higher near the ground surface (15 and 45 cm), maintaining a relative proportion as the elevation of the anemometers increases (190 cm), and in proportion to the flow on the deflation basin. This suggests that streamline convergence is optimal below 1 m and commences the process of re-stabilising by a height of about 2 m. Wind flow is oblique to the flank of the NTA, accelerating as it encounters the 28° slope, 12 m wall. Topographic steering accelerates flow at the toe of the flank forming a jetstream[10], aligned ~ 330° at the toe of the flank. Flow accelerates mid slope, due to the bedform being both convex and the steepest part of the wall. Again, the magnitude of the vertical wind speed is significantly higher near ground surface (15 and 45 cm), and maintains relative proportion as the elevation of the anemometers increases (190 cm). Flow decelerates at the crest, at the height of the top anemometer, probably in response to both separation of flow and turbulence in flow

[10] Indicated by mega ripples with a wave length of ± 1 m, extend from the lee of the neck up onto the stoss.

due to the proximity of 3 m high erosion knolls, with a 30 percent ground cover of *Spinifex sericeus*.

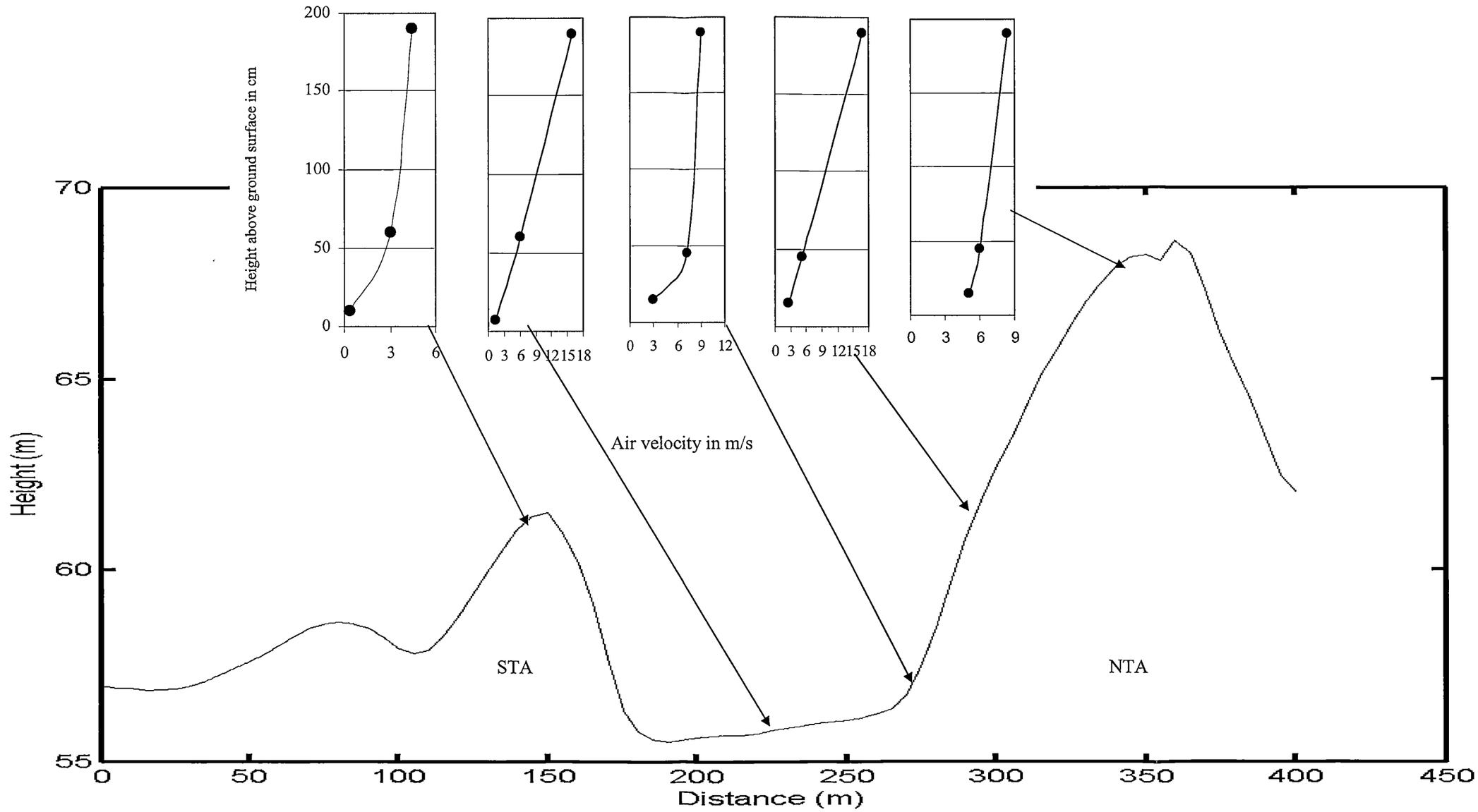

Figure 4.17. Measured wind velocity profiles from a transect aligned north to south, across the parabolic dune profile, with the location of masts. The dune profile is GPS measured (see section 5.1.3.3, Chapter 5 for details).

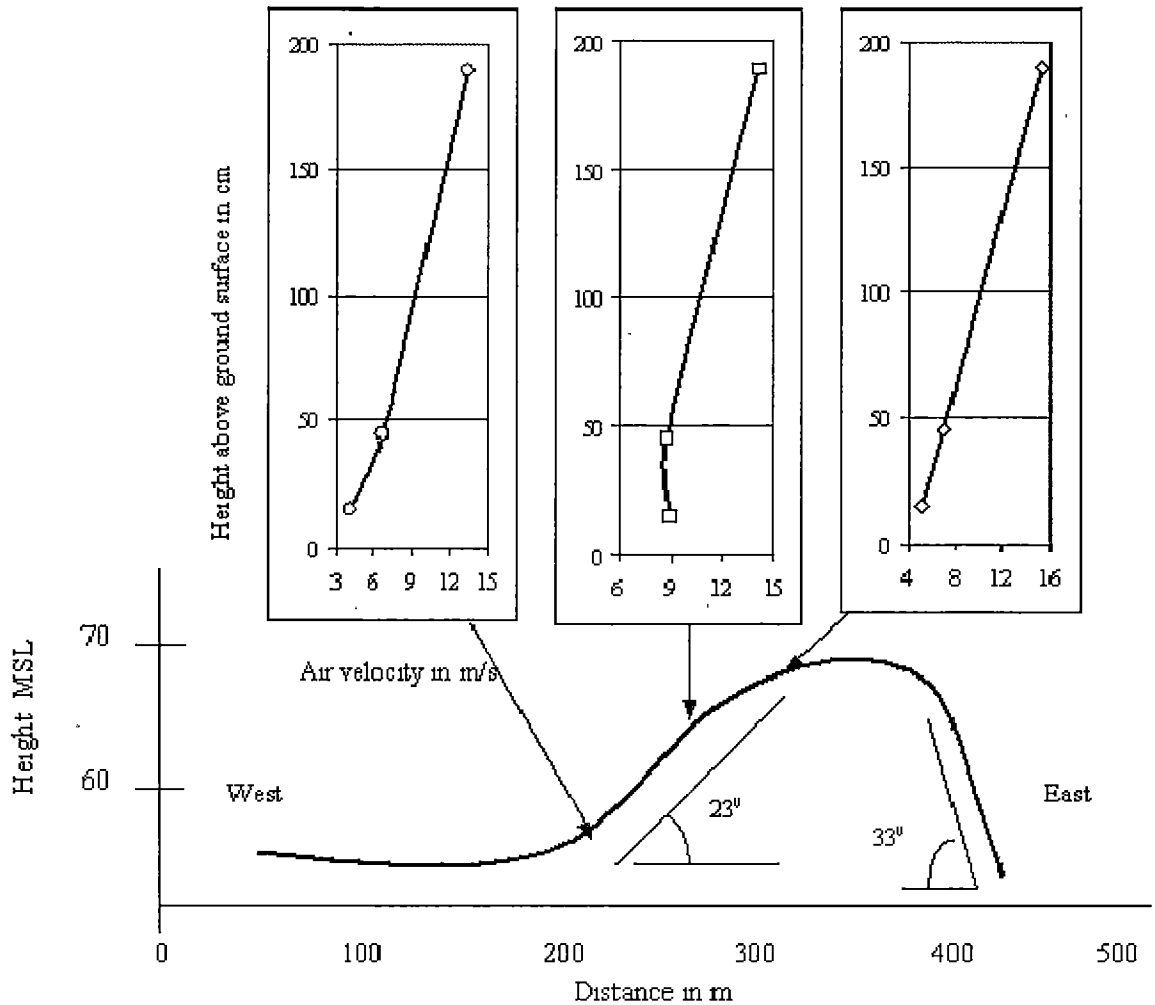

Figure 4.18. Measured wind velocity profiles on stoss and the location of masts. The dune profile is GPS measured.

Figure 4.19, based on field observations, shows the wind speed and azimuths for each wind profile, with a designated line colour indicating the height of the wind vane and anemometer - red 25 cm, blue 45 cm, and black 190 cm. Approach of flow at the base of the flank is oblique throughout the wind profile, with wind vanes aligned consistently in the direction of flow for the duration of the sample. Mid slope, flow is topographically steered by the remnant buttress, with flow almost parallel to the topography. Persistent oscillation in wind vanes, of ± 10° in vanes close to ground surface and ± 5° at 190 cm, during the recording run, is indicative of multi-directional, turbulent flow. Flow on the crest is topographically steered between the buttress and the erosion knolls, and aligned almost parallel to contour. The wind vanes consistently pointed in the direction of flow for the duration of the sample.

Flow up the deflation basin, at the time of sampling, was aligned with the axis of the dune; the wind vanes aligned consistently with direction of flow. The combined alignments of the deflation basin flow and the flow at the base of toe of NTA lends weight to the interpretation that approach flow to the NTA flank from the deflation basin is oblique due to topographic steering.

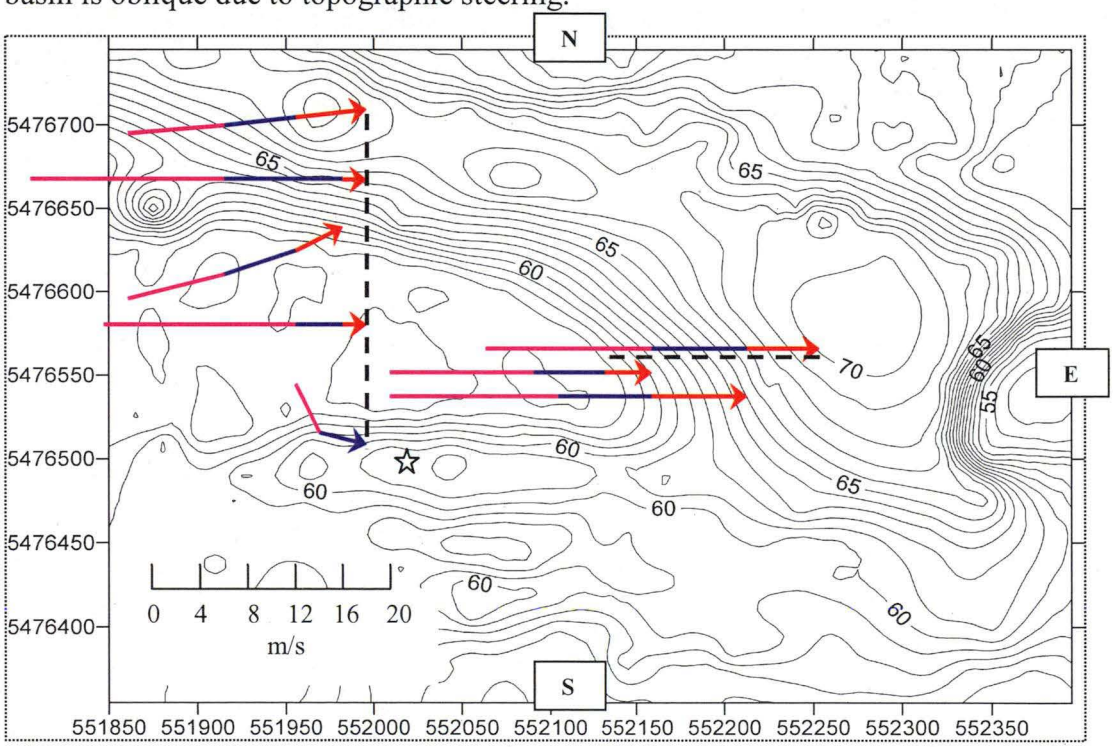

Figure 4.19. Location of azimuths and wind speeds for eight wind profiles.

The contour map is GPS surveyed (Epoch 1) and shows the eastern portion of the parabolic dune, comprised of the stoss, lee slipface, NTA, STA and deflation plain (840 m in length, from west to toe of lee slipface. Total length is 1,900 m).
Line colour indicates the height of the wind vane and anemometer above ground surface: red 15 cm, blue 45 cm and purple 190 cm.
Note: the stoss wind profiles have been offset from their field line sequence to display the azimuths for each wind profile. Wind flow is from the west.
The – – – show the location of the transects. ☆ shows the location of the 2 m met. station.

A flow visualisation experiment, in association with the wind velocity profiles and wind vanes, provides reliable imagery of flow up the stoss, flow separation at the lee slipface, and wake flow downstream of the slipface. Figure 4.20a is a schematic interpretation[11] of the flow visualisation on the stoss, indicative of secondary flows. Figure 4.20b illustrates toe and crest flow visualisation on the stoss.

Observations made in the field were:

⇒ Flow remained close-to-the-bed from the toe of the stoss to mid slope.

⇒ Between mid slope and the crest, a backflow occurs which flows in a roll down slope towards the mid slope.

⇒ Smoke plume between toe of stoss and mid slope, indicated that flow diverged 10° south of the main west to east flow direction of 91°.

⇒ At the crest of the stoss, the smoke drifted to a height of 180 cm above the ground surface, continuing to expand downwind as it flowed towards the lee crest.

⇒ Flow separated at the lee crest:
  - o a component of the smoke plume flowed close-to-the-bed of the slipface from crest to toe whilst the slipface was in shadow, and
  - o lee eddies formed in the wake of the slipface;
  - o a smoke plume flowing downstream just below the elevation of the crest of the lee slipface suggests that streamline constriction continued several hundred metres in the wake flow before reattachment to the main streamflow.

Given that the assessment of wind flow on the stoss is indicative, due to it being constrained by the number of TAs, and by the visualisation experiment, it is inappropriate to join dots between wind profiles to generate a profile of flow up the slope. However, under the wind flow conditions at the time of sampling flow with the TAs, and with the aid of the combined wind velocity profiles, azimuths and flow visualisation on the stoss, the following interpretation is made.

The neck and the axis of the parabolic dune are aligned downwind in a west to east direction; the azimuth for wind direction on the deflation basin during sampling was 91°, and on the stoss 90°. Smoke plumes indicated that flow remained close-to-the-bed from the toe of the stoss to mid slope, indicating that the inner layer is well defined. The stoss from approximately the 58 m to 63 m contours is concave under the influence of downwind flow, and probably the form of the bed reflects the pattern of airflow[12]. The wind profile indicates that mid slope, close-to-the-bed, wind speeds are high (8.7 m/s [15 cm] and 8.9 m/s [45 cm]), some 3.6 m/s above the threshold velocity, with the shortest roughness length at 0.009 (z_0 in m).

Commencing between the crest and mid slope of the stoss, extending down slope some 50 m, the flow visualisation indicated a reverse rotational flow to a height of ~ 3 m was present. The presence of a reverse rotational flow could explain the concave stoss bedform during and following episodes of high velocity wind speeds. The area between mid slope and crest is also the steepest part of the wall. Robertson

[11] Derived from photographs taken simultaneously with the release of smoke flares.

[12] The stoss has a high porosity, indicating large pore spaces, rendering the bed susceptible to ease in sediment transport.

- Rintoul (1990:70) described a similar flow pattern, reporting it as a 'dominant flow pattern (of) a spiral flow moving along the windward face' and associated with higher wind speeds (about 7 m/s) at the control station. She observed 'Reductions in wind speed coincided with a change in flow pattern as the flow moved upslope and became incorporated into the fast-moving airstream that crossed the dune crest.'

At the crest of the stoss, flow visualisation and the wind profile indicated that threshold velocity was maintained close-to-the-bed. Downwind of the crest, the smoke plume expanded to a height of 180 cm above ground surface, continuing expansion downwind as it flowed towards the lee crest. Field observation and photography indicated that an active saltation layer to a height of 30 cm extended from the crest of the stoss to the lee crest, a distance of some 40 m.

Pye and Tsoar (1990:37) reported that an abrupt change in surface inclination and a sharp edge causes airflow to separate because it is not capable of reaching an infinitely large velocity at the lee crest. At Croppies Bay (Figure 4.20a), airflow approached the sharp edge of the crest of the lee slipface direct, rather than oblique (indicated by ripple bedform which ran parallel to crest along the length of the slipface), and then the airflow separated into three distinct components. At the time of the flow visualisation experiment the lee slip face was in shadow, and therefore not receiving direct solar radiation resulting in thermal heating, and this may explain a component of the smoke plume flowing very close-to-the-bed from crest to toe with no eddies. At the toe of the slipface, a portion of this 'bed hugging' smoke plume separated, and flowed over the canopy of vegetation. The greater proportion of the smoke plume flowed downwind of the lee slipface, approximately 1 m below the elevation of the crest of the lee slipface, extending about 100 m before descending to the ground and dissipating. A portion of this downwind flow separated, forming faintly-defined lee eddies.

Considering that lee slipfaces of west to east aligned parabolic dunes are predominantly in shadow, notably during the hottest phase of the day, sampling in shadow contributes to the broader interpretation of airflow on lee slipfaces in downwind flow. In accordance with the flow visualisation above when there is no solar radiation on the bed, it is evident that the formation of lee eddies appears muted, and that there is a 'dead zone' of airflow close-to-the-bed extending down to the toe. This close-to-the-bed flow disperses over vegetation and in the process drops the fine particles in saltation, which inundates plants, reducing the roughness factor. The smoke plume associated with the downwind wake flow expanded in width as distance from slipface increased, then descended to ground some 100 m downwind of the slipface. Downwind (~150 m) of the slipface are a series of sandy knolls (remnants of a nested parabolic dune); 250 m in advance is an intact nested parabolic dune with trailing arms, stoss and deflation basin. The windward slopes of these bedforms – knolls, stoss and north trailing arm – are eroding up to 250 m in advance of the present lee slipface. This is congruent with the proposal of Hogbom (1923, in Olson, 1958:261) that a zone of erosion is located downwind of a lee slipface due to acceleration of the wind in the area of descending streamlines; the capacity of this wind to erode is enhanced because it has dropped the saltation load.

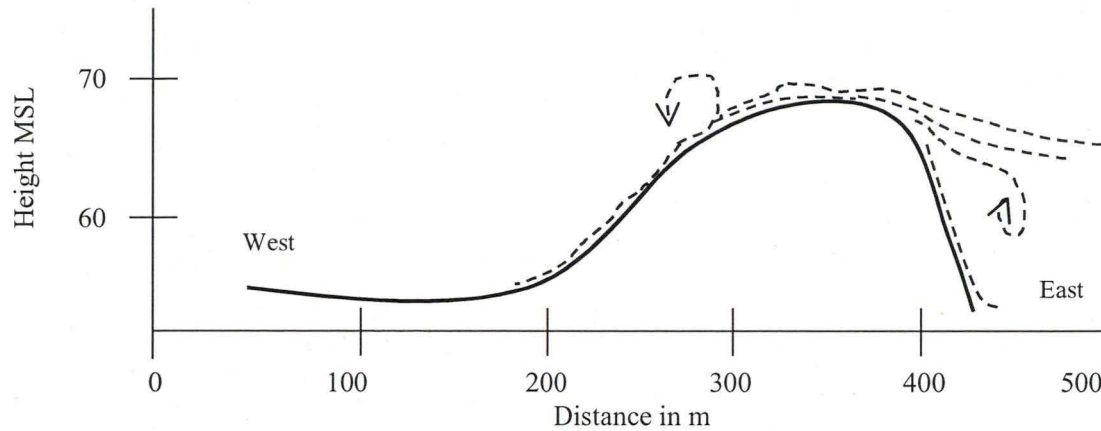

Figure 4.20a. Flow visualisation on stoss. GPS surveyed profile.

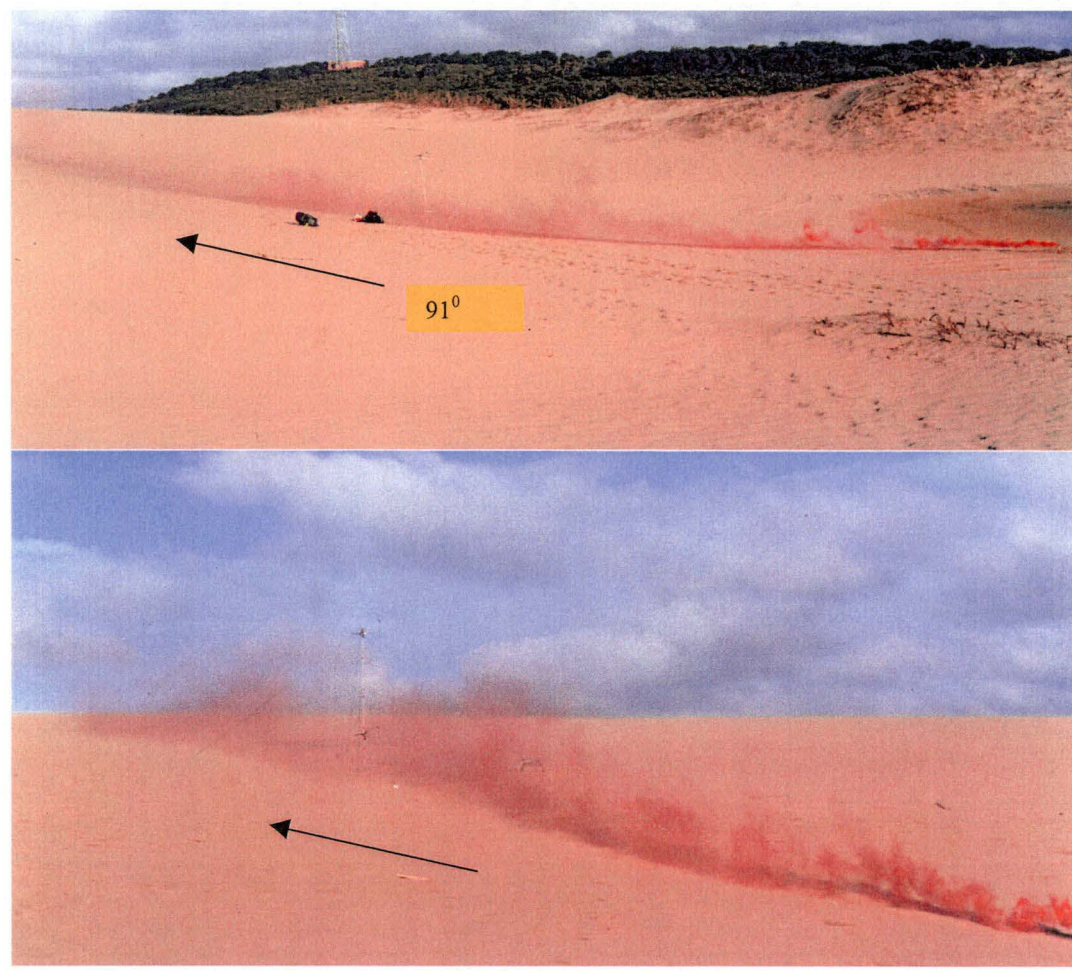

Figure 4.20b. Examples of toe and crest flow visualisation on stoss. Arrows indicate the direction of flow towards crest.

4.7.5 Parabolic windflow pattern

Flow in parabolic dunes, because of the downwind 'U' shape of the bedform, and the presence of a high-walled neck which constricts flow, will mostly result in wind speeds and wind flow patterns unlike inland linear or transverse dunes. In this example at Croppies Bay (Figure 4.21) with above threshold wind speed conditions[13], wind flow accelerates as it leaves the sea and encounters a 20° slope from the beach to the surrounding landform. This profile crowds the streamlines and accelerates the flow. The accelerated flow is further constricted as it is funnelled between the trailing arms[14], then constricted again as it flows through the neck (14 m high walls) of the parabolic dune, producing a concentrated stream or jet (Oke, 2000:185). Flow expands on exiting the neck, creating lee eddies on the abutting trailing arms, with the jet remaining intact for downwind flow. The wall of the trailing arms and stoss compress the streamlines both laterally and vertically and flow remains constrained along the length of the dune. Jets develop parallel to the toe of the NTA, extending along the length of the flank between the neck and the remnant buttress and from the lee of the buttress up the wall of the stoss.

Flow is aligned with the axis of the dune up the deflation basin. For wind speeds above threshold, there is no evidence of stalling at the toe of the stoss; streamlines compress and accelerate on encountering the wall of the stoss with effective flow, remaining close to bed in the inner layer. Compression of flow up the stoss does not increase progressively from toe (1.56 $u*$ m/s) to crest (1.75 $u*$ m/s), instead at mid-slope, where the stoss is concave, $u*$ is 1.05 m/s. The form of the concave bed is reflected in the pattern of airflow: commencing between the crest and mid slope of the stoss and extending down slope some 50 m, flow visualisation indicated a reverse rotational flow to a height of ~ 3 m. Flow remained close-to-the-bed at the crest, due to a 40 m wide ridge between the crest of stoss and crest of lee slipface. Zones of separation occur at the crests of the stoss and lee slip face, and the lateral walls of the stoss.

Airflow separated at the crest of the lee slipface. On the lee slipface, when there is no solar radiation to heat the bed, the formation of lee eddies appears muted, and there is a 'dead zone' of airflow attached to the bed between crest and the toe. Descending accelerating streamlines reattached downwind, eroding windward slopes of a nested parabolic dune located some 250 m in advance of the lee slipface.

The zones of separation on the NTA are influenced by wind flows from two directions. Firstly, the form of the parabolic dune steers and accelerates flow downwind along and up the flank, and secondly, the across-dune wind vector (RDD 68°) enters the dune over the lower south trailing arm and is then steered topographically. The flow approach is oblique to the flank from both sources. Shear stress ($u*$) on the flank more than doubles between the toe (1.03 $u*$ m/s) and mid-slope (2.27 $u*$ m/s), decreasing nearly five-fold at the crest to 0.48 $u*$ m/s, to form a zone of separation. Airflow downwind is topographically steered between an eroding remnant buttress and erosion knolls on the flank crest. Flow accelerates on the 23° up-slope between the buttress and knolls, flowing parallel to flank crest. The

[13] 68% of the recorded wind survey period.
[14] Trailing arms precede the neck and are located between shore and neck.

remnant buttress causes lee wake flows on the flank. Both the oblique and parallel flows converge downstream at a zone of separation, forming a zone of accretion between remnant ridges.

The airflow pattern on the south trailing arm is complex. Placement of the 2 m wind mast (see Figure 4.1) on the crest, in addition to the parallel alignment of trough blowouts and deflation basins, indicates that the predominant flow is topographically steered parallel to the arm. The faster rate of lateral migration indicates a secondary flow across the wall.

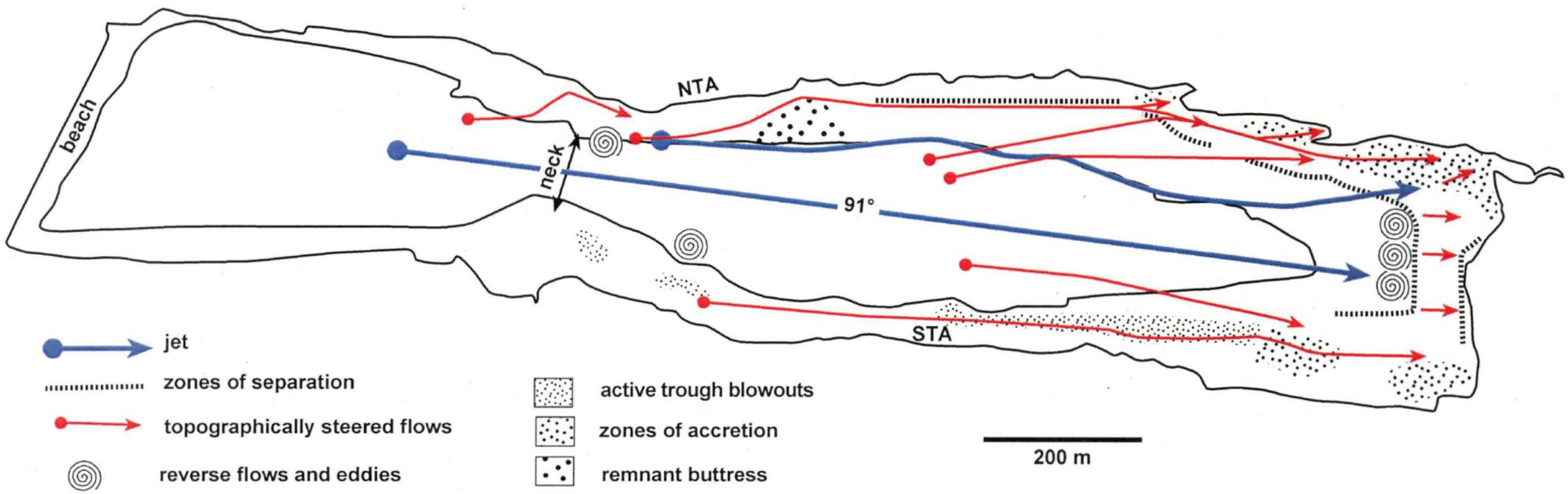

Figure 4.21. Downwind wind flow pattern and topographic steering of flow over Croppies Bay parabolic dune. Plan view image generated from 1999 aerial photo with the Arcview program.

4.8 Sand dune mobility

Indices have been developed to model dune field mobility using simple atmospheric parameters to categorise dune activity. Applying Croppies Bay data to Lancaster's (1997) mobility index, Equation 2.10, yields the migration (M) values shown in Table 4.10.

Table 4.10. Croppies Bay units for calculating M by six monthly intervals and M by seasons.

	Six monthly intervals			Seasons			
	Year	Dry[2]	Wet	Summer[3]	Autumn	Winter	Spring
W[1] (%)	71	68	62	77	75	63	66
P (mm)	55	46	65.4	41.9	55.7	68.8	55
E (mm)	77	114	40.2	133.5	60.2	33.5	80.4
P/E	0.71	0.4	1.6	0.31	0.92	2.1	0.68
M	**100**	**170**	**39**	**248**	**81**	**30**	**97**

[1]Derived from Table 4.5 for seasons and wind data sorted by six month intervals.

[2]The six month intervals are designated by the transition linked with high evaporation / low rainfall (October to March) to low evaporation / higher rainfall (April to September), see Figure 4.6.

[3]Summer months are December, January and February, etc, which have been defined previously.

Where: W = the percentage of days during a year when the sand moving capacity of the wind is > than the site threshold of 4.5 m/s;
P/E = the ratio of the mean annual precipitation (P) to mean annual potential evaporation (E).

M = > 200 fully active dunes
M = 100 to 200 dunes partially fixed by vegetation on slopes
M = < 100 crests of dunes active
M = < 50 inactive dunes (fixed by vegetation).

Table 4.10 shows that winds were above threshold (W) 71% of the year, and the annual migration value, (M) of 100 conceals the range of dune activity. The seasonal indices of mobility (M) range between a fully active dune in summer (M > 200) to an inactive dune in winter (< 50). The W value in autumn is high at 75% whilst M is 81, compared with summer when the W value is 77% and M 248. This indicates that dune activity is a function of aridity (P/E). For both the summer season[15] and dry six month interval the P/E ratio fell below 0.50, indicative of semi-arid conditions, and the annual P/E ratio is less than 1, indicating a net moisture deficit.

An analysis of the mobility index by dry and wet six monthly period provides a better indication of the feedback between P/E on dune migration – for six months evapotranspiration exceeds precipitation (see Figure 4.6) with a mean deficit of 410 mm. Solar radiation for this period is greater than twofold (mean 24 MJ/^{2}), compared with the wet six monthly period. The atmospheric conditions, commencing with the dry six monthly period, which contribute towards aridity in the

[15] Derived from 43 years of BoM data, see Figure 4.6.

dune system, are reflected in the M of 170, which accommodates Lancaster's (1997) mobility index of the dunes being partially fixed by vegetation on slopes. During the winter months, although the W value remains high (62%), it is apparent that precipitation influences the migration value (M 39), and by inference indicates that dune migration is significantly less than during the period conducive to aridity. The contrast between dry six monthly period aridity, comparable to drought conditions, and the winter P surplus conditions, lends itself to an evaluation of conditions conducive to increased dune mobility.

Lancaster's (1997) annual dune mobility index has enabled the calculation of dune mobility in an actively mobile coastal long-walled parabolic dune. Analysis of wind and P/E data by season and by six monthly periods reveals a pattern of summer/spring aridity, contrasted by surplus P in winter, predicated by the P/E index.

Tsoar and Blumberg (2002:1151) argue that rainfall is not a decisive factor in fixing sand dunes. They proposed that wind erosion is the main limiting factor of vegetation growth on dunes due to a combination of the frequency and magnitude of wind above threshold speed and variability in wind direction, resulting in either higher or lower rates of erosion on windward surfaces.

Lancaster's (1997) equation with the component W (the percentage of days during a year when the sand moving capacity of the wind is > 4.5 m/s) reduces this influence to a single parameter, and this may be adequate for inland desert dunes. It seems that components of the Tsoar and Blumberg (2002) argument pertain for the Croppies Bay site. Field observation supports the Tsoar and Blumberg (2002) proposal that plants retreat on actively mobile windward slopes and are unable to colonise these slopes.

Tsoar and Arens (2004:9) proposed a mobility index of above or below 500 DP (m/s) related to Fryberger's (1980) classification of wind-energy environments, with above 500 DP deemed high wind-energy. However, on revisiting Fryberger's (1980:150) classification of wind-energy environments, his categories are high > 206, intermediate 103 to 205, and low < 102 DP (m/s). Fryberger's (1980) categories were derived predominantly from inland arid sites, where wind-energy has a lower range than coastal environments. Given the discussion above, it seems probable that the 500 DP cited as a cut-off between high and low wind-energy environments may be derived from a sample of high wind-energy environments. The threshold needs to be within the range accommodating Fryberger's (1980) categories, and accommodating of higher coastal wind energies. It is beyond the immediate scope of this present study to undertake this task, but it warrants further work.

Applying Croppies Bay data to Tsoar and Arens (2004:9) modified Fryberger's (1980) wind resultant equation, yields the rate of dune migration q (DP) shown in Table 4.11. There are constraints embedded within the wind resultant data, in that the intervals of data analysis are directly connected with the measurement of changes in elevation on erosion pins, rather than with seasons. The data ranges do fit within the phases of the two six monthly periods.

The annual DP (q) 160 yields a low wind-energy environment with the Tsoar and Arens (2004) index, or an intermediate wind-energy environment with Fryberger's (1980) categories. Given that the Croppies Bay DP ranges between 150 and 2671[16] (mean 1172) m/s, the intermediate wind-energy category is a better approximation of the wind-energy environment. Parabolic dunes have been classified as a bedform indicative of intermediate wind-energy (Cook, 1986; Woodroffe, 2002).

The wind resultant data (Table 4.11) displays a more even distribution of wind-energy between the two six monthly periods than the Lancaster (1997) index, with the t (W) value for the dry six month period marginally higher (52%) than the wet six month period. Applying Tsoar and Arens (2004) index (Equation 2.12) to the data, wind resultant 9 (in the wet period) meets their high wind-energy threshold. Eighty percent of the DP values are in Fryberger's (1980) high wind-energy category.

Table 4.11. Croppies Bay units for calculating q by dry and wet six month periods.

Six month periods	Wind resultant[1]	t (W)	DP (q)	RDP/DP
Dry	2	79	343	0.4
	3	74	270	0.2
	4	76	290	0.1
	5	48	96	0.8
	6	84	365	1.0
Wet	1	14	1.5	0.8
	7	83	420	0.8
	8	81	352	0.8
	9	84	537	0.6
	10	70	341	1.0
Annual DP (q)	Annual	**68**	**160**	**0.6**

[1] Refer Figure 4.13.

In contrast to the Lancaster (1997) index, the range of data required to generate the Tsoar and Arens (2004) index is based upon effective wind speeds, and the range of data does display the dune migration rate q (DP) linked with the magnitude of directional variability in effective winds (RDP/DP), and the direction of transport (RDD[17]).

Table 4.11 shows that both six month periods have low DPs associated with low directional variability (> 0.8) indicating that not all wind events with low directional variability are effective. Fifty percent of the whole wind resultant data set occurs in the low directional variability category, and forty percent of the wet six month period t (W) resulted in DPs > 300 with an RDP/DP of 0.8 or greater, the period when precipitation exceeds evapotranspiration.

[16] Refer Table 4.7 and Figure 4.13.

[17] See Table 4.6.

Given that rainfall increases the threshold shear velocity by increasing the moisture content in sand and promotes the growth of plants (Sherman and Hotta, 1990; Namikas and Sherman, 1995), a prolonged phase of decline in rainfall associated with increases in wind speed and air temperature are probably predictive of decreased plant cover and reduced moisture content in sand, thus promoting increased availability of sediment. Lancaster's (1997) index, when applied to the Croppies Bay data, indicates an intra-year pattern of aridity linked with the summer season (P/E 0.3; M 248) / dry six month period (P/E 0.4; M 170) that promotes aeolian activity, followed by diminished aeolian activity during the winter season (P/E 2.1; M 30) / wet six month period (P/E 1.6; M 39). The Tsoar and Arens (2004) indices, when applied to the Croppies Bay data, suggest that precipitation is not the sole determinant of aeolian activity, evidenced by the wet six month period DP (q), indicated in Table 4.11, which shows that effective sand transport occurs between late autumn and late winter with a narrow unimodal wind flow (RDP/DP > 0.8).

The Lancaster (1997) and Tsoar and Arens (2004) indices are practical, indicative tools that facilitate the calculation of sand dune mobility by applying different atmospheric parameters. The parameters that comprise the Lancaster (1997) index (W is wind speed, and P/E is mean annual precipitation to mean annual potential evaporation) are readily accessible from national meteorological agencies, such as BoM, although as discussed elsewhere, wind data derived from 10 m masts is not directly applicable to deriving an effective wind shear threshold, or for collecting a representative range of wind speeds that characterise close to the ground wind flow. Annual dune migration (M) masks the range of dune activity, thus obscuring climatic conditions that promote the evolution of form. Unpacking the seasonal and data of six month periods reveals distinct patterns between P/E and the potential influence of wind on process and form. Similarly, the Tsoar and Arens (2004) annual migration value of 500 DP (m/s) mutes the influence embedded in the range of values in the intra-year data, which promotes aeolian activity. Again, looking at the data by six month periods improves the capacity of the index to analyse sand dune mobility. A strength of the Tsoar and Arens (2004) index is that it is based on the Fryberger (1980) wind resultant method which uses only effective wind velocities, expressed as drift potential (DP), which is a measure of the energy of surface winds and their effectiveness in transporting sand. Both the Lancaster and the Tsoar and Arens indices to some extent complement each other, separately addressing functional components that influence dune mobility and jointly rounding out factors that drive dune mobility. However, the capacity of simple yearly indices to calculate dune mobility are restricted by a number of factors, some of which are mentioned below.

Given the findings of Ash and Wasson (1983), Lancaster (1997), Tsoar and Illenberger (1998) and Tsoar and Blumberg (2002), it seems probable that it is not a definitive matter of rainfall versus wind speed as the key to defining dune mobility. Rather it is likely to be a series of linked feedback mechanisms, of which there are several examples. First, Tsoar and Blumberg (2002) note the association between human activity, in the form of grazing stock, and dune mobility. Several authors (Bird, (1993); Ash and Wasson (1983); Gaylord and Stetler (1994); Mowling (1998)) have also identified this association, finding that when grazing and/or firing to promote green pick either ceased or commenced, there was a time lapse response of either an increase or decrease in vegetation cover followed by either a decline or an increase in dune activity. Second, vegetation cover and density directly affect sand

mobility by increasing the surface roughness length (Bressolier and Thomas, 1977), and, conversely, inundation of plants by wind blown sand promotes dune activity by reducing their protective cover and modifying wind flow. Third, extreme wind events or prolonged periods of wind flow that exceed threshold wind velocity, combined with narrow unidirectional wind flow (low RDP/DP value), are the most effective at transporting large volumes downwind. Conversely, as Lancaster (1997:336) found, a combination of low wind speeds and growth of vegetation contributed to a decline in dune area due to sand being trapped in interdune areas. Fourth, Ash and Wasson (1983:23) found that the percentage of days with sand moving winds is high in the belt of zonal westerly flow, and that dune mobility in coastal dunes is limited by vegetation and controlled by precipitation and evaporation. Similarly, Gaylord and Stetler (1994:111) reported 'variations in temperature affect overall sand dune mobility primarily by controlling rates of evaporation and transpiration.' Fifth, a continuing source of sediment for re-working maintains the downwind migration of coastal dunes.

4.9 Future trends

As a way of investigating future trends in dune activity, an analysis of a number of meteorological data sets for Croppies Bay, including air temperature, rainfall and wind speeds, was undertaken.

An analysis of the relationship between the meteorological parameters (from monthly measurements) of wind speed, air temperature and rainfall for the period 1940 to 2003 for Croppies Bay indicates a trend of increasing wind speeds (r^2 = 0.408) and air temperature (r^2 = 0.703), accompanied by a decline in rainfall (r^2 = 0.154). A fifteen-year running mean correlation of these atmospheric parameters (Figure 4.22) yields a correlation between increasing air temperature and declining rainfall of r^2 = 0.90, and between increasing wind speed and declining rainfall of r^2 = 0.95. The trend per year (based on the fifteen-year running mean correlation) for wind is an increase of 0.0316 m/s, air temperature an increase of 0.0369°C, and a rainfall decrease of 2.550 mm. These predicted trends are in keeping with the findings of Umina and Weeks et al. (2005:692), who compared BoM data from 36 low altitude weather stations located along the eastern coast of Australia. Umina and Weeks et al. (2005:692) reported an increase in the mean temperature at a rate of 0.1° to 0.3° every 10 years, and a decline in rainfall at a rate of 10 to 70 mm per year, indicating that the eastern coast of Australia is gradually becoming warmer and drier.

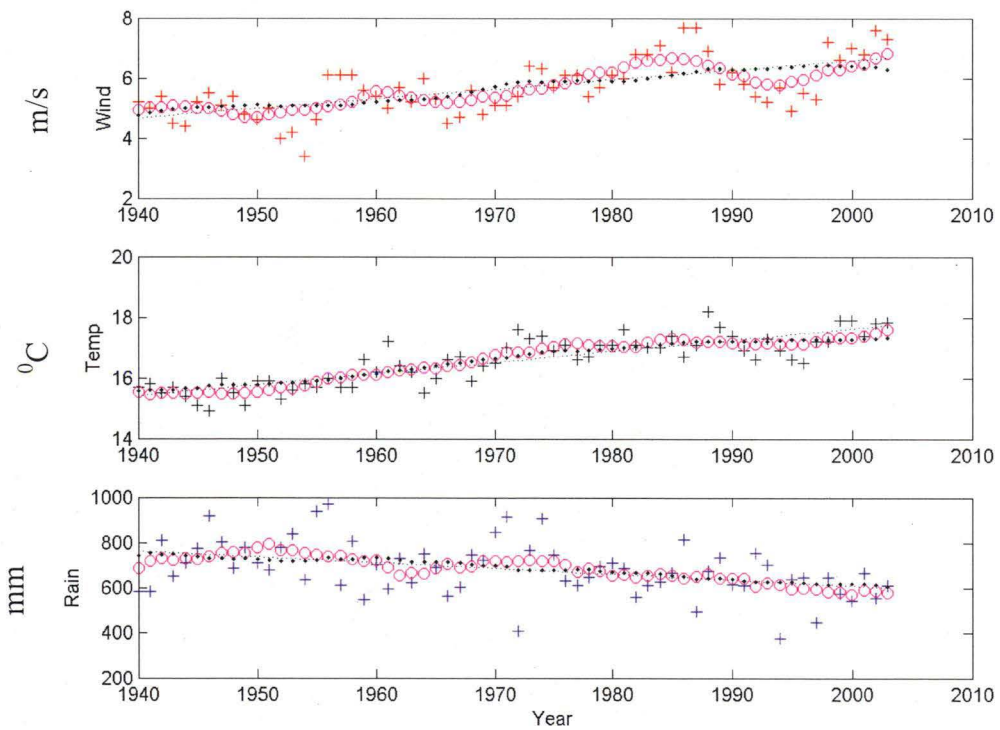

Figure 4.22 . Running mean of annual wind speed, air temperature and rainfall for the period 1940 to 2003, Croppies Bay.

Symbols indicate the 5-year running mean (O), 15-year running mean (...), and the linear regression line (---) to the original data (+). Data sourced from BoM Low Head (wind speed and air temperature), Bridport and Waterhouse (rainfall).

To determine the impact of these predicted trends on sand dune activity, three periods into the future (2014, 2029 and 2054) were selected and the P/E value calculated at intervals of 10 years (- 25.5 mm), 25 years (- 63.75 mm) and 50 years (- 127.5 mm). The evaporation rate and wind speed for the Lancaster index were maintained at the 2004 rates, and based on the six month period transitions in Figure 4.6. It was assumed that the dry phase would extend to 7 months, incorporating April. The total predicted P/E values were then averaged over the seven months and applied to the Lancaster dune migration index. The results of these predicted trends on dune mobility are shown in Table 4.12.

Table 4.12. Predicted trends on dune mobility: applying Lancaster's (1997) indices to calculate M and P:E.

	Six month periods				Seasons			
Trend intervals	Indices value	Year	Dry	Wet	Summer	Autumn	Winter	Spring
2004	M	100	170	39	248	81	30	97
2014	M	104	183	39	275	85	30	101
2029	M	128	226	41	320	91	30	110
2054	M	122	283	40	428	104	30	124
2004	P/E	0.71	0.36	1.4	0.31	0.92	2.1	0.68
2014	P/E	0.68	0.36	1.6	0.28	0.88	2.1	0.65
2029	P/E	0.6	0.3	1.5	0.24	0.82	2.1	0.6
2054	P/E	0.58	0.24	1.5	0.18	0.72	2.1	0.53

Table 4.13. Predicted trends on dune mobility: applying Tsoàr and Arens (2004) index to calculate DP (q).

Year	Predicted trend	m/s	DP (q)
2004		8.1	160
2014	0.316	8.4	188
2029	0.79	8.9	237
2054	1.58	9.9	360

The same time intervals were applied to the Tsoar and Arens (2004) index to calculate DP (q) by adding the predicted increment of increase in wind speed to the 2004 mean site wind speed of 8.1 m/s. The results of these predicted trends on dune mobility are shown in Table 4.13.

Table 4.12 shows that under the predicted future climatic conditions, aridity (P/E) progressively increases markedly in three seasons, summer, autumn and spring, with the summer predicted to change classification unit from semi-arid to arid by 2054. The extension in the duration of aridity is linked with changes in dune mobility, reflected in the annual M indices, which indicates that the dune remains partially fixed by vegetation. Analysis of the inter-year data predicts that within 25 years the dry six-month period will change classification units to be fully active offset by a

continuation of the 'fully fixed' classification in the wet six-month period. The primary message contained in Table 4.12 is one of a predicted drift towards increased mobility typified by progressive increases in M over the 50-year prediction period. The seasonal analysis indicates that three seasons contain shunts in classification class from a status of partially fixed to fully active dunes. The data analysis of wind-energy, DP, complements the findings of M and P/E, indicating a progressive increase in the mean effective annual wind speed, almost double the 2004 site threshold wind speed of 4.5 m/s within 25 years.

The combination of a predicted reduction in rainfall (19%) over 50 years and an increase in air temperature (7.4%) are likely to increase the incidence of drought, accompanied by a reduction in plant cover. Bridgeman (in Knight and Orford et al. 1998:198) suggested that a 20% reduction in precipitation in the southern continents would contribute to an increase in dune mobility due to droughts. It is unknown at this stage whether the current interval of seven months of effective winter rainfall will be shortened in duration, or, whether the present five low rainfall months become drier, or, whether the incidence of rainfall is reduced throughout the year.

There are no regional historical analogues of droughts available to assess and compare the effect of prolonged changes in rainfall, wind speed and air temperature on coastal dune mobility. However, predicted atmospheric conditions are approaching those suggested by Bowden (1981, 1983), Sprigg (1979), and Colhoun (1991) as occurring during the Last Glacial phase. Sprigg (1979) inferred, based on the orientation and morphology of the longitudinal dunes, that winds were drier and consistent with a zonal westerly flow of greater intensity and velocity. Bowden (1981, 1983) calculated that a mean wind speed of 9.7 m/s was necessary to generate the bedforms of the longitudinal dunes that were emplaced in NE Tasmania during the Last Glacial phase. Colhoun (1991) suggested that precipitation was about 50% lower than present values inferring drier conditions that contributed to aeolian activity, and that air temperatures were 4 to 7°C cooler during that phase. Their suggestions do provide a framework in which a range of atmospheric parameters contributed to a phase of active dune mobility adequate for the emplacement of longitudinal dunes (Ainslie Sand) that are 10s of kilometres in length.

An earlier study (Mowling, 1998), located 5 km south of this study site, used a time series of digitised aerial photographs to describe the morphology of a portion of an extensive transgressive Holocene dunefield, 1949 – 1997. For the period 1949 to 1964, comparative analysis of the aerial photographs established a phase of natural revegetation – an increase of 14%, followed by a subsequent increase of 4% over a 20-year period, followed by a decline in area of natural vegetation for the period 1984 to 1997. The 1949 to 1964 phase of revegetation coincided with a period of below average wind speeds of 4.7 m/s (0.9 m/s below mean), nominal below average air temperature of 15.9°C (0.6°C below mean), and rainfall 48.7 mm above average. This interval is indicative of climate values that promoted revegetation of dunes, and may provide a predictive tool illustrative of the range of atmospheric parameters conducive to the natural fixing of dunes. Sustained movement away from these conducive values are associated with a decline in vegetation cover. Hesp and Hyde (1996) and Wolfe (1997) established that prolonged drought accompanied, or followed by, strong winds, can lead to a reduction in vegetation cover, the remobilisation of fixed or partially fixed dunes, accompanied by an increase in the

number of blowouts, leading to the merging of parabolic dunes into an actively mobile sand sheet or transgressive dunefield.

Lancaster (1997:334) defined minor climate change as short-term with an incidence of decades to centuries. He observed that the limited duration of El Niño-Southern Oscillation periods (5 – 7 years) compared to those associated with glacial-interglacial cycles (1,000s of years) are of short duration but have regional significance in the form of droughts. Hesp (2003) established a correlation between El Niño-Southern Oscillation periods and high migration rates of low and narrow (0.5 m high, 60 m wide) parabolic dunes in New Zealand and Holland. Analysis between the above Croppies Bay data set, and the contemporaneous El Niño-Southern Oscillation period[18], indicated no apparent association or correlation for this study site.

Neither wind nor sediment availability are limiting factors on downwind migration at Croppies Bay. Heath vegetation abuts the toe of the lee flanks and dune[19] vegetation grows on the lee of flanks of this parabolic dune, thus plant growth is robust when remote from actively mobile windward slopes and lee slip faces. What is distinct from transgressive dunes to the north and south of this study site is deflation and bed scour down to the water table. There is free standing water in shallow deflation hollows both within the deflation basin, aligned along the external margins of the trailing arms, and within the heathland for > 60% of the year. At the base of the stoss, sand is saturated intermittently for several months. Thus, hydrology may be a contributing factor in the formation and maintenance of the trailing arms as the nose of the parabolic dune migrates downwind. A sustained reduction in rainfall over 32 years may have reduced the influence of hydrology on the lateral outer margins of the north trailing arm, facilitating lateral migration.

In conclusion, analysis of wind, rainfall and air temperature data indicates that with increased aridity and a linked increase in DP, aeolian activity is predicted to increase. Under the influence of the current atmospheric parameters, a long-walled parabolic dune has actively mobile windward slopes and continues to evolve downwind. The cumulative response to the ten, twenty five and fifty year predicted trend of increasing aridity for three seasons (summer, autumn, spring) and the associated increase in DP is a projected decrease in plant cover, the re-activation of fixed dunes, and the merging of active and re-activated dunes into an actively mobile dune field which will transgress abutting land to the east. The trend predictions are independent of external factors such as fire, or an increase in the rate of off-road recreational activities which will probably contribute to the development of a positive feedback between reduced vegetation cover and the liberation of sand for deflation, resulting in wind acceleration close to the ground.

---

[18] www.cgd.ucar.edu/cas/catalog/climind/soi.html;

[19] Open to closed canopy tall shrubland of *Acacia sophorae*, *Leucopogon parviflorus*, *Olearia axillaris*.

4.10 Summary

To date, empirical field based studies that describe the feedback between wind flow patterns and flow close to the ground on the evolution of dune form are few in number and have been located extensively in desert dunes or confined to relatively small blowouts in coastal frontal dunes. Robertson-Rintoul's (1990) research described near-surface wind flow over a parabolic dune using arrays of cup-anemometers and flow visualisation. However, she did not look at the broader influence of wind-resultants or seasonal flow on dune form. Finigan and Neil et al. (1990), with the aid of a wind tunnel and a 1000:1 scale model of a symmetrical parabolic dune, analysed the wind flow pattern and the influence of topographic steering on dune form. Gaylord and Stetler (1994), Wolfe, (1997) and Muhs and Maat (1993) evaluated climatic conditions that promote or diminish aeolian activity in inland dune fields. Lancaster (1997) and Tsoar and Arens (2004) developed indices to calculate sand dune mobility.

This research presents an analysis and description of the feedback between seasonal wind flow patterns and near-surface wind flow on the evolution of a parabolic dune form. This is accompanied by an analysis of the relationship between the atmospheric parameters of wind speed, rainfall and air temperature on aeolian processes at Croppies Bay to determine which circumstances promote an increase or a decrease in dune mobility in a temporal and spatial context. An evaluation of the capacity of indices designed to calculate sand dune mobility, and their applicability to the study site, has been undertaken. Based on a search of the existing scientific literature, this empirical description of the feedback between seasonal wind flow patterns and near-surface wind flow on the evolution of a parabolic dune form, accompanied by predictive trends on coastal dune mobility, this research fills significant gaps.

The predominant wind pattern at Croppies Bay is typified by a prevailing westerly and southwesterly flow with a mean site wind speed of 8.1 m/s, and site maximum wind speed of 48 m/s. Thirty-two percent of wind flow occurs below 4.5 m/s, which represents the threshold below which effective sediment transport does not occur. High velocity wind events, characterised by the average number of days with records of wind speeds greater than 12 m/s, occur 27% of the year, and 68% of wind speeds are above threshold velocity. Summer and autumn have the highest frequency of high velocity winds, and spring has the highest frequency of wind speeds below threshold. There is a distinct seasonal and diurnal pattern to the wind flow although the prevailing wind flow from the west is strongest in all seasons between midday – 6 pm. During late spring, summer and early autumn months (November to March), the thermally driven land-sea breeze system is effective in transporting sediment.

By applying Fryberger's (1980) method it has been determined that the study site at Croppies Bay experiences an intermediate-energy wind environment. The annual resultant drift potential (RDP) for this study site is 7652 VU (vector units), ranging from 150 to 2659 VU. Sixty percent of recorded wind events generated DPs greater than 1,000, with an autumn recording period generating a DP of 2671 (VU). The annual resultant drift direction (RDD) for this site is 69°. Seasonal vector averaged

wind speeds indicate that summer and autumn have potentially higher resultant distances of sand transport than spring and winter.

The quantitative and qualitative evaluation of near-surface air flow on windward slopes was accomplished using arrays of thermo anemometers set at heights of 15, 45 and 190 cm above ground surface on 2 m masts, accompanied by wind vanes at the same heights, and flow visualisation on the stoss and lee slipface.

The wind velocity profiles on the windward slopes demonstrated that the intrusion of the dune into the stream flow affects the vertical velocity gradients close to the dune surface, and that flow acceleration varies over the dune profile and between windward slopes. This is demonstrated by the wind shear velocity profiles derived by applying the Frank and Kocurek (1994) equations.

Shear stress ($u*$) more than doubles between toe on the flank of the NTA (north trailing arm) (1.03 $u*$ m/s), and mid-slope (2.27 $u*$ m/s), decreasing nearly five-fold at the crest to 0.48 $u*$ m/s. Mid-slope on the flank is both convex and the steepest part of the 28^0 slope wall, thus apparently contributing to a convergence of streamlines, generating an increase in pressure, which results in an increase in $u*$ with a roughness length (z_0) of 0.041 m. In contrast, the stoss from toe (1.56 $u*$ m/s) to crest (1.75 $u*$ m/s) does increase, but not progressively. Mid-slope, where the stoss is distinctly concave, $u*$ is 1.05 m/s, with the shortest roughness length (z_0) of 0.009 m. The wind shear velocity profiles were not log-linear due to saltation seen during the simultaneous 30 minute recording phases.

Flow visualisation confirmed that the form of the stoss bed reflects the pattern of airflow in above-threshold wind flows. Flow remained close-to-the-bed from the toe of the stoss to mid slope, indicating that there is no stalling of flow or back eddies. Between mid slope and the crest, a 3 m high reverse rotational flow down-slope towards the mid slope explains the feedback that forms a concave bed, when mean wind speed is in excess of 7 m/s. At the crest of the stoss, both the wind shear velocity and smoke plume indicate that wind speed below a height of 20 cm is above threshold, with separation of flow commencing at elevations above 30 cm and increasing in depth downwind. Flow approached direct to the lee crest, separating at the crest into three: 1) flow close-to-the-bed of the slipface from crest to toe whilst the slipface was in shadow; 2) lee eddies formed in the wake of the slipface; 3) streamline constriction continued several hundred metres in the wake flow before reattachment to streamflow.

The sand dune mobility indices of Lancaster (1997) and Tsoar and Arens (2004) complement each other by extending the interpretative capacity of each respective index.

Analysis of the relationship between the atmospheric parameters of wind speed, air temperature and rainfall for the period 1940 to 2003 for Croppies Bay indicates a trend of increasing wind speeds ($r^2 = 0.408$) and air temperature ($r^2 = 0.703$), accompanied by a decline in rainfall ($r^2 = 0.154$). A fifteen-year running mean correlation of these atmospheric parameters predicts, per 50 years, an increase of 1.6 m/s (19.5% of current value) in wind speed, an increase of 1.8°C (11% of current

value), and a decrease in rainfall of 127.5 mm (19% of current value). The cumulative response to this predicted trend would lead to a reduction in plant cover, contributing to an increase in aeolian activity, resulting in a re-activation of fixed dunes, which are then projected to merge into an actively mobile dune field and transgress abutting land to the east.

CHAPTER 5

Flow and morphodynamics

5.0 Introduction

This chapter presents quantitative data of topographic changes and sediment movement for a coastal parabolic dune and links these data to seasonal wind flow dynamics and geomorphic changes. It aims to contribute to our understanding of the relationship between wind flow and process response in a long-walled parabolic dune. Previous studies have been model based such as Finnigan and Neil (1990), or qualitative such as Robertson-Rintoul (1990), or based on small blowouts located in foredunes such as Gares (1992) and Hesp and Hyde (1996). David and Wolfe (1999) and Lancaster (1985), who worked on inland dunes, which experience more moderate wind regimes than coastal dunes, have provided constructive benchmark work. Fryberger (1980) contributed the wind resultants technique indicating the direction of sand transport.

There have been a number of previous studies that have used traditional geomorphic survey methods combined with either remote or in situ wind data to describe the influence of flow dynamics on blowouts, for example Hesp and Hyde (1996), Gares (1992); Gares and Nordstrom (1995), Fraser and Bennett et al. (1998). To date, there are very few published field based surveys that have integrated traditional geomorphic survey methods with kinematic GPS (Stokes and Goudie et al. 1999; Mitasova and Overton et al. 2005) to generate quantitative data that accurately portrays topographic changes and sediment movement, linked to wind flow patterns. Thus this chapter addresses a series of gaps in the literature regarding the interplay between flow, process and form on the evolution of a long-walled coastal parabolic dune.

The specific objectives of this chapter are to determine the influence of wind speed, wind direction and the frequency of wind events on dune morphodynamics, and to quantify the dune migration rates and dune volumetric changes for temporally spaced wind events.

5.1 Methods

5.1.1 Reconnaissance and ground truthing

Following the acquisition of the temporally spaced aerial photographs, the Croppies Bay transgressive dunefield, beach, headlands and the Ainslea sand formation (Bowden, 1981) were ground-truthed by vehicular and foot traverses to verify the bedform features contained in the aerial photographs. A Garmin 12 GPS (accurate to ± 5 m) was used to locate key bedforms.

5.1.2 Rectification of aerial photographs

To determine the temporal and spatial evolution of the Croppies Bay parabolic dune a comparison of a sequence of vertical aerial photographs was undertaken to determine the longer-term changes in dune morphology and the rate of downwind migration.

Following an assessment of the quality (crispness and definition in the image, contrast in tone and texture) and scale of aerial photographs held by the Department of Primary Industries Water and Environment Office, Hobart, Tasmania, a sequence of four aerial photographs were selected, extending over a fifty year period – 1949, 1964, 1984, and 1999[1]. These photographs were scanned using the HP Deskscan Software and saved as uncompressed TIFF images.

A series of clearly defined natural and anthropogenic ground control features, common to each sequence of aerial photographs, were identified. These ground control features were subsequently located in the field and registered with a Garmin 12 GPS (accurate to ± 5 m), generating 125 waypoints. The single sequence of aerial photographs were then ortho rectified and georeferenced using the *Arcview* computer program. The rectified aerial photographs were accurate to 10 m, within each rectified image and between each sequence.

The *Arcinfo* program was applied to digitise the bedform boundaries in each sequence of aerial photograph, forming polygons of the:

- external periphery of the parabolic dune – defined by the interface between tonal / textural characteristics of mobile sand and vegetation;
- periphery of the deflation plain – defined by tonal / textural characteristics indicative of the interface between toe of dune and plain;
- neck of parabolic dune;
- beach and high tide;
- foredune;
- trailing arms;

[1] The aerial photographic information is summarised in Appendix 4.

- lee slipface;
- sandsheets on the deflation plain – defined by tonal / textural characteristics;
- extant nested parabolic dune bedforms, both mobile and fixed;
- vegetation.

These digitised boundary polygons were colour coded for each aerial photograph sequence, and could be turned on and off between aerial photograph sequences in the *ArcView* program, to facilitate temporal / spatial comparisons between sequences. The area of each polygon was calculated to compare temporal / spatial transitions between fixed and mobile bedforms, the rate of downwind and lateral migration, and changes in vegetation cover.

The rate of dune displacement was calculated using the method developed by Finkel (1959; 1961). By comparing the scale-identical ortho rectified, digitised aerial photo sequences, the net displacement in the horizontal plane was determined over a given time. The net displacement was then divided by the time interval between each sequence to calculate the displacement rate, expressed in unit distances per unit time. Ground truthing was undertaken between 2000 and 2003 to verify interpretation of bedform features on the aerial photographs by visiting the bedforms in the field.

5.1.3 Ground survey

The present study used a combination of techniques to determine dune morphodynamics and dune migration patterns over a period of about four years (2000 – 2004). The techniques incorporated the installation of thirty-three erosion pins and an on-site meteorological station, and repeated dune surveys using GPS measurements and GIS techniques.

5.1.3.1 Erosion Pins

Thirty-three, one metre 16 x 16 mm long hardwood stakes were used as erosion pins (EPs) to record and then analyse the spatial distribution of deflation and accretion within the parabolic dune. On the stoss, the one metre stakes were replaced with one-centimetre circumference aluminium rods measuring 2 m in length for the last 12 months of the recording period. Each EP had a stainless steel label attached which had hand-punched numbers that identified the location on the deflation plain or stoss. The EPs were installed around the periphery of the deflation plain (n = 21), at the mid-line of the stoss (n = 7), at the base of the lee slip face (n = 3), and aligned 91° up the centre of the deflation plain (n = 2). The EP locations are shown in Figure 5.1. Surface elevation changes and downwind and lateral migration of the stoss and dune toe were recorded at irregular intervals over a thirty-month period using a high quality fabric metric tape measure. Deflation pits or accretion mounds that developed at the base of the EPs were levelled with the aid of the side of a ruler to the same ground surface height as the surrounding area prior to taking measurements.

The intervals of measurement of changes in surface elevation at each EP, the downwind migration of the head of the dune, and the lateral migration of the trailing arms, were synchronised with the intervals of downloading the on-site wind data, to enable analysis of the discrete interaction of wind events on deflation or accretion of sediment. Subsequently, these synchronised intervals of wind data were applied to generate the wind resultant sand roses (Fryberger, 1980) (Chapter 4, Figure 4.13, Table 4.4).

The measurement of changes in surface elevation is problematic due to the cycles of deflation and accretion over time. The equation developed by Pluis (1992:664) to calculate surface elevation changes addresses this problem and was applied in this study. The mean surface elevation change for each EP was characterised by the net change in surface elevation (Lc) and the sum of all changes (Lt):

$$Lt = 1/n_p \sum(A + D) \qquad \text{Equ 5.1}$$

where A and D, respectively, are the increase and decrease in surface level height between individual recording periods, and n_p is the number of pins per bedform unit (viz. stoss, toe of stoss , toe of NTA and STA respectively, and toe of lee slipface).

The location, height, and surface elevation changes at the erosion pins provided a direct check against the GPS measurements and subsequent GIS data analyses.

5.1.3.2 Copper erosion pins measuring changes in surface elevation during measurement of close to the ground wind flow

With the aim of acquiring an erosion or an accretion rate, five one meter grids comprised of nine very fine (1 mm) copper EPs (welding rods) were deployed 1 m upwind from selected arrays of thermo anemometers (TAs) on both the windward flank and stoss to simultaneously measure changes in ground surface level with the thirty minute duration close to the ground wind flow measurements, as discussed in Chapter 4, 4.7.2. The height of each EP was measured before and after the wind flow measurements.

Mean elevation change for each 1 m^2 area (Lc′) was characterised by the net change as

$$Lc' = \sum (A'-D') \qquad \text{Equ 5.2}$$

where A' and D' respectively are the increase and decrease in mean surface height of each pin over the recording period. Using the measured bulk density, changes in elevation could be converted to sediment transport rates in $g/m^2/s^{-1}$.

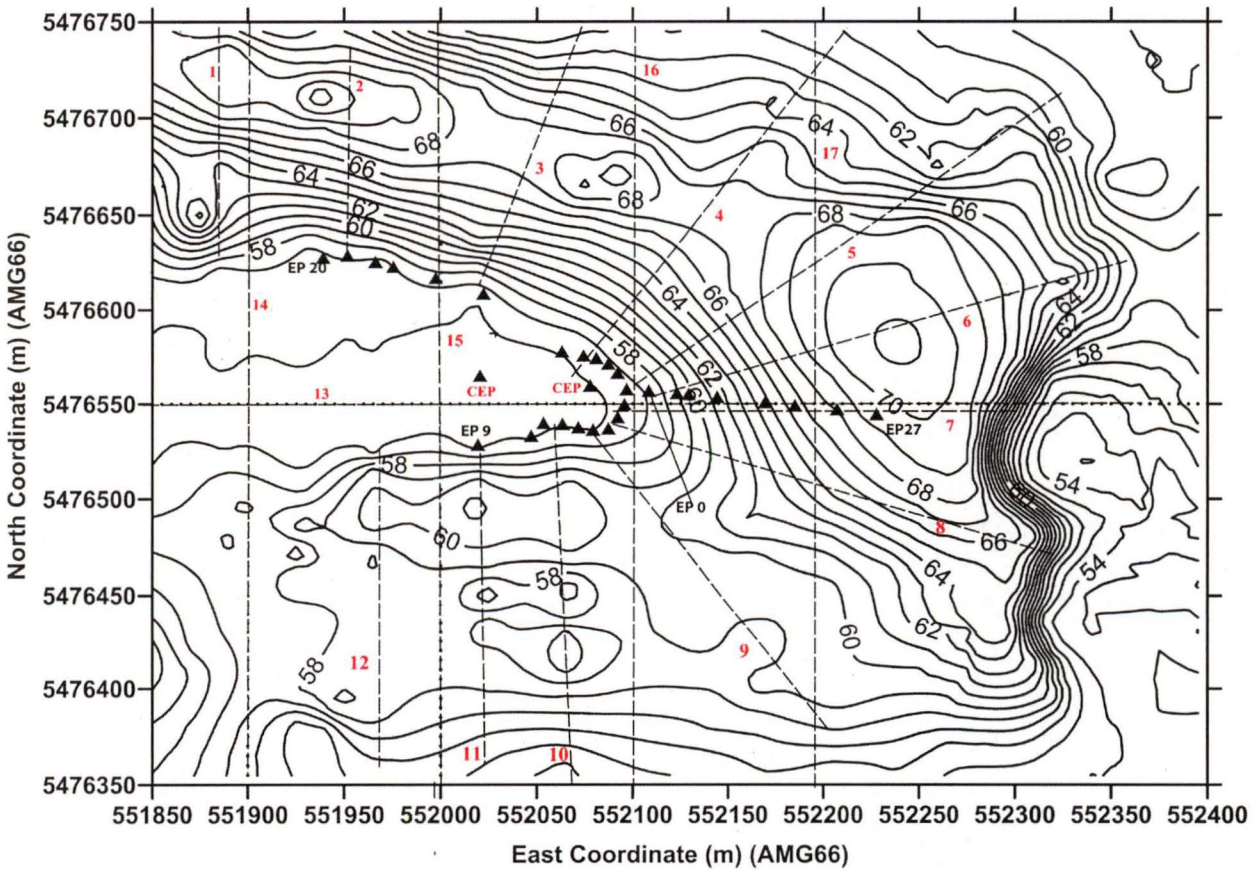

Figure 5.1. Location of the erosion pins (▲) on stoss, periphery of deflation plain, and central alignment; central erosion pins (CEP). Location of GPS profiles 1 to 17 (– – – – –). The topographic map is generated from Epoch 1 GPS data.

5.1.3.3 GPS Surveys

The GPS field surveys were conducted with the assistance of third-year surveying students from the University of Tasmania. Figure 5.2a shows the control network for the dune survey which was comprised of six stations sited on the periphery of the parabolic dune system. This network was established in April 2000, using conventional survey techniques of traversing using a 5 sec Sokkia total station instrument, and after adjustment, defined three-dimensional coordinates of the six points with precisions of a few cm.

Static GPS techniques (using dual-frequency Ashtech Z-Surveyor units) were used to coordinate the position of a main control station (ST0 1, shown in Figure 5.2a), located on the STA of the parabolic dune to the north of the Croppies Bay study site. Using this control station as a base, kinematic GPS data were collected using Ashtech Reliance rover units (single frequency) at sampling intervals (epoch data rate) of between 1-20 secs. The dune system was mapped by walking with the GPS rover units across the dune surface in a series of profiles along and across the dune, at a profile spacing of about 20 m. Along each profile, with data rates of between 1 - 20 secs and at walking pace, coordinated points were at a horizontal spacing of about 1 - 20 m intervals. Figure 5.2b shows an example of one that developed the profiles for Epoch 5.

Table 5.1. Kinematic GPS survey dates, sampling rates at Croppies Bay parabolic dune.

		Interval between	Sampling Rate	
Epoch	Date	surveys - days	Seconds	Points
1	29.4.2000	-	5	488
2	28.4.2000	151	2	5514
3	12.11.2001	411	.1	4592
4	3.5.2002	162	20	784
5	5.9.2002	125	1	10,897
6	22.8.2003	351	1	17,496

Each dune survey took about 4-6 hours to complete. The positions and heights of the erosion pins were taken during most of the GPS surveys, although not all EPs were observed. The GPS data were then reduced using Ashtech Reliance processing software and output in AMG66 grid coordinates and orthometric (mean sea level) heights. In the GPS processing, horizontal and vertical accuracies of each profile point were estimated, with typically accuracies of 2–5 cm in horizontal and 3–10 cm in vertical. Any point with greater than 50 cm in horizontal and vertical accuracy was excluded – about 5% of the data. The GPS profile data were then interpolated onto a 5 m by 5 m horizontal grid using kriging (with a linear variogram model) to produce contour models of the dune system.

A number of cross-sections were selected at various locations across the dune area, shown in Figure 5.1, and heights interpolated to these cross-section locations from the contour models, again using kriging. These cross-sections are called Profiles in the later

section of this chapter but they should not be confused with the original measured GPS profiles. The cross-section profiles were interpolated at selected sites for later analyses and are a result of the field surveys.

Field based surveys undertaken in remote locations, where heavy electronic equipment has to be repeatedly carried in through dense heathland vegetation, followed by traverses across an actively mobile dune (Figure 5.1), are subject to equipment failure that cannot typically be fixed in the field. Table 5.1 shows the variability between sampling rates, due to GPS equipment failure. The kinematic GPS surveys that generated the measurements for Epochs 1 and 4 covered the full dune area, generating a comparative database sufficient to construct topographic models.

The application of kinematic GPS to measure dune morphology and changes in ground surface elevation also enables the quantification of dune migration rates and the calculation of bulk volume transport rates. Stokes and Goudie et al. (1999:211) developed a series of indices to quantify morphological parameters that are extracted from the measured data collected from barchan dunes in the south western Desert of Egypt. These indices have been applied in this study, as follows:

$$\text{Dune reconstitution time} = \frac{\text{dune length}}{\text{dune velocity}} \qquad \text{Equ 5.3}$$

The dune measurements for length were taken from toe of stoss to toe of lee slipface, or, from toe of flank of trailing arms on the deflation plain to toe of lee flank. Embabi (1987) used the mid-point on the slipface of barchan dunes because it is the best means of locating the precise position of each dune, and, because the maximum dune width is coincidental with this position. Embabi (1987) established that the mid-point provided the most reliable variable, and thus was easily measured. In the instance of a parabolic dune with a 3:1 ratio (length : width), the width of the dune in cross section is narrower at the toe than at mid slope, due to the 30° receding angle of slope of the parallel trailing arms. Thus, in the Croppies Bay example of a parabolic dune, mid slope is also wider.

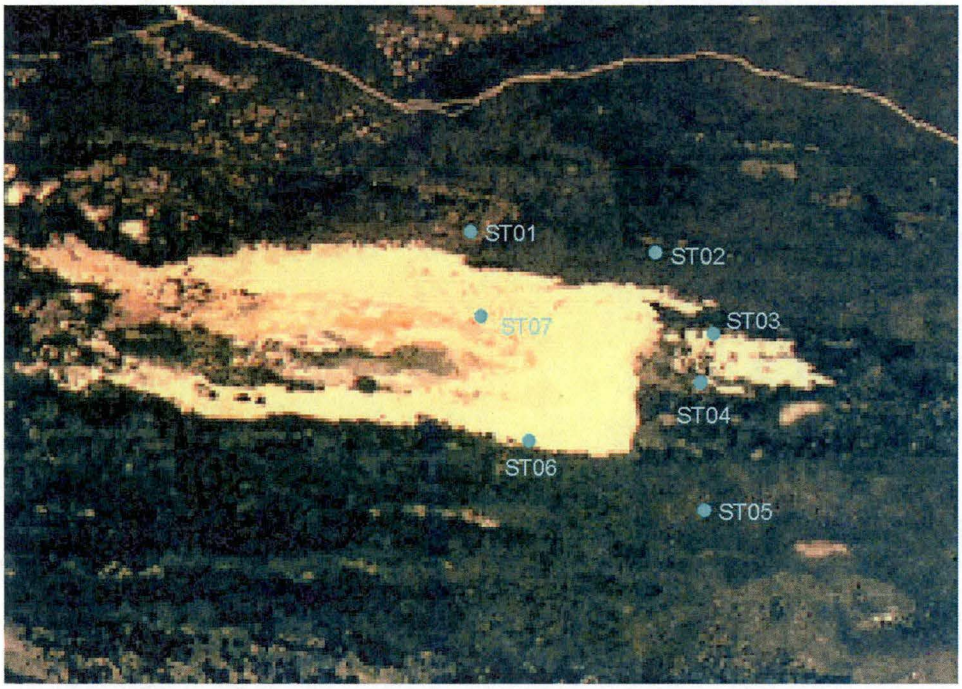

Figure 5.2a. Control network for the dune survey - comprised of 6 stations sited on the periphery of the parabolic dune system and toe of NTA.

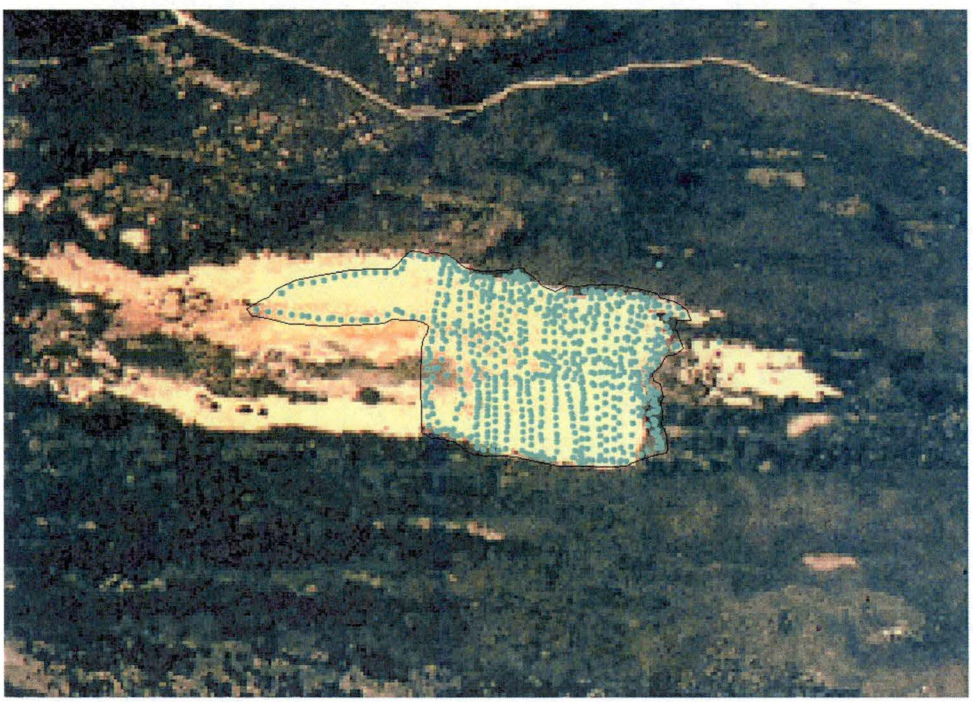

Figure 5.2b. Epoch 5 survey profiles, displayed on a scanned image of the 1999 aerial photograph.

5.2 Results and Discussion

This section of the thesis presents the results generated from the analysis of the temporally spaced aerial photographs, and ground truthing of aerial photography. It is followed by an analysis and discussion of the relationship between flow dynamics, sand transport direction and dune morphodynamics.

5.2.1 Reconnaissance and ground truthing

The reconnaissance and ground truthing of the Croppies Bay transgressive dunefield elaborated upon the status of the bedform features contained in the sequence of aerial photographs. The extracted features are shown in Figure 5.3a. Figure 5.3b shows a scanned image of the 1997 1:42,000 aerial colour photograph. Many of the bedform features shown in Figure 5.3a are obscured by natural vegetation in Figure 5.3b. The features that are clearly evident in Figure 5.3b are: the headlands, beaches interspersed by smaller headlands, the mobile parabolic dune (study site), the northern abutting parabolic dune, remnant trailing arms, a portion of the Ainslie Sand formation (Bowden, 1981), and a dolerite ridge that extends south to form a portion of the NTA neck of the study site parabolic dune. The south flank of the dolerite ridge and crest are extensively overlain by aeolian sand, with small outcrops of talus dolerite.

Figures 5.4a and 5.4b show the Croppies Bay parabolic dune from two views – east and west. These two Figures show the distinct tonal contrasts which distinguish the deflation basin, mobile sand, sand sheet overlaying the deflation basin and vegetation.

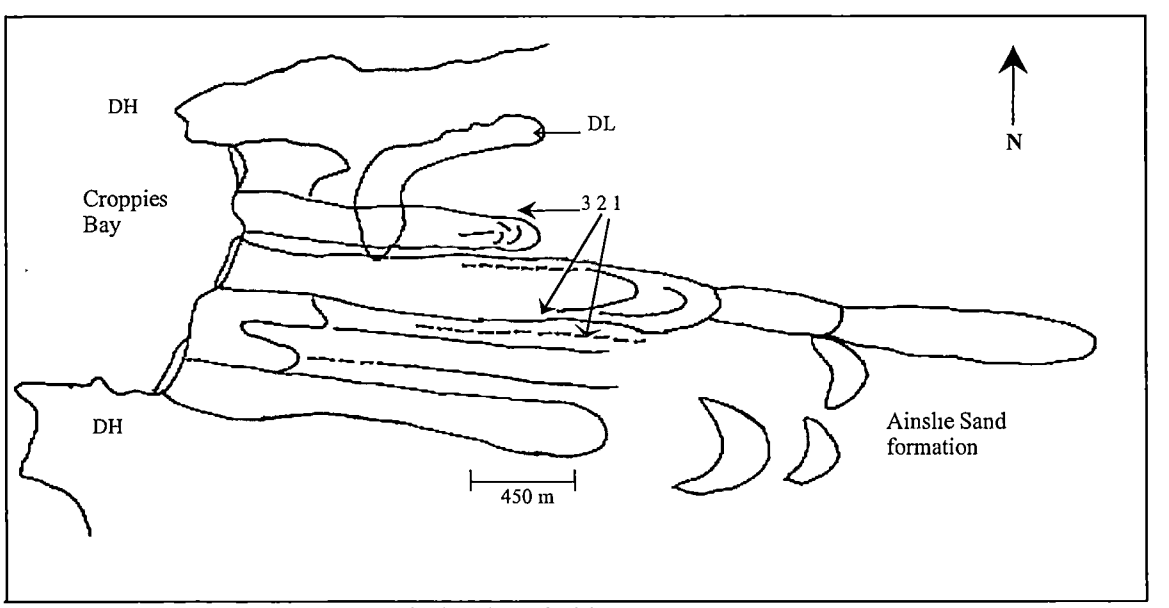

Figure 5.3a. Croppies Bay parabolic dunefield.

Dolerite Headlands (DH); Dolerite ridge (DL); Nested parabolic dune heads ⊃
Truncated – – – – and relict ——— trailing arms.
1: Indicative location of blown out NTA. 2: increased exposure of STA to SW sector winds. 3: parabolic dune located north of study site.

Figure 5.3b. Scanned image of the 1:42,000 1997 aerial photograph, showing the Croppies Bay transgressive dunefield, and the study site parabolic dune.

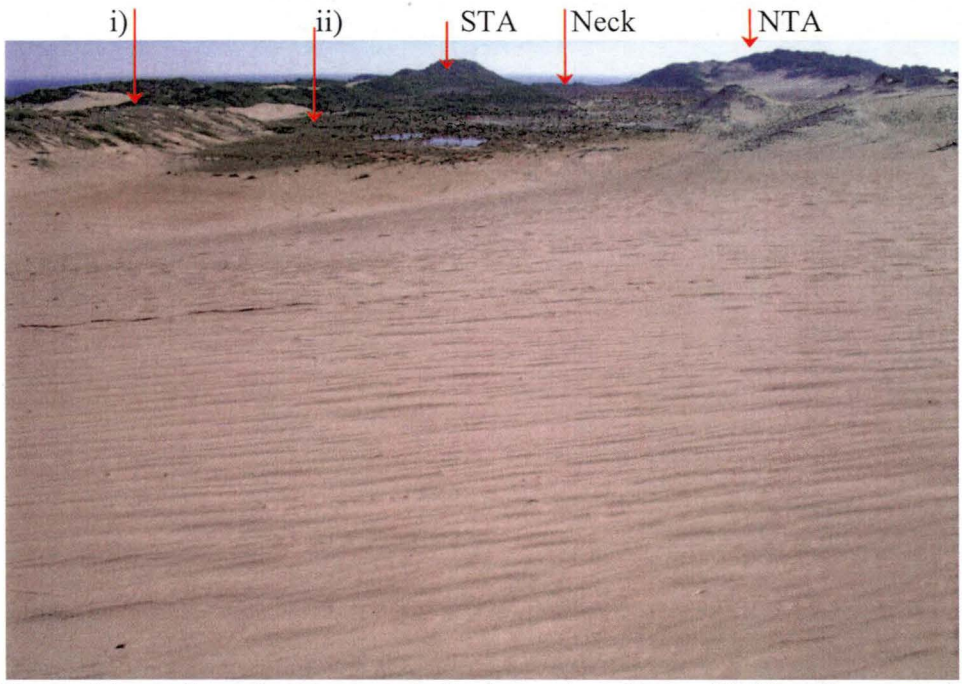

Figure 5.4a. Croppies Bay parabolic dune viewed west (2004). Shows: i) Spinifex sericeus ground cover on the south trailing arm (STA); ii) sedgeland colonising deflation plain; the neck of the dune, and north trailing arm(NTA). In the foreground is the stoss and windward slope of NTA with ripple bedforms.

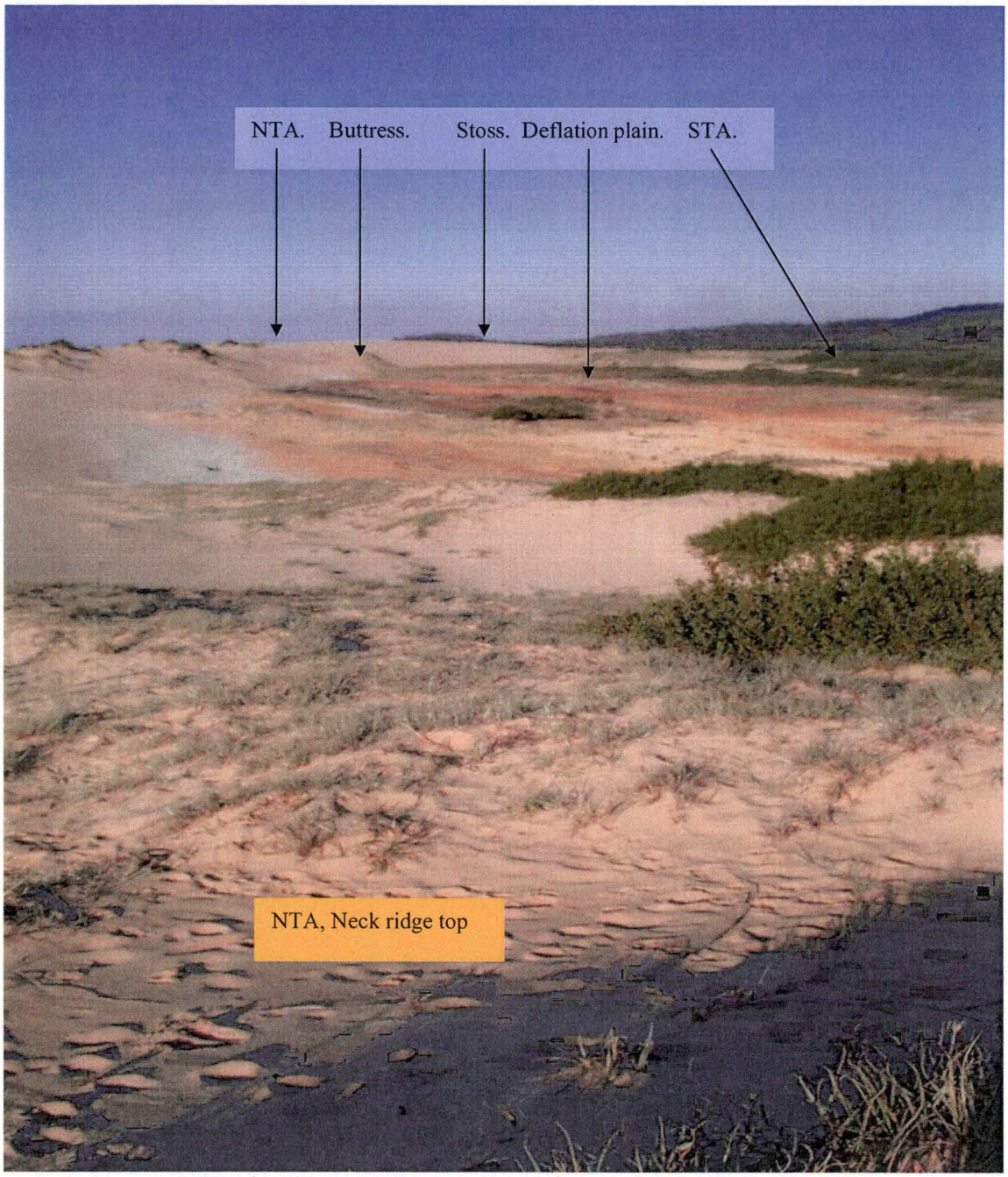

Figure 5.4b. Croppies Bay parabolic dune viewed east (2004) towards the stoss, taken from the ridge of the neck (14 m above deflation plain) of the NTA. Orange tones indicate the extent of the deflation plain, the lighter tones and areas of green indicate areas overlain by sand sheet.

5.2.2 Aerial photography

This section presents the findings of a comparison of the sequence of ortho rectified, georeferenced and digitised vertical aerial photographs to determine, firstly, the temporal and spatial morphological changes in the Croppies Bay parabolic dune, and secondly, the downwind and lateral migration rates.

5.2.2.1 1949 aerial photograph

The notable feature in the 1949 aerial photograph is an extensive fire that had incorporated the entire Croppies Bay transgressive dune field, the two headlands, and the Ainslie Sand formation (Bowden, 1981, 1983). Analysis of 1949 aerial photographs indicates extensive loss of natural vegetation. The response of the Croppies Bay parabolic dune to a loss of vegetation cover – arguably, the wind was more effective closer to the ground following removal of the roughness features of shrubs and grasses – is illustrated in Figures 5.5 and 5.7.

The 1949 image (Figure 5.7) shows the aerodynamic envelope of the blowout, which extended downwind 4,500 m. A low (< 2.5 m in height[2]) and narrow (average width of 70 m) bedform commences 2,300 m from the shore. The narrow width and the alignment of the bedform, particularly the eastern 3,000 m, suggests that topographic steering focussed the flow of an unimpeded jet stream on an exposed mantle of sand overlying a hard pan (mantle depth of 53 to 75 cm, overlying the B_2 horizon of indurated coffee rock).

Abutting the northern boundary of the eastern 3,000 m bedform are a series of disjunct elongated deflation basins, some measuring several 100 m in length, and up to 50 m in width. It remains undetermined whether these deflation basins partially sourced the sediment that formed the relatively uniform bedform, or whether the jetstream propelled the narrow flow of sediment downwind. If the sediment was derived from these deflation basins to form the aerodynamic bedform, the process of deflation was from north to accretion south, but this seems improbable. This aerodynamic bedform remains a distinct feature in subsequent aerial photo sequences, and is also clearly evident in the field.

Other morphological features shown in the 1949 image, are: (i) the deflation basin (150 m west to east), is confined to the western portion of the dune, commencing 30 m to the lee of the foredune. (ii) The stereo aerial photographs show portions of the rims of fixed and partially fixed nested parabolic heads which are incorporated into the aerodynamic envelope of the parallel trailing arms. There is no evidence in the 1949 aerial photographs that the series of nested parabolic dune heads had been breached, but this is due to the partially bleached image of the blowout, and (iii) unimpeded connectivity of beach sediment source with blowout.

[2] Height and uniformity of bedform determined during fieldwork, 2003.

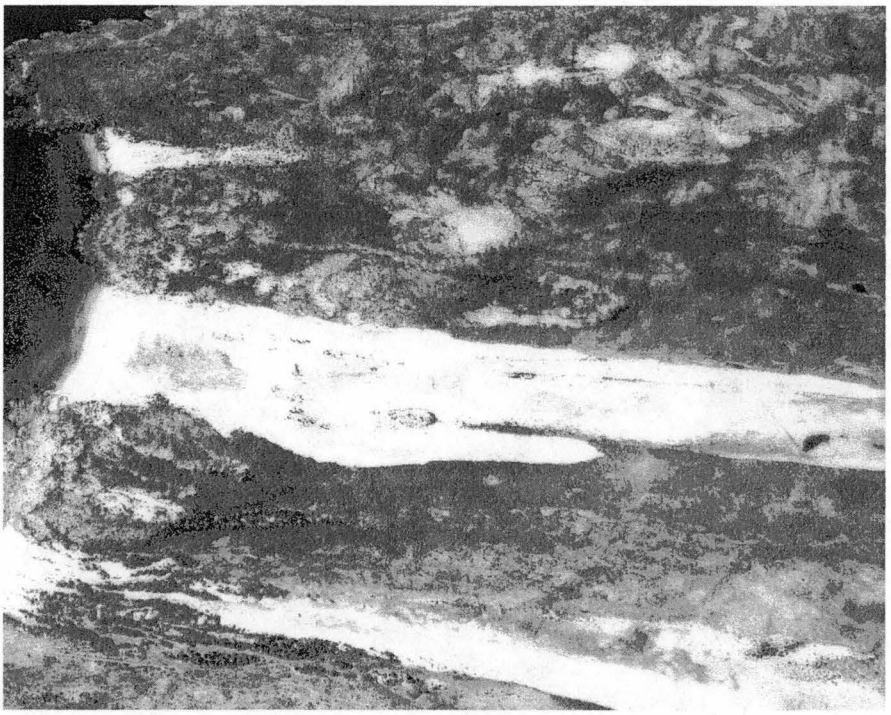

Figure 5.5. 1949 Arcview aerial photo (black and white image), showing the western portion of the Croppies Bay parabolic dune.

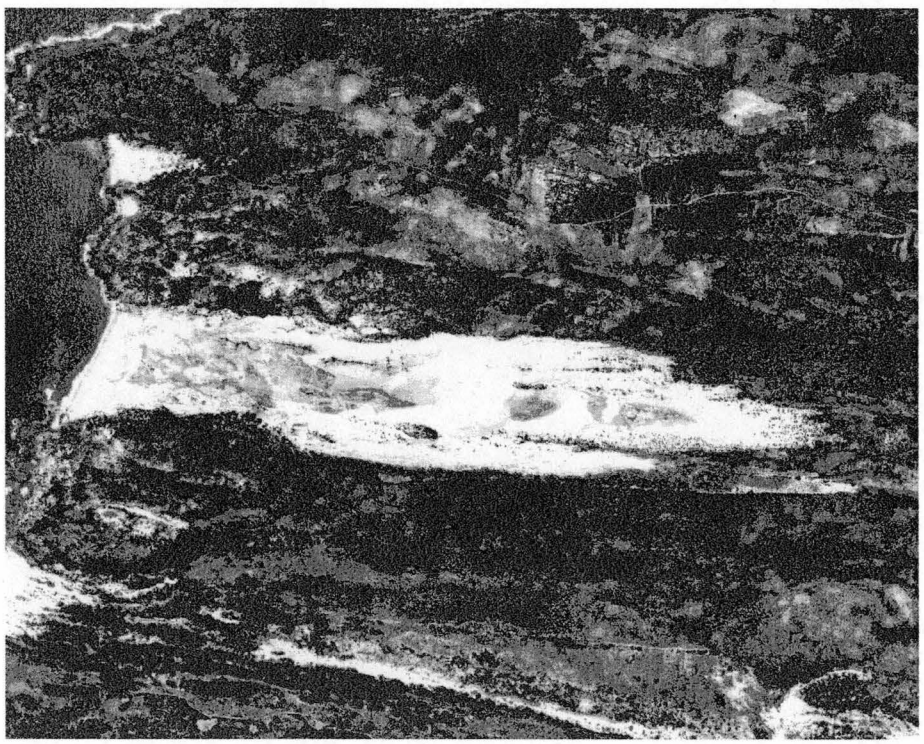

Figure 5.6. 1964 Arcview aerial photo (black and white image), showing Croppies Bay parabolic dune.

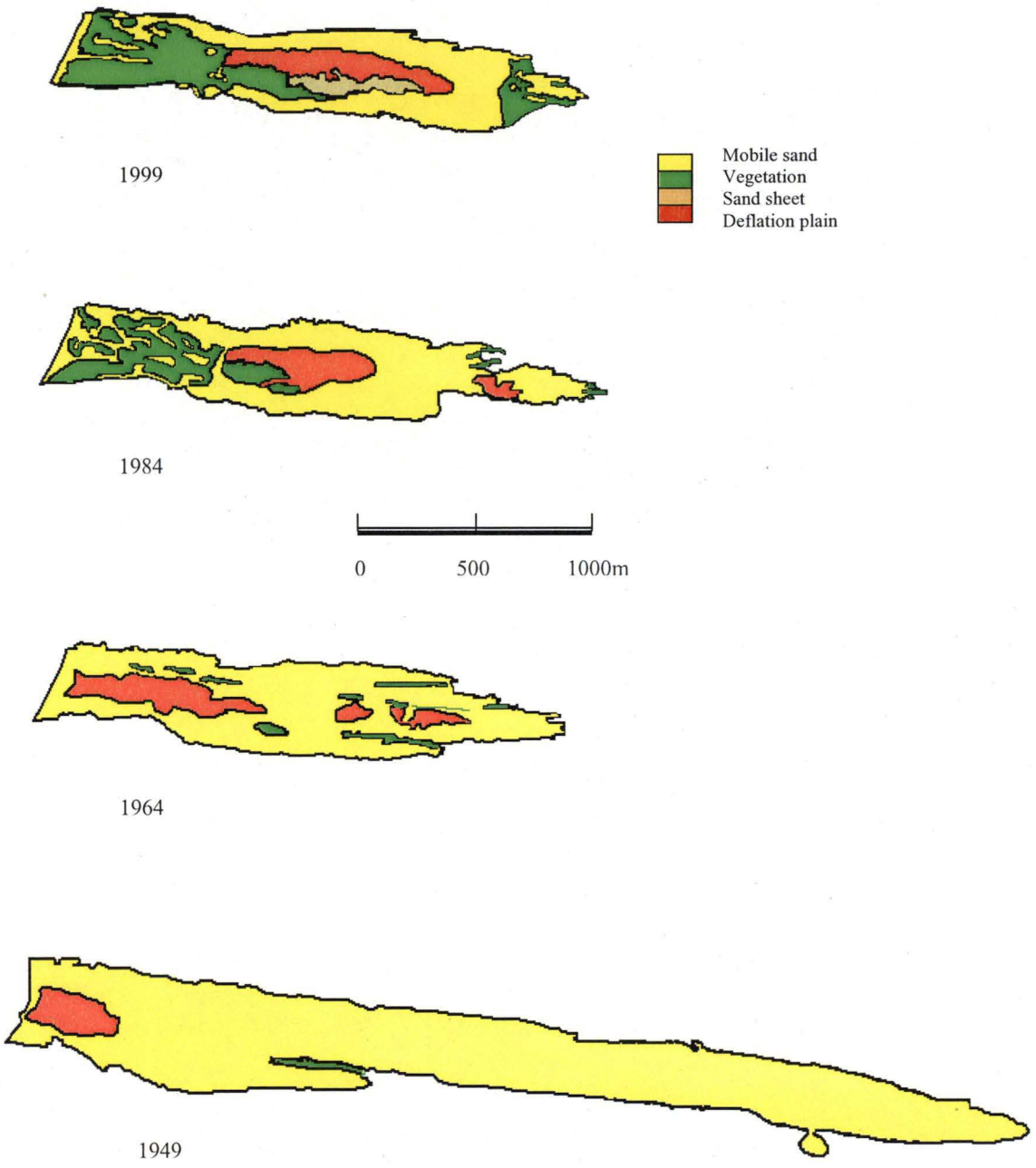

Figure 5.7. Temporal and spatial changes in the morphology of Croppies Bay parabolic dune, derived from a sequence of digitised, ortho rectified, and georeferenced aerial photographs.

Table 5.2. Temporal and spatial changes in the morphology of Croppies Bay parabolic dune, derived from the fifty-year sequence of digitised, ortho rectified, and georeferenced aerial photographs.

Descriptor	Aerial photograph sequences			
Parabolic dune	**1949**	**1964**	**1984**	**1999**
Area (m^2)	1,225,588	658,553	625,295	662,109
Perimeter (m)	11,598	7,483	7,487	5,885
Total length (m)	4,469	2,257	2,361	1,930
Transect 1 width (m)	330	315	284	338
Transect 2 width (m)	432	338	298	254
Transect 3 width (m)	358	399	372	373
Transect 4 width (m)	238	179	215	363
Deflation plain				
Area (m^2)	47,937	79,944	67,175	134,184
Perimeter (m)	1,026	2,091	1,933	2,421
Length (m)	363	852	671	1,019
Sand sheet				
Area (m^2)				21,161
Perimeter (m)				1,415
Length (m)				313
Vegetation canopy cover (cc)				
Canopy cover (area m^2)	0	16,599	131,418	242,836
% increase in canopy cover as a function of total area of dune	0	2.5	21	37
% increase between sequences as a function of 1999 area		2.5	17.3	16.8
Lateral migration, 1949 to 1999				
North arm migration at transect 3 (m)				78
South arm migration at transect 3 (m)				53
North arm migration at transect 4 (m)				53
South arm migration at transect 4 (m)				82
Downwind migration, lee slipface (m) interval between aerial photographs		32.8	27.3	22.6
Average rate of migration / 50 years				27.5

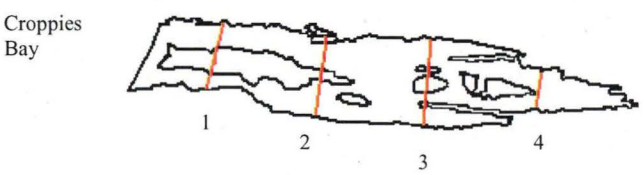

Figure 5.8. Location of transects 1 to 4. The location of the north to south transects in each aerial photograph sequence (1949, 1964, 1984, 1999) are identical. The outline in this image is the digitised 1964 image.

5.2.2.2 1964 aerial photograph

Figure 5.7, image 1964, Figure 5.6 and Table 5.2 show the following distinct morphological changes between 1949 and 1964. The sediment source from beach to parabolic dune remains intact through a dissected foredune. The deflation plain extended downwind some 850 m, extending through the neck of the parabolic dune. Two additional areas of deflation plain are revealed and these are linked with earlier emplacements of nested parabolic dunes. The process of fixing of the mobile dune by vegetation was afoot, with a nominal 16,600 m^2 (2.5%) of natural vegetation evident in the aerial photograph. Revegetation is evident on the NTA, west of the neck, and on the rim of an extant trailing arm, and in the southwest sector in the lee of the STA. The STA had lost vegetation cover resulting in an increase in the area of mobile sand. The periphery of the eastern portion of the blowout has attenuated due to fixing by vegetation of the low relief blowout present in the 1949 image. The nested parabolic heads remain mobile.

5.2.2.3 1984 aerial photograph

In the interval of thirty-five years (1964 – 1984), the key spatial transitions, shown in Figures 5.7 and 5.9, include an increase from 16,600 m^2 to 131,400 m^2 (21%, as a function of total area of dune) in dune fixed by natural vegetation. This fixing of a mobile landscape has occurred extensively on the deflation plain west of the neck of the parabolic dune; evidently, the vegetation is fragmented by mobile sand. For this to occur, the 1949 deflation basin must have been overlayed by sediment because there is no apparent tonal/textural indication of indurated coffee rock present in the aerial photograph. Connectivity between beach sediment source and the parabolic dune remains intact through the dissected foredune. The deflation plain, characterised by an indurated B_2 horizon, extends east of the neck. (iv) Fixing of the 1964 deflation plain proceeds in the southwest sector, namely in the lee of both the neck and STA. The NTA, STA, and head of the parabolic dune remain mobile and devoid of vegetation. The periphery of the eastern portion of the blowout continued to attenuate due to fixing by vegetation of the low relief blowout as shown in the 1949 image. The next phase of downwind migration of the parabolic head is evident, viz. the interface between the attenuation – the interface between previously emplaced parallel trailing arms and the two lobes north and south of the parabolic head.

5.2.2.4 1999 aerial photograph

Figures 5.7 and 5.10, and Table 5.2 show the changes in dune morphology and vegetation cover that have taken place in the interval of fifty years. The total area of the mobile parabolic dune has nearly halved (45%), the length of the mobile dune has decreased by 57% in response to fixing of the low aerodynamic bedform, and the area of the deflation plain has more than doubled in area. Thirty seven percent of the parabolic dune is fixed by natural vegetation, primarily on the earlier phases of deflation plain which are located

west of the neck, in the lee of the STA, and at the eastern end of the dune, which are also associated, principally, with deflation basins linked with earlier emplacements of dune heads. Connection to beach sediment is constrained to a single foredune blowout, which extends several hundred metres downwind into the western portion of the parabolic dune. The fragmentation in vegetation evident in the 1984 aerial photograph has reduced in area. Sand sheet overlays the deflation plain in the lee of the STA. Over the fifty-year period, the windward slopes, and crests of both trailing arms, the lee of the neck, and the head of the parabolic dune (stoss, crest and lee slipface) have remained both free of vegetation and mobile. Due to lateral migration of both trailing arms, relict late succession assemblages of plant species (shrubs to 3 m) that were growing on earlier emplacements of dune ridges, have been eroded (refer to Figure 5.7 1964 image for the location of linear remnant vegetation). Overall, the dune maintains its mobile parabolic bedform.

5.2.3 Downwind and lateral migration

The aerial photographs show a succession of nested parabolic heads, separate to and excluding the aerodynamic bedform discussed in 1949 above. The eastern outlying parabolic head is 3,350 m from shore, and is similar in aerodynamic form to the current head that is migrating downwind, namely 13 m high at crest, 30° lee slipface and 25° stoss slope angle. It is partially fixed by vegetation on the lee slipface and approximately the southern half of the stoss and STA. The NTA and STA of this outlying parabolic head remain intact and contiguous. The vegetation on the stoss and the south aspect of the NTA has died back due to defoliation caused by descending streamlines; these windward slopes are now remobilised.

A second nested parabolic head is located 3,000 m from shore, and has a similar aerodynamic form to the other two parabolic heads, except that it has been breached by wind activity. Again, it is also partially fixed by vegetation on the lee slipface and approximately the southern third of the stoss and STA. The NTA and STA of this outlying parabolic head are disjunct. The vegetation on the stoss and NTA south aspect has died back and the windward slopes are eroding.

At 3,000 m from shore there are a series of disjunct and truncated fixed windward slopes with angles of 26° and lee slipfaces that resemble components of the head of a parabolic dune. Based on field assessment it is reasonable to interpret these bedforms as relicts of a breached parabolic dune head. These bedforms have been breached at their junctions with both trailing arms. The breach from the NTA is some 80 m in width, having deflated to the deflation basin, whereas the breach on the STA is smaller, some 30 m in width, and the level of the breach is several metres above the deflation basin.

The inference to be drawn from the combination of the relict NTA truncated bedforms and the current functioning NTA is that wind flow is topographically steered and accelerated along the toe of the 13 m high wall of the NTA. In above threshold wind flows from the west and southwest sectors this results in the formation of a jet stream (Figure 4. 21). This jet stream flows up the stoss and along the junction between the

NTA and the stoss (Figure 4. 21). Based on the patterns of defoliation of vegetation and erosion, and on the more extensive breaching of earlier emplaced dune heads at the junction between the NTA and the stoss, it is evident that the descending accelerating streamlines re-attach downwind of the lee slipface and extend several hundred metres downwind.

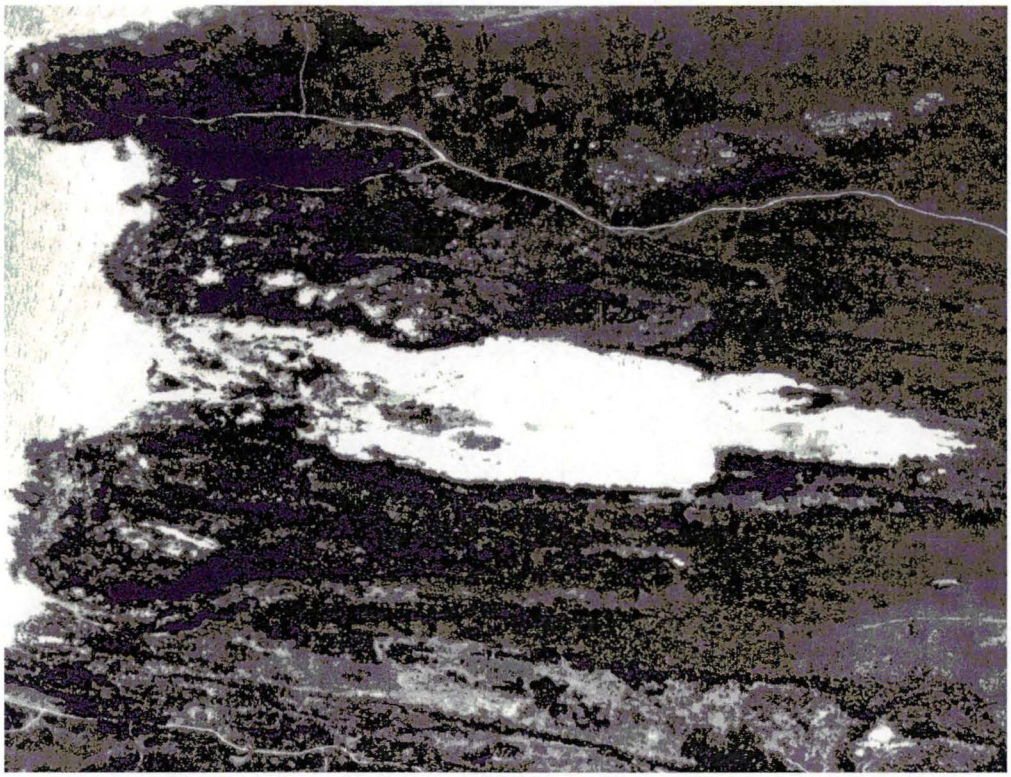

Figure 5.9. 1984 Arcview aerial photo (black and white), showing Croppies Bay parabolic dune.

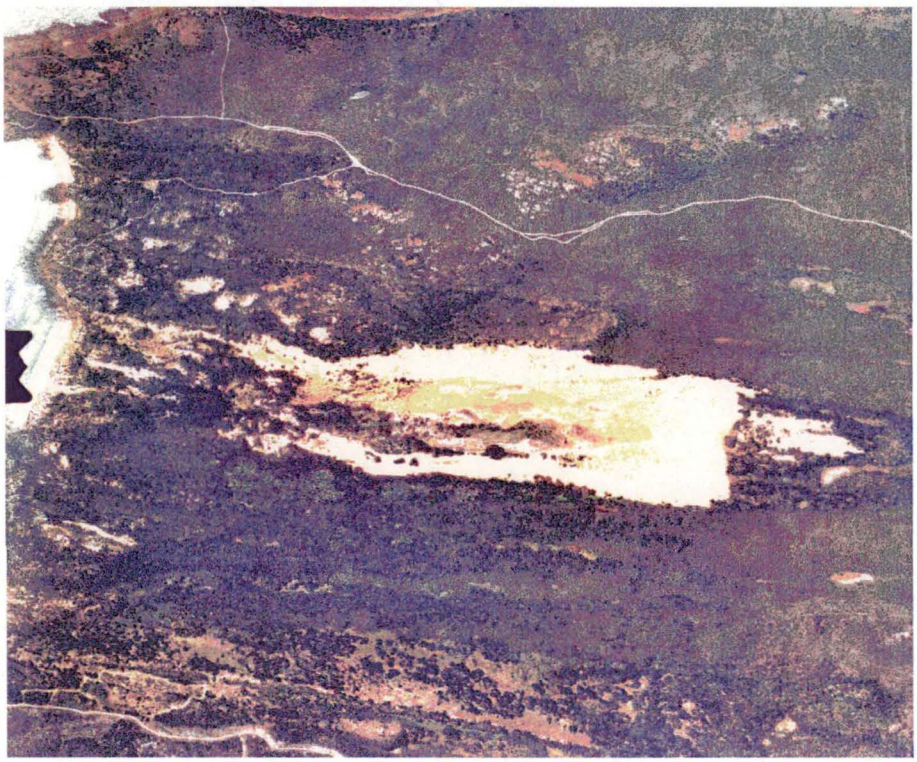

Figure 5.10. 1999 Arcview aerial photo, showing Croppies Bay parabolic dune.

Table 5.2 shows that over the duration of the study of the Croppies Bay parabolic dune, the stoss migrated downwind at annual rates of 33 m in the 1949 to 1964 interval, 27 m between 1964 and 1984, and 22 m in the 15 years between 1984 and 1999. The average rate of migration for the fifty-year period was 27.3 m/year. The progressive decline in the rate of annual migration may be attributed to: a decrease in the effective wind speed due to increasing distance from shore; an increase in the proportion of the deflation plain fixed by vegetation upwind, arguably increasing the roughness length, and to ground-moisture in the dunes (David and Wolfe, 1999; Prill, 1968). In addition, the barrier of the previously emplaced stoss wall(s) impedes the process of downwind migration. Further work is required to determine the properties of the impedance. Reading the geomorphic landscape of the relict bedforms downstream of the current migrating dune head, combined with the flow visualisation, suggests the following: (a) the proximity of a series of nested parabolic dunes, accompanied by the encroachment of the newest parabolic dune head, probably promotes turbulent air flow; (b) positive feedback between jetstream flow forms breaches in relict bedforms, which in turn funnel wind flow, resulting in acceleration of flow, combined with lee eddies. This results in erosion and the liberation of sediment for transport. (c) The proportion of bedforms downwind that are fixed by vegetation declines, results in an acceleration between the processes of (a), (b) and (c).

The presence of a sequence of nested relict parabolic dune heads, some of which have been breached, forming truncated components of earlier heads, indicates that there have been two processes:

(i) remobilisation of the bed in response to defoliation or sand inundation of plants ➡ erosion ➡ breaching in advance of the migrating head;.

(ii) incorporation of truncated bedforms into the migrating head.

Field work confirmed that subsequent to the downwind passage of the latest migrating head, truncated bedforms re-emerge upwind, apparently stranded from their original emplacement sequence.

Arguably, the trailing arms, once emplaced, function as parallel walls confining each subsequent entrained downwind pulse of sand. Each downwind pulse of sand has equilibrated with the wind regime, forming a parabolic head. Over an interval of fifty years, the latest in a series of parabolic dune heads has migrated downwind to a distance of 1,567 m. As discussed in Chapter 3, sediment analysis indicates that sand is derived from several sources – beach, mantle, and lateral migration of trailing arms, deflation of the indurated coffee rock, and deflation of the trailing arms. These sources remain sufficient to fuel these morphodynamic processes. Based on analysis of the aerial photographs and ground-truthing, it seems evident that previously emplaced nested parabolic heads are also a source of sediment. As discussed in Chapter 4, 4.7.4, a zone of erosion is located downwind of a lee slipface due to acceleration of the wind in the area of descending streamlines. Present day erosion of previously emplaced parabolic heads, 150 m and 250 m, respectively, downwind of the current lee slipface, is liberating sediment for transport. Similarly, as the dune head migrates downwind over the sandy deflation basin(s) sediment is recycled to the stoss toe.

An analysis of the location of the periphery of the trailing arms (measured at Transects 1 to 4, Figure 5.8, Table 5.3) indicates that the smaller STA has migrated north at more than twice the rate of the NTA – 106 m and 45 m, respectively – between 1949 and 1999. When combined with an analysis of the lengths of Transects 1 to 4 in Table 5.2 and Figure 5.8 for the same period, it is clear that the parabolic dune has extensively maintained similar peripheral dimensions. Table 5.2 shows that there has been no significant increase in width of the parabolic dune at Transects 1 and 3, a decrease in width of 178 m at Transect 2, and an increase in the width of the head of the parabolic dune of 125 m by 1999. It seems evident, that, to some extent, the faster rate of lateral migration of the STA must regulate the width of the deflation basin, thus maintaining the equilibrium of the aerodynamic envelope between wind regime and the dimensions of the parabolic dune. This fosters feedback between the dunes asymmetry due to south westerly flow across the STA, and the predominant downwind flow along the axis.

Table 5.3. Lateral migration (m), 1949 – 1999.

	1949 to 1964		1964 to 1984		1984 to 1999		1949 to 1999		1949 to 1999 Average/yr	
	STA	NTA	STA	NTA	STA	NTA	STA	NTA	STA	NTA
Transect 1[1]	48	36	18	24	0	28	130	12	2.6	0.2
Transect 2	89	0	40	0	0	0	137	43	2.7	0.9
Transect 3	34	68	16	0	0	0	53	78	1	1.6
Transect 4	58	11	34	70	170	0	81	50	1.6	1

[1] Refer to Figure 5.8 for location of transects.

Figure 5.3a, shows the Croppies Bay transgressive dune. The NTA of the parabolic dune immediately south of the study site (site 1 in Figure 5.3a) has largely been blown out; there was no intact NTA in the 1949 air photo. Arguably, the removal of extensive segments of a trailing arm increases the exposure of an adjacent lee parabolic dune (Site 2 in Figure 5.3a) to across land wind flow from, in this case, the south west sector, possibly resulting in an increase in the rate of lateral migration and a re-equilibration of the STA to the 'new' effective wind flow. This process could explain the marked asymmetry of the Croppies Bay parabolic dune. The question is "has the STA at Site 2 always had a level some 8 m lower than the NTA? Topographic evidence, using in-situ evidence from range poles, in adjacent bedforms, suggests that the STA at Site 2 may have been higher. For example, the parabolic dune immediately north of the study site (Site 3 in Figure 5.3a) is a relict dune fixed by heath vegetation. It is not as distinctly asymmetric as Site 2; there is an average of 1.5 m height difference between the STA and the NTA. Similarly, the height of the STA and NTA dunes (using GPS data) that form the neck of Site 2 parabolic dune are 13 and 14 m above the deflation plain, respectively. Whilst the NTA neck height seems congruent with the downwind ridge height, the 13 m height of the STA neck seems anomalous.

To date there are no known publications, other than Mowling & Coleman (2003), that report lateral migration in a long-walled parabolic dune. Asymmetry in parabolic dunes may well be an indicator of lateral displacement due to cross flow of wind, and lateral displacement may be a common morphodynamic process.

5.2.4 Relationship between flow dynamics, direction of sand transport and morphodynamics

A significant amount of information concerning the relationship between flow dynamics, sand transport directions and dune morphodynamics can be gained by comparing wind resultant sand roses (Fryberger, 1980) for intra-year periods, with the measurement of surface level changes derived from GPS generated profiles and erosion pins. This component of the thesis describes sequentially the results of both the repeated kinematic GPS surveys, from which the topographic dune models and selected dune profiles were compiled, and the erosion pin data, to develop a clear view of the relationships between flow dynamics, direction of sand transport and dune morphodynamics.

5.2.4.1 Repeated Kinematic GPS surveys

This section of the thesis addresses the results of the field work that measured changes in surface elevation over a period of 1,200 days using repeated Kinematic GPS surveys, which consisted of profiles crisscrossing the dune system, with planimetric accuracies typically in the range of 2 - 5 cm and vertical accuracies of 3 - 10 cm. The GPS data, using kriging, were then used to construct topographical models of the dune system on 5 m x 5 m grids. Six surveys of the site were used to develop base maps of the dune topography and to measure changes in surface elevation of the dune.

To derive the temporal and spatial morphological changes in the Croppies Bay parabolic dune the interpolated grid of elevation data from each epoch were overlayed and then subtracted to provide the elevation change data. The topographic models were used to generate cross-section profiles.

5.2.4.2 Topographic models

Figure 5.11 compares the topographic models and shows the zones of erosion and accretion over a period of 724 days. The kinematic GPS generated elevation models (Figure 5.11) illustrate, at this large scale, the maintenance of the aerodynamic envelope of the parabolic bedform, and at the micro scale contrast the displacement patterns of accretion and deflation that maintain the dune form as it migrates downwind and laterally. Figure 5.11 also contrasts the primary morphodynamic changes which consist of the downwind migration of the stoss, accompanied by a slower rate of lateral displacement of the two trailing arms, enlargement of deflation plain, and the evolution of a trough blowout in the STA. The crests of the parabolic head, the NTA and the STA remained at much the same heights. Over the thirty-month interval between Epochs 1 and 4, volumetric change for the surveyed site was in the range of 656,400 m^3.

Figure 5.11 shows that the geomorphic pattern of change between Epochs 1 and 4 was of significant deflation from the windward NTA, resulting in deposition of sediment towards the ENE, and enlarging a corridor between the crest of the previously emplaced trailing arm and the recently emplaced crest. This displaced sediment has increased the width of the parabolic head in the ENE sector. Downwind deflation of a trough blowout, located in the STA, combined with deflation of the stoss, contributed to displacement of sediment into the SE sector, and this resulted in the broadening of the head of the parabolic dune. Deflation of sediment from the windward slope of the NTA, deflation plain and stoss accumulates against the wall of the previous emplacement of the NTA, forming a 'plateau' which is located in the ENE sector. The location and dimensions of the 'plateau' have remained similar over the duration of the six Epochs.

Overall, the topographic models, in combination with the GPS generated profiles (explained below), demonstrate that parabolic dunes transfer sediment landward and extend downwind and laterally by deposition on lee slopes. In addition, the patterns of deflation and accretion on existing bedform ridges, which alter the slope angles, demonstrates an on-going process of aeolian modification since emplacement.

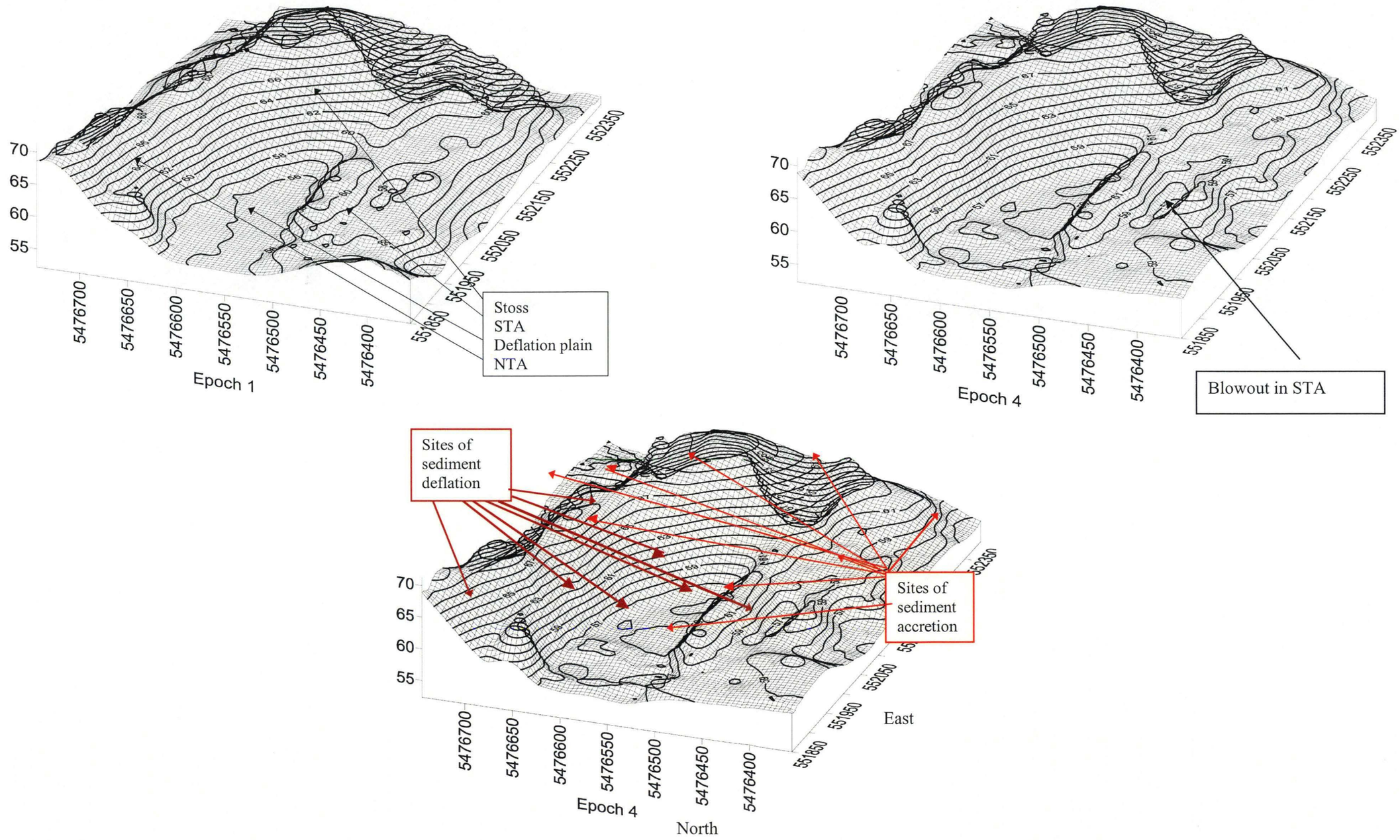

Figure 5.11. Temporal and spatial morphological changes between Epochs 1 and 4. Volumetric change for the site between Epochs 1 and 4 is in the range of 656,400 m³, the deflation plain increased in area 10% – 13%.

5.2.5 Surface elevation change

5.2.5.1 Erosion Pins

Repeated measurements of surface elevation at each erosion pin (EP) coincided with the downloading of on-site meteorological data, enabling subsequent comparison with wind resultant sand roses (Figure 4.13 a and b; Tables 4.4 and 4.5, Chapter 4) to determine the influence of relatively direct and oblique wind flows on dune morphodynamics. Two hundred and ninety EP surface elevation measurements were recorded. The GPS surveyed placement of the erosion pins, shown in Figure 5.1, provided data on surface elevation changes and on the prevailing direction of dune migration for discrete periods. As explained below, in section 5.2.6, there is a distinct temporal-spatial relationship between wind flow and variation in the changes in surface elevation and the direction of dune migration.

Measurement of surface elevation changes became obsolete as the EPs progressively became isolated on the deflation plain due to lateral migration of the NTA and downwind migration of the head of the parabolic dune. As the EPs became isolated, they provided a useful benchmark demarcating the periphery of the deflation plain at the commencement of the study, against which the rate of migration could be measured using a magnetic compass aligned on two EPs centrally located on the deflation plain, shown in Figure 5.1.

The general pattern of surface elevation changes included the following:

- Deflation rates for the NTA deflation plain varied between -6 mm to -136 mm. Phases of accretion occurred as sediment was transported down the deflation plain, forming shadow dunes, followed by deflation due to further lateral migration.

- Surface elevation changes measured on EPs located at the toe of the STA, demonstrated cyclic patterns of accretion and deflation. This cyclicity occurred in response to an enlargement of the deflation plain at the base of the head of the parabolic dune (deflation) and advance of the STA on to the deflation plain (accretion). EPs that were located at the eastern margin of the south trailing arm, where deflation occurred, initially deflated 155 mm. Accretion rates were in the range of 60 mm. Sediment derived from the deflation of the STA, and the advance of the trailing arm, was partially captured by a sparse sedgeland of (< 20% ground cover) prostrate *Carex pumila* and tussocks of *Austrofestuca littoralis*.

Table 5.4 shows the changes in ground surface elevation for the stoss. The erosion pin data for the deflation plain is presented in Appendix 3. The specific patterns of surface elevation changes are discussed in section 5.2.6.

Table 5.4. Stoss erosion pin data.

Sand Rose number	Survey interval dates	Interval between surveys (days)	Erosion Pin Number						
			21	**22**	**23**	**24**	**25**	**26**	**27**
-	November 2000	24	-32	-3	3	19	26	29	25
1	November-December 2000	19	9	-33	-44	-45	-51	-43	-45
-	October - February 2001	68	-10	-424	-661	-665	-475	-323	-697
2	February - May 2001	85	5	-39	-187	-272	-265	-210	-217
3	May - August 2001	110	-28	-227	-526	-607	-582	-508	-520
-	August - September 2001	20	2	-48	-60	-83	-62	-117	-133
7	September-November2001	55	7	-660	-187	-494	-502	-515	-152
9	November 01-March 2002	128	9	-248	-785	-604	-755	98	-518
10	March - May 2002	44	-7	-28	-57	-612	-119	-80	-61
-	May – August 2002	90	5	-106	-763	-848	-760	-850	-986
-	August 2002	1	2	-120	3	-15	-2	-19	-6
-	August – October.2002	77	-2	-173	-395	-617	-581	-561	-554
	Total	721	40	-2109	3659	4843	4128	3099	3864
		Lc 0.14	-5.6	-295	-512	-678	-578	-434	-541
		Ave/day	0.75	3	5.3	7	6	4.5	5.6

5.2.5.2 Copper erosion pins measuring changes in surface elevation during measurement of close to the ground wind flow

The results of the synchronised measurement of surface elevation changes using copper EPs during the thirty-minute close to the ground measurement of wind flow are shown in Table 5.5. Field observation during the measurement period suggested that sediment was moving through in ripple bedform on both the stoss and the NTA, shown in Figure 5.12. The amplitude of the ripple lengths differed between the toe and crest, and between stoss and flank, as discussed in Chapter 4. The data indicates that the net change in surface elevation was nominal, with the exception of mid slope on the NTA where there was net accretion of 59 mm that equates to 26.7 grams/m^2/s^{-1}. The shadow dune in the lee of the buttress probably explains this net accretion; the placement of the mast was at the extremity of the shadow dune tail. The remaining net results indicate sediment was moving through the sample grid.

The net 59 mm accretion mid slope of the NTA explains the linear wind shear velocity in Figure 4.15, Chapter 4. Although sediment was in suspension during the measurement of close to ground wind flow, net accretion was occurring.

The grams/m^2/s^{-1} is not a measurement of q, the sand transport rate; it is an areal measurement of the volume of sediment transported over a thirty-minute period. On reflection, following analysis of this data, a combination of before and after photographs of the 1 m^2 grid would have enabled a comparison of the location of the ripples, thus providing a displacement rate. In addition, the use of sediment traps would have

provided a weight of sediment passing a single point, rather than an areal measurement derived from erosion pins from which q could have been calculated volume.

Table 5.5. Surface elevation changes (mm) measured over a thirty-minute period.

	Stoss				North trailing arm – windward flank					
EP no.	Toe	rate / minute	Crest	rate / minute	Toe	rate / minute	Mid slope	rate / minute	Crest	rate / minute
1	-9	-0.3	1	0.03	20	0.6	71	2.4	7	0.2
2	11	0.4	19	0.6	3	0.1	15	0.5	8	0.3
3	-46	-1.5	33	1.1	10	0.3	35	1.2	-120	-4
4	20	0.6	-3	-0.1	5	0.2	84	2.8	14	0.5
5	-2	-0.06	13	0.4	9	0.3	58	1.9	22	0.7
6	52	1.7	7	0.2	5	0.2	105	3.5	20	0.6
$Lc' = 0.16$	4.3	0.1	11.6	0.4	8.3	0.3	59	2.0	7.8	0.3
$g/m^2/s^{-1}$	1.59		5.19		4.2		26.75		4.7	

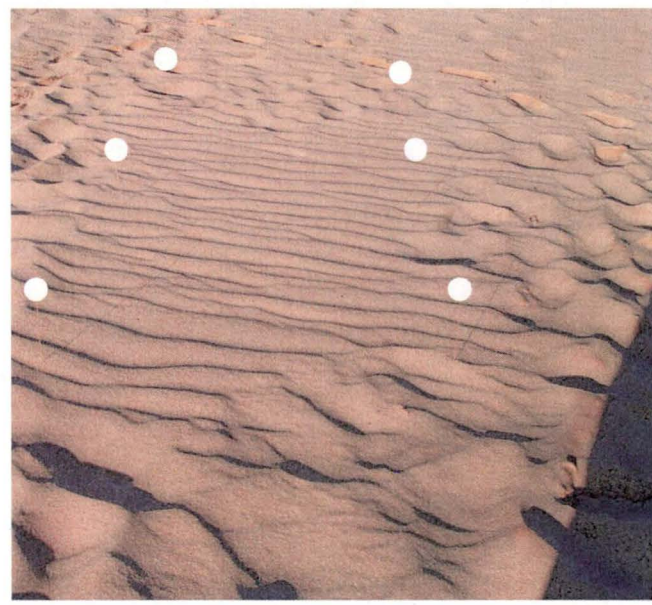

Figure 5.12. Ripple bedform mid slope, NTA with copper erosion pins in a 1 m^2 grid. The location of the top of the erosion pins is indicated by ○ .

5.2.6 Wind resultant sand roses, combined with erosion pin and GPS

The Annual wind resultant sand rose RDD of 68.6° and RDP/DP of 0.63 shows (Figure 4.13 b) that the predominant flow is towards the NE, but this conflation of annual wind data obscures the influence of seasonal wind patterns on the dune morphology. The following section combines the EP data with GPS generated profiles and the Fryberger (1980) wind resultant sand roses to determine the relationship between seasonal wind flow and patterns of accretion and deflation on dune morphodynamics and the evolution of a coastal parabolic dune.

Table 4.5, Chapter 4, shows the vector average wind speed by season. This data indicates that winter experiences the highest variability in direction of wind flow, followed by spring; autumn and summer experience lower variability. Figure 4.13 a and b, Chapter 4, display the wind resultant sand roses which are linked with the EP survey periods.

5.2.6.1 South Trailing Arm

Sediment at the toe of the STA was primarily depositional, due to lateral displacement onto the deflation plain. However, several wind events contributed to deflation of sediment in spring and autumn. For example, wind flow towards the east yield wind resultant sand roses (SR) 1, 2 and 5, with RDDs of 0°, 87° and 89° respectively, and result in retreat of the toe, particularly on the EPs located closest to the junction between the stoss and STA. The GPS Profiles 14, 12, 15, 11, 10, and 16 (Figures 5.17, 5.18) Epoch 3 (Figure 5.1 shows the locations of the Profiles), when viewed in sequence from west to east, show the morphodynamic response of the windward STA to direct approach winds. Commencing the visual sequence at Profile 12, the lower windward flank and crest deflated 40 cm and 60 cm (vertical accuracies of 3-10 cm), respectively. The gradient of the walls of the trough blowout (shown in Figure 5.11), which is embeded into the STA, remained unchanged, suggesting that the sediment was transported east, along the flank and crest of the STA. Profiles 10 and 11 show that the gradient of the STA flank changed, deflating from toe to crest, resulting in a transport of sediment of sufficient volume to fill the trough blowout. This indicates that the principal direction of sediment transport was towards about 120° across the crest of the STA, showing evidence of topographic steering. The STA azimuth shown in Figure 4.19 (Chapter 4) confirms that flow experiences topographic steering in certain wind flow directions. Profile 17 (Figure 5.16) shows that sediment was also transported downwind along the flank and crest of the STA, increasing surface elevation in the SE sector of the dune head. Arguably, the directions of sediment transport indicates topographic steering and acceleration of wind flow along the flank of the STA when winds have a relatively direct approach, as in SR 2 and 5, or across dune as in SR 1. Under these flow regimes lateral migration of the STA stalls, and the south sector of the deflation basin extends SE, transporting sediment up the stoss and across the junction between the stoss and STA, and so contributing to the enlargement of the dune head.

The same trough blowout, mentioned above, continued evolving downwind. GPS profiles 12, 11, 10 (Figure 5.17), indicate a cyclic process of accretion and deflation,

evolving from a narrow (30 m) and shallow (4 m) blowout with a single stoss in Epoch 1, to a series of three 'nested' blowouts in Epoch 5. The narrow elongated form of the trough blowout was evident between Epochs 1 to 2. Epoch 3 recorded a truncation of the blowout due to sediment inundating the eastern two thirds of the blowout, as described above. The Epoch 4 image indicated the formation of a saddle in the trough, separating the narrow blowout into two bedforms – a saucer blowout to the west and the formation of a narrow trough blowout to the east. By Epoch 5, the trough blowout had evolved into a series of two saucer blowouts and a re-emerging trough blowout situated downwind. The necks of the saucer blowouts are aligned on 95° and the neck of the trough blowout on 93°, indicating topographic steering and turbulent flow along the wall of the STA.

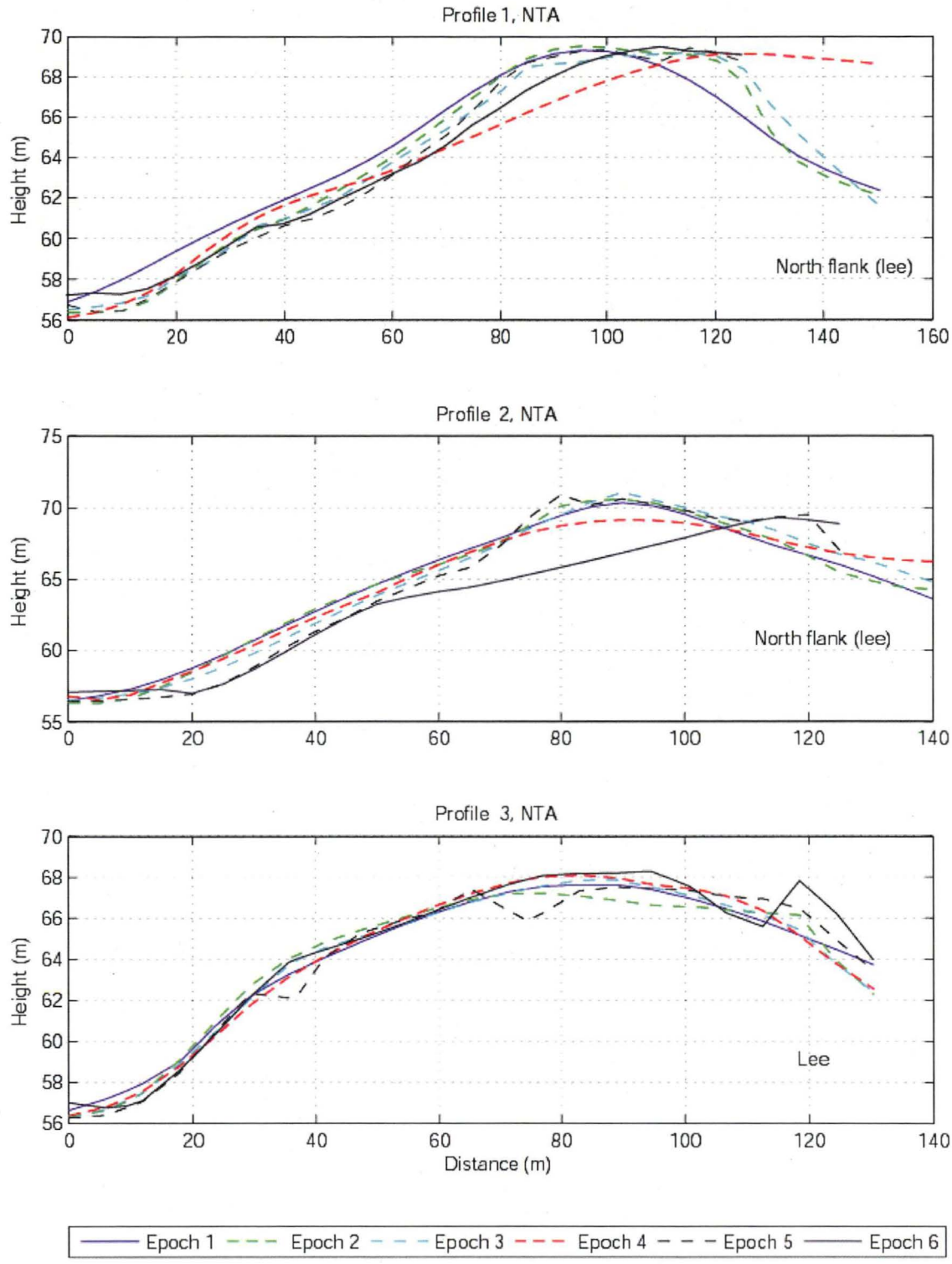

Figure 5.13. North trailing arm, Profiles 1, 2, 3.

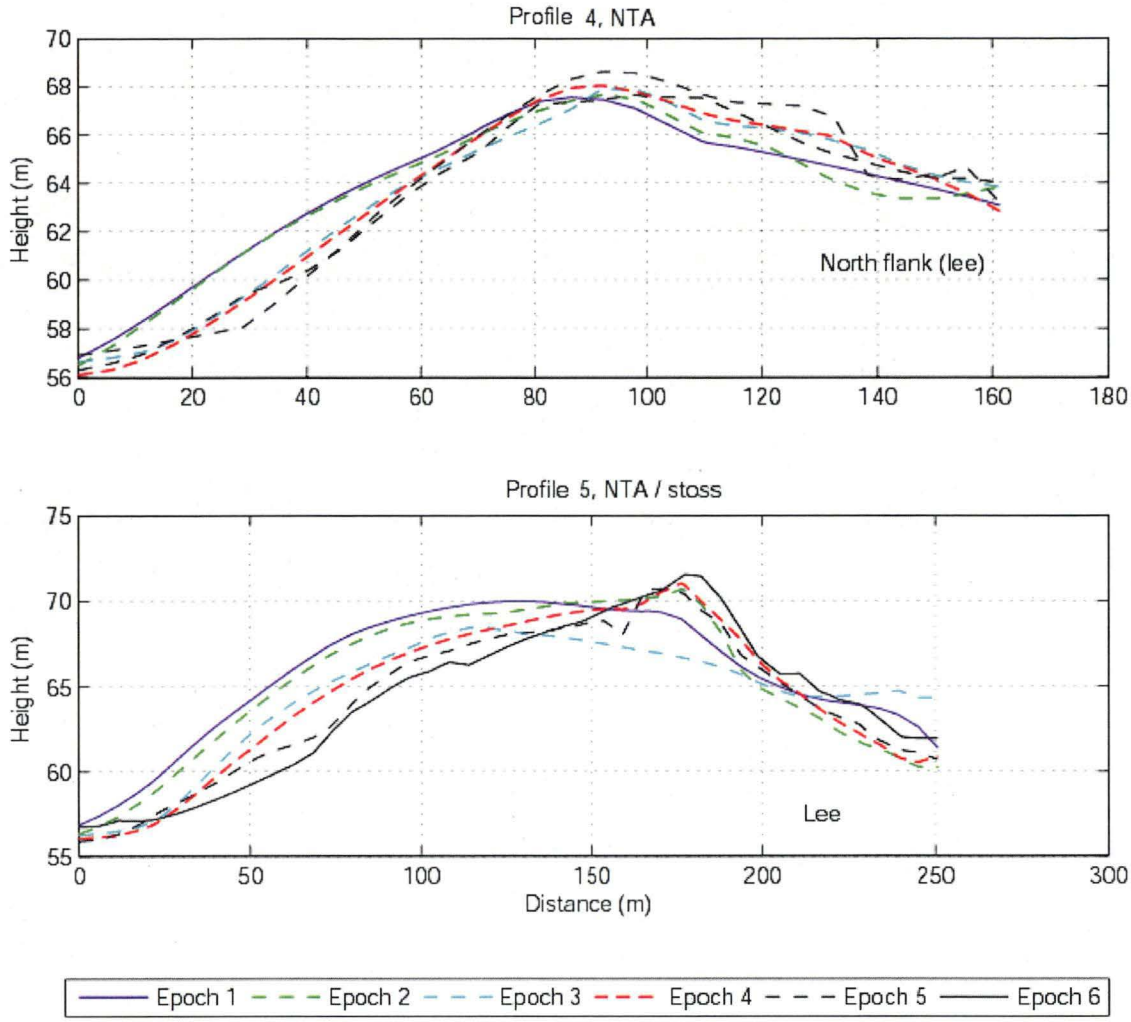

Figure 5.14. North trailing arm and stoss. Profiles 4 and 5.

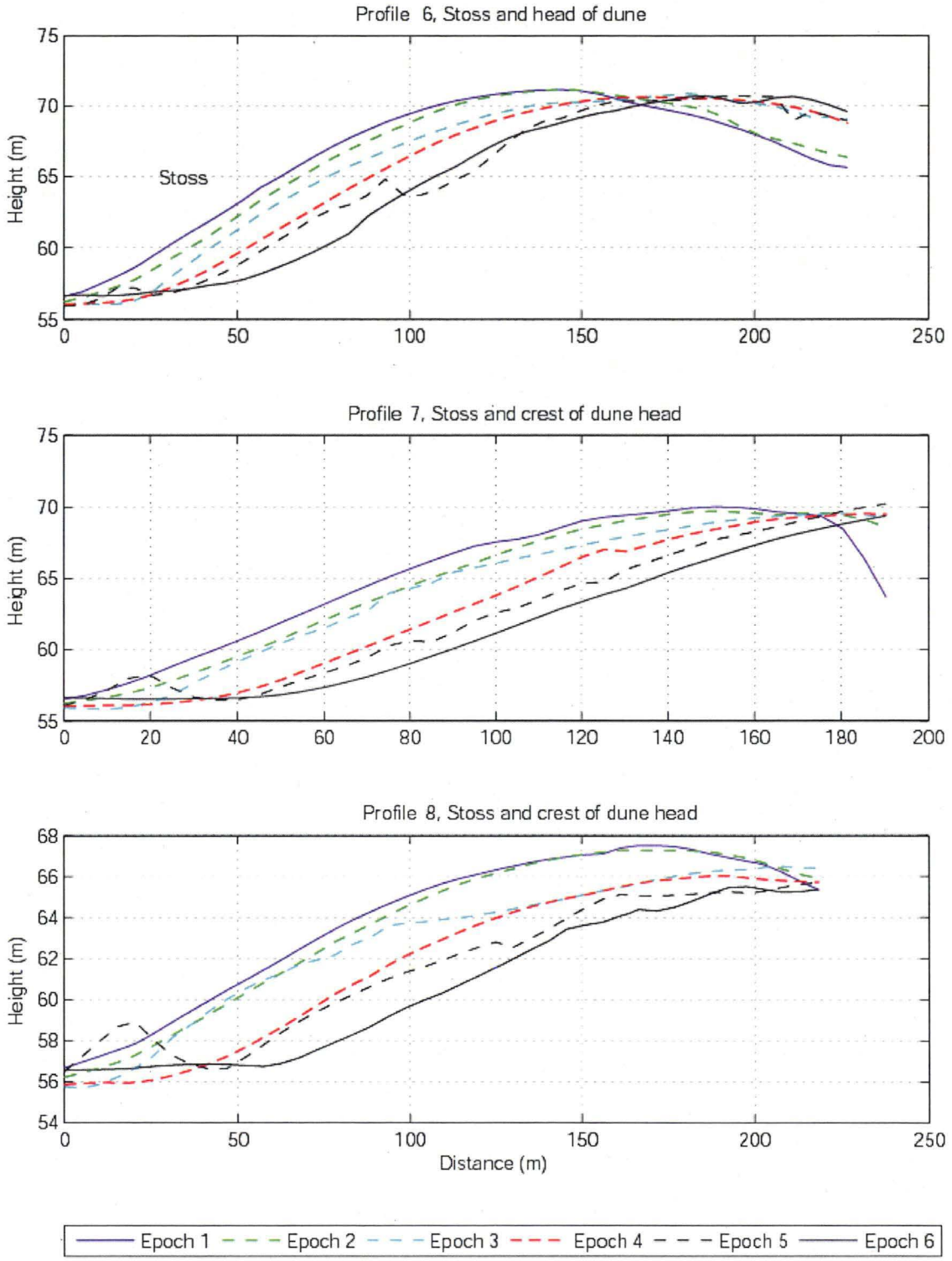

Figure 5.15. Stoss and head of dune. Profiles 6, 7, 8.

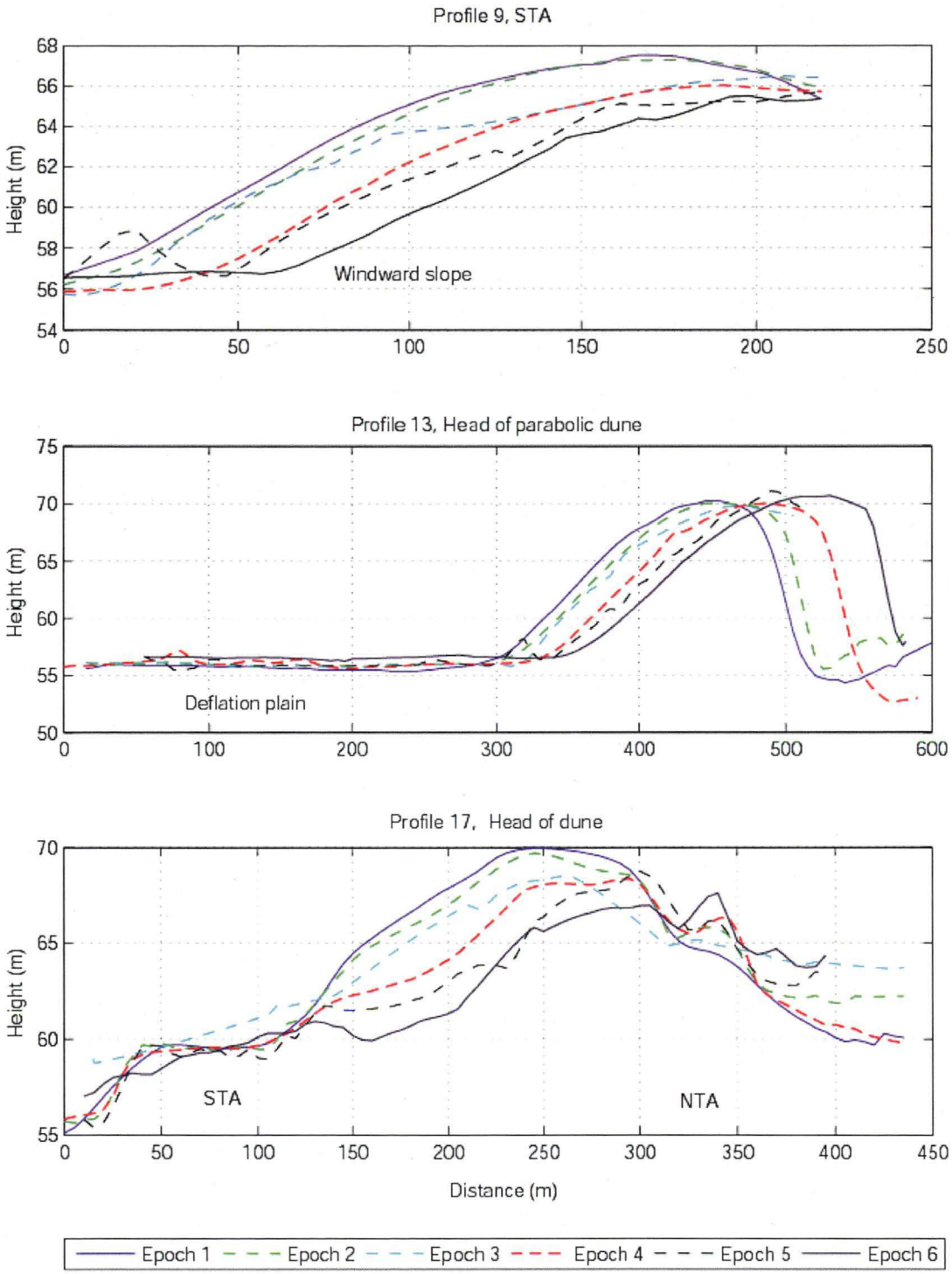

Figure 5.16. STA and head of parabolic dune. Profiles 9, 13, 17.

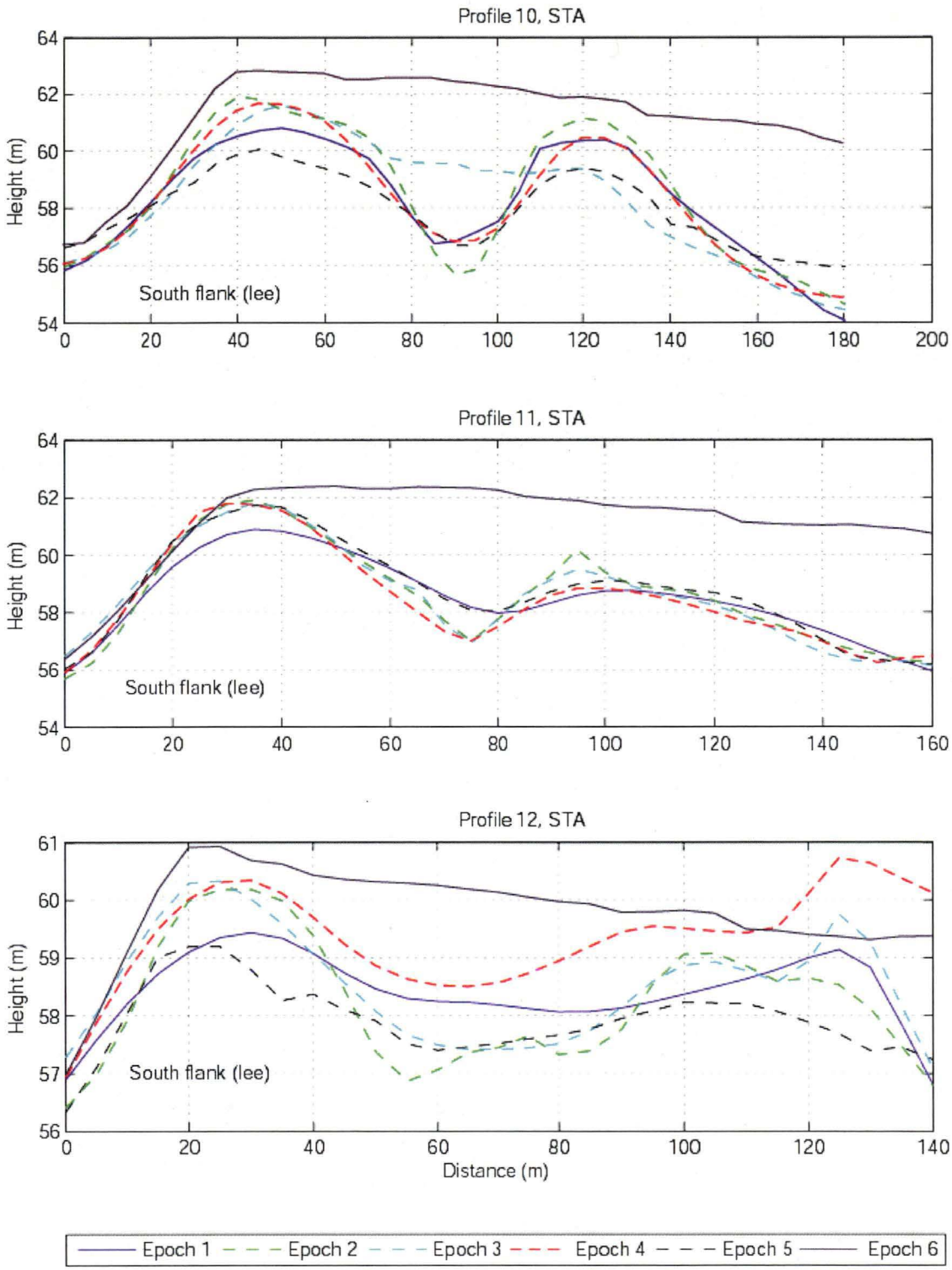

Figure 5.17. STA. Profiles 10, 11, 12.

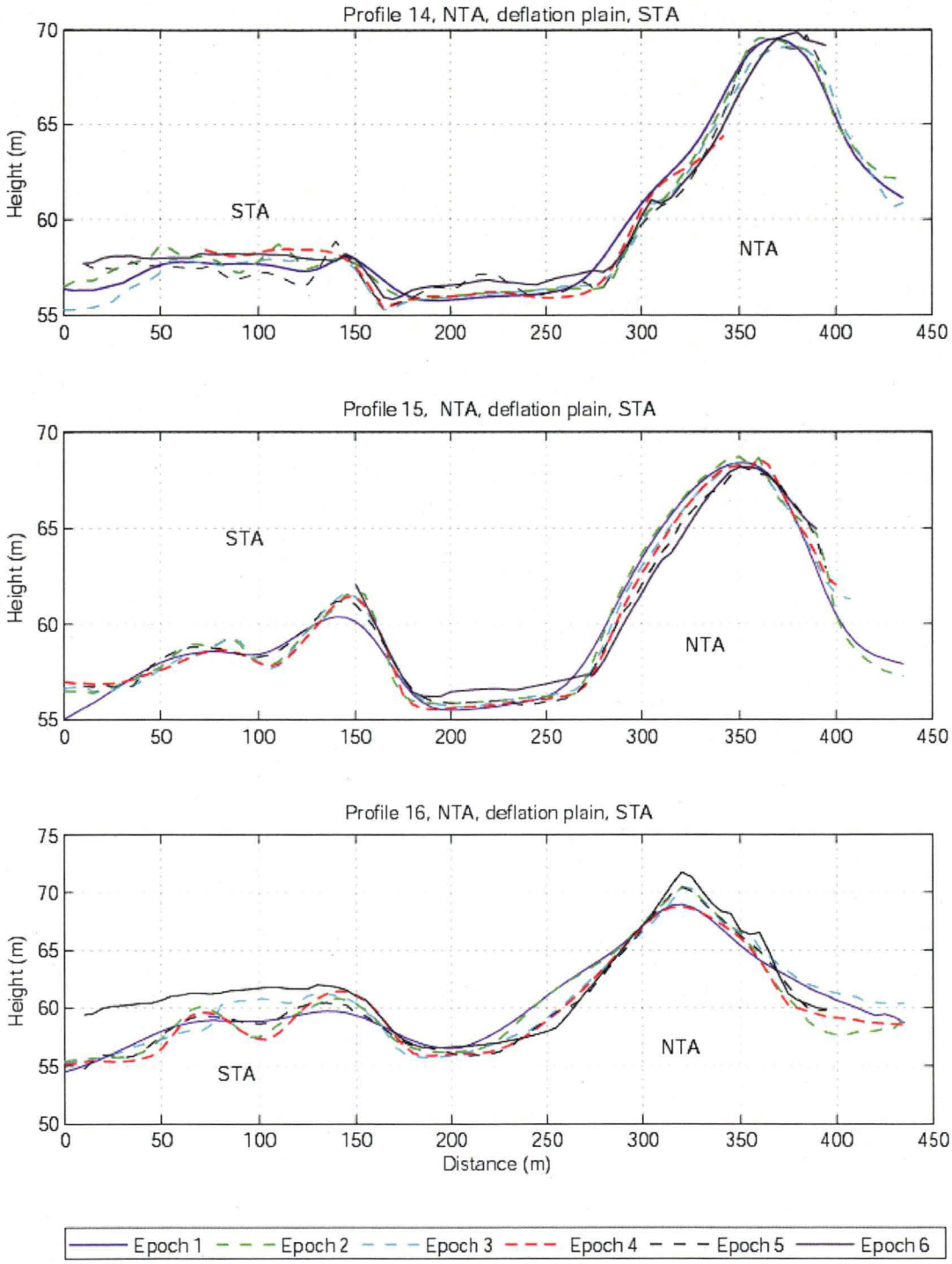

Figure 5.18. South to North traverses. Profiles 14, 15, 16.

5.2.6.2 Lateral displacement

GPS Profiles 1, 14, 15, 16 (Figures 5.13, 5.18), combined with EP data, display the rate of lateral displacement ENE of both trailing arms between Epochs 1 and 6. The planimetric accuracies were typically in the range of 2–5 cm and EPs 18, 19 and 20, and verified the GPS Profile distances. Calculation of the rate of displacement is acquired by locating the toe of the flank of the trailing arms, indicated by the interface between the horizontal and an increase in slope angle. The final displacement measurement of EPs on the deflation plain occurred with the Epoch 5 survey.

GPS Profiles 1, 14, 15, 16(Figures 5.13, 5.18), indicate that the NTA was displaced ENE a total of 21 m, 25 m, 20 m, and 50 m respectively. EPs 18, 19, and 20 are located between Profiles 14 and 15, and the horizontal displacement distances were within the range of ± 90 cm of the Profile figures. EPs 10, 11, 12, 13 are located between Profiles 15 and 16, the displacement distances recorded on ground were within ±200 cm of the Profile figures. This variation between EP and GPS horizontal distances is explained by the GPS grids, which are 5 x 5 m. This smoothes measurements over small scales. The lateral displacement increased the area of the deflation plain by 10% – 13%, between Epochs 1 and 4.

GPS Profiles 14, 15 and 16 (Figure 5.18), indicate that the STA was displaced laterally onto the deflation basin 10 m at Profile 15. Profile 14 indicates some fluctuation in advance and retreat over the interval of the GPS surveys – Epochs 1 and 2 recorded the toe of the STA some 14 m in advance of subsequent Epochs, indicating a retreat of 14 m at this point in the flank. Profile 16, measured at Epoch 5 to link with measurement of EPs, indicates retreat by 14.6 m of the flank from the deflation plain. This compares with measurements at EPs 1, 2, 3, of 39 m, 24 m and 7.8 m respectively.

The GPS recorded rates of lateral migration for the STA and NTA appears to contradict the results from the aerial photograph analysis, which indicated that the smaller STA migrated ENE at more than twice the rate of the NTA – 106 m and 45 m, respectively – between 1949 and 1999. However, the lateral migration measurements were derived from different sources. The measurements for the sequence of aerial photographs were taken from the periphery of the dune because of a lack of clear definition between the toe and deflation basin. In contrast, the repeated kinematic GPS surveys had planimetric accuracies typically in the range of 2–5 cm and vertical accuracies of 3–10 cm and the topographical models of the dune system were generated on 5 m x 5 m grids. This level of accuracy enabled clear definition of the transition between the toe and deflation basin, but the kinematic GPS surveys did not extend to the periphery of the dune. Three questions are posited by this contradiction: 1) are the rates of lateral displacement recorded by kinematic GPS fluctuating around a rate derived from longer recording periods? 2) Is there an incipient transition towards an alignment with the vector wind flow, rather than the surface winds being topographically steered up the axis of the dune? 3) Are a series of meteorological parameters interacting in a process – response feedback that manifest as changes in the bedform?

In regard to the first question, Table 5.3 compares the rates of lateral migration derived from the sequence of aerial photographs. The data in Table 5.3 demonstrate that there is considerable variability between the sequences and between rates of migration of the STA and the NTA over recording intervals of 15, 20, and 50 years. The kinematic GPS surveys extended over a period of three years. Figure 5.7 indicates that the current head of the parabolic dune, between the 1949 to 1964 aerial photos, extended beyond the parallel boundaries of the trailing arms. Based on ground-truthing of the aerial photographs, this extension probably occurred for the first time since the initial emplacement of the parabolic dune. Reading the geomorphic landscape indicates transition in the status quo of the aerodynamic envelope. Thus in regard to question one above, the kinematic GPS surveys probably reflect short-term fluctuations in the rate of lateral migration. The geomorphic transitions that have occurred in the head of the dune lead into questions two and three, as follows.

Finigan and Neil et al.'s (1990:93) investigation of wind flow pattern around a 1000:1 scale model of a symmetrical parabolic dune in a wind tunnel found that it was the orientation and extent of the separation zones that indicated the direction of the dune growth. Of relevance to this study was their finding that as the wind vector approached 30° the dune was aligned with the vector not the dune axis and that the dune was no longer steering the wind. Finigan and Neil et al.'s (1990:93) findings provide useful comparative benchmarks against which to test whether the Croppies Bay parabolic dune is aligning with the vector flow. There are comparative constraints embedded in Finigan et al.'s findings, namely that their wind flow pattern was modelled on a symmetrical parabolic dune, while the Croppies Bay dune is asymmetric.

The following interpretation of the influence of wind flow pattern on lateral dune displacement incorporates the results from Chapter 4, namely Figure 4.13 and Table 4.4 wind resultant sand roses, the wind azimuths in Figure 4.19, and Figure 4.21. These Figures and Table display the recorded wind flow pattern for Croppies Bay parabolic dune, derived from close to the ground measurement of wind speeds and wind direction, and flow visualisation.

The separation zones, displayed in Figure 4.21, Chapter 4, are orientated along the crests of the NTA and stoss, crest of the lee slipface, and the SE sector of the stoss. The most extensive separation zones are associated with the NTA and stoss.

Table 5.6 compares the annual and intra-year wind resultant drift directions (RDDs) to assess the alignment of wind flows. Sixty percent of the recorded intra-year wind flows are 12° below the Finigan et al. 30° benchmark, resulting in an Annual RDD of 22.4°. Four wind flows were recorded with angles of less than 15° off the axis (i.e. winds flowing up the axis of the dune) indicating that the surface winds are topographically steered. Two wind flows were aligned with the wind vector rather than the dune axis. These were SR 4, 56.7 and SR 10. SR 4, which exceeded the 30° indicative benchmark described by Finigan et al.; despite the RDP of 127 being relatively low due to a diffuse modal wind flow, the wind flow occurred during summer, when it is relatively dry and has the most effective sand transport capacity. SR 10, 28.3 approached the 30°

indicative benchmark, the RDP of 2659 (the largest on-site wind record, Table 4.4, Chapter 4) resulted from a narrow unimodal wind flow during spring. A third wind flow, SR 6, RDP 874, which exceeded the 30° indicative benchmark is along the axis but in a reverse direction, i.e. 1740. Including fieldwork this confirmed that this wind event was topographically steered.

Table 5.6. Annual and intra-year wind resultant drift directions.

Sand Rose	RDD°	Axis alignment 91° minus RDD°	RDP
1	0	0	150
2	86.6	4.4	404
3	68.4	22.6	291
4	34.3	56.7	127
5	88.8	2.2	580
6	265	174	874
7	72.7	18.3	935
8	74.9	16.1	864
9	76.98	14	767
10	62.7	28.3	2659
Annual	68.6	22.4	7652

Based on this analysis, the dune remains predominantly aligned with the dune axis. Extreme wind events originating from the SW to SSW sector align with the wind vector (SR 10), particularly the narrow unidirectional wind flows, or prolonged periods of flow that exceed threshold velocity (SR 7). Both wind flows are the most effective at transporting large volumes of sediment up and across the NTA.

However, given the apparent robustness of the Croppies Bay parabolic dune form since the initial emplacement, we can pose the question 'Are the displacements of the dune head in the ENE and ESE sectors purely explained by wind flow, or are other factors influential?' A review of the BoM Low Head wind data (1940 to 2003) does not indicate an increase in the proportion of wind events or an increase in wind speed from the SW sector. The sequence of aerial photography indicated that the NTA from the parabolic dune located south of the Croppies Bay dune has extensively deflated, the sediment being displaced downwind and possibly laterally. Based on a comparison with the bedform of parabolic dunes in the surrounding area, it can be assumed that the deflated NTA was ~ 9 to 11 m in height. Arguably, the reduction of this roughness feature has increased the surface wind flow and wind speed from that sector. It has also facilitated flow across land, where that previous flow had been topographically steered.

In relation to question three, above, the change in morphology of the dune head in the form of an increase in width, due to sand flow extending beyond the parallel boundaries of the trailing arms, could well reflect process – response to a separate driving force, namely an early indicator of a trend towards aridity (P/E) that was discussed in Chapter 4. A component of the thirty-two year decline in rainfall, particularly in the seasons associated with evaporation exceeding precipitation (see Tables 4.12 and 4.13, Chapter

4), is the reduction in free surface water in the deflation plain and abutting Ainslie Sand formation (Bowden, 1981, 1983), and a reduction in capillary moisture in the dune base for extended periods. The height of the water table is decisive in determining the extent and duration of surface water, and is replenished by rainfall and depleted by evapotranspiration. David and Wolfe (1999:226) reported that recharging by precipitation is more efficient through active dune sand, and that surfaces depressed by the dune may provide a higher supply of water. Further, David and Wolfe (1999:234), in a study of inland parabolic dunes in Canada, proposed the concept of a dune activity cycle – defined as the succession of aeolian events between two successive phases of complete dune stabilisation. Their proposition is that moisture in a fixed dune is depleted during periods of prolonged drought due to evapotranspiration, with plants gradually exhausting the available moisture to the base of the roots. The depth of moisture exhaustion, or the resulting thickness of dry sand, reflects the measure of climate stress accumulated in the dune. Subsequent disruption of the vegetation cover due to fire, grazing, or increased wind shear is likely to trigger an activity cycle, which, once started, extends quickly over the entire dune because the sand below the surface has become dry and is easily transported, resulting in relatively high migration rates.

The trends discussed in Chapter 4, 4.9 Tables 4.12, and 4.13, predict that aridity (P/E) will extend in duration and be accompanied by a progressive increase in the mean effective wind speed. So, what is the status of the water table during the summer dry period? To answer this a series of pit holes were dug to locate the height of the water table in summer. Generally, the water table was within 70 cm of ground surface at the head of the deflation plain, within 90 cm on the deflation plain, and within 120 cm of ground surface on the Ainslie Sand formation on the northern periphery of the NTA. Field observations, over the duration of the study, found that there are no extensive surface water bodies in the vicinity during the dry season. There are small perennial soaks situated at the toe of the NTA neck and on the south periphery of the STA, although water levels are significantly lower than winter levels. Following sustained rain periods during winter, surface water occurs in deflation basins located on the dune periphery in the Ainslie Sand formation, and the deflation plain, particularly at the head of the deflation plain where sand is supersaturated for extended periods. Field observation in transgressive coastal dunes generally, and on site, has informed the opinion that ground surface water bodies in particular, and moist to wet ground surface conditions generally, impede dune migration due to saturation of flank and lee toes by capillary moisture. For example Table 3.4, Chapter 3, shows the moisture content at the toe of the flank of the NTA 0.4%, and the toe of the lee slipface 6.4%. The undertaking of a more extensive project, involving the seasonal collection of core samples from multiple traverses on the dune, including the peripheral Ainslie Sand formation and the deflation plain, is required to determine the influence of moisture content on the maintenance of the parabolic dune form.

In summary, a series of meteorological parameters and geomorphic bedforms have combined, influencing an increase in width of the head of the parabolic dune in the ENE and ESE sectors and the accelerated rate of lateral displacement of the NTA. These include:

(i) The walls of the three nested parabolic dune heads located downwind of the current converging migrating head causes wind turbulence. Arguably, this causes the wind to flow around an obstacle as well as over it. In response to this process sediment is transported both to the sides of the obstacle and downwind, falling out of suspension on the downwind and ENE and ESE lee slipfaces.

(ii) The reduction of the north wall of the parabolic dune, located immediately south of the Croppies Bay study site, has changed the equilibrium in the interplay between wind flow and resultant dune form in the Croppies Bay transgressive dunefield (Figure 5.3a). Arguably, the reduction of the wall has exposed the study parabolic dune to extreme wind events or prolonged periods of flow that exceed threshold velocity from the SSW and SW sectors. Under the influence of these high or sustained velocity wind flows, the dune aligns with the wind vector in twenty percent of recorded wind events. The response to these wind events is to displace the wall of the NTA ENE.

(iii) A third component, aridity, arguably accelerates the rate of lateral displacement. In parabolic dunes, ground moisture, and precipitation onto bare sand, causes cohesion of sand grains, impeding downwind and lateral migration by increasing the shear velocity of the sand. A sustained period of below average rainfall, accompanied by above average air temperatures and an average site wind speed of 8.1 m/s, probably resulted in an extended period when the ground water level was lower for several months each year. Thus, there is less cohesion on the lateral peripheries and the head of the migrating dune, combined with drier sand on the dune, which is consequently available for transport.

5.2.6.3 Head of parabolic dune

This section describes the interaction between changes in ground surface elevation caused by discrete wind flow regimes on dune morphodynamics. GPS Profiles 5, 6, 7, 8, 9, 13, and 17 (Figures 5.14, 5.15, 5.16), combined with EP data (Tables 5.7, 5.8, and 5.9, Figure 5.19) and wind resultant sand roses (Figure 4.13 a and b), display the rate and pattern of displacement of the head of the parabolic dune.

Transitions in the atmospheric parameters occur in mid and late Spring, October and November, when the evaporation rate commences to exceed rainfall (Figure 4.6), and solar radiation (Table 4.2) and air temperature increases (Table 4.1). Analysis of wind and P/E data by season and by six monthly periods revealed a pattern of summer/spring aridity (Chapter 4, 4.9), indicating conditions conducive to increased dune mobility. Table 5.6 and Figure 5.19 show the seasonal surface elevation changes that occurred at the periphery of the deflation basin and on the stoss. Summer, when precipitation (126 mm) amounts to only 31% of potential evapotranspiration (400 mm) in an average year, recorded the highest rates of deflation and downwind migration at the head of the dune (Figure 5.19) and lateral migration of the NTA. Loose packing of sediment on the stoss (high porosity, average of 73.5% to a depth of 1.5 m) enables sand entrainment to commence at lower wind speeds, compared with sediment on the flank of the NTA. This is reflected in Table 5.7, where seasonality has less influence on deflation.

Table 5.7. Intra-year and seasonal deflation rates on the stoss by sand rose over a period of 721 days.

Year	Season	Deflation (mm)	Accretion (mm)	Lc 0.14	Interval between surveys (days)	Sand Rose number
November 2000	Late Spring	-35	+102	9	24	-
November-December 2000	Late Spring-early Summer	-261	+9	456	19	1
October - February 2001	Spring - Summer	-3255	0	350	68	-
February - May 2001	Autumn	-1190	+5	35	85	2
May - August 2001	Autumn - Winter	-2998	0	392	110	3
August - September 2001	Winter	-503	+2	166	20	-
September-November2001	Spring	-2510	+7	135	55	7
November 01-March 2002	Spring - Summer	-2910	+107	420	128	9
March - May 2002	Autumn	-964	0	70	44	10
May – August 2002	Winter	-4313	+5	22	90	-
August 2002	Winter	-162	+5	603	1	-
August – October 2002	Winter - Spring	-2883	0	426	77	-
	Total	-21,984	+242	Ave 429		

The speed-up ratios, discussed in Chapter 4, 4.7.3, demonstrate (NTA 1.7, stoss 1.3 crest to toe, at the height of 15 cm above ground surface, Table 4.8) that as elevation increases potential sediment transport increases (Lancaster, 1985:590). Thus, a threshold wind velocity on the deflation plain (4.5 m/s) will effectively be 7.6 m/s on the NTA crest and 5.8 m/s on the stoss crest, an increase of 58% and 77% respectively. When wind

velocity is below threshold on the deflation plain, say 3.5 m/s, increasing dune height increases the wind velocity to 5.9 m/s on the NTA, and 4.5 m/s on the stoss. Effectively, this extends the periods of sediment transport and rates of erosion for the upper slopes and crest of the NTA and stoss.

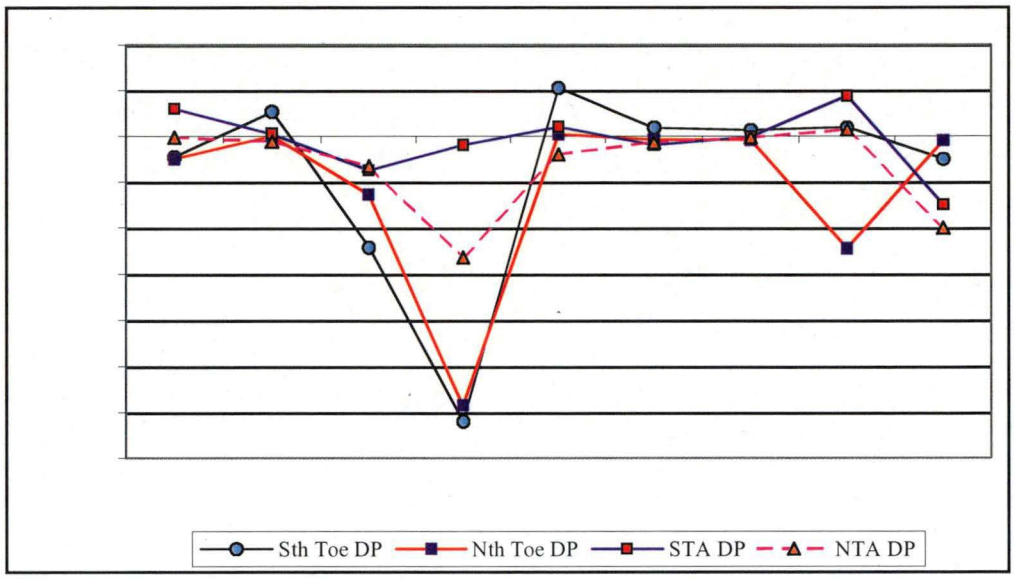

Figure 5.19. Seasonal surface elevation changes at the periphery of the deflation basin. The erosion pins were deployed at the toe of the stoss, and the toe of both trailing arms.
(Sp – Spring; Su – Summer; A – Autumn; W – Winter)

Table 5.7 shows the surface elevation changes on the stoss: EP 21 recorded the least changes in surface elevation due to its early isolation on the deflation plain; the higher rates of deflation at EPs 24 and 25 reflect the higher shear velocity ($u*$) due to topographically accelerated flow being compressed mid slope. Over the duration of 691 days, the toe of the stoss migrated 34 m from EP '0' (Figure 5.1), with an annual migration rate of 18 m/yr. The lee slipface migrated downwind 37 m, with an annual migration rate of 21.5 m/yr (mean value). Table 5.8 shows the progressive rate of downwind migration of the lee slipface. There are too few measurements by season to determine a relationship.

The influence of wind events on rates of migration is compared with the wind resultant sand roses in the following section below.

Table 5.8. Surface elevation changes (mm) on the stoss – 721 days.

EP No.	Lc 0.14	Lt 0.14	Total	Ave/day
21	-5.6	16.5	-40	-0.75
22	-295	-295	-2,109	-3
23	-512	514	-3,659	-5.3
24	-678	683	-4,843	-7
25	-578	585	-4,128	-6
26	-434	469	-3,099	-4.5
27	-541	548	-3,864	-5.6

Table 5.9. Progressive mean migration rate of the lee slipface.

Lee Slip Face Survey Date	Survey Interval (Days)	Advance Rate (m)	Advance rate per day (mm)	Sand rose Number
10.12.00				
16.2.01*	69	4.8	6.9	-
11.5.01	84	2.3	2.8	2
18.9.01	140	5.8	4.1	4
28.9.01	10	0.7	6.8	5
12.11.01	45	2.6	5.7	7
20.3.02	128	5.0	3.9	9
3.5.02	44	4.9	11	10
31.8.02	120	9.2	7.6	-
18.10.02	48	1.7	3.5	-
Total	619	36.8	5.9	

*Leap Year

Profile 13 (Figure 5.16) displays the west to east displacement of the dune head and the changes in surface elevation of the deflation basin and stoss. The notable features in profile 13 include the progressive increase in depth to about 1 m of sand on the deflation basin. Progressive deflation of sediment at the toe of the migrating stoss resulted in a shallow basin, which contained water following rain, and super-saturated sand following evaporation of surface water, and a dry bed during summer. Epochs 1 to 6 indicate an equal 53 m displacement from toe of stoss to toe of lee slipface, an average of 22.6 m / year, compared with the annual migration rate of 21.5 m/yr (mean value) acquired from the measurement of EP. The variability in elevation between Epochs 1, 4 and 6 at the toe of the lee slipface is explained by transgression of the dune over (respectively) deflation basins (1 and 4) and the fixed foot slopes of previously emplaced stosses. Recording of contours ceased at the crest of the lee slipface for Epochs 3 and 5, and recording of contours ceased at the toe of the slipface. Repeated surveys over an interval of 1200 days demonstrate the process of downwind displacement of the dune head – deflation of the windward slope, accretion of lee. We can examine changes in morphology by taking measurements off the Epoch graphs using the x and y-axis, and by extracting the distances from the data. Table 5.10, which compares the measurement of Epochs 1, 2, 4, and 6 at the heights of 60 and 65 m on Figures 5.13, 5.14, suggests

that the width of the dune head has progressively increased, whilst the height of the dune remains consistent within ± 1 m. The possible reason for this progressive increase in width is that the dune head has encountered an obstruction downwind in the form of a previously emplaced fixed dune head, which is impeding downwind migration, and the aerodynamic envelope is responding to disequilibrium due to increased turbulence. Figure 5.20 shows a contextual oblique low altitude flight view of the head of the dune.

GPS Profiles 5, 6, 7, 8, and 9 (Figures 5.14, 5.15, 5.16) expand on the pattern of deflation and displacement discussed above for Profile 13 (Figure 5.16). Profile 7 (Figure 5.15) is aligned almost parallel to profile 13 and elaborates on the progressive sequence of deflation, indicating a deflation rate of about 7 m over 1200 days (about 6 mm / day) at EPs 24 and 25, which is similar to the EP derived daily rates of -7 and -6 mm. The slightly concave topography between contours 60 to 64 m is evident in profiles 5 to 8 and 13 (Figures 5.14, 5.15, 5.16) in Epochs 3 and 5. The pattern of

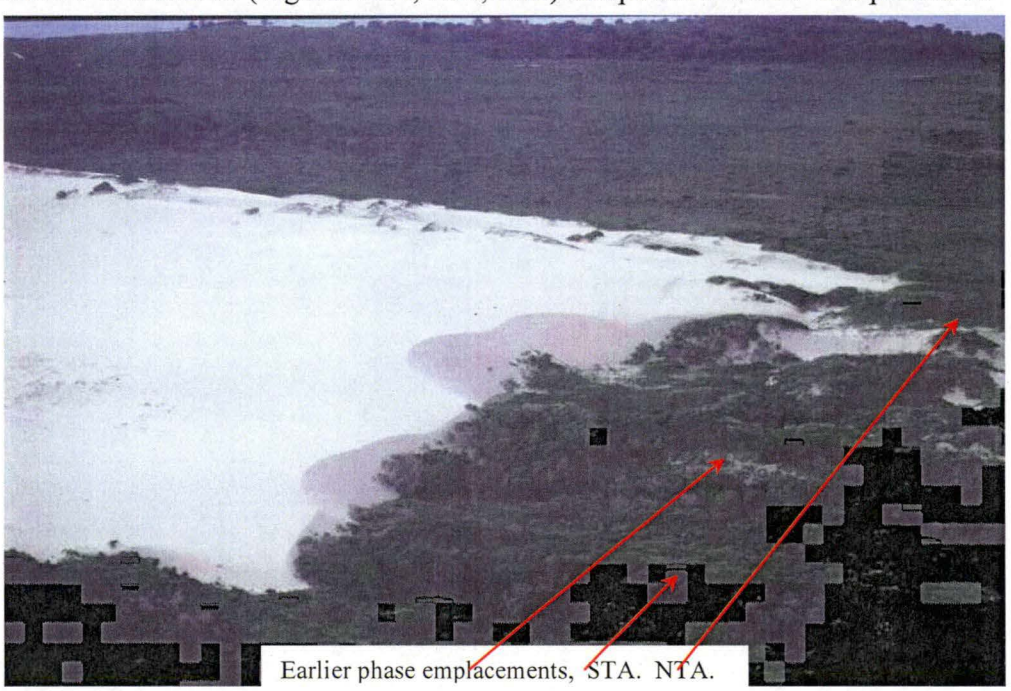

Figure 5.20. Head of parabolic dune, oblique low altitude air photo, 2003.

deflation measured with EPs and GPS on the stoss indicates consistently higher rates between contours 60 to 64 m (Figure 5.1), which is congruent with compression of air flow, and/or to the patterns of flow that are conducive to the formation of a reverse flow role encountered during the flow visualisation experiment discussed in Chapter 4.

Table 5.7 shows the influence that the direction of wind flow has on the pattern of deflation on the stoss. All recorded wind flows resulted in deflation of the stoss, except SR 1, which is discussed below.

The narrow unimodal off shore flow, which generated SR 6, surprisingly, given the lee flow, deflated sediment in descending order from the crest of the stoss to the 62 m contour, EP 23 (Figure 5.19). The autumn narrow unimodal flow, SR 10, with an RDP of 2659, deflated 612 mm of sediment at EP 24 at a rate of 13.6 mm/day, compared with the bracketing EPs 23 and 25, which deflated at rates of 0.6 mm and 2.6 mm/day. Profiles 5, 6, and 8, Epoch 5 display a distinct concavity on the stoss between contours 62 and 64. This concavity is also evident in the north to south profile 17 (Figure 5.16.). EP 24, at the time of the survey, was located at about the 62 m contour, which is about the same height as the STA. Flow originated from the SSW with DP 1910, and SW DP 747, and had sufficient shear velocity to displace the lee slipface at a rate of 11 mm/day, or 4.9 m in 44 days.

Examples of surface winds that are topographically steered up the axis of the dune are recorded in SRs 1, 2, 8, and 9. The response of the stoss bed to these flows is shown in Figure 5.21. Wind flows from the north west (SR 1) (Figure 5.21) are typically associated with high pressure cells, warm winds and stable conditions, generally with light dry winds. Their capacity to transport sediment is generally low on the lower contours of windward slopes, increasing in capacity on crests. The north west across dune wind flow of SR 1 resulted in an accretion of sediment on the stoss above the 62 m contour (Figure 5.1, EPs 23 to 27), and deflation of the stoss toe (EP 21).

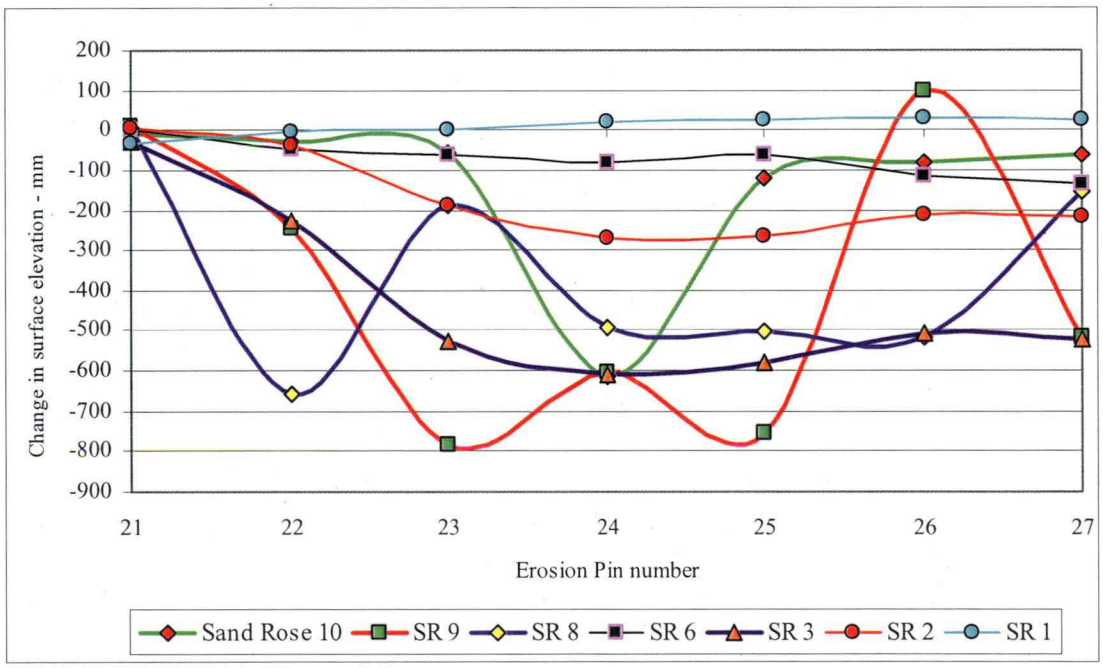

Figure 5.21. Stoss: change in mm ground surface elevation per day by wind resultant sand rose.

The response of the bed of the stoss to the autumn SR 2 flow is nominal deflation at EPs 21 and 22, and as flow was compressed, commencing at the 62 m contour, shear velocity increased steadily from EP 23, with highest deflation at EPs 24 and 25, and then

reducing deflation towards the crest (EPs 26, 27). Under the influence of this wind flow the lee slipface advanced at a rate of 2.8 mm/day. In contrast, SR 9, with nearly double the RDP of SR 2, (767 to 404) deflated significantly more sediment at EP 23 (4:1), EP 24 (2:1) and EP 25 (nearly 3:1), yet the advance rate of the lee slipface was not reflected in the magnitude of the advance rate, at 3.9 mm/day (Table 5.9). Similarly, contrasting the effective displacement capacity of SR 10 with SR 9, where the magnitude between RDP is about 3.5 times greater, the advance rate of the lee slipface is 2.8 times faster with the narrow unimodal flow of SR 10. SR 2 and SR 10 were recorded during autumn; SR 9 was recorded over summer and early autumn. The sediment transport capacity indicated by these three sand roses is associated with the period when evaporation exceeds precipitation and when the migration (M) values are at their highest.

Profiles 16 and 17 (Figures 5.16, 5.18), which traverse the dune head, incorporating both trailing arms, display the patterns of displacement and topographic changes in the bedform. The process has been of deflation of both the deflation plain and the flank of the NTA. The flank of the NTA in Epochs 1 and 2, was slightly convex. Deflation of some 3 m of the windward slope has realigned the slope angle of the flank, probably in response to the accelerated flow of the jetstream which is aligned along the toe of the NTA. Table 5.10 compares the measurement of Epochs 1, 2, 4, and 6 by applying the 68 m contour as a benchmark for dune height and the 60 m contour as a benchmark to compare dune width. Profile 16 shows that the combination of deflation of the windward slope and lateral displacement of the NTA at this location at a height of 60 m has reduced the width of the dune by 99 m, and sediment has been transported to the lee slope, increasing the width an average of 50 m at the 60 m contour. The crest of the NTA has increased in height 9 m.

Profile 17 (Figure 5.16), incorporates the NTA, the plateau on the head of the dune and the STA. The notable features in profile 17 include the progressive deflation of the plateau and the northerly displacement of the dune. By applying an intersect between the X-axis 60 m contour, and the 250 m Y-axis in Profile 17, the elevation of the dune at this point has deflated 4 m and migrated north 50 m (Table 5.10). Over the duration of 1200 days the angle of the windward slope has progressively changed through the processes of deflation and displacement of sediment, from slightly convex in Epoch 1 to concave in Epoch 6. This is illustrated by taking an intersect between contours 65 and 60 on the X-axis, and 150 to 250 m on the Y-axis. Table 5.10 shows the width of the dune in the area of the NTA, and in the area of the plateau, it has decreased between Epochs by 56 m.

Table 5.10. Temporal-spatial changes in the width and height by selected Epochs.

Profile 13	Dune Height	Dune Width
Epoch	60m contour	65m contour
1	173	125
2	173	130
4	178	130
6	186	139
Profile 16	68m contour	60m contour
1	62.7	174
2	70	80
4	62.7	75
6	71.9	75
Profile 17	65-70m contour	65m contour
1	70	163
2	69	180
4	68	161
6	66	107

Displacement of sediment along Profile 17 (Figure 5.16) has been to the north, forming knolls due to sediment accumulating against the obstacle of vegetation. Ground surface elevation has increased on the northern lee flank some 3 m due to sediment flow. The 58 m elevation of the dune head between 50 and 125 m on the Y-axis has remained relatively consistent over the duration of the study. Profile 13 (Figure 5.16) shows the downwind displacement of the head of the dune in the period of 1200 days.

Applying the Stokes and Goudie et al. (1999:211) indices to the GPS data to describe the morphological parameters of dune reconstitution time, net displacement value and net rollover transport rate, elaborates on the basic dune displacement rates derived from the sequence of aerial photographs discussed above in section 5.2.2 and transforms the migration rates into volume sediment transport rates, as follows.

The head of the parabolic dune is comprised of sediment with high porosity (average of 73.5%) medium sized grains from mid slope to stoss crest (average 1.56ϕ) and the lee slipface is formed from very fine to silt sediment (average 3.97ϕ) (Table 3.2). This loose packing of medium size grains on the stoss, combined with an average site wind speed of 8.1 m/s, and shear velocity midslope of 1.05 $u*$, results in a dune reconstitution time of 8.9 years. Compared with the Stokes and Goudie et al. (1999:203) dune reconstitution time : volume, theirs is 8.99 years : 40,252 m^3, that of the present study is 8.9 years : 100,796.8 m^3. Arguably, the dune head, given more than twice the volume of the barchan dune, is reconstituting more than twice as fast. The higher threshold wind velocity at Croppies Bay probably explains some of this difference. Other factors that probably contribute to the differential include the partial (the dune head is confined by

parallel trailing arms) compared to the entire reconstitution of a barchan dune, and to the sediment packing and grain size.

5.2.6.4 North Trailing Arm

The combined influence of higher sediment packing, well to very well ϕ sorting of grains, and mean medium grain size (M_z ϕ 1.5) and slightly convex topography on the windward flank of the NTA (located approximately at Profile 2, Figure 5.1) results in an increase in the shear velocity ($u*$) mid slope. Cumulatively, this contributes to a slower rate of deflation relative to the stoss.

Given the sediment characteristics of the windward flank of the NTA, the relatively slower rate of deflation is reflected in the sequence of GPS profiles 1, 14, 2, 15, 3 and 16 (Figures 5.13, 5.18). These sequences of profiles traverse the NTA and extend 200 m downwind from the remnant buttress to the junction of the trailing arm with the head of the dune. Generally, they show progressive deflation of the windward slope, maintenance of the angle of slope in profiles 1, 2, and 3, and transition in slope angle in profile 4, from slightly convex in Epochs 1 and 2, to concave in Epoch 4, followed by a steeper slope angle in Epoch 6. The change in slope angle can largely be attributed to lateral migration, given the relocation of the slope angle evident at the 58 m contour intersecting the 25 m Y-axis, generating some 3 m of deflation. Dune crest has been displaced 12.5 m north at profile 2. Figure 5.22 shows the crest of the NTA.

The volume of the NTA, shown in Table 5.11, was calculated by deriving end area volumes from profiles 14, 15, and 16 (Figure 5.18). For each profile, dune height was calculated from contour 56 m to crest of dune. The extrapolation was necessary, as the roving GPS survey did not commence at the toe of the lee flank. The width was calculated at the base of the dune, from the toe of slope on the deflation basin, and an extrapolated base derived from a perpendicular angle intersecting the 56 m contour on the northern lee flank. This extrapolation probably resulted in an underestimate of the total volume of some 1,000 m^3.

The NTA volume in Epoch 1 was ~995,295 m^3 and ~879,180 m^3 in Epoch 6, giving a deflation volume of –116,115 m^3 ± 1,000 m^3 over a period of 1,200 days. The width and height measurements shown in Table 5.11 indicate that the process of deflation and lateral displacement between the two Epochs has changed the form of the NTA. Dune height decreased in the three profiles by an average of 73 cm. Dune width at profiles 16 and 17 decreased, narrowing the width of the trailing arm by 14 and 18 m respectively, whilst profile 18 increased in width by 3 m. Figure 5.22 illustrates a typical section of the crest of the NTA.

Table 5.11. NTA morphology data.

Profile No	NTA				
Epoch 1	Dune height at crest	Dune width at base	m^3	Total m^3	Volume of sediment transported m^3
16	13.1	174.5	476,095	995,295	-116,115
17	13.2	187.5			
18	13	209	519,200		
Epoch 6					
16	12.7	159.9	415,750	879,180	
17	12.6	168.8			
18	11.8	212.5	463,430		

The narrowing of the dune width suggests that deflation of sediment from the windward flank is not a process of direct transfer to the lee flank, but rather a transfer of sediment along the wall of the flank towards the dune head, and the direction congruent with the annual sand rose resultant of RDD 68.6°, which is reflected in the widening of the dune and which may account for the 3 m increase in width at profile 16. Figure 3.2, Chapter 3, shows the location of sediment (Sample 1) that has been winnowed during the process of transport, and deposited in a corridor that is forming between the relict ridge formed by eroding knolls with remnant vegetation, and a series of knolls and shadow dunes that are forming a nascent crest, shown in Figure 5.11, Epoch 4.

Field observation of the segment of NTA, located between the truncated buttress and the neck, indicates that the lateral displacement of this segment has inundated the Ainslie Sand formation which previously separated the northern parabolic dune and the study dune (Figure 5.3a). The ground surface level, that previously separated the two dunes, has been elevated by sand accumulation several metres, arguably forming a ramp of sand bridging the crest of the lower STA with the encroaching NTA. Currently the NTA is incorporating the western portion of the STA of the northern parabolic dune, inundating vegetation in the process.

Thus, a first appraisal suggests a process of lateral displacement by deflation from windward flank to lee. A second appraisal of the trailing arms suggests, based on kinematic GPS measurements, that a reduction in the width of the trailing arms reduces the volume of the dune. Arguably, the rate of lateral displacement increases as displacement volume decreases, showing a positive feedback in the system.

This process of lateral displacement, crab-like across the landscape, of an asymmetric parabolic dune, may explain the placement of truncated trailing arms emplaced within the walls of fixed and mobile parabolic dunes, and larger transgressive dune fields. Examples of this relict displacement are indicated in Figure 5.3a, in the parabolic dune located north of the study site, and the current example of the remnant buttress, located at 551860, 5476650 (north coordinate) 65 m contour Figure 5.1. The buttress is aligned with the northern wall of the neck and the trailing arms of the nested parabolic dune heads located downwind (Figures 5.3a).

Figure 5.22. The crest of the NTA showing the distribution of relict vegetation on eroding knolls (background) and shadow dunes formed in the lee of *Spinifex sericeus* (foreground). Located between GPS profiles 14 to 16.

5.3 Summary

This chapter has presented quantitative data acquired from repeated surveys of ground surface level by using kinematic GPS and arrays of erosion pins, linked to an analysis of seasonal wind flow patterns derived from an on-site climate station, to describe process – response in the bedform of a long-walled parabolic dune. Analysis of temporally spaced aerial photography extended the duration of the survey by fifty years, and downwind and lateral migration rates have been established. In addition, the morphodynamic evolution of the parabolic bedform, in response to changes in vegetation cover, increased aridity, and emplaced downwind obstacles, has been established.

The objectives of this chapter have been achieved by determining the influence of wind speed and wind direction, and the frequency of those wind events on dune morphodynamics, which, in turn, have been linked to the dune sand transport potential and direction of sand movement. The new technology of kinematic GPS has demonstrated its capacity to provide reliable GPS data to construct temporally spaced three-dimensional topographic models of the dune system with planimetric accuracies typically in the range of 2-5 cm and vertical accuracies of 3-10 cm.

The findings of this study are consistent with Lancaster (1985) and Lie and Skidmore et al. (2005:295), namely that the majority of sand transport is generated by moderate velocity wind flows which have a higher frequency of occurrence. Forty one percent of wind events occur in the moderate velocity category (4 to < 12 m/s), twenty seven percent occur in the high velocity category of > 12 to > 20 m/s. Some seventy percent of wind events are topographically aligned, maintaining the parabolic dune form, although across-dune flow from the SW sector results in lateral migration of the trailing arms, with the smaller STA migrating ENE at more than twice the rate of the NTA. This asymmetrical rate of lateral displacement maintains the 3:1 length to width ratio of the parabolic dune by maintaining the dimensions of the deflation basis, which in turn maintains the dynamic equilibrium of the aerodynamic envelope of the dune form.

An analysis of intra-year wind resultant drift directions found that the dune remains predominantly aligned with the dune axis. Extreme wind events originating from the SW sector align with the wind vector about twenty percent of the time, resulting in displacement of the NTA and north east component of the dune head, as follows.

Extreme wind events with a narrow unimodal flow that occur during the dry summer season have the capacity to transport large volumes of sediment in short periods. An example of this is the wind resultant sand rose 10, with an RDP of 2659, which deflated 612 mm of sediment from mid slope of the stoss, transporting the sediment ENE across the NTA and downwind. This same wind event displaced the lee slipface downwind at a rate of 11 mm / day (mean value), totalling 4.9 m after 44 days. SR 10 displaced the NTA in a NE direction – the toe of the NTA windward flank retreated from the deflation plain in the NE sector by 50 m in 44 days.

This study of a parabolic dune achieved planimetric accuracies typically in the range of 2-5 cm and vertical accuracies of 3-10 cm, which compares favourably with the study by Stokes and Goudie el al. (1999). The total number of survey points per survey in the present study are several magnitudes greater than those of Stokes and Goudie et al. (1999:205) for similar sized dunes, and their survey points ranged between 75 to 150, ours between 488 to 17,496.

The level of accuracy achieved in the repeated kinematic GPS surveys provided reliable GPS data that were used to construct three-dimensional topographic models of the dune system on 5m x 5m grids using kriging. Sequences of two dimensional cross-section profiles were selected at representative locations across the dune area, and heights were interpolated to these cross-section locations from the topographic models, again using kriging. The topographic models displayed the general patterns of displacement and accretion of sediment that maintain dune form. The two-dimensional cross-section profiles, when read in sequence clearly display the pattern of process-response between direction of sand movement, influenced by wind speed and wind direction, on morphodynamics. A series of morphological parameters were extracted from the kinematic GPS data to quantify dune migration rates, dune volumes, and dune reconstitution time.

Volumetric change for the study site over an interval of thirty months was in the range of 656,400 m^3. The volume of the NTA at the first survey, Epoch 1, was in the range of 995,300 m^3, by Epoch 6, an interval of 1,200 days later, the volume of the NTA had reduced to 880,000 m^3, indicating that the windward flank had deflated in the range of 116,000 m^3. Deflation resulted in a narrowing of the width of the NTA, suggesting that deflation of sediment from the windward flank was not a process of direct transfer to the lee flank, rather the bulk of the sediment transfer was along the wall of the windward flank up the stoss wall. Thus, based on kinematic GPS measurements, the reduction in the width of the NTA reduces the volume, and arguably, the rate of lateral displacement increases. Analysis of the sequence of aerial photography indicated an increase in the rate of lateral displacement, which was initially interpreted as a function of vector aligned extreme wind events, but, analysis of the GPS profiles and intra-year sand roses indicates that topographically steered moderate wind events erode the windward flank altering the slope angles. This demonstrates an on-going process of aeolian modification since emplacement.

To date, there are no known publications, other than Mowling & Coleman (2003), that report lateral migration in a long-walled asymmetric parabolic dune. This study's measured migration rate of a parabolic dune head remains one of the highest reported, with a mid slope volume of 393,737.5 m^3, and a migration rate of 21.5 m/yr (mean value) measured over 4 years, and 27.3 m/yr measured from a fifty year sequence of ortho-rectified, georeferenced, digitised aerial photography. The head of the dune reconstitutes at the rate of 8.90 years, with a volume of 100,796.8 m^3. This compares with the Stokes and Goudie et al. (1999:203) comparable barchan dune reconstitution time : volume of 8.99 years : 40, 252 m^3.

5.4 Conclusion

The integration of temporally spaced aerial photographs with the ground survey methods of kinematic GPS and erosion pins provided quantitative data and qualitative information about the short and longer term morphodynamic transitions occurring in a long-walled parabolic dune. Analysis of vertical aerial photographs provided comparative data on temporal and spatial transitions, and the lateral and downwind rates of migration were determined. The collection of six epochs of GPS data substantiated the patterns and rates of migration located in the aerial photographs, and enabled the accurate calculation of dune volumes of the northern trailing arm and parabolic dune head. In addition, the GPS data provided short-term images of morphodynamic changes that were linked with short-term wind resultant sand roses, to determine, firstly, the effective capacity of specific wind flows in transporting sediment downwind or laterally, and, secondly, to determine which wind flows resulted in an accelerated migration rate. The erosion pins, particularly the seven pins deployed on the stoss, provided useful data on the pattern of deflation and accretion in response to specific sand roses.

CHAPTER 6

Conclusions

6.0 Introduction

To acquire an understanding of the interaction between the wind flow pattens on the migration rate and evolution of a mobile coastal long-walled parabolic dune, this thesis has integrated measurements of close-to-the-bed wind flow up the walls of the dune and along the deflation plain with an analysis of the sediment and the current and predicted dune mobility. Geomorphic mapping of changes in ground surface topography of the dune, obtained using repeated kinematic GPS, has been linked with wind flow events to explain the relationship between dune morphodynamics and mobility. This integrated approach has provided quantitative evidence demonstrating the feedback between the prevailing wind regime and seasonal and discrete wind flow events on the dune bed.

The primary results from the present study are as follows.

6.1 Sediment sources

As a component of determining the composition of the sediment available for transport, particularly the size range, this research presented an analysis of a reworked Quaternary quartz mantle and, based on a scientific literature search, is the first analysis of the textural parameters of the windward and lee slopes that form a long-walled coastal parabolic dune.

The interesting result from the Croppies Bay sediment analysis is that where parabolic dunes migrate downwind substantial distances from shore, although they may remain connected to source beach sediment, the degree of subsequent sorting and reduction in grain sizes is the result of wind action rather than the more usual derivative of a limited size-range of beach material.

Ninety five percent of the Croppies Bay parabolic dune sediment is sourced from the reworking of an aeolian Quaternary mantle of quartz sediment ('Ainslie Sand' formation) (Bowden, 1981) that had reworked an earlier phase of late Quaternary marine sediment ('Stumpys Bay Sand' formation) (Bowden, 1981). Large and small fragments of biogenic carbonate calcite, indicative of downwind transport of modern beach material, comprised an average three percent of the Croppies Bay dune sediment, increasing in proportion on specific deposition and lee bedforms. The low proportion of biogenic calcite may be a function of the distance from shore and the process of aeolian abrasion of relatively 'soft' grains.

The processes of aeolian abrasion and winnowing have significantly transformed the Ainslie Sand formation two sediment size classes, from coarse to very coarse grains (average 77%), fine grains (average 18%) and a low proportion of silt and clay (average 3%) to the finer sediment size classes of medium (30%) to fine to very fine sand (42%), silt (8%), and coarse grains (17%) with an average grain size of 2.45 ø.

The combination of high porosity (stoss 73%, lee slipface 76%) with sub angular low sphericity grains on the stoss indicates that the sediment is loosely packed, with a high proportion of voids, and easily entrained by the wind. Pryor (1973) reported porosities of 49% – 53% for coastal dunes, and Pye and Tsoar (1991:80) reported that porosities for desert dunes range between 25% – 50%.

Given that the depth of the 'Ainslie Sand' formation is 53 – 75 cm overlaying an indurated B2 horizon, it is reasonable to deduce that there is an adequate source of sediment to fuel on-going down wind and lateral dune migration.

6.2 Site wind flow

An objective of this study was to determine the processes that drive a long-walled, asymmetric, actively mobile coastal parabolic dune. Within this context, the west to east 90° axis alignment of Croppies Bay parabolic dune is in response to on-shore intermediate wind-energy zonal westerly surface flows. High velocity wind events, characterised by the average number of days with records of wind speeds greater than 12 m/s, occur twenty nine percent of the year; summer[1] receives the highest frequency of high velocity winds. Forty two percent of wind events occur in the moderate velocity category (4.5 to < 12 m/s). The average yearly site wind speed is 8.1 m/s, and the site maximum wind speed, measured 1,500 m from shore, is 48 m/s.

Annual and seasonal analysis of wind resultant sand roses, applying Fryberger's (1980) method, indicates that winter experiences the highest variability in the direction of wind flow, followed by spring. Autumn and summer experience the lowest variability. Each of the prime compass directions have effective winds, which resolve into an annual resultant drift direction (RDD) of 69°, with an annual drift potential (DP) of 7652 vector units. Seventy percent of wind events are topographically aligned with the dune axis. Twenty percent of wind events are aligned with the SW wind vector. Effective wind flows originating from the east and north sectors stall the rates of downwind and lateral migration.

[1] Summer: December, January, and February.

6.3 Atmospheric parameters

6.3.1 Dune mobility

This research has presented the results generated from the objective of identifying the influence of specific atmospheric parameters on aeolian processes – under what circumstances does dune mobility increase, remain stable or decrease?

Applying Lancaster's (1997) sand dune mobility indices shows that winds were above threshold 71% of the year. During the summer, when precipitation (126 mm) amounts to 31% of potential evaporation (400 mm), the P/E ratio[2] fell below 0.50 which is indicative of semi-arid conditions, and the annual P/E ratio is less than 1, indicating a net moisture deficit. During summer, winds were above threshold 77% of the specific period, compared with winter when winds were above threshold 63% of the specific period, and the P/E ratio was 2.1.

The trend reported by Umina and Weeks et al. (2005:692) along the eastern coast of Australia of an increase in the mean temperature at a rate of 0.1° to 0.3° every ten years, and a decline in rainfall at a rate of 10 to 70 mm, corresponds with the trends identified at Croppies Bay. The ten-year trend at Croppies Bay (based on a fifteen-year running mean correlation) is for an increase in air temperature of 0.4°C, a decline in rainfall of -25.5 mm, and an increase in wind speeds by 0.3 m/s.

To date, there is no firm evidence that the dune's on-going mobility is in response to the post 1970s atmospheric conditions, this may be due to a lag between the response of the vegetation cover on the dune to the changes in atmospheric conditions that are conducive to increased aridity.

6.3.2 Measurement of potential sand movement rate

Potential sand movement rates were calculated using the Lettau and Lettau (1978) Equation 4.3. The actual transport rates were significantly lower than those predicted by Equation 4.3. Given this result, the decision was taken to rely on field-measured rates of migration rather than equations based on laboratory-derived constants. There is a need for components of the sediment transport equations to be refined to accommodate the complexities encountered in measuring flow in field conditions.

6.3.3 Measurement of dune migration rate

The asymmetric long walls of the Croppies Bay parabolic dune extend downwind 1,700 m to the head of the dune. The crests of the north trailing arm (NTA) and the stoss rise 13 m above the deflation plain; the south trailing arm (STA) rises 8 m above the deflation plain. Constrained by the walls of the trailing arms, the head of the parabolic dune, with a volume of 100,800 m^3, reconstitutes at the rate of 8.90 years. This

[2] P/E is the ratio of the mean annual precipitation (P) to the mean annual potential evaporation (PE).

reconstitution rate is driven by an average yearly wind speed of 8.1 m/s, and is reflected in the downwind migration rate of 21.5 m/yr (mean value) measured over four years, and 27.3 m/yr measured from a fifty year sequence (1949, 1964, 1984 and 1999) of ortho-rectified, georeferenced, digitised aerial photography. The difference between the 21.5 m/yr and the 27.3 m/yr is due to a measured progressive slowing down in the migration rate, from 33 m in the period 1949 – 1964, to 27 m between 1964 – 1984, and to 22 m between 1984 – 1999. The progressive decline in the rate of annual migration may be attributed to a decrease in the effective wind speed due to increasing distance from shore, an increase in the proportion of the deflation plain fixed by vegetation upwind (arguably increasing the roughness length), and to ground-moisture in the dunes.

In a similar wind regime to that of the present study site, Cooper (1958) reported a maximum migration rate for Oregon parabolic dunes, based on ground surveys, of 2.84 m/yr. He also recorded advances of 10.75 m/yr for a slipface 10 m high that had access to beach sand. Pye (1990), based on analysis of aerial photography, reported a maximum migration rate of 5.6 m/yr for a dune system in tropical north Queensland. Wiedermann (1990:178) reported a migration rate in a coastal parabolic dune of 4.3 m/yr measured over 24 years from on site field measurements. Mowling (1998) reported a migration rate of 17 m/yr based on a sequence of georeferenced, digitised aerial photography for a dune system located 5 km south of the present study site.

Within the context of the above rates of migration, the 21 m/yr recorded at this study site is high. It may be partially explained by the high porosity (average 75%) of the sediment that forms the dune head; by the annual narrow unimodal sand drift potential with an RDD of 69° resulting in the hairpin 3:1 planform of the parabolic dune, and by the availability of sediment for transport.

The size of the Croppies Bay dune may also influence the rate of migration. For example, Finkel (1961) recorded smaller barchan dunes moving faster than larger dunes, that is, annual displacement had an inverse relationship with dune volume. Stokes and Goudie et al. (1999:203), by applying both traditional and kinematic GPS techniques, also reported that the reconstitution time of smaller barchan dunes (volumes in the range of 45,027 m^3) was five times faster than barchan dunes with volumes in the range of 437,635.3 m^3. Alas, Stokes and Goudie et al. (1999) did not report on grain size parameters, and their threshold wind velocities had a range of 3 to 7.5 m/s, which are within the range of the coastal wind speeds recorded at Croppies Bay. Given the migration rates reported by others (Cooper (1958), Pye (1990), Wiedermann (1990), Mowling (1998), direct comparison of migration rates remains elusive without the reporting of the variables that may influence downwind migration and the displacement rates of dunes. This study found that the influential variables include:

- measurement of the wind regime in-situ 2 m above the ground surface provided a reliable indication of the flow exerted on the bed;
- planform, height of dune and dune volume;
- sediment texture and composition parameters, and the availability of sediment;
- P/E;
- proximity to shore, and the

- ground hydrology.

At Croppies Bay, effective vector winds flowing from the SW sector drive the lateral migration of the trailing arms (walls). The average lateral migration rate for the STA is 1.9 m/yr, for the NTA a rate of 0.9 m/yr. The differential rates of lateral displacement maintain the 3:1 ratio of the parabolic dune by maintaining the dimensions of the deflation basin, which in turn maintains the dynamic equilibrium of the aerodynamic envelope of the dune form. Measurement of changes in ground surface levels using erosion pins and repeated surveys with kinematic GPS provided quantitative evidence, which demonstrated that lateral displacement of the trailing arms recycles and reworks sediment. An example of this is the decrease in width and height of the NTA. Over an interval of 1,200 days, dune width decreased by an average of 16 m, and the dune height decreased by an average of 73 cm, giving a deflation volume of -116,115 m^3 ±1,000 m^3. The narrowing of the NTA indicates that sediment is transported primarily downwind, rather than to lee slopes.

To date there are no known publications, other than Mowling and Coleman (2003), that report lateral migration in parabolic dunes. Asymmetry in parabolic dunes may well be an indicator of lateral displacement due to cross flow of wind, and lateral displacement may be a common morphodynamic process.

6.4 Wind flow over a parabolic dune – interaction between wind flow and dune form

The results from this study confirms the earlier work reported by Pye and Tsoar (1990) that wind flow in parabolic dunes, because of the downwind 'U' shape of the bedform, and the presence of a high-walled neck which constricts flow, results in wind speeds and wind flow patterns unlike inland linear or transverse dunes.

The results from this study confirms and expands upon the earlier work reported by Walker and Nickling (2002) of interaction between wind flow and the dune form, by determining that there is considerable feedback between the form of the dune bed and wind flow. The primary expansions are presented below.

The findings of this research diverge from the findings of Lancaster (1985), Lancaster and Nickling et al. (1996), Frank and Kocurek (1996), McKenna Neuman and Lancaster et al. (1997) and Wang and Dong et al. (2002) who found that due to compression of flow up the slope of a dune, shear stress progressively increases.

The divergent findings of this research are as follows.

- When wind flow was measured in above threshold wind speeds (average of 7.5 m/s on the stoss at a height of 45 cm and 14 m/s at a height of 190 cm above ground surface) with sediment entrained, shear stress (u_*) did not progressively

increase from toe to crest of dune due to the feedback between dune topography and wind flow.

- The flank of the north trailing arm (28° slope angle) is convex at mid slope, which contributes to a convergence of streamlines, generating an increase in pressure, which results in an increase in $u*$ and roughness length (z_0).
- Flow visualisation on the stoss (23° slope angle) indicated a reverse rotational flow to a height of ~ 3 m commencing at the crest and reconnecting with the bed approximately mid slope.
- The stoss, under these flow conditions, has a concavity mid slope and lower $u*$ and z_0 of 1.05 m/s and 0.009 m, respectively, compared with toe 1.56 $u*$, and crest shear stress 1.75 $u*$, and roughness lengths of 0.063 z_0 m and 0.062 z_0 m, respectively. It remains undetermined whether the concavity was a response in the bed to the reverse rotational flow, or to streamlines converging mid slope. In the latter situation, arguably, it could be expected that shear stress would be higher, probably indicating that the concavity is in response to the reverse rotational flow.

The results from this study confirm Lancaster's (1985) work, which reported that the main effect of velocity speed-up on windward slopes is to extend the duration and increase the volume of potential sand movement on the upper slopes and crests of the windward slopes. The speed-up ratios calculated for Croppies Bay confirm Lancaster's (1985:587) findings on desert dunes.

Under the influence of downwind surface flow, the convergence of streamlines on windward slopes results in an acceleration of flow. For example, in a mean wind speed of 4.5 m/s on the deflation plain, a slope angle of 23° between toe of dune and crest over a distance of 100 m (measured at right angles from height of dune crest to deflation plain over which the dune is migrating) accelerates wind speed 1.3 times, or 30% on the stoss. This compares with the flank of the NTA, where under the same downwind flow conditions as the stoss, flow approach is oblique, the speed-up ratio is 1.7, an increase of 70%, up a slope angle of 28° over a distance of 60 m.

The results from this study confirm the findings of Finigan and Neil et al. (1990) that multiple zones of flow separation develop when winds flow up the axis of the dune and are topographically steered.

By comparing wind resultant sand roses (Fryberger, 1980) for intra-year periods with measurements of surface level changes derived from repeated kinematic GPS generated profiles and erosion pins, the relationship between flow dynamics, sand transport directions and dune morphodynamics has been determined.

The kinematic GPS surveys consisted of profiles crisscrossing the dune system, with planimetric accuracies typically in the range of 2–5 cm and vertical accuracies of 3–10 cm, at average sampling rates at 5 s. This high level of accuracy in the GPS data enabled the construction of three-dimensional topographic models of the dune system on 5 m x 5 m grids. Six GPS surveys of the site were used to develop base maps and

profiles of the dune topography, which enabled the measurement of changes in surface elevation and dune morphology over an interval of 1,200 days.

Eighty six percent of recorded wind flow events resulted in deflation of the stoss, although not all wind events are as effective in transporting sediment to the lee slipface. The feedback between different flow regimes on the topography of the stoss is distinct, for example:

- Narrow unimodal flows that are aligned with vector flow originating from the SW, upon entering the parabolic dune, are topographically steered and accelerate. Evidence of compression of flow as it encounters the wall of the stoss is reflected in the response of the bed. Changes in ground surface level measured with kinematic GPS and erosion pins demonstrated that in response to compression of flow, a distinct and highly localised concavity formed mid slope – 612 mm of sediment deflated at a rate of 14 mm/day between the 60 to 64 m contours. Down slope (toe of slope to the 60 m contour) deflated at a rate of 0.6 mm/day, and, between the 65 m contour to the crest (70 m contour) deflation occurred at a rate of 2.6 mm/day. In response to this wind flow, and the distinct pattern of deflation on the stoss, the head of the dune migrated downwind at the rate of 11 mm/day.

- Topographically steered narrow unimodal off shore flows, for example Sand Rose 6 with an RDP of 874, effectively stall downwind migration of the dune head. Under the flow conditions recorded for Sand Rose 6, the slope angle of the lee slipface increased by 1° to 34°, and the crest of the lee slipface was perpendicular to the lee slope to a height of about 1.3 m. The stoss deflated from the crest to the 62 m contour (deflation plain contour 54 m), resulting in a more gradual slope on the stoss.

- Topographically steered wide unimodal on shore flows, for example Sand Rose 2 with an RDP of 404, deflate the stoss between contours 23 m and 66 m forming a concavity in the stoss. The flow is, arguably more dissipative and less effective in transporting sediment downwind, which is reflected in the head of the dune migrated downwind at the rate of 2.8 mm/day.

6.5 Future trends

One of the primary goals of the present research has been to identify the influence of specific atmospheric parameters on aeolian processes. Namely, under what circumstances does dune mobility increase, remain stable or decrease?

An analysis of the relationship between wind speed, air temperature and rainfall has been undertaken for a period of sixty-three years using monthly measurements from the Bureau of Meteorology data. This analysis indicates a trend of increasing wind speeds and air temperature, accompanied by a decline in rainfall. A fifteen-year running mean of these atmospheric parameters yielded significant correlations with trends per year

(based on the fifteen-year running means) of 0.0316 m/s for wind, 0.0369°C for air temperature, and 2.550 mm for rainfall.

To determine the impact of these predicted trends on sand dune activity, three periods into the future, 2014, 2029 and 2054, were selected and the P/E value calculated at intervals of 10 years (- 25.5 mm), 25 years (- 63.75 mm) and 50 years (- 127.5 mm). The results of these predicted trends on dune mobility are that under the predicted future climatic conditions, aridity (P/PE) progressively increases markedly in three seasons, summer, autumn and spring, with the summer predicted to change classification unit from semi-arid to arid by 2054. The extension in the duration of aridity is linked with changes in dune mobility, reflected in the annual M indices, which indicate that the dune remains partially fixed by vegetation. Analysis of the inter-year data predicts that within 25 years the dry six-month period will change classification unit to be fully active offset by a continuation of the 'fully fixed' classification in the wet six-month period. The primary message is one of a predicted drift towards increased mobility typified by progressive increases in dune migration (M) over the fifty-year prediction period. The seasonal analysis indicates that three seasons contain shunts in classification class from a status of partially fixed to fully active dunes. The data analysis of wind-energy, DP, complements the findings of M and P/E, indicating a progressive increase in the mean effective annual wind speed, almost double the 2004 site threshold wind speed of 4.5 m/s, within 25 years.

The combination of a predicted reduction in rainfall (19%) over 50 years and an increase in air temperature (7.4%) are predicted to increase the incidence of drought, accompanied by a reduction in plant cover.

6.6 Proposed characteristic features of parabolic dunes

It is important to note that after undertaking an extensive review of all the relevant literature to date regarding coastal parabolic dunes, not one study or research paper has provided a detailed listing of key characteristic features of parabolic dunes in terms of what actually makes them function. Consequently, for the first time, selected features are now inventoried to serve as a catalyst and resource for future dune morphological research. Those characteristics identified for the first time as a result of this research are highlighted in italics.

- *Quantitative and qualitative data presented in the present study indicate that the parabolic dune form is promoted through a series of feedback processes between wind flow, bedform and water – both ground water and precipitation.*
- Simple parabolic dunes are U or V shaped in planform due to two trailing arms that point upwind. Most dunes have a steep terminal lee slipface located at the downwind end. The trailing arms may be partially mobile on the windward side, or partially or wholly fixed by vegetation (Mowling and Coleman, 2003).

- Continued movement of parabolic dunes is governed by the source and the amount of sand available, the strength and directional variability of the wind, and the terrain over which the dunes move (Pye, 1990).
- Parabolic dunes generally deflate down to a hardpan, forming a deflation plain or basin.
- The hairpin dune form compresses the airflow both vertically and horizontally (Pye and Tsoar, 1990).
- Multiple zones of flow separation develop when winds flow up the axis of the dune and are topographically steered.
- The central axis is aligned with the prevailing wind direction, and
- the dune extends downwind and laterally by deposition on lee slopes.
- The presence of a high, steep walled neck compresses surface wind flow through the topographic constriction, accelerating turbulent flow; jetstreams form in the neck and flow downwind aligned with the central dune axis. *In the Croppies Bay example of a long-walled parabolic dune, the jetstream flow, formed in on shore surface flow conditions, is (re)compressed as it encounters the wall of the dune head (stoss) between the topographic contours of 62 m to 66 m. The response of the bed to this compressed flow is deflation, forming a distinct concavity in the stoss.*
- *Flow expands on exiting the neck forming lee eddies on the flanks of the north and south trailing arms, scouring sediment from bare surfaces which is transported both downwind along the flank of the north and south trailing arms (NTA and STA), up slope on the flank of the NTA to the lee slip face, and laterally across the deflation plain from the STA.*
- *In on shore wind flow conditions > 8 m/s a narrow jetstream forms at the toe of the north trailing arm forming mega ripples comprised primarily of very coarse to medium sand. This jetstream flows up the interface between the wall of the NTA and the stoss, maintaining mega ripples comprised of coarse to fine sand, transporting sediment to the lee slipface.*
- *In some downwind flow conditions, when wind flow is up axis and > 7 m/s close to the ground surface, a reverse rotational flow to a height of ~ 3 m commences at the crest of the stoss and reconnects with the bed approximately mid slope.*
- Ground water and moisture (precipitation) in unvegetated dunes regulates the dune form (David and Wolfe 1999). Moisture causes cohesion of sand grains, impeding downwind and lateral migration, by increasing the shear velocity of the sand in the dune.
- *Ground moisture impedes lateral and downwind migration; conversely in prolonged droughts a decline in the height of the ground water promotes the rate of dune migration.*
- *Reworking of previously emplaced late Quaternary sediments that occur as a mantle to depths greater than 0.5 m provides sufficient sediment to fuel dune mobility, supplemented by beach sediment.*
- *The process of aeolian abrasion and winnowing reduces coarse to very coarse sediment two sediment size classes to medium to fine sand.*
- *The process of lateral and downwind migration cannibalises sediment, fuelling dune mobility.*

- *Asymmetry in form is a response to two wind flows, one up axis, the second across the dune, the process — response to these flows is for the smaller south trailing arm to migrate laterally at twice the rate of the north trailing arm, resulting in the maintenance of the hairpin form with a 3:1 ratio (length : width).*
- *The parabolic dune form, particularly the actively mobile narrow hairpin forms where flow close to the ground accelerates due to topographic steering, function as rapid conveyers of sediment to the hinterland.*

This inventory of parabolic dune features indicates for the first time, that both:

1. a new benchmark for the understanding of parabolic dune morphodynamics has been set, and
2. this thesis has served as a major catalyst for the broadening of such a knowledge base.

In final summary, this thesis has presented both quantitative and qualitative field-based data that describes the interaction between discrete wind flow events on dune morphodynamics.

The application of repeated GPS surveys over the dune profile, followed by the interpolation of the GPS profile data onto a 5m by 5m horizontal grid using kriging has enabled the production of contour models of the dune system.

Furthermore, the combined output of wind data, measured changes in ground surface elevation using erosion pins and GPS, and contour models of the dune, has produced reliable results which can clearly define the downwind and lateral migration rates of a coastal long-walled parabolic dune.

Consequently, I believe this data set will facilitate the modelling of wind flow, sediment transport rates and dune morphodynamics.

References and Bibliography

Abuodha, J. O. Z. (2003). "Grain size distribution and composition of modern dune and beach sediments, Malindi Bay coast, Kenya." Journal of African Earth Sciences **36**: 41-54.

Ahlbrandt, T. S. (1980). Textural parameters of eolian deposits. A study of global seas. Tunbridge Wells, Kent, England. Castle House Publications, Ltd.: 21-52.

Allen, J. R. (1974). "Reaction, relaxation and lag in natural sedimentary systems: general principles, examples and lessons." Earth-Science Review **10**: 263-342.

Allen, J. R. L. (1970). Physical processes of sedimentation. An introduction. London, George Allen and Unwin Ltd.

Anderson, J. L. and I. J. Walker (2006). "Airflow and sand transport variations within a backshore parabolic dune plain complex: NE Graham Island, British Columbia, Canada." Geomorphology In press: 2-18.

Anderson, R. S. and B. Hallet (1986). "Sediment transport by wind - toward a general model." Geological Society of America Bulletin **97**: 523-535.

Andrews, B. D., P. A. Gares, et al. (2002). "Techniques for GIS modeling of coastal dunes." Geomorphology **48**: 289-308.

Anthonsen, K., L. (1997). Evolution of a parabolic dune, Rabjerg Mile, Skagen Odde, and its relation to other Danish dune formations. EUCC Dune Seminar, Skagen, Denmark.

Anthonsen, K. L., L. B. Clemmensen, et al. (1996). "Evolution of a dune from crescentic to parabolic form in response to short-term climatic changes: Rabjerg Mile, Skagen Odde, Denmark." Geomorphology **17**: 63-77.

Anton, D. and P. Vincent (1986). "Parabolic dunes of the Jafurah Desert, Eastern Province, Saudi Arabia." Journal of Arid Environments **11**: 187-198.

Arens, S., Q. Slings, et al. (2004). "Mobility of a remobilised parabolic dune in Kennermerland, The Netherlands." Geomorphology **59** (1-4):175-188.

Arens, S. M. (1996). "Rates of aeolian transport on a beach in a temperate humid climate." Geomorphology **17**: 3-18.

Arya, P., S. (1988). Introduction to micrometeorology. London, Academic Press, Inc.

Ash, J. E. and R. J. Wasson (1983). "Vegetation and sand mobility in the Australian desert dunefield." Zietschrift Fur Geomorphologie. N.F. Suppl.-Bd. **45**: 7-25.

Aylor, D., E., Y. Wang, et al. (1993). "Intermittent wind close to the ground within a grass canopy." Boundary-Layer Meteorology **66**: 427-448.

Bagnold, R. A. (1941). The Physics of Blown Sand and Desert Dunes. London, Chapman and Hall.

Bailey, S. D. and C. S. Bristow (2004). "Migration of parabolic dunes at Aberffraw, Anglesey, North Wales." Geomorphology **59**: 165-174.

Barrett, N. and S. Wilcox (2001). Biological surveys and habitat mapping of proposed marine protected areas on the Tasmanian North and North East coasts. Hobart, TAFI: 34-42.

Belly, P.-Y. (1964). Sand movement by wind, with Adendum 2 by Abdel-Latif Kadib, US Army Corps of Engineers, Coastal Engineering Research Centre: **85**.

Beslar, H. (1983). "The response diagram: distinction between aeolian mobility and stability of sands and aeolian residuals by grain size parameters." Zeitschrift fuer Geomorphologie. **45** (Supplementband): 287-301.

Best, A. I. and D. E. Gunn (1999). "Calibration of marine sediment core loggers for quantitative acoustic impedance studies." Marine Geology **160**: 137-146.

Bigarella, J. J., A. H. Alessi, et al. (1969). "Textural characteristics of the coastal dune, sand ridge, and beach sediments." Boletim Parananse de Geosciencias.

Bigham, J. M. and J. M. Bartels (1996). Methods of Soil Analysis Part 3 Chemical Methods. Madison, Wisconsin, USA, Soil Science Society of America, Inc. American Society of Agronomy, Inc.

Bird, A. C. F. (1993). The coast of Victoria. The shaping of scenery. Melbourne, Melbourne University Press.

Bird, E. C. F. (1993). Submerging coasts : the effects of a rising sea level on coastal environments. Chichester, England, John Wiley & Sons.

Blumberg, D. G. and R. Greeley (1993). "Field studies of aerodynamic roughness length." Journal of Arid Environments **25**: 39-48.

Borne, K., Chen D., et al. (1998). "A method for finding sea breeze days under stable synoptic conditions and its application to the Swedish West coast." International Journal of Climatology **18**: 901-914.

Bowden, A. R. (1981). Coastal sands of northeastern Tasmania: geomorphology and groundwater hydrology. School of Geography & Environmental Studies. Hobart, University of Tasmania.

Bowden, A. R. (1983). "Relict terrestrial dunes: legacies of a former climate in coastal northeastern Tasmania." Zeitschrift fur Geomorphologie **45** (Supplementband): 153-174.

Breed, C., S., McCauley, et al. (1989). Wind erosion forms. Arid Zone Geomorphology D. S. G. Thomas. London, Belhaven Press: 284-307.

Bressolier, C. and Y.-F. Thomas (1977). "Studies on wind and plant interactions on French Atlantic coastal dunes." Journal of Sedimentary Petrology **47**(1): 331-338.

Brookfield, M. E. and T. S. Ahlbrandt (1983). Early post-depositional modification of aeolian dune sands. Elesevier.

Bullard, J., E. (1997). "A note on the use of the "Fryberger method" for evaluating potential sand transport by wind." Journal of Sedimentary Research **67**(3): 499-501.

Bullard, J. E., D. S. G. Thomas, et al. (1997). "Dunefield activity and interactions with climate variability in the southwest Kalahari." Earth Surface Processes and Landforms **22**(2):165-174."

Burkinshaw, J. R. and I. C. Rust (1993). "Aeolian dynamics on the windward slope of a reversing transverse dune, Alexandria coastal dunefield, South Africa." Aeolian sediment, ancient and modern. Special Publication, 16, International Association of Sedimentologists. K.L. Pye, N. Blackwell, Oxford: 13-21.

Butler, A., F., Althaus, et al. (2002). "Assessment of the conservation values of the Bass Strait sponge beds area." A component of the Commonwealth Marine Conservation Assessment Program 2002-2004: report to Environment Australia, December 2002. Hobart, CSIRO Marine Research: **64**.

Butler, D. R. and S. J. Walsh (1998). "The application of remote sensing and geographic information systems in the study of geomorphology: an introduction." Geomorphology **21**: 179-181.

Butterfield, G. R. (1993). Sand transport response to fluctuating wind velocity. Turbulence: Perspectives on flow and sediment Transport. N. J. Clifford, French, J.R. and Hardisty, J. Chichester, John Wiley & Sons: 305-335.

Butterfield, G. R. (1999). "Application of thermal anemometry and high-frequency measurement of mass flux to aeolian sediment transport research." Geomorphology **29**: 31-58.

Castro, I. P. (1971). "Wake characteristics of two-dimensional perforated plates normal to an air-stream." Journal Fluid Mechanics **46**: 599-609.

Chepil, W. S., F. H. Siddoway, et al. (1962). "Climatic factors for estimating wind erodibility of farm fields." Journal Soil Water Conservation **17**: 162-165.

Clemmensen, L. (1986). "Storm-generated eolian sand shadows and their sedimentary structure, Vejers Strand, Denmark." Journal of Sedimentary Petrology **56**: 520-527.

Clifford, N. J., J. R. French, et al., Eds. (1993). Turbulence: perspectives on flow and sediment transport. Chichester, John Wiley & Sons Ltd.

Colhoun, E. A. (1978). "The late Quaternary environment of Tasmania as a backdrop to man's occupance." Records of the Queen Victoria Museum, Launceston. **61**: 1-12.

Cook, P. G. (1986). "A review of coastal dune building in eastern Australia." Australian Geographer **17**: 133-143.

Cooper, W. S. (1958). "Coastal sand dunes of Oregon and Washington." Geological Society of America **Memoir(72)**: 1-162.

Cooper, W. S. (1967). "Coastal dunes of California." Geological Society of America **Memoir(104)**: 1-125.

Council, N. R. (1992). Coastal Meteorology, a review of the state of the science. Washington, National Academy Press.

Craig, M., S. (2000). "Aeolian sand transport at the Lanphere Dunes, Northern California." Earth Surface Processes and Landforms **25**: 239-253.

Crutcher, H. L. (1956). "On the standard vector-deviation wind rose." Journal of Meteorology **14**: 28-33.

David, P. P., S. A. Wolfe, et al. (1999). "Activity cycle of parabolic dunes based on morphology and chronology from seward sand hills, Saskatchewan." Holocene climate and environmental change in the Palliser Triangle: a geoscientific context for evaluating the impacts of climate change on the Southern Canadian Prairies. Geological survey of Canada, Bulletin 534. R. E. Lemmen D.S. and Vance, Geological survey of Canada. **534:** 223-238.

Davidson-Arnott, R. G. D., K. MacQuarrie, et al. (2005). "The effect of wind gusts, moisture content and fetch length on sand transport on a beach." Geomorphology **68**: 115-129.

Davies, J. L. (1978). Beach sand and wave energy in Tasmania. Landform evolution in Australasia. J. L. Davies, and Williams, M.A.J. Canberra, ANU Press.

Dean, W. E., Jr. (1974). "Determination of carbonate and organic matter in calcareous sediments and sedimentary rocks by loss on ignition: comparison with other methods." Journal of Sedimentary Petrology **44**(1): 242-248.

Dekker, L., W., and C. Ritsema, J. (1994). "Fingered flow: the creator of sand columns in dune and beach sands." Earth Surface Processes and Landforms **19**: 153-164.

Donald R. Coates, ed. (1973). Coastal Geomorphology. Binghamton, N.Y, State University of New York.

Dong, Z., X. Liu, et al. (2003). "The aerodynamic roughness with a blowing sand boundary layer (BSBL): A redifinition of the Owen effect." Geophysical research letters **30**(2): 19-1-19-4.

Draga, M. (1983). "Eolian activity as a consequence of beach nourishment; observation at Westerland (Sylt), German North Sea coast." Zeitschrift fuer Geomorphologie **45** (Supplementband): 303-319.

Edyvane, K., H. Krikman, et al. (2000). Regional classification of Tasmanian coastal waters (stage 3): marine habitat mapping - final report. Hobart, Parks and Wildlife Service, Tasmania, and CSIRO Marine Research. 1-24.

Embabi, N. (1987). "Dune movement in the Kharga and Dakhla Oases depressions, the Western Desert, Egypt." Bulletin of the Geographic Society of Egypt **60**: 35-70.

Filion, L. (1987). "Holocene development of parabolic dunes in the central St. Lawrence Lowland, Quebec." Quaternary Research **28**: 196-209.

Findlater, P. A., D. J. Carter, et al. (1990). "A model to predict the effects of prostrate ground cover on wind erosion." Australian Journal Soil Research **28**: 609-622.

Finkel, H. J. (1959). "The barchans of Southern Peru." Journal of Geology **67**: 614-647.

Finkel, H. J. (1961). "The movement of barchan dunes measured by aerial photogrammetry." Photogrammetric Engineering **27**(3): 357-365.

Finnigan, J. J., D. Neil, et al. (1990). "Modelling the wind flow pattern around a parabolic sand dune." Mathematics and Computers in Simulation **32**: 89-94.

Folk, R. L. (1971). "Longitudinal dunes of the northwestern edge of the Simpson Desert, Northern Territory, Australia. 1. Geomorphology and grain size relationships." Sedimentology **16**: 5-54.

Folk, R. L. and W. C. Ward (1957). "Brazos River bar: a study in the significance of grain size parameters." Journal of Sedimentary Petrology **27**: 3-26.

Frank, A. and G. Kocurek (1994). "Effects of atmospheric conditions on wind profiles and aeolian sand transport with an example from White Sands National Monument." Earth Surface Processes and Landforms **19**: 735-745.

Frank, A. and G. Kocurek (1996). "Toward a model for airflow on the lee side of aeolian dunes." Sedimentology **43**: 451-458.

Frank, A. J. and G. Kocurek (1996). "Airflow up the stoss slope of sand dunes: limitations of current understanding." Geomorphology **17**: 47-54.

Fraser, G. S., S. W. Bennett, et al. (1998). "Windflow circulation patterns in a coastal dune blowout, south coast of Lake Michigan." Journal of Coastal Research **14**(2): 451-460.

Freeman, T. (2002). WinRose' v0.95. MS-Windows. Hobart.

Fryberger, S., G. (1980). Dune forms and wind regime. A study of global sand seas. Tunbridge Wells,Kent, England., Castle House Publications Ltd: 137-170.

Furberg, M., D. G. Steyn, et al. (2002). "The climatology of sea breezes in Sardinia." International Journal of Climatology **22**: 917-932.

Gardner, R. and S. McLaren (1999). "Infiltration and moisture movement in coastal sand dunes, Studland, Dorset, U.K.: preliminary results." Journal of Coastal Research **15**(4): 936-949.

Gares, P., A. (1992). "Topographic changes associated with coastal dune blowouts at Island Beach State Park, New Jersey." Earth Surface Processes and Landforms **17**: 589-604.

Gares, P., A., and F. Nordstrom Karl (1995). "A cyclic model of foredune blowout evolution for a leeward coast: Island Beach, New Jersey." Annals of the Association of American Geographers **85**(1): 1-20.

Gares, P. A. (1988). "Factors affecting eolian sediment transport in beach and dune environments." Journal of Coastal Research **3**(Special issue): 121-125.

Gaylord, D. R. and L. D. Stetler (1994). "Aeolian-climatic thresholds and sand dunes at the Hanford Site, south-central Washington, U.S.A." Journal of Arid Environments **28**: 95-116.

Gerety, K. M. (1984). Problems with determination of U. Proceedings of international workshop on the physics of blown sand.

Gibbons, G. S. (1967). "Shell content in quartzose beach and dune sands, Dee Why, New South Wales." Journal of Sedimentary Petrology **37**(3): 869-878.

Goldsmith, V. (1989). "Coastal sand dunes as geomorphological systems." Proceedings of the Royal Society of Edinburgh **96B**: 3-15.

Gomes, N., C. Andrade, et al. (1992). Sand transport rates in the Troia-Sines Arc, southwest Portugal. Coastal dunes form and process. P. Nordstrom K.F., N. and Carter B. Chichester, John Wiley & Sons Ltd: 33-38.

Goudie, A. S. and A. Watson (1981). "The shape of desert sand dune grains." Journal of Arid Environments **4**: 185-90.

Greeley, R., D. G. Blumberg, et al. (1996). "Field measurements of the flux and speed of wind-blown sand." Sedimentology **43**: 41-52.

Griffith, D. A. and C. G. Amrhein (1991). Stastical analysis for geographers. New Jersey, Prentice-Hall.

Hamilton, L. J. (1997). Bibliography of wind-wave data and publication for the coastal regions of Australia. Report DSTO-GD-0116, Department of Defence.

Hardisty, J. (1993). Frequency analysis of sand transport in a turbulent air flow. Turbulence: Perspectives on flow and sediment transport. N. J. Clifford, French, J.R. and Hardisty, J. Chichester, John Wiley & Sons: 295-304.

Heap, A. D., G. R. Dickens, et al. (2001). "Late Holocene sediment in Nara Inlet, central Great Barrier Reef platform, Australia: sediment accumulation on the middle shelf of a tropical mixed clastic/carbonate system." Marine Geology **176**: 39-54.

Hesp, P. (1983). "Morphodynamics of incipient foredunes in New South Wales, Australia." Dev. in Sed. **38**: 325-342.

Hesp, P. (2001). "The Manawatu dunefield: environmental change and human impacts." New Zealand Geographer **57**(2): 33-40.

Hesp, P., A., and R. Hyde (1996). "Flow dynamics and geomorphology of a trough blowout." Sedimentology **43**: 505-525.

Hsu, S. A. (1971). "Measurement of shear stress and roughness length on a beach." Journal of Geophysical Research **76**(a): 2880-2885.

Hsu, S. A. (1971). "Wind stress criteria in eolian sand transport." Journal of Geophysical Research **76**(b): 8684-8686.

Hsu, S. A. (1973). "Computing eolian sand transport from shear velocity measurements." Journal of Geology **81**: 739-743.

Hubble, G. D. (1946). A soil survey of part of Waterhouse Estate, County of Dorset, North-East coast, Tasmania. Bulletin No 204. Melbourne, Council for Scientific and Industrial Research: 1 - 59.

Hugenholtz, C. H. and S. A. Wolfe (2005). "Biogeomorphic model of dunefield activation and stabilisation on the northern Great Plains." Geomorphology **70**: 53-70.

Hunt, J. C. R., S. Leibovich, et al. (1988). "Turbulent shear flows over low hills." Q.J.R. Meteorology Soc. **114**: 1435-1470.

Hunter, R. A., B. M. Richmond, et al. (1983). "Storm-controlled oblique dunes of the Oregon coast." Geological Society of America Bulletin **94**: 1450-1465.

Illenberger, W., K., and I. C. Rust (1988). "A sand budget for the Alexandria coastal dunefield, South Africa." Sedimentology **35**: 513-521.

Inman, D. L. (1952). "Measures for describing the size distribution of sediments." Journal of Sedimentary Petrology **22**(3): 125-145.

Inman, D. L., G. C. Ewing, et al. (1966). "Coastal sand dunes of Guerrero Negro, Baja California, Mexico." Geological Society of America Bulletin **77**(August): 787-802.

Jackson, P. S. and J. C. R. Hunt (1975). "Wind flow over a low hill." Q.J.R. Meteorology Soc. **101**: 929-955.

James, P. M. (1984). Sand blows - indicators of past climatic changes? Focus on Stradbroke: new information on North Stradbroke Island and surrounding areas, 1974-1984. A. P. Stradbroke Island Management Organization. Brisbane, Boolarong Publications.

Jennings, J. B. (1983). A history of Bridport. Launceston, Prestige Bookbinders.

Jennings, J. N. (1957). "On the orientation of parabolic or U-dunes." Journal of Geography **123**(4): 474-480.

Jennings, J. N. (1958). "The submarine topography of Bass Strait." Proceedings Royal Society Victoria: 49-72.

Jennings, J. N. (1969). The geological history of Bass Strait. Bass Strait, Australia's last frontier. Sydney, The Australian Broadcasting Commission: 17-25.

Jensen, J. L., K. R. Rasmussen, et al. (1984). "The Hanstholm experiment 1982. Sand grain saltation on a beach."

Johnson, J. W. (1963). Sand movement on coastal dunes. Federal inter-agency sedimentation, Washington, D.C., US Government Printing Offiice.

Jorgensen, D. W. (1992). "Use of soils to differentiate dune age and to determine spatial variation in aeolian activity, north-east Colorado, USA." Journal of Arid Environments **23**: 19-34.

Jungerius, P. D. and F. v. d. Meulen. (1988). "Erosion processes in a dune landscape along the Dutch coast." Catena **15**: 217-228.

Jungerius, P. D. and F. van der Meulen (1989). "The development of dune blowouts, as measured with erosion pins and sequential air photos." Catena **16**: 369-376.

Jungerius, P. D. and F. van der Meulen (1992). A geometrical approach to monitoring blowout development from aerial photographs using a Geographical Information System (GIS). Coastal Dunes. Carter, Curtis and Sheehy-Skeffington (eds). Rotterdam, Balkema.

Jungerius, P. D., A. J. T. Verheggen, et al. (1981). "The development of blowouts in 'De Blink', a coastal dune area near Noordwijkerhout, The Netherlands." Earth Surface Processes and Landforms **6**: 375-396.

Karman, T. v. (1934). "Turbulence and skin friction." Journal of Aeron. Sci. **1**: 1-20.

Kawamura, R. (1951). Study on sand movement by wind. Reports of Physical Sciences Research. No.3-4 Volume 5, October, 1951. Tokyo, Institute of Tokyo University: 95-112.

Kirkpatrick, J. B. and S. Harris (1999). The disappearing heath revisited. A guide to the conservation and ecology of the flora and communities of Tasmanian lowland heathlands. Hobart, Information Solutions Works, P/L.

Klijn, J. A. (1990). "The younger dunes in the Netherlands; chronology and causation." Catena Supplement **18**: 89-100.

Knight, J., J. D. Orford, et al. (2002). "Assessment of temporal changes in coastal sand dune environments using the log-hyperbolic grain-size method." Sedimentology **49**: 1229-1252.

Knight, J., J. D. Orford, et al. (1998). "Facies, age and controls on recent coastal sand dune evolution in North Norfolk, Eastern England." Journal of Coastal Research **26**: 154-161.

Knight, M., D. S. G. Thomas, et al. (2004). "Challenges of calculating dunefield mobility over the 21st century." Geomorphology **59**: 197-213.

Kochel, R. C. and J. C. Miller (1997). "Geomorphic responses to short-term climatic change: an introduction." Geomorphology **19**: 171-173.

Kocurek, G. and R. Dott, H., jr. (1981). "Distinctions and uses of stratification types in the interpretation of eolian sand." Journal of Sedimentary Petrology **51**(2): 579-595.

Kocurek, G. and R. C. Ewing (2005). "Aeolian dune field self-organisation - implications for the formation of simple versus complex dune-field patterns." Geomorphology **72**: 94-105.

Krumbein, W. C. (1936). "Applications of logarithmic moments to size frequency distribution of sediments." Journal of Sedimentary Petrology **6**(1): 35-47.

Lambeck, K. (2002). "Sea level change from Mid Holocene to Recent Time: an Australian example with global implications." Ice Sheets, Sea Level and the Dynamic Earth Geodynamics Series (**29**): 33-50.

Lambeck, K., Yokoyama, Y. and Purcell, T. (2002). "Into and out of the Last Glacial Maximum: sea-level change during Oxygen Isotope Stages 3 and 2." Quaternary Science Reviews **21**: 343-360.

Lancaster, N. (1982). "Dunes on the Skeleton Coast, Namibia (South West Aftrica): geomorphology and grain size relationships." Earth Surface Processes and Landforms **7**: 575-587.

Lancaster, N. (1985). "Variations in wind velocity and sand transport on the windward flanks of desert sand dunes." Sedimentology **32**: 581-593.

Lancaster, N. (1986). "Grain-size characteristics of linear dunes in the southwestern Kalahari." Journal of Sedimentary Petrology **56**(3): 395-400.

Lancaster, N. (1988). "Controls of eolian dune size and spacing." Geology **16**: 972-975.

Lancaster, N. (1991). The orientation of dunes with respect to sand-transporting winds: a test of Rubin and Hunter's gross bedform-normal rule. NATO Advanced Research Workshop on sand, dust, and soil in their relation to aeolian and littoral processes, University of Aarhus, Sandbjerg, Denmark.

Lancaster, N. (1996). "The role of field experiments in studies of dune dynamics and morphology." Annals of Arid Zone **35**(3): 171-186.

Lancaster, N. (1997). "Response of eolian geomorphic systems to minor climate change: examples from the southern Californian deserts." Geomorphology **17**: 333-347.

Lancaster, N. and P. Helm (2000). "A test of a climatic index of dune mobility using measurements from the southwestern United States." Earth Surface Processes and Landforms **25**: 197-207.

Lancaster, N., W. G. Nickling, et al. (1994). Sediment flux and airflow on the stoss slope of a barchan dune. Response of eolian processes to global change: abstracts of a workshop. Desert Research Institute.

Lancaster, N., W. G. Nickling, et al. (1996). "Sediment flux and airflow on the stoss slope of a barchan dune." Geomorphology **17**: 55-62.

Lee, J. (1987). "A field experiment on the role of small scale wind gustiness in aeolian sand transport." Earth Surface Processes and Landforms **12**: 331-335.

Lettau, K. and H. Lettau (1978). Experimental and micrometeorological field studies of dune migration. Exploring the world's driest climate. K. Lettau and H. H. Lettau. Madison, Center for Climatic Research, University Wisconsin.: 110-147.

Linacre, E. (1992). Climate data and resources a reference and guide. London and New York, Routledge.

Liu, L. Y., E. Skidmore, et al. (2005). "Dune sand transport as influenced by wind directions, speed and frequencies in the Ordo Plateau, China." Geomorphology **67**: 283-297.

Livingstone, I. (1986). Geomorphological significance of wind flow patterns over a Namib linear dune. Aeolian Geomorphology, Proceedings of the 17th Annual Binghampton Symposium.

Lofdahl, L. and M. Gad-el-Hak (1999). "MEMS-based pressure and shear stress sensors for turbulent flows." Meas. Sci. Technol. **10**: 665-686.

MacKinnon, K. (1980). Climatic survey, Tasmania. Region 3, Northern. Canberra, Bureau of Meteorology, Dept of Science and the Environment: 1-64.

Mason, C. C. and R. L. Folk (1958). "Differentiation of beach, dune and aeolian flat environments by size analysis, Mustang Island, Texas." Journal of Sedimentary Petrology **28**(2): 211-226.

Mason, P. J. and R. I. Sykes (1979). "Flow over an isolated hill of moderate slope." Quaterly Journal of Royal Meteorological Society **105**: 383-395.

Masselink, G. and C. B. Pattiaratchi (2001). "Characteristics of the sea breeze system in Perth, Western Australia, and its effect on the nearshore wave climate." Journal of Coastal Research **17**(1): 173-187.

Mattox, R. J. (1954). A study of sand dunes. Geology. Michigan, State University of Iowa, USA: 149.

McCaul, S. G. (1996). The effect of dune topography on wind flow and sand transport Brooklands Spit; Pegasus Bay. Geography. Canterbury, University of Canterbury, New Zealand: **175**.

McDonald, R. C., R. F. Isbell, et al. (1984). Australian soil and land survey field handbook. Melbourne. Inkata Press.

McFadgen, B. G. (1985). "Late Holocene stratigraphy of coastal deposits between Auckland and Dunedin, New Zealand." Journal of the Royal Society of New Zealand **15**(1): 27-65.

McKee, E. D. and W. C. Ward (1983). Eolian Environment. Carbonate depositional environments. P. A. Scholle, D. G. a. Bebout and C. H. Moore. Tulsa, The American Association of Petroleum Geologists: 131-170.

McKenna Neuman, C., N. Lancaster, et al. (1997). "Relations between dune morphology, air flow, and sediment flux on reversing dunes, Silver Peak, Nevada." Sedimentology **44**: 1103-1113.

Meteorology, B. o. (2003). Solar radiation data. Hobart.

Meteorology, B. o. (2003). Station data. Rainfall: Low Head, Bridport, Waterhouse.

Meteorology, B. o. (2004). Wind speed Low Head, Swan Island, Waterhouse. Hobart.

Meteorology, B. o. (2004). Station data. Rainfall and evapotranspiration, Scotsdale. Hobart.

Middleton, G. V. (1984). Mechanics of sediment movement. Massachusetts, Massachusetts Institute of Technology.

Mikkelsen, H. E. (1989). "Wind flow and sediment transport over a low coastal dune." Geoskrifter **32** (Aarhus University Geologisk Institute.): 1-46.

Mitasova, H., M. Overton, et al. (2005). "Geospatial analysis of a coastal sand dune field evolution: Jockey's Ridge, North Carolina." Geomorphology **72**(1-4): 204-221.

Mowling, F. A. (1998). Changes in the morphology of Waterhouse coastal dune system since 1949. School of Geography & Environmental Studies. Hobart, University of Tasmania: 111.

Mowling, F. A. and R. Coleman (2003). Temporal spatial analysis of dune morphology. Coastal GIS 2003: an integrated approach to Australian coastal issues. Wollongong Papers on Maritime Policy, 14, Wollongong, NSW, Australia.

Muckersie, C. and M. J. Shepherd (1995). "Dune phases as time-transgressive phenomena, Manawatu, New Zealand." Quaternary International **26**: 61-67.

Muhs, D. H. (1985). "Age and paleoclimatic significance of Holocene sand dunes in Northeastern Colorado." Annals of the Association of American Geographers **75**(4): 566-582.

Muhs, D. R. and V. T. Holliday (1995). "Evidence of active dune sand on the Great Plains in the 19th Century from accounts of early explorers." Quaternary Research **43**: 198-208.

Muhs, D. R. and P. B. Maat (1993). "The potential response of eolian sands to greenhouse warming and precipitation reduction on the Great Plains of the USA." Journal of Arid Environments **25**: 351-361.

Mulligan, K. R. (1988). "Velocity profiles measured on the windward slope of a transverse dune." Earth Surface Processes and Landforms **13**: 573-582.

Mulligan, K. R. (1995). Field methods in a study of the process-response system controlling dune morphology, Salton Sea, California. Desert Aeolian Processes. P. Tchakerian Vatche. London, Chapman & Hall: 131-150.

Murray-Wallace, C. V. and A. Goede (1991). "Aminostratigraphy and electron spin resonance studies of late Quaternary sea level change and coastal neotectonics in Tasmania, Australia." Zeitschrift fuer Geomorphologie **35**(2): 129 - 149.

Namikas, S. L. (2003). "Field measurement and numerical modelling of aeolian mass flux distributions on a sandy beach." Sedimentology **50**: 303 - 326.

Namikas, S. L. and S. D.J. (1998). "AEOLUS II: an interactive program for the simulation of aeolian sedimentation." Geomorphology **22**: 135-149.

Nanson, G. C., X. Y. Chen, et al. (1992). "Lateral migration, thermoluminescence chronology and colour variations of longitudinal dunes near Birdsville in the Simpson Desert, central Australia." Earth Surface Processes and Landforms **17**: 807-819.

Ni, J. R., Li, Z., and C. Mendoza (2004). "Blown-sand transport rate." Earth Surface Processes and Landforms **29**: 1-14.

Nickling, W., G., and R. Davidson-Arnott, G.D. (1990). Aeolian sediment transport on beaches and coastal sand dunes. Proceedings Canadian Symposium on Coastal Sand Dunes.

Nordstrom, K., F. (1990). "Changes in the volume of coastal dunes in New Jersey, USA." Ocean and Shoreline Management **14**: 1-10.

Nordstrom, K., F. (2000). Beaches and dunes of developed coasts. Cambridge, Cambridge University Press.

Nordstrom, K. and N. Psuty. (1990). Coastal dunes: form and process. Chichester, John Wiley & Sons Ltd.

Oke, T. R. (2000). Boundary Layer Climates. London, Mathuen.

Olson, J. R. (1958). "Lake Michigan dune development 1 wind velocity profiles." Journal Geology **66**: 254-263.

Owen, P. R. (1964). "Saltation of uniform grains in air." Journal of Fluid Mechanics **20**: 225-242.

Pearce, K. I. and I. J. Walker (2005). "Frequency and magnitude biases in the 'Fryberger' model, with implications for characterising geomorphically effective winds." Geomorphology **68**: 39-55.

Pethick, J. (1984). An introduction to coastal geomorphology. London, Edward Arnold.

Pirazzoli, P. A. (1991). World atlas of Holocene sea-level changes / Paolo Antonio Pirazzoli ; assistant, Jean Pluet. Amsterdam, Elsevier.

Pluis, J. L. A. (1992). "Relationships between deflation and near surface wind velocity in a coastal dune blowout." Earth Surface Processes and Landforms. **17**: 663-673.

Pluis, J. L. A. and B. De Winder (1990). "Natural stabilization." Catena (Supplement 18): 195-208.

Prill, R. C. (1968). Movement of moisture in the unsaturated zone in a dune area, southwestern Kansas. Prof. Paper.: D1-D9.

Pryor, W. A. (1973). "Permeability-porosity patterns and variations in some Holocene sand bodies." American Assoc. Petroleum and Geology Bulletin **57**: 162-189.

Psuty, N., P., J. R. Allen, et al. (1988). "Spatial analysis of dune crest mobility, Fire Island National Seashore, New York." Journal of Coastal Research **Special Issue No. 3** (Autumn): 115-120.

Pugh, D., J. Hunter, et al. (2002). "A comparison of historical and recent sea level measurements at Port Arthur, Tasmania." The International Hydrographic Review 3(3): 1-20.

Pye, K. (1982). "Negatively skewed aeolian sands from a humid tropical coastal dunefield, Northern Australia." Sedimentary Geology **31**: 249-266.

Pye, K. (1983). "Coastal dunes." Progress in Physical Geography **7**: 531-557.

Pye, K. (1983). Early post-depositional modification of aeolian dune sands. Developments in Sedimentology, Eolian Sediments and Processes. M. E. Brookfield and T. S. Ahlbrandt. Elesevier. **38:** 197-222.

Pye, K. (1983). "Formation and history of Queensland coastal dunes." Zeitschrift fuer Geomorphologie **45** (Supplementband): 175-204.

Pye, K. and H. Tsoar (1990). Aeolian sand and sand dunes. London, Unwin Hyman.

Ranwell, D. S. (1972.). Ecology of salt marshes and sand dunes. London, Chapman and Hall.

Ranwell, D. S. (1979). Strategies for the management of coastal systems. Ecological processes in coastal environments. Jeffries,R.L. and Davy, A.J. Oxford, Blackwell Scientific: 515-528.

Raper, J., D. Livingstone, et al. (2003). Constructing a geomorphological database of coastal change using GIS. Coastal and marine geo-information systems. D. R. Green and S. D. King, Kluwer Academic Publishers, Netherlands : 399-413.

Rasmussen, K. R. (1989). "Some aspects of flow over coastal dunes." Proceedings of the Royal Society of Edinburgh **96B**: 129-147.

Rasmussen, K. R. and M. Sorensen (1999). "Aeolian mass transport near the saltation threshold." Earth Surface Processes and Landforms **24**(5): 413-422.

Rasmussen, K. R., M. Sorensen, et al. (1985). Measurement of saltation and wind strength on beaches. Proceedings of International Workshop on the Physics of Blown Sand., Aarhus University, Department of Theoretical Statistics.

Rayment, G. E. (1992). Australian laboratory handbook of soil and water chemical methods. Port Melbourne, Inkata Press.

Rice, M. A. (1991). "Grain shape effects on aeolian sediment transport." Acta Mechanica **Supplement** (1): 159-166.

Ritter, D. F. (2004). Wind processes and landforms. Process Geomorphology. Dubuque, Iowa, Wm. C. Brown.

Roberston-Rintoul, M. J. (1990). A quantitative analysis of the near-surface wind flow pattern over coastal parabolic dunes. Coastal dunes: form and process. K. Nordstrom and N. Psuty. Chichester, John Wiley & Sons Ltd: 57-78.

Rowe, R. D., S. F. Benjamin, et al. (1981). "Field studies of stable air flow over and around a ridge." Atmospheric Environment **16**(4): 643-653.

Royal Australian Navy, H. S. (1989). Cape Barren Island, 1:250,000, Commonwealth of Australia, Royal Australian Survey Corps : Sheet SK 55-3, Edition 1, Cape Barren Island, National Bathymetric Map Series.

Rubin, D. M. and R. E. Hunter (1987). "Bedform alighnment in directionally varying flows." Science **237**(July): 276-278.

Rubin, D. M. and H. Ikeda (1990). "Flume experiments on the alignment of transverse, oblique, and longitudinal dunes in directionally varying flows." Sedimentology **37**: 673-684.

Rust, I. C. (1990). "Coastal dunes as indicators of environmental change." Suid-Afrikaanse Tydskrif vir Wetenskap **86**(July-October): 299-301.

Sadr, R. and J. C. Klewicki (2000). "Surface shear stress measurement system for boundary layer flow over a salt playa." Measurement Science and Technology **11**: 1403-1413.

Sarre, R. D. (1989). "Aeolian sand drift from the intertidal zone on a temperate beach: potential and actual rates." Earth Surface Processes and Landforms **14**: 247-258.

Shanmugam, S. and M. Barnsley (2003). Quantifying landscape / ecological succession in a coastal dune system using sequential aerial photography and GIS. Coastal and marine geo-information systems. D. R. Green and S. D. King, Kluwer Academic Publishers, Netherlands : 247-260.

Sharp, R. P. (1963). "Wind Ripples." Journal Geology **71**: 617-36.

Sherman, D. J. (1990). A method for measuring aeolian sediment transport rates. Proceedings Canadian Symposium on Coastal Sand Dunes, Guelph, Ontario.

Sherman, D. J. and B. O. Bauer (1993). "Dynamics of beach-dune systems." Progress in Physical Geography **17**(4): 413-447.

Sherman, D. J. and S. Hotta (1990). Aeolian sediment transport: theory and measurement. Coastal dunes: form and process. K. F. Nordstrom, N. P. Psuty and R. W. G. Carter. NY, John Wiley & Sons Ltd: 17-37.

Short, A. D. (1988). "Holocene coastal dune formation in Southern Australia: a case study." Sedimentary Geology **55**: 121-142.

Sinclair, B. J. (2001). "Biolologically relevant environmental data: Macros to make the most of microclimate recordings." Cryoletters **22**: 125-134.

Skidmore, E. L. (1965). Assessing wind erosive forces direction and relative magnitude. Proceedings of the Soil Science Society of America.

Sprigg, R. C. (1979). "Stranded and submerged sea-beach systems of southeast South Australia and the aeolian desert cycle." Sedimentary Geology **22**(1-2): 53-96.

Stapor, F. W., J. P. May, et al. (1983). "Eolian shape-sorting and aerodynamic traction equivalence in the coastal dunes of Hout Bay, Republic of South Aftrica." Developments in Sedimentology. Eolian Sediments & Processes (**38**): 149-164.

Stockton, P. H. and D. A. Gillette (1990). "Field measurement of the sheltering effect of vegetation on erodible land surfaces." Land Degradation and Rehabilitation **2**: 77-85.

Stokes, S., A. S. Goudie, et al. (1999). "Accurate dune displacement and morphometric data using kinematic GPS." Zietschrift Fuer Geomorphologie **Nov. (Supplementary, 116.)**: 195-214.

Story, R. (1982). Notes on parabolic dunes, winds and vegetation in Northern Australia. Division of Water and Land Resources Technical Paper No. 43, CSIRO: 1-33.

Tanner, C. B. (1963). Basic instrumentation and measurements for plant environment and micrometeorology. Wisconsin, Dept of Soil Science, College of Agriculture, University of Wisconsin.

Tchakerian, V., P., Ed. (1995). Desert Aeolian Processes. London, Chapman & Hall.

Tengberg, A. (1995). "Nebka dunes as indicators of wind erosion and land degradation in the Sahel zone of Burkina Faso." Journal of Arid Environments **30**: 265-282.

Thom, A. S. (1971). "Momentum absorbtion by vegetation." Quarterly Journal of the Royal Meteorological Society **91**: 414-428.

Thom, B., P. Hesp, et al. (1994). "Last glacial 'coastal' dunes in Eastern Australia and implications for landscape stability during the Last Glacial Maximum." Palaeogeography, Palaeoclimatology, Palaeoecology **111**: 229-248.

Thom, B. G. (1978). Coastal sand deposition in southeast Australia during the Holocene. Landform Evolution in Australasia. J. Davies and M. A. J. Williams. Canberra, Australian National University Press: 197 - 214.

Thom, B. G. and J. Chappell (1975). "Holocene sea levels relative to Australia." Search **6**: 90 - 93.

Thom, B. G. and P. S. Roy (1985). "Relative sea levels and coastal sedimentation in southeast Australia in the Holocene." Journal of Sedimentary Petrology **5**(2): 257-264.

Thomas, D. S. G., Ed. (1989). Arid Zone Geomorphology. London, Belhaven Press,.

Thomas, D. S. G. and H. C. Leason (2005). "Dunefield activity response to climate variability in the southwest Kalahari." Geomorphology **64**: 117-132.

Thomas, D. S. G. and H. Tsoar (1990). The geomorphological role of vegetation in desert dune systems. Vegetation and Erosion: processes and environments. J. B. Thornes. Chichester, John Wiley & Sons: 474-489.

Thomas, I. (1991). The Holocene Archaeology and Palaeoecology of Northeastern Tasmania. Geography and Environmental Studies. Hobart, University of Tasmania: 412.

Thompson, C. H. (1983). "Development and weathering of large parabolic dune systems along the subtropical coast of eastern Australia." Zeitschrift fuer Geomorphologie. vol.45, **45** (Supplementband): 205-225.

Thornthwaite, C. W. (1931). "The climate of North America according to a new classification." Geog. Rev. **21**: 633-55.

Thornthwaite, C. W. and J. R. Mather (1957). "Instructions and tables for computing potential evapotranspiration and water balance." Publications in climatology. Laboratory of climatology, Centerton, NJ. **10**: 185-311.

Tsoar, H. (2005). "Sand dunes mobility and stability in relation to climate." Physica **A 357(1)**: 50-56.

Tsoar, H. and S. M. Arens (2003). Mobiliza & ccedil; & atilde; o E Estabiliza & ccedil; & atilde; o De Dunas Em Climas & Uacute; midos E Secos (Mobilization and stabilization of sand dunes in humid and arid climates). Mercator **2**(3): 131-145.

Tsoar, H. and D. G. Blumberg (2002). "Formation of parabolic dunes from barchan and transverse dunes along Israel's mediterranean coast." Earth Surface Processes and Landforms **27**: 1147-1161.

Tsoar, H. and W. Illenberger (1998). "Re evaluation of sand dunes' mobility indices." J of Arid Lands Studies **7S**: 265-268.

Umina, P. A., A. R. Weeks, et al. (2005). "A rapid shift in a classic clinal pattern in *Drosophila* reflecting climate change." Science **308**: 691-693.

UNESCO (1979). Map of the world distribution of arid regions. MAB Technical Note 7.

Unwin, D. M. (1980). Microclimate measurement for ecologists. London, Academic Press.

Visher, G. S. (1969). "Grain size distributions and depositional processes." Journal of Sedimentary Petrology **39**(3): 1074-1106.

Walker, I. J. (2002). Advances in research on dune-airflow-sand transport dynamics: incorporating secondary flow and sand transport processes. ICARS5/GCTE-SEN Joint Conference, International Center for Arid and Semiarid Lands Studies, Texas Tech University, Lubbock, Texas, USA, International Center for Arid and Semiarid Lands Studies.

Walker, I. J. and W. G. Nickling (2002). "Dynamics of secondary airflow and sediment transport over and in the lee of transverse dunes." Progress in Physical Geography **26**(1): 47-75.

Walsh, S. J., D. R. Butler, et al. (1998). "An overview of scale, pattern, process relationships in geomorphology: a remote sensing and GIS perspective." Geomorphology **21**: 183-205.

Wang, X., Z. Dong, et al. (2002). "Relations between morphology, air flow, sand flux and particle size on transverse dunes, Taklimakan sand sea, China." Earth Surface Processes and Landforms **27**: 515-526.

Warren, A. (1976). "Dune trend and the Eckman spiral." Nature **259**: 653-654.

Wasson, R. J. (1983). "A test of granulometric control of desert dune geometry." Earth Surface Processes and Landforms **8**: 301-312.

Wasson, R. J. and P. M. Nanninga (1986). "Estimating wind transport of sand on vegetated surfaces." Earth Surface Processes and Landforms **11**: 505-514.

Watson, A. (1987). "Variations in wind velocity and sand transport on the windward flanks of desert. sand dunes." Sedimentology **34**: 511-516.

Weng, W. S. and et al. (1991). "Air flow and sand transport over sand dunes." Acta Mechanica **Supplement** (2): 1-22.

Wentworth, C. K. (1922). "A scale of grade and class terms for clastic sediments." Journal of Geology **30**: 377-92.

Whisenant, S., G. (1999). Repairing damaged wildlands a process-orientated, landscape-scale approach. Cambridge, Cambridge University Press.

White, B. R. and H. Tsoar (1998). "Slope effect on saltation over a climbing sand dune." Geomorphology **22**: 159-180.

Whitney, M., I. (1981). "Eolian features shaped by aerodynamic and vorticity processes." Developments in Sedimentology **38**(Eolian sediments and processes): 223-246.

Wiedemann, A. M. et al. (1998). "Coastal foredune history and development, Oregon, USA." Journal of Coastal Research (**Special Issue 26**): 45-51.

Wiggs, G. F. S., R. J. Atherton, et al. (2002). The dynamic effects of moisture on the entrainment and transport of sand by wind. Proceedings of ICARS5/GCTE-SEN

Joint Conference, Texas, Tech University, Lubbock, Texas, USA, International Center for Arid and Semiarid Lands Studies, Pub.

Wiggs, G. F. S., I. Livingstone, et al. (1996). "The role of streamline curvature in sand dune dynamics: evidence from field and wind tunnel measurements." Geomorphology **17**: 29-46.

Wilcox, F. A. and R. W. G. Carter (1977). "An environmental approach to the restoration of badly eroded sand dunes." Biological Conservation **11**: 279-291.

Willetts, B. B. (1989). "Physics of sand movement in vegetated dune systems." Proceedings of the Royal Society of Edinburgh **96B**: 37-49.

Wilson, I. G. (1972). "Aeolian bedforms - their development and origins." Sedimentology **19**: 173-210.

Wolfe, S. A. (1997). "Impact of increased aridity on sand dune activity in the Canadian Prairies." Journal of Arid Environments **36**: 421-432.

Wolfe, S. A. and P. P. David (1997). "Parabolic dunes: examples from the Great Sandhills, southwestern Saskatchewan." Canadian Geographer **41**(2): 207-13.

Wolfe, S. A. and W. G. Nickling (1993). "The protective role of sparse vegetation in wind erosion." Progress in Physical Geography **17**: 50-68.

Wolman, M. G. and J. P. Miller (1960). "Magnitude and frequency forces in geomorphic processes." Journal of Geology **68**: 54-74.

Woodroffe, C., D. (2002). Coasts: form, process, and evolution. Cambridge, Cambridge University Press.

Woolard, J. W. and J. D. Colby (2002). "Spatial characterizaton, resolution, and volumetric change of coastal dunes using airborne LIDAR: Cape Hatteras, North Carolina." Geomorphology **48**: 269-287.

Wright, L. D. and B. G. Thom (1977). "Coastal depositional landforms: a morphodynamic approach." Progress in Physical Geography **1(3)**: 412-459.

Wrigley, N. (1985). Categorical data analysis for geographers and environmental scientists. New York, Longman.

Zhibao Dong, Xiaoping Liu, et al. (2003). "The aerodynamic roughness with a blowing sand boundary layer (BSBL): a redefinition of the Owen effect." Geophysical research letters **30**(2): 19 (1-4).

Appendix 1. Wind data – Figures 4.9 to 4.13.

Surface wind data were analysed using the 'WinRose' v0.95, MS-Windows based program (Freeman, 2002). Wind direction and speed were calculated for 8 sectors (sector bins of 45 degrees). Maximum site wind speed is highlighted in each table.

Whole Year
00:00 to 06:00

	Frequency (%)								
	Classes m/s						Site m/s		
Direction	>4 to <8	>8 to <12	>12to<16	>16to<20	>20	Total (%)	Calm	Max	Min
N	0.7	0.38	0.29	0.03	0.01	1.41	4.2	25.5	8.95
NE	1.34	0.61	0.25	0.09	0.04	2.33	4	23.6	8.34
E	10.77	4.3	1.44	0.62	0.44	17.57	4	27.7	8.27
SE	4.01	1.82	0.62	0.2	0.09	6.74	4	27.5	8.08
S	1.1	0.45	0.06	0.03	0.03	1.67	4	45	7.37
SW	2.31	3.36	2.85	1.47	0.48	10.46	4	26.9	11.76
W	2.89	2.78	3.05	2.35	1.08	12.15	4	28.5	12.66
NW	1.05	1.1	0.61	0.19	0.13	3.08	4	28.3	10.16
Total	24.17	14.79	9.17	4.98	2.3	55.41			

Matched 6881; Unmatched 18601; Bad Data 83; Total Readings 25565

Calm (<4.00 m/s) 44.59%
Site maximum (m/s) 45.00
Site mean (m/s) 5.99

06:00 to 12:00

	Frequency (%)								
	Classes m/s						Site m/s		
Direction	>4 to <8	>8 to <12	>12to<16	>16to<20	>20	Total (%)	Calm	Max	Min
N	1.68	1.65	0.67	0.14	0	4.14	4	18.8	9.12
NE	1.69	2.57	2.06	0.36	0.1	6.78	4	27.1	10.72
E	6.41	5.68	3.46	1.18	0.47	17.19	4	25.1	10.05
SE	2.61	1.65	0.93	0.6	0.16	5.95	4	21.3	9.78
S	1.23	0.32	0.06	0.1	0.03	1.74	4	21.9	7.52
SW	2.29	2.7	1.89	1.59	0.3	8.78	4	31.2	11.59
W	3.04	3.89	5.06	3.56	1.96	17.51	4	39.2	13.58
NW	2.12	2.58	0.75	0.33	0.24	6.02	4	33.9	9.93
Total	21.08	21.02	14.88	7.86	3.27	68.11			

Matched 6974; Unmatched 18508; Bad Data 83 Total Readings 25565

Calm (<4.00 m/s) 31.89%
Site maximum (m/s) 39.20
Site mean (m/s) 7.96

12:00 to 18:00

Direction	Frequency (%) Classes m/s						Site m/s		
	>4 to <8	>8 to <12	>12to<16	>16to<20	>20	Total (%)	Calm	Max	Mean
N	2.76	2.6	1.57	0.37	0.06	7.36	4	22.8	9.6
NE	1.39	2.79	4.73	2.17	0.19	11.27	4	22.2	12.85
E	2.72	3.98	3.95	2.16	0.65	13.45	4	31.7	12.19
SE	0.49	1.02	1.02	0.59	0.27	3.39	4.3	25	12.82
S	0.27	0.22	0.2	0.06	0.06	0.8	4.1	25.1	10.81
SW	0.96	0.85	0.85	1.21	0.78	4.64	4	33.2	14.25
W	5.22	7.86	7.26	6.74	6.11	33.18	4	34.3	14.23
NW	2.93	4.38	1.65	0.33	0.32	9.61	4.1	33.6	10.1
Total	16.74	23.7	21.22	13.62	8.42	83.7			

Matched 6959; Unmatched 18523; Bad Data 83; Total Readings 25565.

Calm (<4.00 m/s) 16.30%
Site maximum (m/s) 34.30
Site mean (m/s) 10.95

18:00 to 24:00

Direction	Frequency (%) Classes m/s						Site m/s		
	>4 to <8	>8 to <12	>12to<16	>16to<20	>20	Total (%)	Calm	Max	Mean
N	1.09	0.67	0.19	0.03	0.01	1.99	4.1	25.5	8.27
NE	2.3	2.14	0.87	0.06	0.01	5.38	4	25.1	8.82
E	10.53	5.27	2.24	0.84	0.33	19.22	4	30.1	8.75
SE	2.32	1.63	0.8	0.17	0.04	4.97	4	25.8	8.98
S	0.65	0.36	0.16	0.07	0.04	1.29	4.1	40	9.29
SW	1.95	2.89	2.8	1.6	1.05	10.29	4	48	12.74
W	4.1	4.21	3.63	3.46	2.67	18.08	4	30.1	13.32
NW	1.86	0.99	0.48	0.32	0.09	3.73	4	30.8	9.26
Total	24.8	18.16	11.17	6.55	4.26	64.95			

Matched 6882; Unmatched 18600; Bad Data 83; Total Readings 25565.

Calm (<4.00 m/s) 35.05%
Site maximum (m/s) 48.00
Site mean (m/s) 7.36

Entire Day – Whole year

Direction	Frequency (%) Classes m/s						Site m/s		
	>4 to <8	>8 to <12	>12to<16	>16to<20	>20	Total (%)	Calm	Max	Mean
N	1.57	1.35	0.69	0.15	0.02	3.78	4	25.5	9.21
NE	1.68	2.01	1.95	0.69	0.09	6.42	4	27.1	11.05
E	7.61	4.87	2.79	1.22	0.48	16.96	4	31.7	9.66
SE	2.35	1.52	0.82	0.4	0.14	5.24	4	27.5	9.56
S	0.83	0.34	0.12	0.06	0.04	1.39	4	45	8.28
SW	1.86	2.5	2.1	1.47	0.66	8.58	4	48	12.36
W	3.77	4.71	4.78	4.04	2.97	20.27	4	39.2	13.68
NW	1.99	2.28	0.88	0.29	0.19	5.62	4	33.9	9.93
Total	21.65	19.58	14.12	8.31	4.59	68.26			

Matched 25482; Unmatched 0; Bad Data 83; Total Readings 25565.

Calm (<4.00 m/s) 31.74%
Site maximum (m/s) 48.00
Site mean (m/s) 8.09

Summer
00:00 to 06:00

Direction	Frequency (%) Classes m/s						Site m/s		
	>4 to <8	>8 to <12	>12to<16	>16to<20	>20	Total (%)	Calm	Max	Min
N	0.57	0.38	0.21	0.03	0.02	1.2	4.2	25.5	9.05
NE	1.53	0.71	0.29	0.1	0.05	2.68	4	23.6	8.38
E	11.37	5.01	1.7	0.74	0.52	19.34	4	27.7	8.46
SE	4.41	2.12	0.74	0.24	0.1	7.61	4	27.5	8.19
S	1.22	0.52	0.07	0.03	0.02	1.86	4	21.1	7.11
SW	2.34	3.6	2.72	1.27	0.29	10.22	4	23.8	11.37
W	2.75	3.17	3.61	2.79	1.27	13.59	4	28.5	13.02
NW	0.91	1.22	0.64	0.22	0.15	3.15	4.2	28.3	10.65
Total	25.11	16.71	9.98	5.44	2.43	59.66			

Matched 5811;Unmatched 19671; Bad Data 83; Total Readings 25565.

Calm (<4.00 m/s) 40.34%
Site maximum (m/s) 28.50
Site mean (m/s) 6.40

06:00 to 12:00

Direction	Frequency (%) Classes m/s						Site m/s		
	>4 to <8	>8 to <12	>12to<16	>16to<20	>20	Total (%)	Calm	Max	Min
N	1.53	1.7	0.45	0.05	0	3.73	4	18.1	8.83
NE	1.87	2.7	2.28	0.43	0.12	7.4	4	27.1	10.83
E	7.04	6.4	4.07	1.41	0.57	19.49	4	25.1	10.2
SE	2.94	1.97	1.12	0.72	0.19	6.94	4	21.3	9.9
S	1.43	0.38	0.07	0.12	0.03	2.03	4	21.9	7.59
SW	2.3	2.7	1.75	1.65	0.33	8.72	4	31.2	11.67
W	3	4.41	5.92	4.14	2.3	19.78	4	39.2	13.85
NW	2.13	2.82	0.89	0.39	0.29	6.52	4	33.9	10.25
Total	22.24	23.08	16.55	8.91	3.83	74.61			

Matched 5824; Unmatched 19658; Bad Data 83 Total Readings 25565.

Calm (<4.00 m/s) 25.39%
Site maximum (m/s) 39.20
Site mean (m/s) 8.71

12:00 to 18:00

Direction	Frequency (%) Classes m/s						Site m/s		
	>4 to <8	>8 to <12	>12to<16	>16to<20	>20	Total (%)	Calm	Max	Min
N	2.08	2.59	1.24	0.14	0.02	6.06	4.1	22.8	9.48
NE	1.46	2.9	5.17	2.54	0.22	12.29	4	22.2	13.04
E	3.09	4.65	4.72	2.57	0.77	15.81	4	31.7	12.28
SE	0.55	1.22	1.22	0.7	0.33	4.02	4.3	25	12.88
S	0.29	0.26	0.24	0.07	0.07	0.93	4.1	25.1	11.05
SW	0.88	0.93	0.88	1.22	0.86	4.75	4	33.2	14.63
W	4.77	8.62	8.22	7.21	7.17	35.99	4	34.3	14.59
NW	3	4.82	1.91	0.39	0.38	10.5	4.1	33.6	10.33
Total	16.12	25.99	23.58	14.85	9.82	90.35			

Matched 5826; Unmatched 19656; Bad Data 83; Total Readings 25565.

Calm (<4.00 m/s) 9.65%
Site maximum (m/s) 34.30
Site mean (m/s) 11.94

18:00 to 24:00

Direction	Frequency (%) Classes m/s						Site m/s		
	>4 to <8	>8 to <12	>12to<16	>16to<20	>20	Total (%)	Calm	Max	Min
N	1.16	0.49	0	0	0	1.65	4.1	10.8	6.94
NE	2.94	3.16	1.47	0.13	0	7.7	4	17.9	9.22
E	6.41	6.76	2.22	0.49	0	15.88	4	19	9.13
SE	1.69	0.98	0.4	0.09	0	3.16	4	19.6	8.73
S	0.09	0.31	0.22	0	0	0.62	6.3	13.3	11.13
SW	0.93	2.71	3.78	1.6	1.07	10.1	4	25.8	13.55
W	3.47	4.63	4.27	5.34	4.23	21.93	4	28.2	14.6
NW	1.11	0.36	0.18	0.13	0.04	1.82	4.2	25.4	8.84
Total	17.79	19.4	12.54	7.78	5.34	62.86			

Matched 2248; Unmatched 23234; Bad Data 83; Total Readings 25565.

Calm (<4.00 m/s) 37.14%
Site maximum (m/s) 28.20
Site mean (m/s) 7.63

Entire Day - Summer

Direction	Frequency (%) Classes m/s						Site m/s		
	>4 to <8	>8 to <12	>12to<16	>16to<20	>20	Total (%)	Calm	Max	Min
N	1.22	1.87	0.75	0.02	0	3.86	4	16.9	9.4
NE	1.81	3.12	3.4	1.24	0.08	9.66	4	21.1	11.7
E	4.87	4.53	2.46	0.84	0.01	12.72	4	20.7	9.61
SE	1.48	0.99	0.51	0.22	0.11	3.3	4	21.6	9.61
S	0.68	0.29	0.07	0	0	1.04	4.1	15.4	7.3
SW	1.41	2.65	2.23	1.52	0.49	8.31	4	25.8	12.46
W	2.95	4.64	5.58	5.62	5.04	23.84	4	39.2	15.16
NW	1.57	2.32	0.58	0.07	0.11	4.64	4	33.9	9.68
Total	15.99	20.41	15.58	9.54	5.85	67.37			

Matched 8293; Unmatched 17189; Bad Data 83; Total Readings 25565.

Calm (<4.00 m/s) 32.63%
Site maximum (m/s) 39.20
Site mean (m/s) 8.48

Autumn
00:00 to 06:00

Direction	Frequency (%) Classes m/s						Site m/s		
	>4 to <8	>8 to <12	>12to<16	>16to<20	>20	Total (%)	Calm	Max	Min
N	0.07	0.2	0.47	0.07	0	0.81	6.6	17.3	13.12
NE	1.28	0.87	0.27	0.13	0.07	2.62	4.6	21.9	9.12
E	14.13	2.15	0.47	0.07	0.07	16.89	4	21.6	6.54
SE	9.02	2.76	1.21	0.74	0.13	13.86	4	21.3	7.84
S	1.14	0.27	0	0	0	1.41	4	9.5	5.58
SW	2.62	3.5	4.04	2.36	1.28	13.8	4.1	26.9	12.84
W	1.75	3.1	3.57	2.02	0.67	11.1	4.4	23	12.66
NW	0.94	1.14	1.14	0.4	0.07	3.7	4.4	20.3	11.2
Total	30.96	14	11.17	5.79	2.29	64.2			

Matched 1486; Unmatched 23996; Bad Data 83; Total Readings 25565.

Calm (<4.00 m/s) 35.80%
Site maximum (m/s) 26.90
Site mean (m/s) 6.65

06:00 to 12:00

Direction	Frequency (%) Classes m/s						Site m/s		
	>4 to <8	>8 to <12	>12to<16	>16to<20	>20	Total (%)	Calm	Max	Min
N	1.21	0.87	0.87	0.2	0	3.15	4.1	18.1	9.62
NE	1.27	2.95	1.41	0.54	0.13	6.3	4.3	20.1	11.01
E	8.65	4.49	2.68	0.27	0	16.09	4	17.6	8.55
SE	6.1	3.22	1.74	0.6	0.27	11.93	4	21.3	9
S	1.74	0.13	0.07	0	0	1.94	4	12.6	5.74
SW	4.22	2.95	2.88	2.14	0.4	12.6	4	21.8	11.14
W	2.08	4.22	3.89	4.02	0.94	15.15	4.6	27.7	13.3
NW	1.27	1.54	0.87	1.54	0.27	5.5	4.5	20.9	12.17
Total	26.54	20.38	14.41	9.32	2.01	72.65			

Matched 1492; Unmatched 23990; Bad Data 83; Total Readings 25565.

Calm (<4.00 m/s) 27.35%
Site maximum (m/s) 27.70
Site mean (m/s) 8.01

12:00 to 18:00

Direction	Frequency (%) Classes m/s						Site m/s		
	>4 to <8	>8 to <12	>12to<16	>16to<20	>20	Total (%)	Calm	Max	Min
N	1.49	2.16	1.62	0.41	0	5.68	4.3	17.6	10.44
NE	1.08	2.97	6.22	2.23	0.34	12.84	4	21.6	13.21
E	3.51	2.43	1.96	1.82	0	9.73	4	19.3	10.66
SE	1.15	2.09	1.49	1.08	0.2	6.01	4.3	21.7	11.93
S	0	0.07	0.14	0.07	0	0.27	9.8	19.6	14
SW	1.35	1.35	1.28	1.76	0.47	6.22	4.4	21.7	13.03
W	6.62	9.46	9.53	6.76	4.19	36.55	4	28.7	13.25
NW	3.51	5.2	1.96	1.35	0.54	12.57	4.2	22.5	10.68
Total	18.72	25.74	24.19	15.47	5.74	89.86			

Matched 1480; Unmatched 24002; Bad Data 83; Total Readings 25565.

Calm (<4.00 m/s) 10.14%
Site maximum (m/s) 28.70
Site mean (m/s) 11.30

18:00 to 24:00

Direction	Frequency (%) Classes m/s						Site m/s		
	>4 to <8	>8 to <12	>12to<16	>16to<20	>20	Total (%)	Calm	Max	Min
N	0.47	0.61	0.34	0	0	1.42	4.2	14.5	9.43
NE	2.1	2.17	1.29	0	0	5.56	4.2	14.8	9.19
E	14.72	4.61	0.95	0.14	0	20.42	4	18	7.26
SE	3.53	3.46	1.22	0.61	0	8.82	4.1	19.2	9.23
S	0.88	0.34	0.34	0.07	0	1.63	4.1	16.6	8.49
SW	2.71	4.21	4.34	2.78	1.15	15.2	4.4	25.2	12.63
W	1.97	4.75	4.48	2.17	2.31	15.67	4.4	24.8	13.52
NW	1.7	0.95	1.29	0.41	0	4.34	4.1	19.3	10.16
Total	28.09	21.1	14.25	6.17	3.46	73.07			

Matched 1474; Unmatched 24008; Bad Data 83; Total Readings 25565.

Calm (<4.00 m/s) 26.93%

Site maximum (m/s) 25.20
Site mean (m/s) 7.94

Entire Day - Autumn

Direction	Frequency (%) Classes m/s						Site m/s		
	>4 to <8	>8 to <12	>12to<16	>16to<20	>20	Total (%)	Calm	Max	Min
N	0.79	0.95	0.86	0.18	0	2.78	4.1	18.1	10.4
NE	1.41	2.21	2.23	0.75	0.15	6.75	4	21.9	11.56
E	10.26	3.51	1.52	0.6	0.02	15.9	4	21.6	7.94
SE	4.94	2.83	1.39	0.77	0.15	10.07	4	21.7	9.09
S	0.97	0.22	0.11	0.04	0	1.33	4	19.6	6.85
SW	2.71	3.09	3.16	2.19	0.86	12.01	4	26.9	12.32
W	3.07	5.39	5.3	3.75	2.08	19.6	4	28.7	13.26
NW	1.83	2.27	1.33	0.9	0.22	6.54	4.1	22.5	10.99
Total	25.96	20.48	15.9	9.18	3.47	74.99			

Matched 5470; Unmatched 20012; Bad Data 83; Total Readings 25565.

Calm (<4.00 m/s) 25.01%
Site maximum (m/s) 28.70
Site mean (m/s) 8.49

Winter
00:00 to 06:00

Direction	Frequency (%) Classes m/s						Site m/s		
	>4 to <8	>8 to <12	>12to<16	>16to<20	>20	Total (%)	Calm	Max	Min
N	1.55	0.3	0	0.06	0.06	1.97	4.2	25.5	7.32
NE	0.9	0.06	0.06	0.12	0.06	1.2	4.1	23.6	7.9
E	11.36	3.71	2.21	1.97	1.73	20.98	4	27.7	9.81
SE	2.63	2.15	1.43	0.18	0.24	6.63	4	27.5	9.71
S	1.26	0.84	0.24	0.12	0.12	2.57	4	45	9.31
SW	2.33	1.97	2.15	0.36	0.12	6.93	4	22.1	10.36
W	4.06	2.39	2.33	2.75	1.61	13.15	4.1	28.5	12.84
NW	1.91	2.21	0.6	0.12	0.12	4.96	4	21.7	8.73
Total	26	13.63	9.03	5.68	4.06	58.4			

Matched 1673; Unmatched 23809; Bad Data 83; Total Readings 25565.

Calm (<4.00 m/s) 41.60%
Site maximum (m/s) 45.00
Site mean (m/s) 6.67

06:00 to 12:00

Direction	Frequency (%) Classes m/s						Site m/s		
	>4 to <8	>8 to <12	>12to<16	>16to<20	>20	Total (%)	Calm	Max	Min
N	1.78	0.23	0.06	0	0	2.07	4	14.6	6.17
NE	1.78	0.46	0	0	0.17	2.41	4	27.1	7.25
E	8.38	6.89	4.42	2.18	1.72	23.59	4	25.1	10.84
SE	2.53	1.78	1.09	0.57	0.06	6.03	4	20.1	9.78
S	0.57	0.11	0.11	0.29	0.11	1.21	4.9	21.9	11.13
SW	2.12	3.21	1.55	1.03	0.29	8.21	4	23.5	10.92
W	2.93	2.07	3.1	2.01	1.32	11.42	4.2	28.5	12.98
NW	1.89	2.18	0.92	0	0.52	5.51	4	28.8	10.23
Total	21.99	16.93	11.25	6.08	4.19	60.45			

Matched 1742; Unmatched 23740; Bad Data 83 Total Readings 25565.

Calm (<4.00 m/s) 39.55%
Site maximum (m/s) 28.80
Site mean (m/s) 7.16

12:00 to 18:00

Direction	Frequency (%) Classes m/s						Site m/s		
	>4 to <8	>8 to <12	>12to<16	>16to<20	>20	Total (%)	Calm	Max	Min
N	3.39	0.92	0	0	0.06	4.37	4	22.8	6.82
NE	3.39	1.27	0.12	0	0.06	4.83	4	22.2	7.01
E	4.14	7.53	7.07	2.3	1.73	22.77	4	31.7	12.34
SE	0.81	1.55	1.32	0.35	0.29	4.31	4.6	25	11.77
S	0.81	0.46	0.69	0.12	0.17	2.24	4.1	25.1	10.94
SW	1.84	1.32	1.15	1.32	0.75	6.38	4	33.2	13.07
W	8.74	5	3.05	3.51	2.24	22.54	4	30	11.35
NW	3.11	1.84	1.61	0.12	0.69	7.36	4.1	33.6	10.67
Total	26.22	19.9	15.01	7.71	5.98	74.81			

Matched 1739; Unmatched 23743; Bad Data 83; Total Readings 25565.

Calm (<4.00 m/s) 25.19%
Site maximum (m/s) 33.60
Site mean (m/s) 8.91

18:00 to 24:00

Direction	Frequency (%) Classes m/s						Site m/s		
	>4 to <8	>8 to <12	>12to<16	>16to<20	>20	Total (%)	Calm	Max	Min
N	1.38	0.72	0	0.12	0.06	2.28	4.2	25.5	8.34
NE	0.78	0	0.06	0	0.06	0.9	4.1	25.1	7.09
E	11.33	4.86	2.7	1.2	1.08	21.16	4	30.1	9.31
SE	3.78	1.98	1.56	0.06	0.18	7.55	4	25.8	8.95
S	1.32	0.42	0.06	0.24	0.18	2.22	4.1	40	10.01
SW	2.64	1.8	0.48	0.24	0.72	5.88	4	48	10.8
W	3.66	4.26	3.12	3.06	2.34	16.43	4	30.1	13.33
NW	2.04	1.62	0.48	0.78	0.3	5.22	4	30.8	10.38
Total	26.92	15.65	8.45	5.7	4.92	61.63			

Matched 1668; Unmatched 23814; Bad Data 83; Total Readings 25565.

Calm (<4.00 m/s) 38.37%
Site maximum (m/s) 48.00
Site mean (m/s) 7.14

Entire Day - Winter

Direction	Frequency (%) Classes m/s						Site m/s		
	>4 to <8	>8 to <12	>12to<16	>16to<20	>20	Total (%)	Calm	Max	Min
N	2.06	0.51	0.02	0.03	0.03	2.65	4	25.5	6.96
NE	1.77	0.43	0.05	0.03	0.08	2.36	4	27.1	7.08
E	8.82	5.85	4.24	1.93	1.59	22.44	4	31.7	10.65
SE	2.43	1.9	1.33	0.31	0.19	6.16	4	27.5	9.88
S	1	0.5	0.29	0.18	0.13	2.09	4	45	10.08
SW	2.14	2.11	1.32	0.77	0.5	6.83	4	48	11.43
W	4.74	3.41	2.99	2.85	1.93	15.91	4	30.1	12.55
NW	2.23	1.96	0.95	0.26	0.4	5.8	4	33.6	10.13
Total	25.19	16.67	11.19	6.35	4.85	64.25			

Matched 6221; Unmatched 19261; Bad Data 83; Total Readings 25565.

Calm (<4.00 m/s) 35.75%
Site maximum (m/s) 48.00
Site mean (m/s) 7.54

Spring
00:00 to 06:00

Direction	Frequency (%) Classes m/s						Site m/s		
	>4 to <8	>8 to <12	>12to<16	>16to<20	>20	Total (%)	Calm	Max	Min
N	0.56	0.48	0.35	0	0	1.4	4.3	15.8	9.03
NE	1.56	0.75	0.32	0.05	0.03	2.71	4	20.3	8.12
E	9.16	5.43	1.48	0.24	0	16.31	4	18.2	8.09
SE	2.63	1.29	0.03	0	0	3.95	4	12.6	7.21
S	1.02	0.35	0	0	0	1.37	4.1	10.8	6.47
SW	2.18	3.92	2.69	1.61	0.32	10.72	4	23.8	11.61
W	2.82	2.82	3.17	2.31	0.99	12.12	4	27.5	12.58
NW	0.7	0.59	0.4	0.13	0.16	1.99	4.2	28.3	10.99
Total	20.63	15.64	8.44	4.35	1.5	50.56			

Matched 3722; Unmatched 21760; Bad Data 83; Total Readings 25565.

Calm (<4.00 m/s) 49.44%
Site maximum (m/s) 28.30
Site mean (m/s) 5.41

06:00 to 12:00

Direction	Frequency (%) Classes m/s						Site m/s		
	>4 to <8	>8 to <12	>12to<16	>16to<20	>20	Total (%)	Calm	Max	Min
N	1.82	2.62	0.88	0.19	0	5.51	4	18.8	9.52
NE	1.82	3.4	3.29	0.45	0.05	9.01	4.2	20.4	11.07
E	4.6	5.59	3.32	1.07	0.08	14.65	4	21.7	10.12
SE	1.26	0.96	0.53	0.61	0.16	3.53	4	21.1	10.85
S	1.34	0.48	0.03	0.05	0	1.9	4.1	18.2	7.19
SW	1.6	2.35	1.66	1.63	0.27	7.51	4	31.2	12.24
W	3.48	4.6	6.44	4.09	2.67	21.28	4	39.2	13.81
NW	2.57	3.18	0.61	0	0.11	6.47	4	33.9	9.05
Total	18.48	23.18	16.76	8.1	3.34	69.87			

Matched 3740; Unmatched 21742; Bad Data 83 Total Readings 25565.

Site minimum (m/s) 0.00
Site maximum (m/s) 39.20
Site mean (m/s) 8.31

12:00 to 18:00

Direction	Frequency (%) Classes m/s						Site m/s		
	>4 to <8	>8 to <12	>12to<16	>16to<20	>20	Total (%)	Calm	Max	Min
N	2.97	3.56	2.27	0.53	0.08	9.41	4	21.9	10
NE	0.59	3.42	6.28	3.16	0.19	13.64	4	21.1	13.68
E	1.74	2.94	3.29	2.22	0.4	10.59	4.2	24.5	12.61
SE	0.08	0.35	0.7	0.51	0.29	1.93	4.4	21.6	15
S	0.13	0.16	0	0.03	0.03	0.35	4.6	20.7	9.43
SW	0.4	0.43	0.53	0.94	0.91	3.21	4	29.8	16.28
W	3.02	8.56	8.32	8.24	8.66	36.79	4	34.3	15.44
NW	2.62	5.24	1.55	0.03	0.05	9.49	4.1	21	9.59
Total	11.55	24.65	22.94	15.64	10.61	85.4			

Matched 3740; Unmatched 21742; Bad Data 83; Total Readings 25565.

Calm (<4.00 m/s) 14.60%
Site maximum (m/s) 34.30
Site mean (m/s) 11.76

18:00 to 24:00

Direction	Frequency (%) Classes m/s						Site m/s		
	>4 to <8	>8 to <12	>12to<16	>16to<20	>20	Total (%)	Calm	Max	Min
N	1.24	0.69	0.2	0	0	2.14	4.1	15.5	7.9
NE	3.1	3.18	1.13	0.12	0	7.53	4.1	17.9	8.84
E	8.22	5.85	2.58	1.01	0.14	17.8	4	22.4	9.23
SE	1.07	0.72	0.32	0.06	0	2.17	4.2	19.6	8.93
S	0.29	0.29	0.14	0	0	0.72	4.1	13.3	8.91
SW	1.3	2.84	3.1	1.74	1.22	10.19	4	25.8	13.4
W	5.18	4.11	3.53	4.31	3.07	20.2	4	28.2	13.32
NW	1.97	0.75	0.17	0.06	0.03	2.98	4	25.4	7.7
Total	22.37	18.44	11.17	7.29	4.46	63.73			

Matched 3455; Unmatched 22027; Bad Data 83; Total Readings 25565.

Calm (<4.00 m/s) 36.27%
Site maximum (m/s) 28.20
Site mean (m/s) 7.35

Entire Day - Spring

Direction	Frequency (%) Classes m/s						Site m/s		
	>4 to <8	>8 to <12	>12to<16	>16to<20	>20	Total (%)	Calm	Max	Min
N	0.7	0.35	0.35	0	0	1.4	4.7	12.4	8.48
NE	2.46	1.75	0.35	0	0	4.56	4	13.6	7.98
E	12.28	4.21	2.11	0.35	0	18.95	4.1	18.1	7.98
SE	2.81	1.05	0	0	0	3.86	4	10.2	6.54
S	0	1.05	0	0	0	1.05	8.7	10.8	9.87
SW	1.75	3.16	4.91	1.75	0.35	11.93	4.6	20.3	12.2
W	4.56	2.46	3.51	2.11	1.75	14.39	4.3	27.5	12.09
NW	0.35	0.35	0	0.35	0	1.05	7.3	16.9	11.03
Total	24.91	14.39	11.23	4.56	2.11	57.19			

Matched 285; Unmatched 25197; Bad Data 83; Total Readings 25565.

Calm (<4.00 m/s) 42.81%
Site maximum (m/s) 27.50
Site mean (m/s) 5.93

Dates for Daylight Saving in Australia

Queensland, the Northern Territory and Western Australia do not participate in Daylight Saving. Which means that Australia has both horizontal and vertical time zones in summer.

New South Wales, Victoria, Australian Capital Territory and Tasmania

- begins at 2 am on Sunday 27 August 2000. Clocks should be turned forward one hour to read 3 am.
- ends at 3 am on Sunday 25 March 2001. Clocks should be turned back one hour to read 2 am (Australian Eastern Standard Time).
- The start and stop DST dates for NSW, ACT, Victoria and SA would be
  28 October 2001 to 31 March 2002
  27 October 2002 to 30 March 2003
  26 October 2003 to 28 March 2004
  31 October 2004 to 27 March 2005
- For the next few years, the start and stop DST dates for Tasmania would be
  7 October 2001 to 31 March 2002
  6 October 2002 to 30 March 2003
  5 October 2003 to 28 March 2004
  3 October 2004 to 27 March 2005
- In NSW, "summer time period" means a period starting at 2 am on the last Sunday in October in each year and ending at 2 am [for the 2nd time] on the last Sunday in the following March.

Appendix 2. Prècis of average annual atmospheric parameters, 1940 – 2003.

Year	Windspeed[1] m/s	Temperature[2] ^{0}C	Rainfall[3] mm	Year	Windspeed[1] m/s	Temperature[2] ^{0}C	Rainfall[3] Mm
1940	5.2	15.7	582.3	1972	5.4	17.6	410.3
1941	5	15.8	585.2	1973	6.4	17.3	767.6
1942	5.4	15.5	810	1974	6.3	17.4	907.1
1943	4.5	15.7	652.2	1975	5.7	16.9	748
1944	4.4	15.4	713.4	1976	6.1	17.1	630.7
1945	5.2	15.1	775.2	1977	6.1	16.6	612.4
1946	5.5	14.9	917	1978	5.4	16.7	647.2
1947	5.1	16	803	1979	5.7	17.1	696.9
1948	5.4	15.5	686.4	1980	6.1	17.1	713.3
1949	4.8	15.1	778	1981	6	17.6	687.7
1950	4.6	15.9	713.2	1982	6.8	17.1	560.6
1951	5	15.9	680.8	1983	6.8	17	610.8
1952	4	15.3	781	1984	7.1	17	626.5
1953	4.2	15.6	840.2	1985	6.2	17.4	669.2
1954	3.4	15.8	637.8	1986	7.7	16.7	814
1955	4.6	15.7	940	1987	7.7	17.1	495.1
1956	6.1	16	971	1988	6.9	18.2	676.6
1957	6.1	15.7	612.8	1989	5.8	17.7	735.9
1958	6.1	15.7	805	1990	6.2	17.4	616.7
1959	5.6	16.6	546.6	1991	5.8	16.9	610.2
1960	5.4	16.2	705	1992	5.4	16.6	755.7
1961	5	17.2	595.9	1993	5.2	17.3	703.4
1962	5.7	16.4	731.9	1994	5.7	16.9	377.2
1963	5.2	16.2	622.2	1995	4.9	16.6	641.4
1964	6	15.5	750.9	1996	5.5	16.5	647.6
1965	5.3	16	692	1997	5.3	17.2	447.6
1966	4.5	16.6	562.7	1998	7.2	17.2	646.4
1967	4.7	16.7	605.6	1999	6.6	17.9	574.2
1968	5.6	15.9	745.7	2000	7	17.9	545.8
1969	4.8	16.4	722.3	2001	6.8	17.4	665.8
1970	5.1	16.5	847.1	2002	7.6	17.82	554.8
1971	5.1	17	913.3	2003	7.3	17.84	613.4
				Mean	5.7	16.57	683.37

[1] Wind speed and [2] Temperature collected at Low Head;
[3] Rainfall collected at Waterhouse Station (1960-2003), Bridport (1940-1959).

Appendix 3. Erosion pin data for the periphery of the deflation plain, Croppies Bay, NE Tasmania, Australia.

Survey interval dates	Interval between surveys (days)	Erosion pin numbers				
		0	1	2	3	4
October-November 2000	22	-24	-9	-3	-7	-3
November-December 2000	19	-35	-23	-157	-8	-20
December - February 2001	68	-237	-157	24	-118	-131
February - May 2001	85	-10	9	-5	-5	29
May - August 2001	110	-21	0	0	0	40
August - September 2001	20	-36	0	0	0	-15
September-November2001	55	35	0	0	0	18
November 01-March 2002	128	15	15	-7	7	75
March - May 2002	44	0	5	5	-1	4
Total	551	363-50=313	189-29=160	172-29=143	139-7=132	169-166=3
$n_b = 5\ 1/5 = 0.2$	Lc 0.2	62.6	32	28.6	26.4	0.6

Survey interval dates	Interval between surveys (days)	Erosion pin numbers				
		5	6	7	8	9
October-November 2000	22	27	23	31	-12	-10
November-December 2000	19	3	3	-75	5	-10
December - February 2001	68	-10	-28	88	-29	-42
February - May 2001	85	12	-1	8	2	-1
May - August 2001	110	15	22	14	13	24
August - September 2001	20	-5	-8	-133	-4	0
September-November2001	55	1	-4	4	1	4
November 01-March 2002	128	4	8	0	7	0
March - May 2002	44	15	-4	-16	0	4
	551	15-77=62	45-56=11	224-145=79	45-30=15	63-28=35
$n_b = 5\ 1/5 = 0.2$	Lc 0.2	12.4	2.2	16	3	7

Survey interval dates	Interval between surveys (days)	Erosion pin numbers				
		10	11	12	13	14
October-November 2000	22	-18	-24	-20	-16	31
November-December 2000	19	-21	-36	-34	-4	-33
December - February 2001	68	-56	-68	-137	-112	-211
February - May 2001	85	-45	-45	-13	-19	113
May - August 2001	110	-232	-20	5	3	-1
August - September 2001	20	12	19	20	3	-2
September-November2001	55	-2	4	2	-2	-5
November 01-March 2002	128	2	13	15	4	-38
March - May 2002	44	0	1	-5	-4	-1
	551	362-2=360	174-18156	209-42=167	157-10=147	291-144=147
$n_b = 5\ 1/5 = 0.2$	Lc 0.2	72.0	31.0	33.0	29	29

Survey interval dates	Interval between surveys (days)	Erosion pin numbers					
		15	16	17	18	19	20
October-November 2000	22	-5	-6	-2	-9	-7	26
November-December 2000	19	-38	0	-2	4	-10	-35
December - February 2001	68	-131	-83	19	-16	-98	-23
February - May 2001	85	-35	-6	26	8	-3	-8
May - August 2001	110	15	5	-15	-1	-1	14
August - September 2001	20	42	54	69	16	68	-1
September-November2001	55	4	-1	-9	-4	3	-9
November 01-March 2002	128	-19	8	-44	-5	4	5
March - May 2002	44	-11	5	10	-5	-2	-6
	551	239-6=178	96-73=23	72-124=52	40-28=12	119-77=42	82-45=37
	Lc 0.16	28.5	4	8	1.9	6.7	5.9

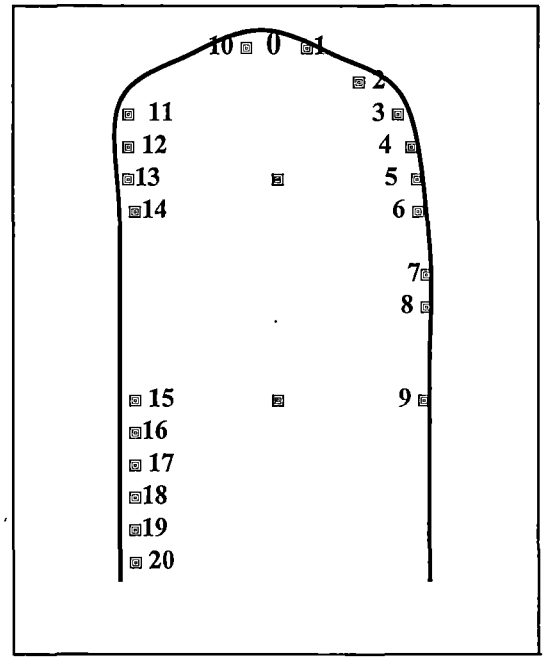

Figure Appendix 2. Indicative location of erosion pins (▣) around the periphery (⟶) of the deflation basin. The two central EPs (▣) are for alignment up the central axis of dune. Figure 5.1 contains the GPS surveyed locations.

Appendix 4. Summary of close-to-the-bed wind flow measurements and aerial photography.

Summary of close-to-the-bed wind flow measurements.

	No. of stations (masts[1]) deployed	No. of sensors[2] deployed	Date	Time of run	Duration of run
Transect 1 North to South over dune profile	4	3/ mast	6.9.03	11.38	30[3] min
Transect 2 Stoss profile	3	3/ mast	6.9.03	1.30 pm	30 min

[1] Figure 4.5 p.55. [2] Thermo anemometers were set at heights of 190 cm, 45 cm and 15 cm and run for 30-minute intervals, [3] preceded by a programmed 'warm-up' phase of 3 minutes.

Summary of aerial photographic information.

Year	Scale[1]	Elevation (feet)	Date taken	Lens Size
1949	1:25,000	11,000	22.3.1949	6 inch
1964	1:32,750	12,500	2.3.1964	4½ inch
1984	1:43,750	23,500	18.10.1984	151 mm
1999	1:20,000	20,100	17.1.1999	151 mm.

[1]Actual scale and elevation adjusted following a review of the DPIWE flight information sheets. Information of lens size for each flight was derived from flight information sheets.

Appendix 5. Measurement of enclosure sensor and probe.

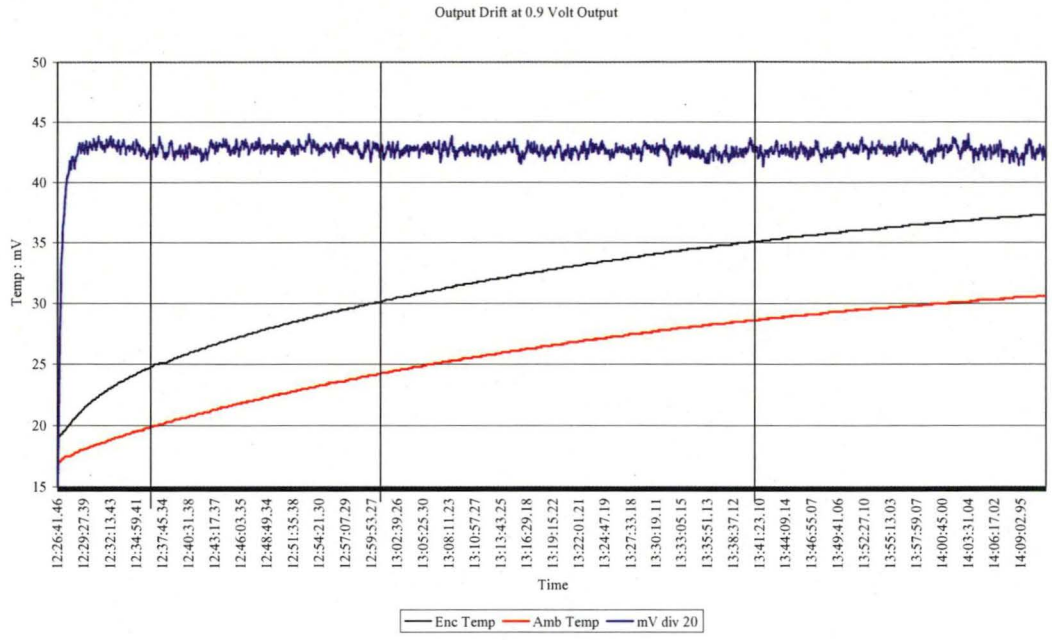

Figure 1. Measurement of enclosure sensor, probe, and additional ambient temperature sensor versus the duration of time of measurement (in hours:minutes:seconds) and applying an output drift of 0.9 Volt output. Refer Section 4.1.3:51, and Figure 4.2:52. Note that the 'Y'axis mV (blue) is divided by 20.

Table 1. Incremental drift of Temperature:m/V at three selected sample intervals shown in Figure 1.

	Commence time min:sec		Increments between sample intervals 1 to 3					
			Increment time 1		Increment time 2		Increment time 3	
Enclosure	12:26	19.2°C	17:10	7.6°C	25:39	5.1°C	41:8	4.9°C
Ambient	12:26	17.0°C	17:10	4.4°C	30:3	3.1°C	58:36	4.9°C

°C difference between Enclosure and Ambient at sample intervals			
2.2°	5.0°	5.8°	6.4°

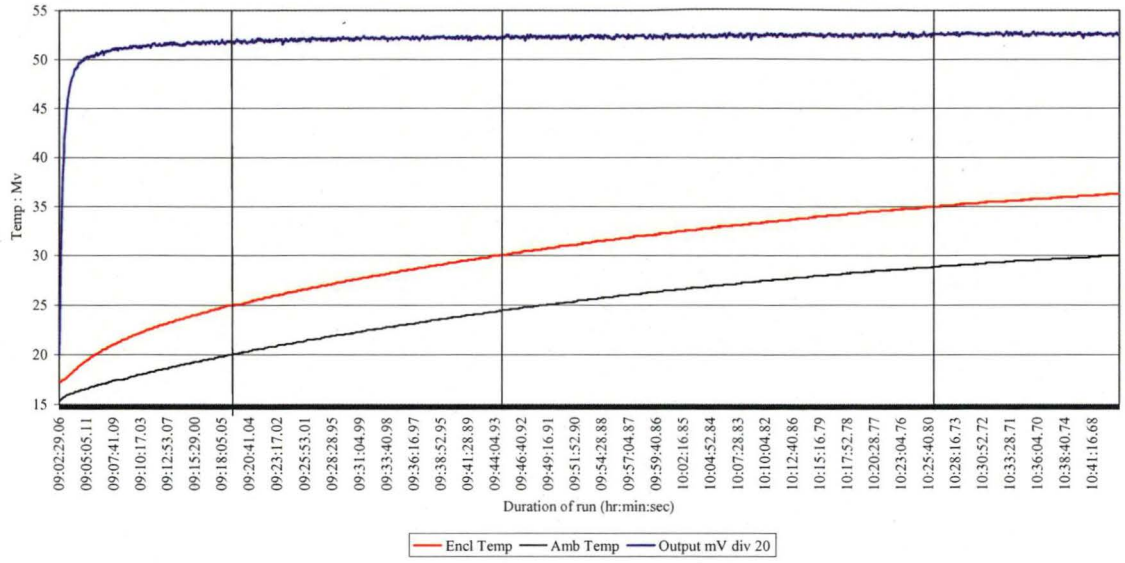

Figure 2. Measurement of enclosure sensor, probe, and additional ambient temperature sensor versus the duration of time of measurement (in hours:minutes:seconds) and applying an output drift of 1.0 Volt output. Refer Section 4.1.3:51, and Figure 4.2:52. Note that the 'Y'axis mV (blue) is divided by 20.

Table 2. Incremental drift of Temperature:m/V at three selected sample intervals shown in Figure 2.

	Commence time min:sec		Increments between sample intervals 1 to 3					
			Increment time 1		Increment time2		Increment time 3	
Enclosure	9:02	17.3°C	17:10	7.6°C	25:39	5.1°C	41:8	4.9°C
Ambient	9:02	15.5°C	17:10	4.4°C	30:3	5.1°C	58:36	4.9°C
°C drift between Enclosure and Ambient at sample intervals								
1.9°			5.0°		5.7°		6.1°	

Both Figures show a distinct increase in Temperature and mV output at the warm-up phase, which has a duration of about five minutes.

The incremental drift in Temp:mV in Figures 1 and 2 can partially be attributed to the increase in temperature in the air flow excluder enclosure (a modified bar fridge). Air temperature increases due to the functioning of the background electrical components. The ambient temperature increase in Figure 1 over a period of 1 hr 39 minutes was 14.3 °C. Figure 2 the ambient temperature increased 13.5°C over a period of 1 hr 35 min. Both the Ambient and Enclosure measurements parallel each other, with a nominal drift in the Enclosure temperature of 4.2°C for both the 1 and 0.9 volt outputs.

Both Figures 1 and 2 show a distinct steady state by the output mV, or Probe, at 1048 m/v. Evidently, the probe output is steady and independent of the Enclosure measurements.

Applying a polynomial regression to the calibration for Croppies Bay TA 8 and to the Enclosure Temperature and mV reading is equivalent to a range of 853 to 570 mV yielding an average 1.47 m/s (range 853 mV 1.87 m/s and 570 mV 1.08 m/s) drift over a one-hour recording period.

Given the following

- The field experiment that measured close-to-the-ground wind flow was undertaken in overcast / cloudy conditions with air temperature ranging between 10 to 12°C, there was no apparent warming of the Enclosure by the sun.
- For each transect run a programmed three minute warm-up was followed by a thirty minute recording period, which was instantly downloaded on to a laptop computer.

Based upon the field weather conditions, and the findings from the above testing of the TAs in controlled conditions, it is reasonable to say that the drift between the Enclosure sensor and the Probe for a recording period of 33 minutes is in the range of less than 1 m/s.